WAPD-TM--1605

DE88 005094

WAPD-TM-1605
Distribution Category UC-78

END-OF-LIFE NONDESTRUCTIVE EXAMINATION OF LIGHT WATER BREEDER REACTOR FUEL RODS

(LWBR Development Program)

D. A. Gorscak

Contributors: W. R. Campbell
J. C. Clayton

Contract No. DE-AC11-76PN00014

October 1987

Printed in the United States of America
Available from the
National Technical Information Service
U. S. Department of Commerce
5285 Port Royal Road
Springfield, Virginia 22161

NOTE

This document is an interim memorandum prepared primarily for internal reference and does not represent a final expression of the opinion of Westinghouse. When this memorandum is distributed externally, it is with the express understanding that Westinghouse makes no representation as to completeness, accuracy, or usability of information contained therein.

Bettis Atomic Power Laboratory West Mifflin, PA 15122-0079

Operated for the U. S. Department of Energy by
WESTINGHOUSE ELECTRIC CORPORATION

FOREWORD

The Shippingport Atomic Power Station located in Shippingport, Pennsylvania was the first large-scale, central-station nuclear power plan in the United States and the first plant of such size in the world operated solely to produce electric power. This program was started in 1953 to confirm the practical application of nuclear power for large-scale electric power generation. It has provided much of the technology being used for design and operation of the commercial, central-station nuclear power plants now in use.

Subsequent to development and successful operation of the Pressurized Water Reactor in the Atomic Energy Commission (now Department of Energy, DOE) owned reactor plant at the Shippingport Atomic Power Station, the Atomic Energy Commission in 1965 undertook a research and development program to design and build a Light Water Breeder Reactor core for operation in the Shippingport Station.

The objective of the Light Water Breeder Reactor (LWBR) program has been to develop a technology that would significantly improve the utilization of the nation's nuclear fuel resources employing the well-established water reactor technology. To achieve this objective, work has been directed toward analysis, design, component tests, and fabrication of a water-cooled, thorium oxide-uranium oxide fuel cycle breeder reactor for installation and operation at the Shippingport Station. The LWBR core started operation in the Shippingport Station in the fall of 1977 and finished routine power operation on October 1, 1982. After end-of-life core testing, the core was removed and the spent fuel shipped to the Naval Reactors Expended Core Facility for detailed examination to verify core performance, including an evaluation of breeding characteristics.

In 1976, with fabrication of the Shippingport LWBR core nearing completion, the Energy Research and Development Administration (now DOE) established the Advanced Water Breeder Applications (AWBA) program to develop and disseminate technical information which would assist U. S. industry in evaluating the LWBR concept for commercial-scale applications. The AWBA program, which was concluded in September, 1982, explored some of the problems that would be faced by industry in adopting technology confirmed in the LWBR program. Information developed includes concepts for commercial-scale prebreeder cores which would produce uranium-233 for light water breeder cores while producing electric power, improvements for breeder cores based on the technology developed to fabricate and operate the Shippingport LWBR core, and other information and technology to aid in evaluating commercial-scale application of the LWBR concept.

All three development programs (Pressurized Water Reactor, Light Water Breeder Reactor, and Advanced Water Breeder Applications) have been conducted under the technical direction of the Office of the Deputy Assistant Secretary for Naval Reactors of DOE.

Technical information developed under the Shippingport, LWBR, and AWBA programs has been and will continue to be published in technical memoranda, one of which is this present report.

(Intentionally Blank)

TABLE OF CONTENTS

TABLE OF CONTENTS (Cont)

TABLE OF CONTENTS (Cont)

LIST OF FIGURES

LIST OF FIGURES (Cont)

LIST OF FIGURES (Cont)

LIST OF TABLES

LIST OF ACRONYMS

ACCEPT	Analysis of Cladding Collapse for Externally Pressurized Tubes (fuel rod analysis program)
ANL-W	Argonne National Laboratory-West
AWBA	Advanced Water Breeder Applications
BOL	Beginning of Life
CHORT	Corrosion and Hydriding of Reactor Tubing (corrosion analysis program)
CHF	Critical Heat Flux
CYGRO	Cylindrical Growth (fuel rod analysis program)
DOE	Department of Energy
DSR	Degradation of Specification Requirements
ECF	Expended Core Facility, Idaho
EDCOT	Eddy Current Oxide Thickness
EFPH	Effective Full Power Hours
EOL	End-of-Life
FIR	Fissile Inventory Ratio
LOCA	Loss of Coolant Accident
LWBR	Light Water Breeder Reactor
MVS	Module Visual Station
NRC	Nuclear Regulatory Commission
PCI	Pellet-Cladding Interaction
PIFAG	Production Irradiated Fuel Assay Gage
PWR	Pressurized Water Reactor
REX	Rod Examination Gage
RIT	Reactivity Insertion Transient
ROBOT	Computer Program for Calculating Rod Bow
RRS	Rod Removal System
RTIPS	Real Time Image Processor Software
RXA	Recrystallization Annealed
SRA	Stress Relief Annealed
VDS	Vertical Disassembly Stand

In-bundle and out-of-bundle (single rod) nondestructive examinations of Light Water Breeder Reactor fuel rods were performed. In-bundle examinations included visual examination and measurement of rod bow, rod-to-rod gaps, and rod removal forces. Out-of-bundle examinations included rod visuals and measurement of fuel rod length, diameter and ovality, cladding oxide and crud thickness, support grid induced cladding wear mark depth and volume, and fuel rod free hanging bow. The out-of-bundle examination also included ultrasonic inspection for cladding defects, neutron radiography for pellet integrity and plenum gap measurements, and gamma scans for in-stack axial gap screening and binary fuel stack length measurements. The measurements confirmed design predictions of fuel rod performance and provided evidence of excellent fuel rod performance for operation of Light Water Breeder Reactor to 29,047 effective full power hours (EFPH).

END-OF-LIFE NONDESTRUCTIVE EXAMINATION OF LIGHT WATER BREEDER REACTOR FUEL RODS

(LWBR Development Program)

D. A. Gorscak

SECTION 1 - INTRODUCTION

As part of the Light Water Breeder Reactor (LWBR) program, spent modules were shipped to the Naval Reactors Expended Core Facility (ECF) in Idaho Falls, Idaho for examination and preparation for long term storage. The examinations were performed to confirm breeding, to assess support structure and fuel rod performance, and to provide a data base for evaluation of design procedures. The end-of-life (EOL) examination program included examinations of entire modules as well as individual components (fuel rods, grids, bolts, etc.). The purpose of this report is to present results of in-bundle and out-of-bundle EOL nondestructive examinations of LWBR fuel rods that were performed to evaluate fuel rod dimensional stability, cladding and fuel pellet integrity, Zircaloy cladding corrosion, and fuel rod crud buildup.

In-bundle examinations included visual examination of each module, rod spacing and bow measurements, and pull force measurements. In-bundle spacing and bow were determined by digitizing 5X video recordings of fuel rods in seven of the 39 LWBR fuel modules. Up to 10,000 spacing measurements and 10,000 rod centerline position measurements were obtained for a single fuel module. Pull forces were measured for all rods removed from spent fuel modules. Measured pull forces were monitored at 0.1 to 0.4-inch increments during rod pull and were compared with limits to assure that fuel rod cladding was not overstressed during removal. The data was also used for analysis of sliding friction and comparisons between rods.

Out-of-bundle examinations included measurement of fuel rod length, diameter, plenum ovality, cladding wear, free-hanging bow, and oxide thickness in the rod examination gage (REX) (Reference 1) specifically designed for examination of LWBR fuel rods. Ultrasonic probes on the REX were also used to screen fuel rods for defects (e.g., partial or through cracks). Nineteen fuel rods were examined with the REX.

Approximately 40,000 diameter measurements per rod were obtained with the REX. Measured diameters were used to determine the axial variation of average fuel rod diameter and cladding ovality. Approximately 1000 oxide thickness measurements per rod were obtained with the REX. Measured oxide thickness was used to study the axial and radial variation of oxide thickness for individual rods and for comparison between rod types.

An orbiting profilometer on the REX was used to determine fuel rod plenum ovality and wear mark depth and volumes. The gage provided surface radial and angular position around the circumference of a fuel rod relative to a fixed coordinate system. Approximately 2500 measurements of the cladding surface were used to determine the depth and volume of an individual wear mark. Approximately 2000 measurements of cladding surface position were used to characterize plenum ovality for a single rod.

Fuel rod free hanging bow was determined by digitizing 5X video recordings with the rod suspended in the REX. End-of-life (EOL) free hanging bow measurements were obtained for comparison with similar measurements obtained

during fuel rod fabrication and for calculation of EOL in-bundle bow of fuel rods.

Out-of-bundle examinations also included neutron radiography of the fuel rods and crud characterization and crud thickness measurements by Argonne National Laboratory-West (ANL-W) and gamma scan of the fuel rods using the production irradiated fuel assay gage (PIFAG) (References 2 and 3) at ECF. Neutron radiography was used to determine pellet integrity, fuel stack length, and to search for spaces between pellets (in-stack axial gaps). Gamma scans were also used to determine fuel stack lengths and to search for in-stack axial gaps. Measured fuel stack lengths were used to calculate fuel stack length changes for comparison with predictions. Crud examinations were performed to determine elemental and isotopic components of the LWBR crud, to determine axial variation of crud thickness, and for comparison among rod types.

The following section (Section 2) presents a brief description of the LWBR core and fuel rod design, with emphasis on features unique to LWBR. Section 2 also presents a brief summary of LWBR operation and discusses selection of rods for the EOL examination program. Section 3 presents a detailed description of each of the EOL examinations. Section 4 presents examination data and comparisons of data with design predictions.

Results from other EOL examinations of LWBR are presented in References 4, 5, 6, and 7. A description of the overall examination process at ECF is presented in Reference 8.

(Intentionally Blank)

SECTION 2 - BACKGROUND

2.1 - GENERAL CORE DESIGN

The objective of the Light Water Breeder Reactor (LWBR) program was the development of technology to improve utilization of the nation's nuclear fuel resources in light water reactors. To achieve this objective, a small (236.6 Mw thermal, 72 Mw electrical) water cooled, thorium cycle breeder reactor was installed and operated at Shippingport, Pennsylvania.

Figure 1 shows a plan cross section of the LWBR core installed in the Shippingport pressurized water reactor vessel. Figure 2 shows a cutaway view of the reactor. The central portion of the core had a seed-blanket configuration consisting of 12 movable-fuel seed assemblies each surrounded by a stationary blanket assembly. The seed-blanket assemblies were designated as Types I, II, or III modules. Zircaloy shells separated each seed and blanket assembly. The seed-blanket assemblies were surrounded by an outer reflector region composed of 15 modules (Types IV and V). The design simulated a large-scale breeder environment in the interior of the core (three Type I modules) with the intent to achieve net breeding in the core.

The core had four distinct fuel regions: seed, standard blanket, power flattening blanket, and reflector. Type I modules contained seed and standard blanket fuel. Types II and III modules contained seed, standard blanket, and power flattening blanket fuel. Types IV and V modules contained only reflector fuel. The seed, blanket, and power flattening fuel regions each contained fissile fuel (U-233) in the form of thoria-urania (ThO_2-UO_2) fuel pellets and fertile material in the form of thoria (ThO_2) fuel pellets. Reflector modules served to restrict neutron losses from the core and contained only ThO_2 pellets.

To enhance breeding performance, the standard blanket region had a high metal-to-water ratio of 2.98. The power flattening blanket fuel region had a lower metal-to-water ratio of about 1.76 and a higher UO_2 concentration than the blanket. The power flattening blanket was located on the outer periphery of the nine seed-blanket assemblies surrounding the three center seed-blanket assemblies. As a result, the overall radial core power distribution was flattened.

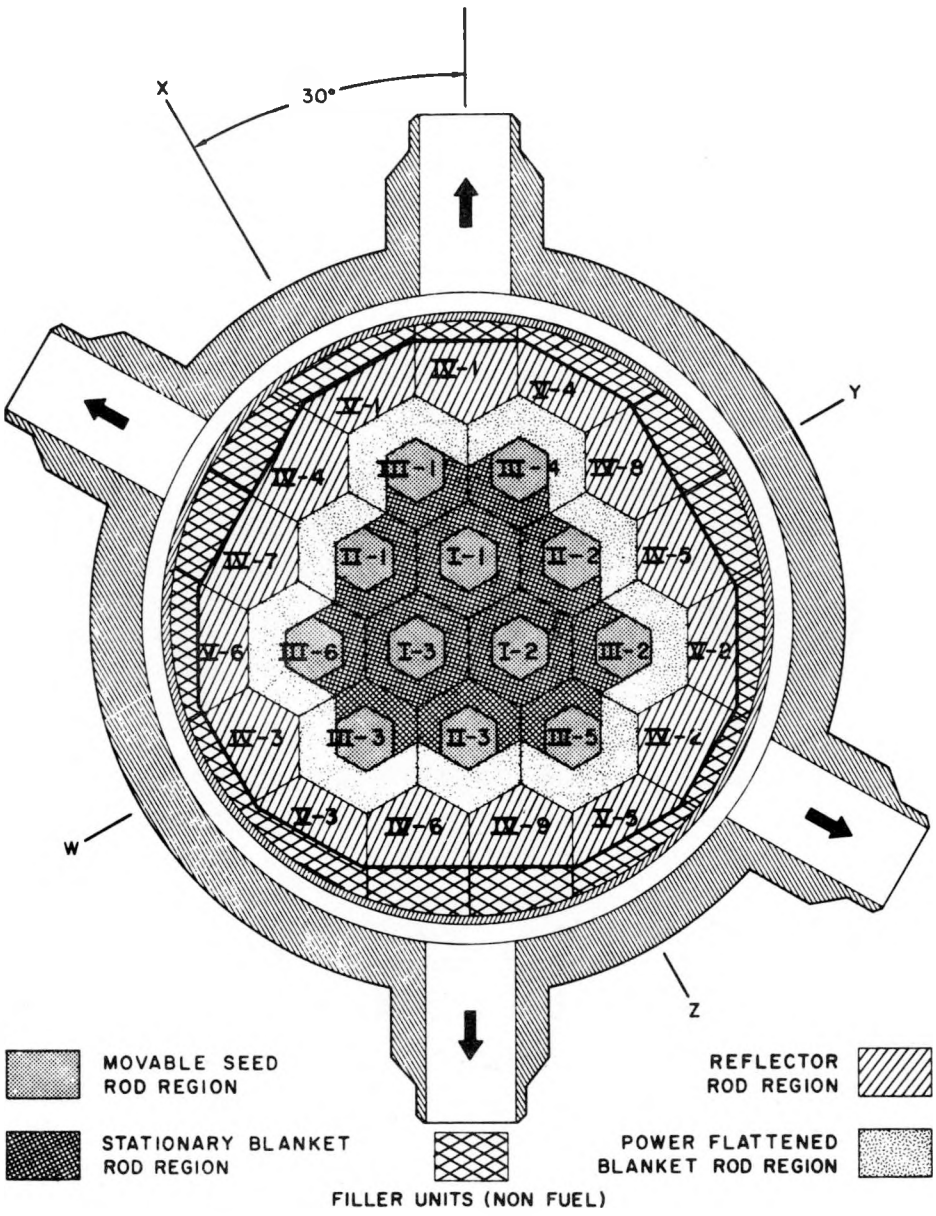

Figure 1 - LWBR Core Module Descriptions

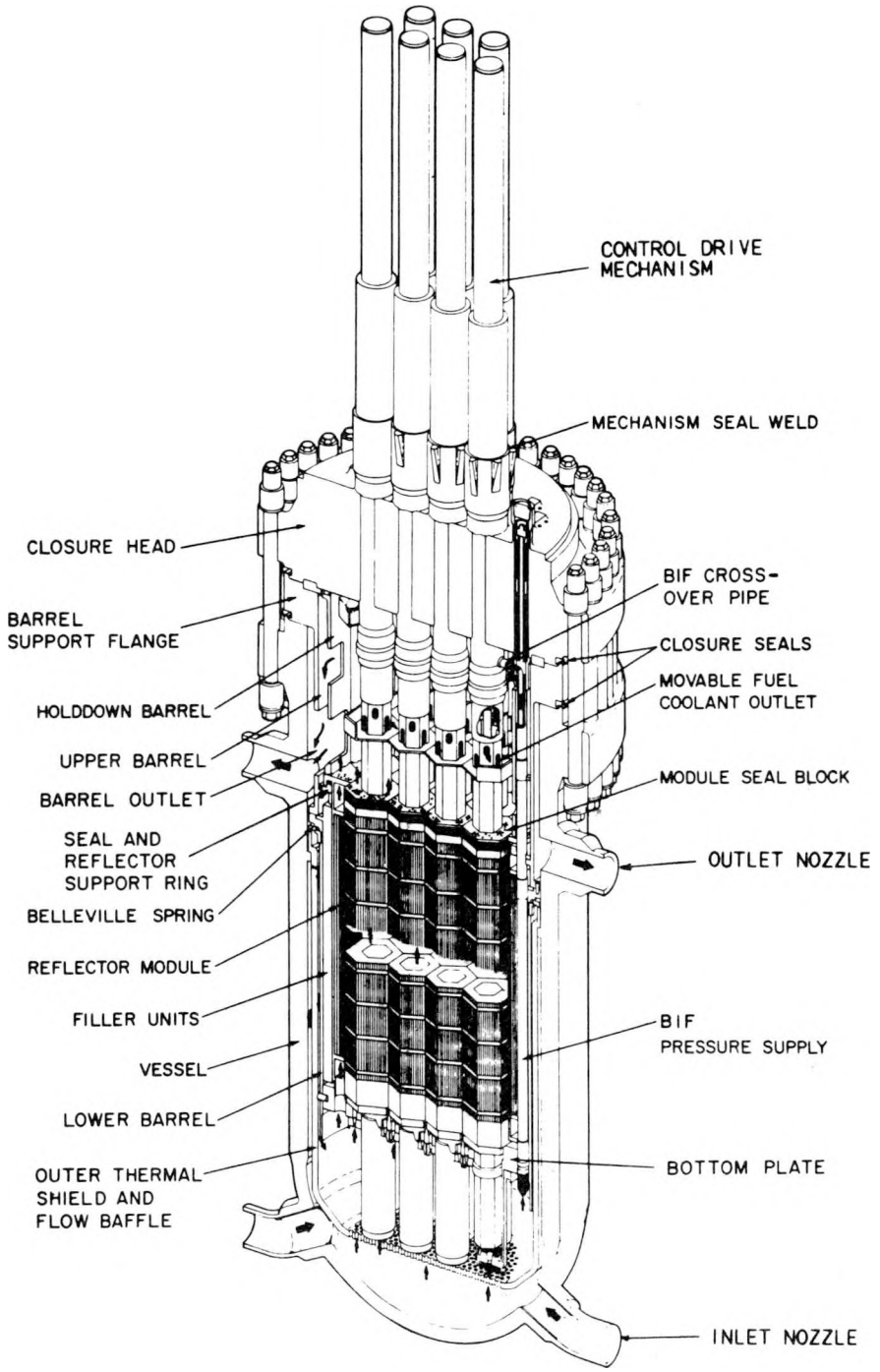

Figure 2 - LWBR Core Reactor Assembly

The four types of ceramic fuel pellets (seed, standard blanket, power flattening blanket, and reflector) were loaded into four sizes of fuel rods. The rods were designated as seed, standard blanket, power flattening blanket, and reflector fuel rods and were loaded into seed, blanket, and reflector fuel modules. Numbers of rods and rod spacing for each module type are summarized below.

Module	Type	Number of Rods	Spacing (in.)
Seed	I	619	0.063
	II	619	0.063
	III	619	0.063
Blanket	I	444/0*	0.058
	II	261/303	0.058/0.103
	III	187/446	0.058/0.103
Reflector	IV	228	0.069
	V	166	0.069

AM-350 stainless steel grids with a hexagonal array were used to support the fuel rods. Each seed module had 9 grids per module. Each blanket module had 8 grids per module. Each reflector module had 6 grids per module. Fuel rods were secured to only one end of the modules. Approximately half of the fuel rods in each module were fixed to the top of the module and the other half to the bottom of the module. Details regarding the support grid design are presented in Reference 9.

2.2 - FUEL ROD DESIGN

2.2.1 - Seed Fuel Rods

LWBR had eight types of seed fuel rods designated as 01, 02, 03, 04, 05, 06, 07, and 08. Figure 3 shows a seed fuel rod. The seed fuel rods had two different binary (UO_2-ThO_2) loadings and four different stack lengths. Loadings and binary stack lengths for seed fuel rods are presented in Table 1. Binary fuel with 5.195 w/o U-fissile material was designated as high zone binary fuel. Binary fuel with 4.325 w/o U-fissile material was designated as low zone binary fuel. Rod types with odd designations (e.g., 01, 03, etc.)

*Standard blanket/power flattening blanket

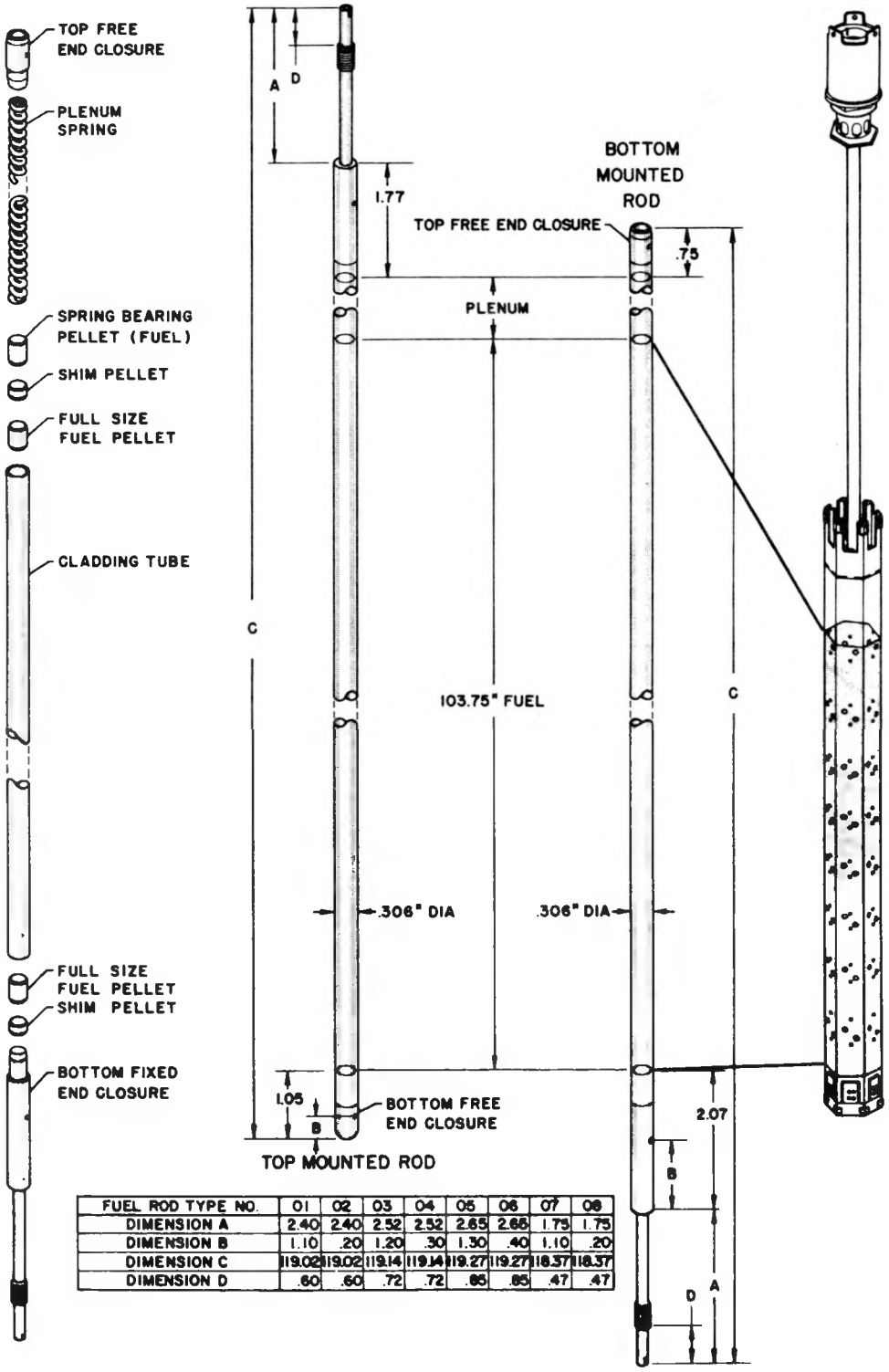

FUEL ROD TYPE NO.	01	02	03	04	05	06	07	08
DIMENSION A	2.40	2.40	2.52	2.52	2.65	2.65	1.75	1.75
DIMENSION B	1.10	.20	1.20	.30	1.30	.40	1.10	.20
DIMENSION C	119.02	119.02	119.14	119.14	119.27	119.27	118.37	118.37
DIMENSION D	.60	.60	.72	.72	.85	.85	.47	.47

Figure 3 - LWBR Seed Fuel Rods

were fixed to a baseplate at the bottom of the module, and rod types with even designations were fixed to a baseplate at the top end of the module to prevent axial movement of the rods.

Table 1 - Seed Binary Fuel Loadings

Type	Composition* w/o U-fissile	Theoretical Density (gm/cc)	Binary Stack Length (in.)
01	4.327	10.035	42.0
02	4.327	10.035	42.0
03	4.327	10.035	56.0
04	4.327	10.035	70.0
05	5.195	10.042	84.0
06	5.195	10.042	84.0
07	4.327	10.035	42.0
08	4.327	10.035	42.0

Seed fuel pellets were right circular cylinders with chamfers on both ends to ease loading into tubing, to facilitate movement of the pellet stack in the tubing during power operation, and to reduce pellet chipping during fabrication, rod handling, and power operation. The pellets had dished ends to reduce axial expansion of the stack. The pellets were sintered to 97-99 percent theoretical density to maximize pellet dimensional stability. Shim pellets of thoria fuel were used near the top and bottom of the fuel stack to make up the desired fuel stack length. A spring-bearing fuel pellet with only one dished end was used at the top of the fuel stack. Dimensions for seed fuel pellets are presented in Table 2. Seed fuel rod cladding was recrystallization annealed (RXA) Zircaloy-4. Heat treatment and material properties for the Zircaloy-4 cladding are presented in Table 3. More detailed information on the characteristics of LWBR cladding is presented in Reference 10. The process used to fabricate the cladding is described in Reference 11. Nominal length of the rods (excluding the end stem) was 116.62 inches. Outside diameter (OD) was nominally 0.306 inch. Cladding

*w/o - weight percent

Table 2 - LWBR Fuel Pellet Dimensions*

UO_2-ThO_2 Pellets

Attribute	Seed	Standard Blanket	Power Flattening Blanket
Diameter	0.2520 ±.0005	0.5105 ±.0005	0.4695 ±.0005
Length	0.615 ±.020	1.785 ±.020	0.700 ±.020
	0.445 ±.020	0.870 ±.020	0.785 ±.020
	----	0.530 ±.020	0.870 ±.020
Chamfer Length	0.015 ±.005	----	----
Chamfer Depth	0.015 ±.005	----	----
Taper Length	----	0.150 ±0.050	0.150 ±0.050
Taper Depth	----	0.003 ±0.002	0.0024 ±0.0014
End Dish Spherical Radius	0.360	1.439	1.161
End Dish Depth	0.009 ±0.003	0.014 ±0.004	0.014 ±0.004

ThO_2 Pellets

Attribute	Seed	Standard Blanket	Power Flattening Blanket	Reflector
Diameter	0.2555 ±.0005	0.5105 ±.0005	0.4695 ±.0005	0.7415 ±.0005
Length	0.530 ±.020	0.615 ±.020	0.44 ±.020	0.740 ±.060
Chamfer Length	0.015 ±.005	0.006 ±.004	0.006 ±.004	----
Chamfer Depth	0.015 ±.005	0.006 ±.004	0.006 ±.004	----
End Dish Spherical radius	0.298	1.439	1.160	3.152
End Dish Depth	0.009 ±.003	0.014 ±.004	0.014 ±.004	0.014 ±.004

*All dimensions in inches, except as noted

Table 3 - LWBR Fuel Rod Cladding Material Properties

Attribute	Seed	Standard Blanket	Power Flattening Blanket	Reflector
Final Heat Treatment Temperature, degrees F	1225 ±25	925 ±25	925 ±25	925 ±25
Final Heat Treatment Time (hrs)	2 - 5	2 - 5	2 - 5	2 - 5
70 F Yield Strength (ksi)*	54.66 49.74	79.77 73.55	80.71 76.13	77.79 72.36
700 F Yield Strength (ksi)*	18.57 17.37	51.14 47.89	53.13 50.67	49.49 46.56
70 F Yield/Ult. Ratio*	1.472 1.405	1.363 1.310	1.359 1.330	1.367 1.330
700 F Yield/Ult. Ratio*	1.951 1.872	1.259 1.212	1.254 1.226	1.288 1.261
70 F Elongation (%)*	29.2 27.04	21.87 20.41	19.63 18.49	23.57 22.16
700 F Elongation (%)*	35.75 32.19	20.61 18.83	18.17 16.90	21.87 20.33

*Average and lower 95/95 tolerance interval

thickness (t) was nominally 0.022 inch, for an OD/t ratio of 13.9. For LWBR system pressure and temperature, the cladding was freestanding (i.e., the cladding would not collapse onto the fuel pellets). The fuel rods had a 10.0-inch plenum at the top of the fuel stack to accommodate fission gas release.

The plenum included an Inconel compression spring at the top of the stack to minimize formation of axial gaps in the stack during handling, normal reactor operation, and shock loading (e.g., from scrams, check value slams, earthquakes, etc.). A top mounted rod had a hemispherical free end to minimize flow induced vibratory wear of the free end of the rod. A bottom mounted fuel rod had a square free end at the top where the end configuration did not affect rod vibration. The rods were backfilled with helium at 1-atmosphere pressure during welding. Physical dimensions for seed fuel rods are summarized in Table 4.

2.2.2 - Blanket Fuel Rods

Figure 4 shows LWBR standard and power flattening blanket fuel rods. LWBR had six types of standard blanket fuel rods designated as 11, 12, 13, 14, 15, and 16 and seven types of power flattening blanket fuel rods designated as 21, 22, 23, 24, 25, 26, and 27. The standard blanket fuel rods had three binary loadings and four stack lengths. The power flattening blanket fuel rods had three binary fuel loadings and four stack lengths. Loading and binary stack lengths for standard and power flattening blanket fuel rods are presented in Table 5. Standard blanket binary pellets with 1.211 w/o U-fissile material were called low zone binary fuel. Standard blanket binary fuel pellets with 1.662 w/o U-fissile material were called medium zone binary fuel. Standard blanket binary fuel pellets with 2.000 w/o U-fissile material were called high zone binary fuel. Loading for low, medium, and high zone power flattening binary fuel pellets were 1.649, 2.005, and 2.733 w/o U-fissile material, respectively. Rod types with odd designations (e.g., 11, 21) were fixed to the bottom of the modules. Rod types with even designations (e.g., 12, 22) were fixed to the top end of the module.

Table 4 - LWBR Fuel Rod Dimensions*

Attribute	Seed	Standard Blanket	Power Flattening Blanket	Reflector
Rod length	116.620 ±.065	117.650 ±.065	117.650 ±.065	110.85 ±0.065
Cladding Type**	RXA	SRA	SRA	SRA
Cladding Outside*** Diameter	0.306 ±.0015 +.003 -.002	0.5715 ±.0015 ±.0025	0.5275 ±.0015 ±.0025	0.832 ±.003
Cladding Inside*** Diameter	0.262 ±.001 ±.002	0.516 ±.001 ±.002	0.475 ±.001 ±.002	0.748 ±.001 ±.002
OD/t	13.9	20.6	20.1	19.8
Pellet Diameter	0.252 ±.0005	0.5105 ±.0005	0.4695 ±.0005	0.7415 ±.0005
Cladding-Pellet Radial Gap	0.0042-0.0057	0.002-0.0035	0.002-0.0035	0.002-0.0045
Plenum Length	10.0 ±.100	9.9 ±.055	9.9 ±.055	3.955 ±.040

*All dimensions in inches, except as noted

**RXA - Recrystallization Annealed
SRA - Stress Relief Annealed

***Average and local tolerance

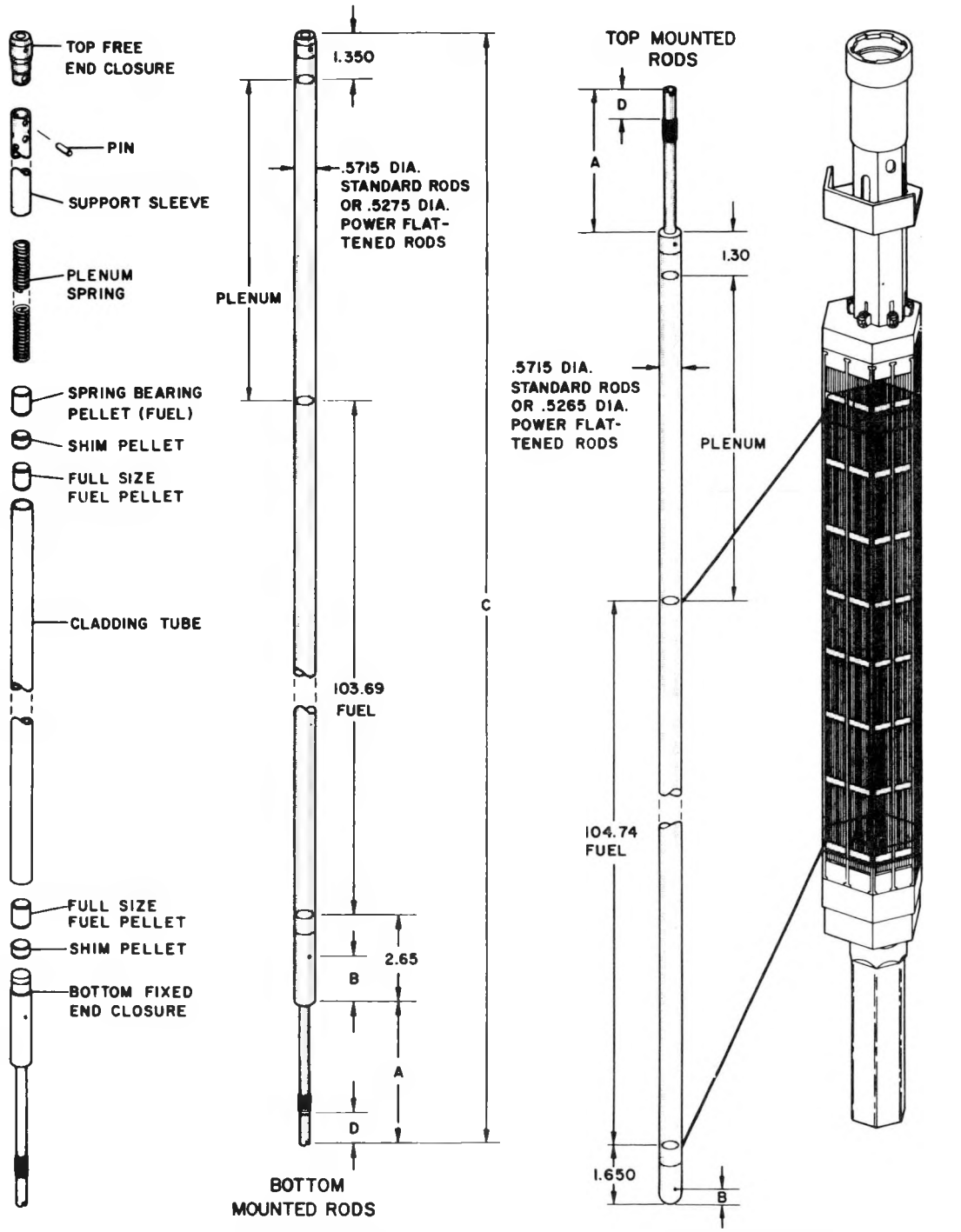

FUEL ROD TYPE NO.	11	12	13	14	15	16	21	22	23	24	25	26	27
DIMENSION-A	4.23	4.23	4.35	4.35	4.47	4.47	4.23	4.23	4.35	4.35	4.47	4.47	4.60
DIMENSION-B	1.40	.50	1.50	.60	1.60	.70	1.70	.80	1.80	.90	1.90	1.00	2.00
DIMENSION-C ± .07	121.9	121.9	122.0	122.0	122.1	122.1	121.9	121.9	122.0	122.0	122.1	122.1	122.3
DIMENSION-D	.78	.78	.90	.90	1.03	1.03	.78	.78	.90	.90	1.03	1.03	1.16

Figure 4 - LWBR Blanket Fuel Rods

Table 5 - Standard and Power Flattening
Blanket Binary Fuel Loadings

Standard Blanket

Type	Composition w/o* U-fissile	Theoretical Density (gm/cc)	Binary Stack Length (in.)
11	1.211	10.009	42.0
12	1.211	10.009	42.0
13	2.000	10.016	70.0
14	1.662	10.013	56.0
15	1.662	10.013	84.0
16	2.000	10.016	84.0

Power Flattening Blanket

Type	Composition w/o* U-fissile	Theoretical Density (gm/cc)	Binary Stack Length (in.)
21	1.649	10.013	42.0
22	1.649	10.013	42.0
23	2.733	10.022	70.0
24	2.005	10.016	56.0
25	2.733	10.022	84.0
26	2.005	10.016	84.0
27	2.733	10.022	84.0

*w/o - weight percent

Standard and power flattening blanket binary fuel pellets were right circular cylinders with tapers on both ends to minimize ridging of the cladding due to pellet hourglassing. The pellets also had dished ends to reduce fuel stack axial expansion. The pellets were sintered to 96-99 percent theoretical density to maximize pellet dimensional stability.

Standard and power flattening blanket thoria fuel pellets were right circular cylinders with chamfers on both ends. The pellets had dished ends and were also sintered to 96-100 percent theoretical density.

Dimensions for blanket fuel rod pellets are also presented in Table 2.

Blanket fuel rod cladding was highly coldworked and stress relief annealed (SRA) Zircaloy-4. Heat treatment and material properties for the cladding are also summarized in Table 3. Rod length (excluding the end stem) was approximately 117.7 inches for both standard and power flattening blanket fuel rods. Cladding outside diameter was nominally 0.5715 inch for standard blanket fuel rods and 0.5275 inch for power flattening blanket fuel rods. Nominal wall thickness was 0.0278 inch for standard blanket fuel rods and 0.0263 inch for power flattening blanket fuel rods. The OD/t ratios were 20.6 and 20.1 for standard and power flattening blanket fuel rods, respectively. For LWBR operating pressure and temperatures, cladding for both standard and power flattening fuel rods was nonfreestanding (i.e., the cladding would collapse onto the fuel pellets after exposure in the core). Both standard and power flattening blanket fuel rods had 9.9-inch plenums at the top to accommodate fission gas release. Both rods had an Inconel sleeve in the plenum to provide internal support for the nonfreestanding cladding. Each standard blanket fuel rod had a 0.53-inch axial gap between the Inconel sleeve and the top of the fuel stack. Each power flattening fuel rod had a 0.495-inch gap at the top of the fuel stack. Each rod had an Inconel compression spring in its plenum to minimize the development of in-stack pellet-to-pellet axial gaps due to handling, differential expansion, and shock loading during operation. Each top mounted rod had a hemispherical free end. Each bottom mounted rod had a square free end. Each rod was also backfilled with helium at 1-atmosphere pressure during welding. Dimensions for standard and power flattening blanket fuel rods are also presented in Table 4.

2.2.3 - Reflector Fuel Rods

Figure 5 shows a reflector rod. Reflector rods had only two rod types, type 31 and type 32. Both contained only thoria pellets. Rod type 31 was attached to the bottom of the module, and rod type 32 was attached to the top of the fuel module.

Reflector pellets were right circular cylinders with square edges and had dished ends to minimize axial expansion of the fuel stack. Dimensions of reflector pellets are also presented in Table 2.

Reflector cladding was highly cold worked and stress relief annealed (SRA) Zircaloy-4. Heat treatment and material properties for LWBR reflector rods are also summarized in Table 3. Rod length was 110.85 inches, excluding the end stem. Cladding nominal outside diameter was 0.832 inch. Cladding thickness was 0.042 inch, for an OD/t ratio of 19.8, making the cladding nonfreestanding for LWBR operating pressure and temperature.

Reflector fuel rods had a 3.955-inch plenum with an Inconel support sleeve. The axial gap between the support sleeve and the top of its pellet stack was nominally 0.230 inch. Each reflector rod had an Inconel compression spring at the top of the fuel stack to minimize the formation of in-stack pellet-to-pellet gaps. Each top mounted reflector fuel rod had a hemispherical free end. Each bottom mounted fuel rod had a square free end. The rods were backfilled with helium at 1-atmosphere pressure during welding. Dimensions for reflector fuel rods are also summarized in Table 4.

2.3 - COMPARISON WITH COMMERCIAL PRESSURIZED WATER REACTOR FUEL RODS

LWBR fuel rods had several features which distinguished them from commercial pressurized water reactor (PWR) fuel rods. Some of the features were required to meet breeding objectives; others were included because they improved fuel rod performance.

2.3.1 - U-233 Fuel

Uranium-233 is chemically similar to partially enriched uranium-235 used to form uranium-oxide fuel for commercial nuclear power fuel rods. However, it had two unique features of importance to LWBR. First, U-233 has a larger

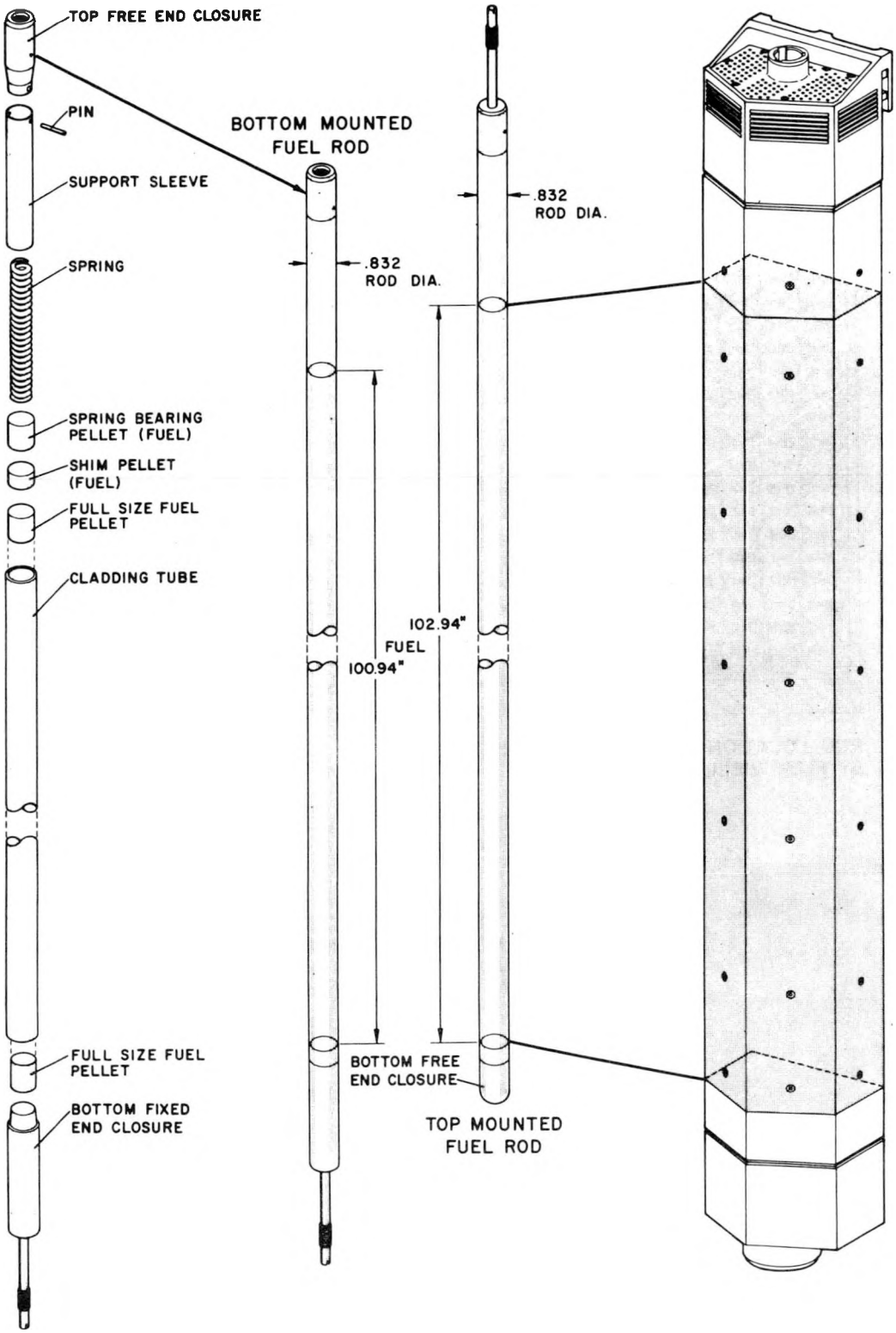

Figure 5 - LWBR Reflector Fuel Rods

neutron regeneration factor (η) in the thermal and epithermal region than U-235. The initial conversion ratio (the ratio of the rate of production of fissile atoms to the rate of destruction of fissile atoms at any instant of time) for the LWBR core was approximately 1.1 at beginning-of-life (BOL) and decreased to 1.0 at 18,000 EFPH. The net fissile inventory for LWBR peaked at 18,000 EFPH when the conversion ratio was 1.0. For continuous 100 percent power operation, the fissile inventory ratio (FIR) for LWBR would be 1.012. Because LWBR was shut down for testing and maintenance and was operated in swingload mode during periods, the average load factor was approximately 80 percent. The peak FIR was larger for reduced load factors because of reduced absorption rate in the fission product poisons Pa-233 and Xe, so that the measured FIR for LWBR was approximately 1.014 (Reference 7).

Second, the fission product yield for U-233 is different from that of U-235. The most important effect that this had on fuel element performance was that twice as much iodine was produced by U-233. Doubling the amount of iodine decreases the threshold stress required for iodine stress corrosion cracking by about 12 percent. However, since U-233 in the thoria system used in LWBR had a much lower total fission gas release at typical operating heat flux conditions, the expected iodine release for LWBR fuel rods was a factor of 2.5 less than U-235, resulting in an increase in threshold stress of 19 percent.

2.3.2 - UO_2-ThO_2 Fuel System

The thorium cycle used in LWBR converted fertile Th-232 to fissile U-233. The thorium cycle was used to take advantage of the high thermal η value of U-233 so as to provide as large an excess of neutrons as possible during the depletion of fissile fuel. The excess neutrons were utilized in the production of fissile U-233 by neutron capture in fertile Th-232.

The thoria-based fuel system has many operating advantages over the urania system, with some fabrication disadvantages. Fabrication difficulties of importance to design included uranium homogeneity, which is difficult to obtain in the single fire process, and attainment of high density because of

thoria's high melting temperature and reduced diffusion coefficients at normal sintering temperature. Attainment of uranium homogeneity limits was achieved by comicronizing and by thoroughly mixing the binary compositions. High density was achieved by using micronized powder and a slightly higher than normal sintering temperature.

At a given heat flux, the margin to fuel melting in LWBR fuel rods compared with commercial fuel rods was almost directly related to thermal conductivity and melting point of the respective fuel systems. Best estimate melting point for UO_2 fuels is about 5100F, compared with about 5950F for UO_2-ThO_2 fuel systems with 2 to 6 w/o UO_2. In addition, the thermal conductivity of the thoria based system was higher than in the urania system.

The thoria system also has reduced fission gas release due to the higher threshold temperatures for release from internal dislocations and grain boundaries, as shown in References 12 through 14.

Pellet-cladding interaction (PCI) during power changes is highly dependent on fuel thermal conductivity and the thermal expansion coefficient. Because the thermal expansion of ThO_2 is less than that for UO_2, the thoria system would have less interaction for comparable conditions (i.e., fuel-cladding gap and fuel pellet temperatures).

Finally, the thoria fuel system is more corrosion resistant than the urania system, where UO_2 can oxidize to U_3O_8 when exposed to hot water. Conversion of UO_2 to U_3O_8 results in a volume increase potentially overstraining the cladding. Test results presented in References 15 and 16 demonstrated the improved corrosion resistance of thoria (with core enrichments of urania) over that of urania.

2.3.3 - Tapered Fuel Pellets

As discussed above, LWBR binary fuel pellets had either tapers (blanket) or chamfers (seed) on the ends of the pellets to minimize end voids in manufacture, to improve axial stack movement capability of the fuel in the cladding, and to reduce PCI effects at the ends of the pellets.

The only fuel rod performance concern related to fuel pellet tapers was associated with grinding tolerances. In general, a taper of 1-mil depth was required to compensate for expected bellmouthing of fuel pellets. Manufacturing tolerance could result in taper depths of 1 to 5 mils. An overly large taper was undesirable because deformation of the nonfreestanding blanket cladding could have resulted in a significant loss of support grid seating force and a reduction in rod-to-rod and rod-to-support structure clearances.

2.3.4 - Low Hafnium Zircaloy Tubing

To enhance breeding, LWBR tubing hafnium content was limited to 50 ppm. Irradiation tests of both low and high hafnium (<50 ppm versus 50 to 100 ppm) did not show any differences attributable to hafnium content.

2.3.5 - RXA Tubing

Commercial reactors generally use cold-worked tubing with final stress relief anneal, whereas the seed of LWBR used highly cold-worked tubing followed by a recrystallization annealing treatment. RXA tubing was selected because it provided more creep resistance during irradiation. RXA cladding also minimized cladding elongation of seed fuel rods which are exposed to peak fluences. Elongation was a concern for rod-to-base plate clearance and potential bow of the small diameter seed rods. Low initial strength of RXA tubing necessitated separation of the fuel from the cladding to minimize pellet-to-cladding interaction (PCI) by using a large fuel-cladding gap and a cladding thickness to maintain low hoop stress (approximately 16,000 psi at 2000 psi system pressure). At 20,000 psi stress and a fast flux of $>5 \times 10^{13}$ n/cm^2-sec, the creep rate of RXA tubing is a factor of 2.6 less than SRA tubing.

Fuel rod up-power and reactivity insertion transient (RIT) capability are dependent on the amount of PCI and strength of the cladding. Although seed fuel rods were expected to have little pellet-to-cladding interaction, the low strength of RXA cladding versus SRA cladding at beginning-of-life required

special reactor startup procedures. Irradiation hardening rapidly increased strength of RXA cladding during operation.

Based on corrosion tests on LWBR tubing (Reference 17), RXA seed tubing had a 25 percent lower corrosion rate than SRA tubing when tested in 680F water.

Overall, at low stress the use of RXA tubing was expected to improve seed fuel rod performance over SRA tubing.

2.3.6 - Fuel Rod Pressurization

Collapse of cladding over axial gaps which formed in the fuel stack during reactor operation led to breeched cladding in some early commercial reactors. Formation of these gaps was due to Zircaloy growth combined with densification of the relatively low density unstable fuel. Causes for collapse of cladding over in-stack axial gaps were recognized early in the LWBR program. To minimize the concern, LWBR used high density stable fuel pellets (as is the case in commercial reactors today) to minimize fuel stack shrinkage. However, unlike commercial reactors where fuel rods are pressurized during fabrication, LWBR rods were backfilled with helium at 1-atmosphere pressure during welding. This, coupled with use of thin cladding in blanket fuel rods to improve breeding, resulted in rods with high hoop stress (approximately 21,000 psi) under external coolant pressure. For these hoop stresses, proximity to collapse of blanket cladding over in-stack and plenum gaps was a design concern. Both analyses and tests were performed to confirm adequacy of the fuel rod design.

2.3.7 - Movable Fuel

Reactivity control in LWBR was obtained by axial motion of the movable seed modules. Reactivity in commercial cores is controlled with hafnium control rods. Each of the 12 seed modules was designed to move independently even though banked module control was used during operation. A buffer system prevented high contact velocities during scrams. The movable fuel assembly scram speed was 6 to 9 ips, which is slower than conventional commercial control systems by approximately a factor of 10. Slower scram speed during

loss-of-flow accidents was compensated for by flywheel generators maintaining flow at a high level to assure adequate thermal protection of fuel rods.

Scram of LWBR subjected seed fuel rods and pellets to shock loads not normally experienced by rods in commercial reactors.

2.3.8 - Fuel Zones

As shown in Figure 6, LWBR had many radial and axial fuel zones to enhance the worth of the movable seeds. The outer four rows of seed rods, called wedge rods, had a partial height of low zone binary fuel with the remainder of each rod composed of thoria. Similarly, for the blanket and power flattening blanket, the inner four rows had a partial height of low and medium zone binary fuel, with the remainder of the rod composed of thoria. Thoria pellets in the wedge rod region of the seed were loaded preferentially at the top of the outer rod rows to form a sequence of decreasing thoria lengths at increasing rod row distance from the seed-blanket interface. Thoria pellets in the blanket were loaded preferentially at the bottom of the binary rods and were arranged similar to the seed to form a sequence of decreasing thoria lengths as the rod row distance from the seed increased.

Zoning of the fuel in LWBR for control and breeding purposes resulted in local rod power peaking factors that were higher than peaking factors for commercial cores.

2.3.9 - Fixed Fuel Rods

As indicated previously, fuel rods in LWBR were firmly attached to either the top or bottom baseplate in each of the fuel modules. In most commercial cores, rods are not fixed and are free to move axially in support grids. Rods were positively attached in LWBR to maintain fuel zone alignment, to minimize grid loads, and to provide space at the top and bottom of the module for coolant flow.

The maximum difference between top and bottom mounted fuel rods in any of the LWBR modules was seven rods. This small difference limited rod growth and thermal expansion loads on module grids.

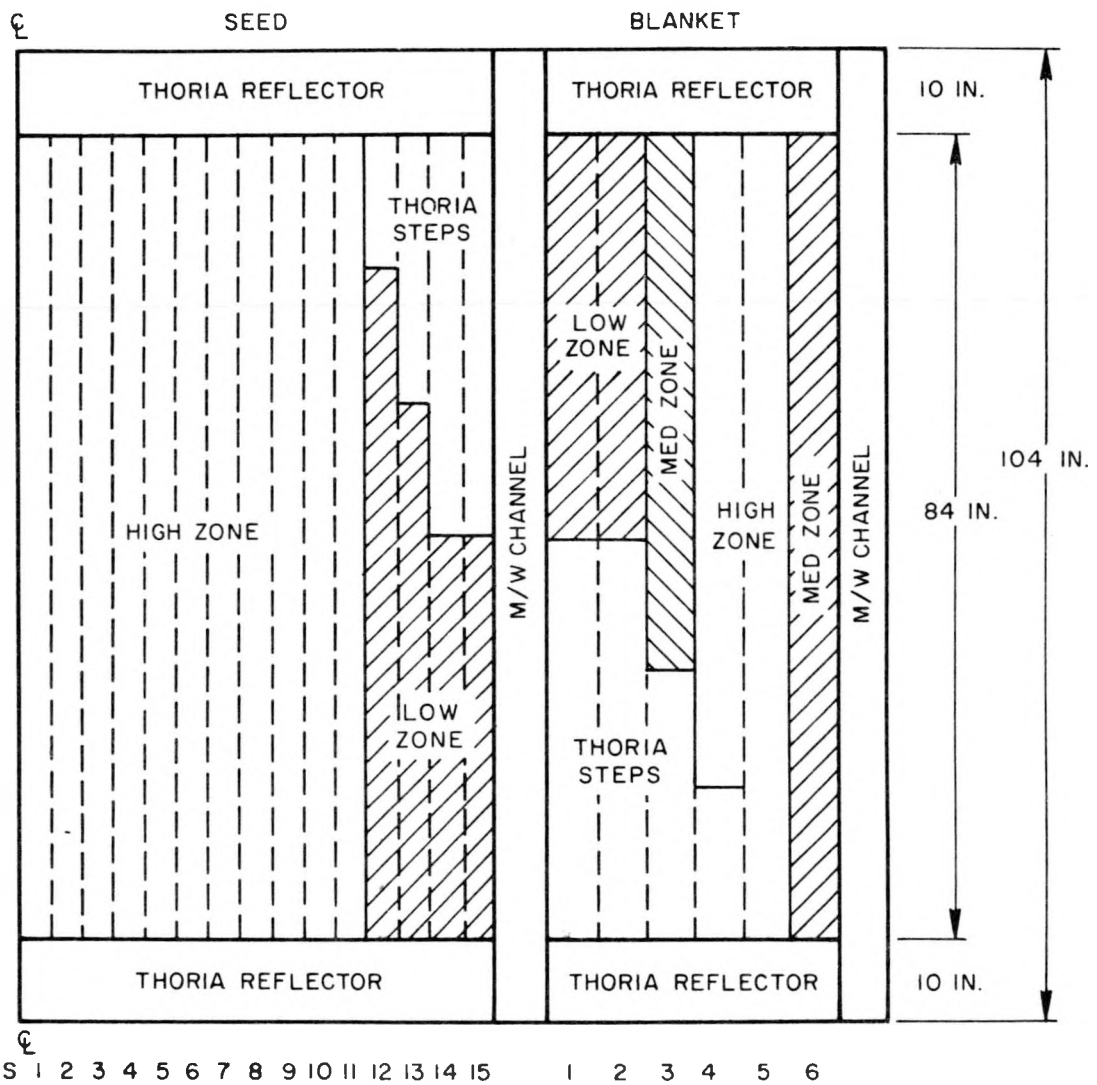

Figure 6 - LWBR Fuel Zones

Bolting fuel rods to top and bottom baseplates resulted in additional demands on the support system. Nonparallelism of the fuel rod and baseplate surfaces and misalignment of the support grid cells with the baseplate resulted in additional bowing of a fuel rod when it was fastened to the baseplate during assembly and during operation of the LWBR core.

2.3.10 - Close Packed Fuel Array

Except for the power flattening blanket region, rod-to-rod spacing was approximately 0.060 inch for LWBR compared with approximately 0.120 inch in commercial cores. (Rod-to-rod spacing was 0.103 inch in the power flattening region.) This tight lattice required more stringent grid and module assembly restrictions than commercial practice to avoid rod-to-grid and rod-to-rod contact. The tight lattice also required tighter limits on potential for flow constriction due to possible fuel rod swelling during a loss of coolant accident (LOCA). Commercial reactors are designed for peak clad temperature during LOCA of 2200F, whereas in LWBR cladding temperatures during a LOCA were restricted to 1800F at beginning of core life and 1500F later in core life.

2.4 - LWBR OPERATION

Originally designed for 18,000 effective full power hours (EFPH) of operation, LWBR was operated for 29,047 EFPH. During most of core life, LWBR was operated as a base load station. During the first three years of operation (18,500 EFPH), the core was subjected to 204 planned swingload cycles to demonstrate fuel element and plant capability to follow load demand for a typical utility power system. A swingload cycle was defined as a power reduction from about 90 percent to operation in the range of 35 to 60 percent power for periods of four to eight hours and then a return to above 90 percent power.

For the initial 18,000 EFPH of operation, maximum allowable reactor power was 72 Mw electric and average coolant temperature was 531F. Reactor coolant pressure was initially 2000 psia and was decreased to 1940 psia at 4325 EFPH, 1870 psia at 7132 EFPH, and to 1815 psia at 10,932 EFPH to minimize potential for cladding collapse, and to reduce cladding temperature in a rod-to-rod contact condition.

After 18,507 EFPH, maximum allowable reactor power was reduced to about 58 Mw gross electric, system pressure was reduced to 1615 psia, and average coolant temperature was reduced to 521F. Again, system pressure was reduced because of cladding collapse and cladding temperature concerns. Reactor power and average coolant temperature were reduced to provide additional margin to CHF and fuel element stress limits at the reduced system pressure.

At 27,419 EFPH, maximum allowable power was reduced to 54 Mw electric. From 27,419 EFPH to 29,047 EFPH, power was reduced from 54 Mw to 43 Mw in 12 steps. These power reductions were required because of the decrease in reactivity of the depleting core.

During the 29,047 EFPH operation of LWBR, the fuel rods were subjected to 60 reactor startups (a power change from below 1 percent power to above 20 percent power), 58 reactor scrams (number of unlatchings of the movable seed modules from any power level, including from zero power after a normal shutdown), 204 planned swingload cycles, and 68 other power cycles in excess of 20 percent.

Detailed information regarding LWBR operation is presented in Reference 18.

2.5 - SELECTION OF FUEL RODS FOR NONDESTRUCTIVE EXAMINATIONS

2.5.1 - Rod Pull Force Measurements

Pull force was measured for all (1072) rods removed from LWBR spent fuel modules. This included 524 rods removed for proof-of-breeding measurements, 12 rods removed for nondestructive examinations in the REX and destructive examinations at Argonne National Laboratory (ANL), and 7 rods removed for only nondestructive examinations in the REX. The remaining 529 rods were removed for fuel rod in-bundle bow and gap measurements and to provide access for seed grid removal.

2.5.2 In-Bundle Bow and Gap Measurements

Fuel rod in-bundle bows and rod-to-rod gaps were measured for one seed module, one reflector module, and five blanket modules. The number of modules was based on obtaining a statistically significant population of data to assess rod thermal performance for gap closure between rods and by the fact that seed and reflector modules had an outer shell that had to be removed to view the rods. The modules examined and their locations in the core are identified in Figure 7.

For the seed module, in-bundle bow and gaps were measured for all peripheral rods and for selected internal fuel rods. Average fluence levels for the selected seed module (SII-3) were approximately 85 percent of the fluence for Type I seed modules. Peak rod fluence in this module was 84 percent of that for the peak fluence seed rod. For the selected reflector module (RIV-4), fuel rod in-bundle bow and gaps were measured for one-half of the peripheral fuel rods and for selected internal fuel rods. This was one of the six most highly exposed reflector modules.

Because blanket modules did not have external shells, in-bundle bow and gaps were measured for a large number of blanket fuel rods, and therefore measured bows of the selected modules should be representative of bow for all blanket fuel rods in LWBR. Except for blanket module III-2, fuel rod in-bundle bow and gap measurements were limited to peripheral fuel rods. In-bundle bows and gaps were measured for peripheral and selected internal fuel rods in blanket module III-2.

2.5.3 - Rod Examination Gage Examinations

Nineteen (six seed, seven standard blanket, three power flattening blanket, and three reflector) fuel rods were examined with the rod examination gage (REX). The REX (Figure 8) was specifically designed for automated inspection of LWBR fuel rods at ECF. The gage had the capability of length measurement of fuel rods, 5X visual examination and video recording of the fuel rods, fuel rod diameter measurement, fuel rod oxide thickness measurement, fuel rod ovality measurements, and fuel rod wear mark depth and volume measurements. The gage also had the capability of ultrasonic screening of the

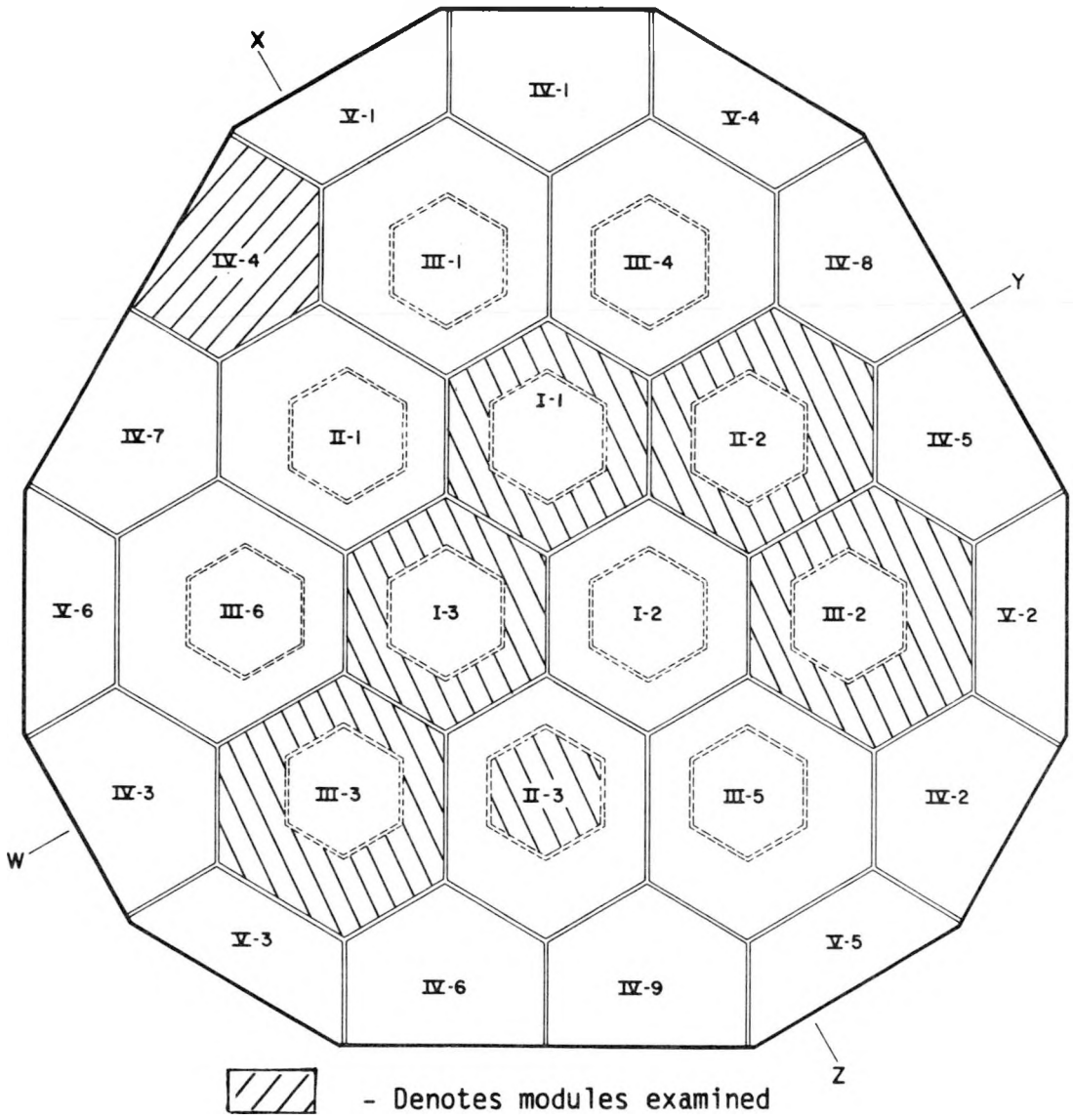

Figure 7 - Fuel Rod In-Bundle Bow and Gap Examination Modules

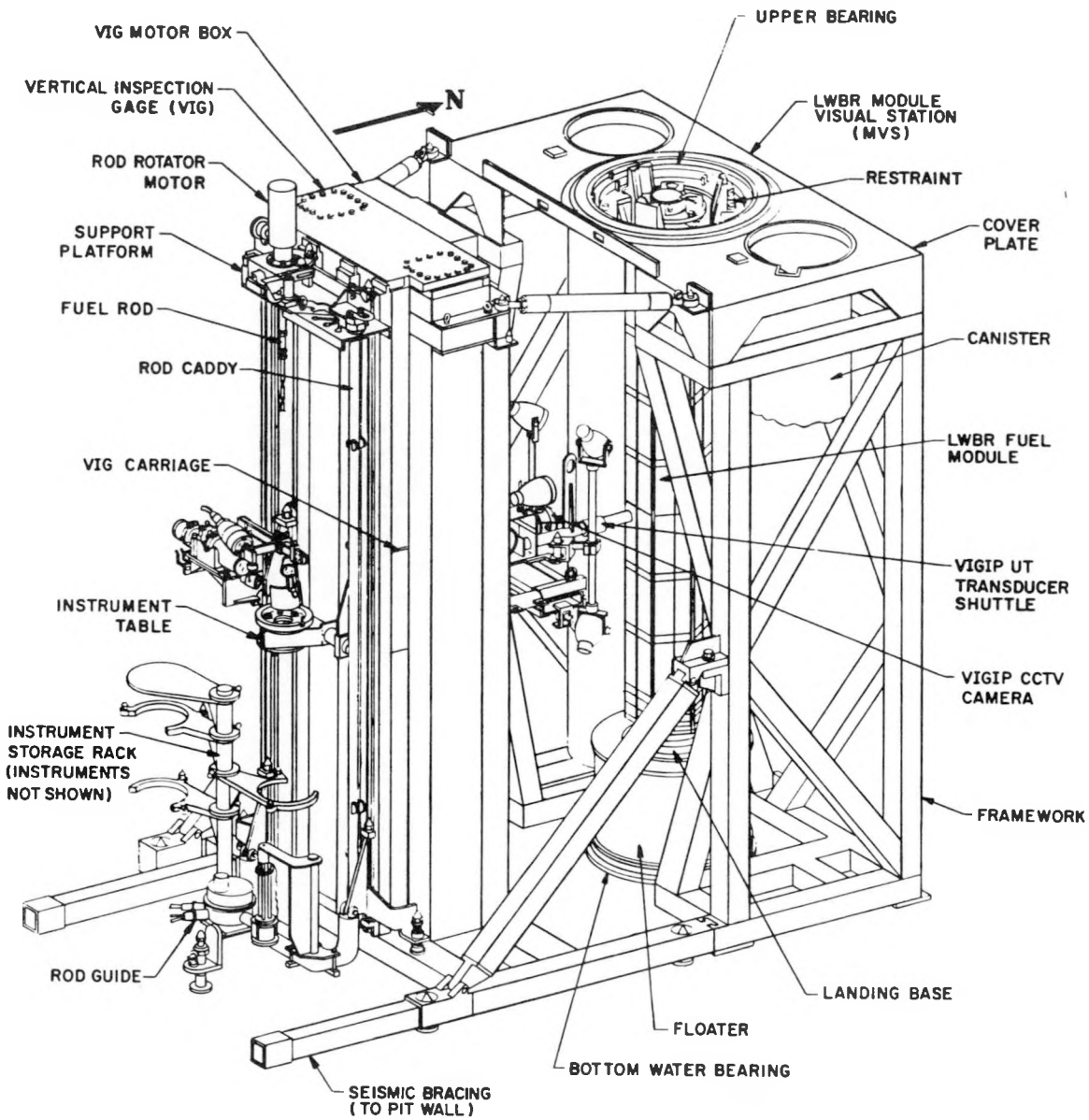

Figure 8 - Module Visual Station (MVS) and
Rod Examination Gage (REX)

fuel rod cladding for defects (e.g., internal and external cracks). Except for the extreme ends of the fuel rods, measurements could be obtained at any angular orientation and at any axial plane. Details regarding the REX design are presented in Reference 1.

The fuel rods selected for examination in the REX are listed in Table 6. Approximate location of the rods in LWBR are shown in Figure 9. Exact position of a fuel rod in the module can be determined with the module fuel rod cell maps presented in Appendix A1. Twelve of the fuel rods examined nondestructively in the REX were also destructively examined. Results from the destructive examinations are presented in Reference 5.

The rods were chosen to evaluate the effects of a broad range of parameters on fuel rod performance. The major parameters investigated were (1) rod type, (2) binary fuel stack length, (3) initial U-233 content, (4) fuel rod mounting (top or bottom), (5) power, (6) fluence, (7) depletion, and (8) gradient (thermal and fast neutron flux). Some of the rods selected had manufacturing deviations (DSR) which restricted location of the rod in the core. Other rods selected had unusual support conditions (e.g., proximity to blanket grid internal tabs or module support posts) or special locations in the module (e.g., boundary fuel rod). Binary stack length, fissile loading, peak fluence, depletion, power, and burnup, and special characteristics for the fuel rods selected are presented in Table 6. As-built data for the selected fuel rods is presented in Appendix A2. Specific examinations performed for each of the REX rods are identified in Table 7. Table 7 also identifies the rods examined in the PIFAG (gamma scan) and examined by ANL (neutron radiography and crud).

2.5.4 - Crud Examinations

Three fuel rods (seed rod 0504502, standard blanket rod 1605629, and reflector fuel rod 3220018) were examined for crud. Crud examinations were performed at Argonne National Laboratory-West. Seed rod 0504502 and blanket rod 1605629 were examined in the REX after chemical decrudding. EOL rod average depletion of the selected seed fuel rod was the peak for seed fuel rods. EOL rod average depletion of the selected blanket fuel rod was 99.7 percent of the

Table 6 - REX Examination Rods

REX Sequence	Rod S/N	Type Mounting	Cell No.	Module	Binary Fuel Length	Fissile Loading (w/o) U	Peak Fluence 10^{20} n/cm-c	Peak Depletion 10^{20} f/cc	Peak Power kw/ft	Peak Burnup MWD/MTM	DE/NDE	Special Characteristics
1	0400736	Top	4M33	SI-1	70.0	4.327	85.0	9.5	6.7	44,500	DE	Diagonal
2	0606773	Top	6B4	SI-1	84.0	5.195	96.5	8.8	4.4	41,200	DE	Peak fluence, no gradient
3	0205071	Top	2Q41	SI-1	42.0	4.327	75.5	11.4	5.5	53,400	DE	Peak depletion, flow hole
4	0507672	Bottom	5L31	SI-1	84.0	5.195	87.9	10.1	4.2	47,300	DE	Hot channel, Max avg depletion
5	1606710	Top	16E57	BI-3	84.0	2.000	73.0	5.1	8.7	22,300	DE	Peak power & fluence, diagonal
6	3102657	Bottom	1A1	RIV-3	--	--	25.9	0.9	3.4	4,100	DE	Apex, wide spring
7	1208823	Top	12A12	BII-2	42.0	1.211	55.4	4.3	6.9	18,700	DE	Intermediate power & fluence, Boundary cell
8	2610746	Top	26E68	BII-2	84.0	2.005	57.7	5.7	8.7	25,200	DE	PFB high power & fluence
9	1105717	Bottom	11A46	BI-3	42.0	1.211	71.4	5.2	8.6	22,800	DE	High power, Tab (sharp edges)
10	1504272	Bottom	15F11	BI-3	84.0	1.622	64.2	4.4	7.4	19,200	DE	DSR on fuel taper, suspected rods touching
11	2514164	Bottom	25K13	BII-2	84.0	2.005	38.6	5.1	8.3	22,300	DE	PFB high power, low fluence
12	2607600	Top	26E19	BII-2	84.0	2.005	58.6	5.5	8.4	24,400	DE	Boundary location between Std Bkt and PFB regions
13	1605629	Top	16E58	BI-3	84.0	2.000	74.1	5.2	8.9	22,800	NDE	Chemically decrudded at ANL-W
14	0504502	Bottom	5L32	SI-1	84.0	5.195	87.9	10.1	4.2	43,300	NDE	Chemically decrudded at ANL-W
15	3107082	Bottom	1A1	RIV-4	--	--	27.8	1.0	3.6	4,500	NDE	Apex, wide spring, peak power, panel clearance
16	3206304	Top	2D10	RIV-4	--	--	7.8	0.2	0.9	900	NDE	Low power location, top mounted reflector
17	1601036	Top	16E71	BI-3	84.0	2.000	70.9	5.0	8.5	22,000	NDE	High power, post dimple
18	1612146	Top	16E20	BII-2	84.0	2.000	59.0	4.3	7.1	19,000	NDE	Boundary location, post dimple
19	0604555	Top	6B3	SI-1	84.0	5.195	96.5	8.8	4.4	41,200	NDE	Adjacent to seed rod 0606773 with ovalling

Nomenclature

DE - Destructive and non-destructive examination rod.
NDE - Non-destructive examination rod.
Diagonal - Rod located at intersection of two segments of hexagonal module.
Apex - Rod at apex of Type IV reflector module.
Wide Spring - Rod located in grid cell with high force spring.
Flow Hole - Rod located next to flow hole in seed shell.
Panel Clearance - Rod located in grid cell with small clearances.
Tab - Rod located near grid sheet-metal connector with potential sharp edges.
Post Dimple - Rod in grid cell with solid (non-sheet-metal) support dimple.
PFB - Power flattening blanket
Std Bkt - Standard blanket

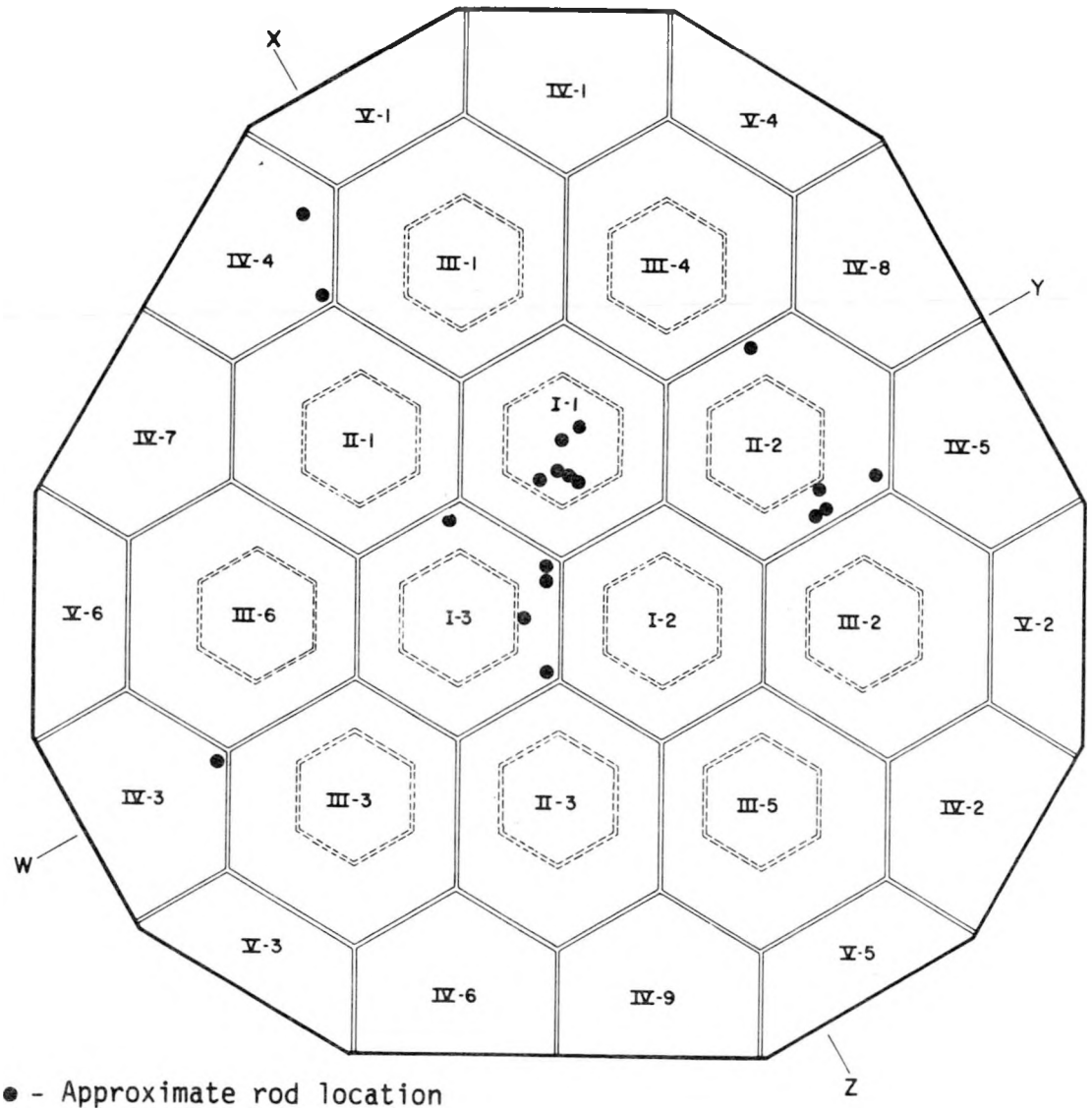

Figure 9 - REX Examination Fuel Rod Locations

Table 7 - Summary of Individual Fuel Rod Examinations

Rod No.	Rod Serial No.	Cell No.	Module	REX Exams								Neutron Radiography	Gamma Scan	Crud
				Length	Visual	Bow	UT	Diameter	Oxide	Ovality	Wear Mark			
1	0400736	4M33	SI-1	X	X	X	X	X	X	X	X	X		
2	0606773	6B4	SI-1	X	X	X	X	X	X	X	X	X		
3	0205071	2Q41	SI-1	X	X	X	X	X	X	X	X	X		
4	0507672	5L31	SI-1	X	X	X	X	X	X	X	X	X		
5	1606710	16E57	BI-3	X	X	X	X	X	X	X	X	X		
6	3102657	1A1	RIV-3	X	X	X	X	X	X		X	X		
7	1208823	12A12	BII-2	X	X	X	X	X	X	X	X	X		
8	2610746	26E68	BII-2	X	X	X	X	X	X	X	X	X		
9	1105717	11A46	BI-3	X	X	X	X	X	X	X	X	X		
10	1504272	15F11	BI-3	X	X	X	X	X	X	X	X	X		
11	2514164	25K13	BII-2	X	X	X	X	X	X	X	X	X		
12	2607600	26E19	BII-2	X	X	X	X	X	X	X	X	X	X	
13	1605629	16E58	BI-3	X	X			X	X	X	X			X
14	0504502	5L32	SI-1	X	X			X	X		X			X
15	0604555	6B3	SI-1	X	X			X					X	
16	3107082	1A1	RIV-4	X	X	X		X	X		X		X	
17	3206304	2D10	RIV-4	X	X	X		X	X		X		X	
18	1601036	16E71	BI-3	X	X			X		X	X		X	
19	1612146	16E20	BII-2	X	X			X		X	X		X	
20	0800227	8Q49	SIII-1										X	
21	3220018	2K4	RIV-9											X
22	1402762	14C48	BI-3										X	
23	1203626	12B27	BIII-2										X	
24	2620628	26G1	BIII-2										X	
25	2621223	26J15	BII-2										X	
26	3116856	1D9	RIV-4										X	
27	1503329	15F56	BI-3										X	
28	1104478	11A27	BI-3										X	
29	0602209	6K27	SI-1										X	
30	0618561	6B1	SIII-2										X	
31	2104416	21A6	BII-2										X	
32	1600616	16E43	BII-2										X	
33	1105055	11A36	BII-2										X	
34	0800117	8Q37	SIII-1										X	
35	0607258	6K14	SIII-1										X	
36	0205154	2Q32	SI-1										X	
37	0301340	3N38	SI-1										X	
38	0702069	7P46	SI-1										X	

average depletion for the peak blanket fuel rod. EOL rod average depletion of the selected reflector fuel rod was 17 percent of the average depletion for the peak reflector fuel rod.

2.5.5 - Neutron Radiography

Neutron radiography was performed on the 12 rods (four seed, four standard blanket, three power flattening blanket, and one reflector) that were destructively examined. Neutron radiography was performed by Argonne National Laboratory West. Specific rods examined are identified in Table 7.

Seed rods 0507672 and 0606773 had 84-inch high zone binary fuel stacks. Seed rod 0400736 had a 70-inch binary fuel stack with low zone fuel. Seed rod 0205071 had a 42-inch binary fuel stack with low zone fuel. Peak depletions of the seed rods examined ranged from 77 to 100 percent of the peak seed fuel rod depletion.

Standard blanket rods 1105717 and 1208823 had 42-inch low zone binary fuel stacks. Standard blanket rod 1606710 had an 84-inch high zone binary fuel stack. Standard blanket rod 1504272 had an 84-inch medium zone binary fuel stack. Peak depletions of the rods examined ranged from 81 to 99 percent of the peak standard blanket fuel rod depletion.

All three power flattening blanket fuel rods (2514164, 2607600, and 2610746) examined had 84-inch high zone binary fuel stacks. Peak depletions ranged from 89 to 100 percent of the peak power flattening blanket fuel rod depletion.

Reflector fuel rod 3102657 had a peak depletion 91 percent of the peak reflector fuel rod depletion.

2.5.6 - Gamma Scan Measurements

Twenty-four fuel rods (nine seed, eight standard blanket, four power flattening blanket, and three reflector) were gamma scanned using the PIFAG (References 2 and 3) to screen for in-stack axial gaps and to determine binary fuel stack length. Nine of the rods selected for gamma scan were also examined with the REX. One of the rods was destructively examined. The rods

were selected to encompass each of the rod types and rod loadings, and to provide a wide range of depletions. Specific rods examined are identified in Table 7.

For the seed rods examined, the rod average depletion ranged from 42 to 94 percent of the average depletion for the peak seed fuel rod. For the standard blanket fuel rods examined, the rod average depletion ranged from 45 to 100 percent of the average depletion for the peak blanket fuel rod. For the power flattening blanket rods examined, the rod average depletion for the ranged from 44 to 97 percent of the average depletion for the peak power flattening blanket fuel rod. For the reflector fuel rods examined, the rod average depletion ranged from 17 to 100 percent of the average depletion for the peak reflector fuel rod.

SECTION 3 - DESCRIPTION OF NONDESTRUCTIVE EXAMINATIONS

3.1 - ROD PULL FORCE MEASUREMENTS

Rod pull forces during removal of rods from depleted LWBR fuel modules were measured to guard against overstressing a rod during disassembly operations. Data from the operation provided a qualitative measure of the residual spring forces in the support grids. High pull force gives an indication of binding of the rod in the support system.

Pull forces were measured automatically by the Rod Removal System (RRS). The RRS (Figure 10) was a computerized system design to remove and transfer LWBR fuel rods in the Naval Reactors Expended Core Facility (ECF). The RRS had a grapple attached to a winch for grasping and pulling fuel rods out of LWBR modules. Details regarding design of the RRS are presented in Reference 19. Pull forces were determined with two load cells in the RRS grapple. Measured forces were recorded using a Digital Equipment Corporation (DEC) MINC-23 computer.

Fuel rods were removed by grappling the rods at winch positions in the range of 5 to 10 inches and withdrawing the rod 0.75 inch at 1 inch/minute. The rod was then rotated 60 degrees to minimize chances of the grid springs and dimples snagging a wear spot as the rod was removed. Rod pull was then continued at 1 inch/minute to a winch position of 14.0 inches. Pull rate was then increased to 12 inch/minute to a winch position of 120.0 inches. Beyond 120 inches, the pull rate was decreased to 1 inch/minute and the RRS was operated in a manual mode. Pull force data were not collected when the RRS was operated in manual mode.

Pull force data were collected at 0.080 to 0.12-inch increments for winch positions up to 14.0 inches and at 0.27 to 0.59-inch increments for winch positions from 14.0 to 120.0 inches. Recorded forces were adjusted for pressure effects on the load cells in the grapple and included rod weight (2 pounds for seed rods, 8 pounds for standard blanket rods, 7 pounds for power flattening blanket rods, and 16 pounds for reflector fuel rods) and grapple drag force (approximately 3 pounds).

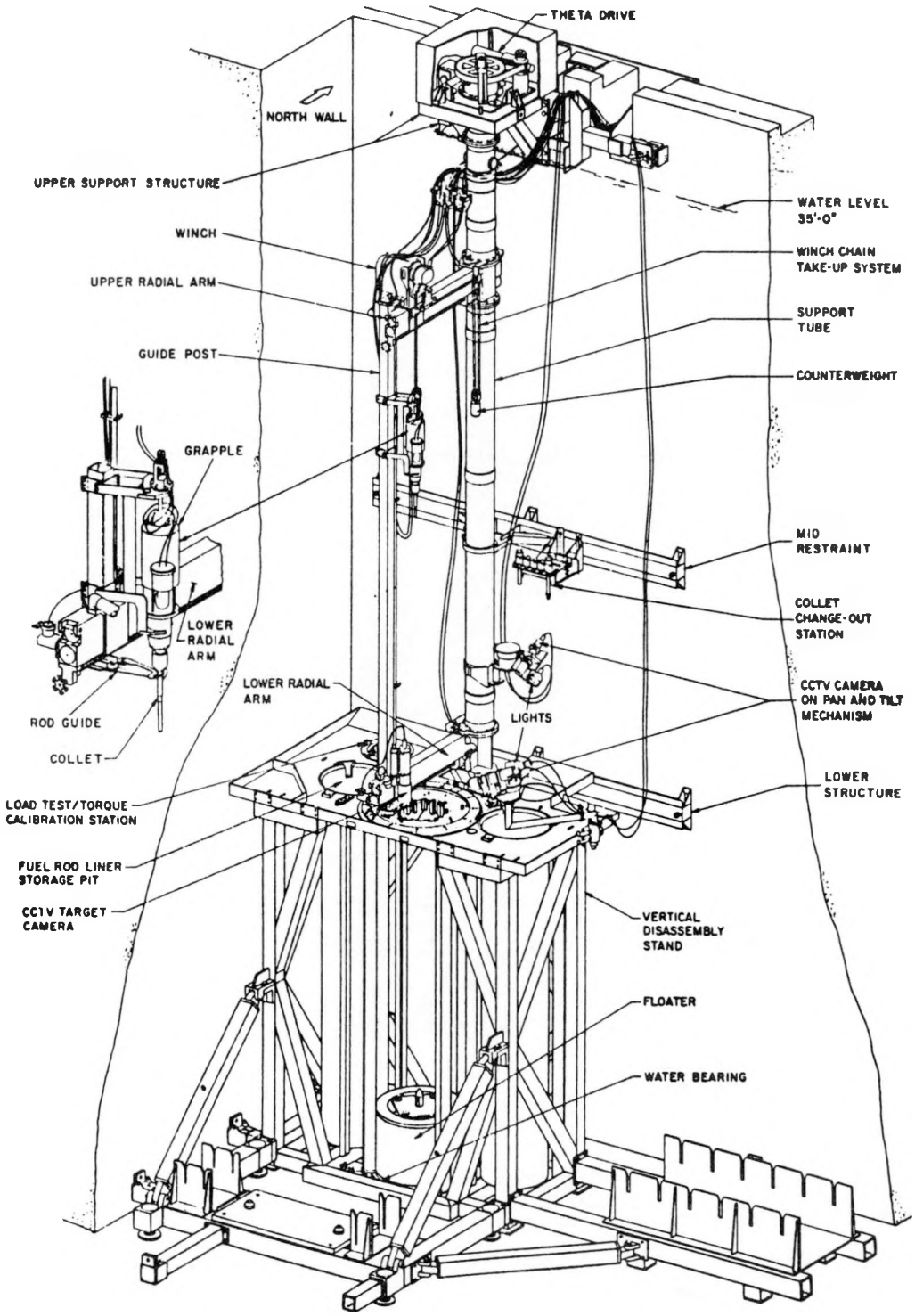

Figure 10 - Rod Removal System

3.2 - IN-BUNDLE BOW AND GAP MEASUREMENTS

For core certification safety analysis, the Nuclear Regulatory Commission (NRC) requires that sufficient data be available to provide a standard deviation of percent gap closure which will not be exceeded with a 95 percent probability. This limiting standard deviation is then used to assess degradation in critical heat flux as a function of gap closure. Standard deviations for the "worst" spans (i.e., the highest standard deviation for all spans) are used.

In order to evaluate LWBR fuel rod performance, EOL rod-to-rod spacing measurements were performed to provide a sufficiently large data base to develop statistical limits on channel closure for each of the fuel rod types similar to those required by the NRC for core certification. Fuel rod in-bundle bow measurements were also performed to develop statistics on rod bow and to provide a data base to evaluate the effects of fuel rod mounting, fuel rod type, and power gradient on fuel rod bow.

Fuel rod in-bundle bow and gaps for LWBR were determined by digitizing video recordings of the fuel rods in LWBR modules. Video recordings were made using the vertical inspection gage inspection package (VIGIP) in the module visual station (MVS) (Reference 1) and similar inspection equipment in the vertical disassembly stand (VDS). The VIGIP (see Figure 8) had an EDO Western high resolution underwater camera mounted on a carriage. The carriage moved axially along a precision granite block on a water bearing. Underwater lights were attached to the carriage above and below the video camera and to the camera for illumination. Lights above and below the camera were offset horizontally. The video image was recorded on 3/4-inch video tape for processing at Bettis Atomic Power Laboratory. A character generator displayed horizontal and axial positions of the camera on the video image. A computer monitored axial position of the camera and notified the character generator to display a "trigger" on the video tape at prescribed elevations. The "trigger" was used to automate analysis of the video tapes.

A TRAPIX 5500 Series Real Time Image Processor with Recognition Concepts, Real Time Image Processor Software (RTIPS), Bettis generated software, and MINC-23 computer were used to digitize the video tapes to determine fuel rod in-bundle bows and rod-to-rod gaps. Rod bow and gaps were determined by dividing the video image into a 515 x 512 block array. Each block (pixel) of the array was digitized by assigning a light intensity value ranging from 0 (black) to 255 (white). The variation in light intensity across the module at prescribed axial planes was then used to detect rod edges.

A double criteria were used in establishing rod edge position:

(1) Sudden change in the first derivative of light intensity in the horizontal direction;

(2) A near constant distribution of light intensity (pixel values) in the vertical direction.

The double criterion distinguished rod edges from mottling of fuel rods. Regions with a near constant vertical distribution and a large change in intensity in the horizontal direction were potential rod edges. Locations of edges were further ensured by limiting the search to preselected gap regions which were updated continuously during the processing.

Figure 11 shows a sample pixel distribution across a rod and two adjacent gaps and edges determined with the edge detection software.
Rod edge position was defined by

$$X(i) = X_o(i) + A\,[(CF)\,P(i) - P_c] \qquad (1)$$

where: $X_o(i)$ = Lateral position (inch) of camera centerline,
$P(i)$ = Edge Pixel location (0 to 511),
A = Amplification factor,
P_c = Pixel position for camera centerline (255),
i = axial elevation index, and

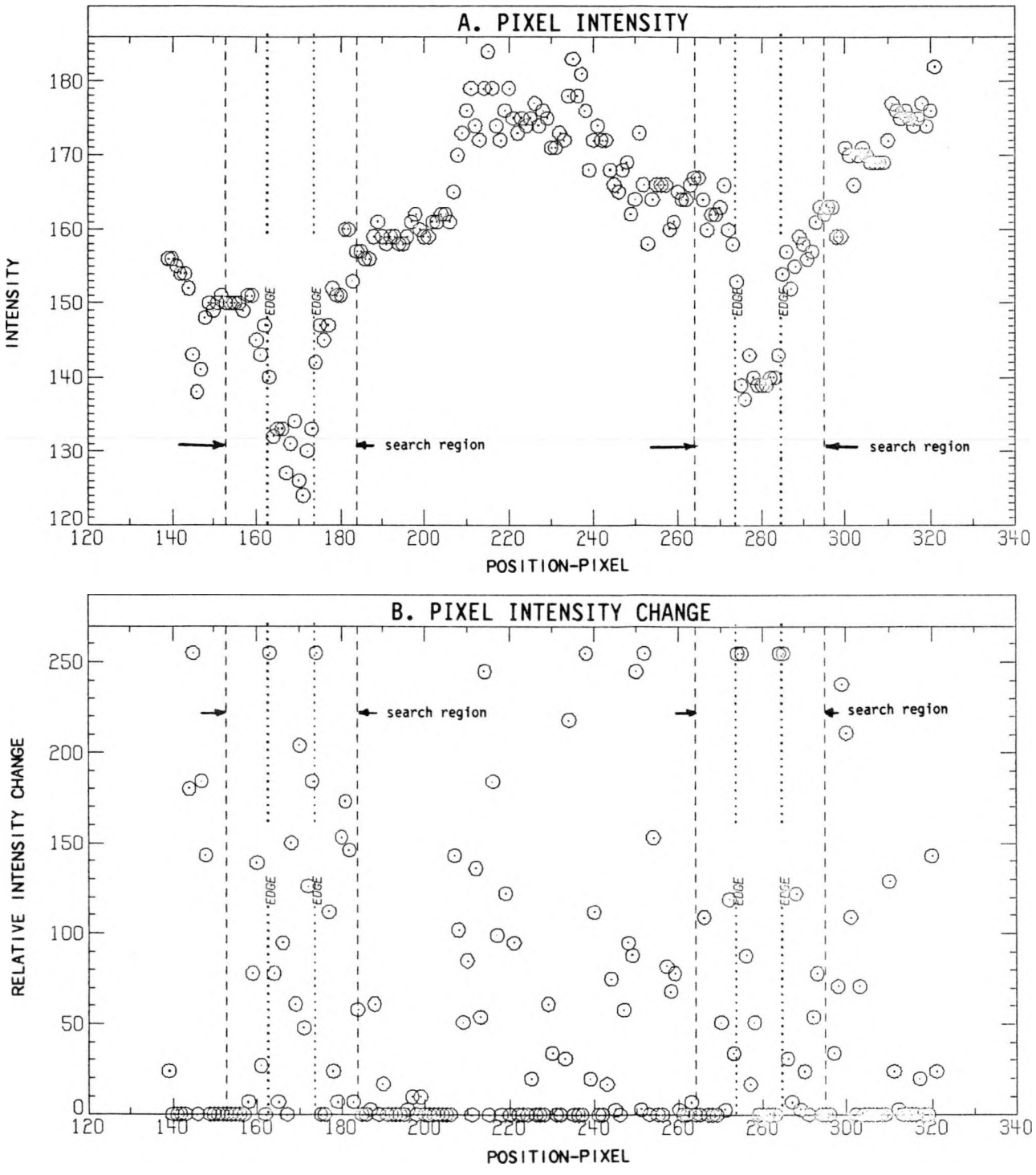

Figure 11 - Pixel Intensity Across a Fuel Rod and Two Gaps

CF is a correction factor which eliminated distortion in the data. The correction factor was given by

$$CF = -231 \times 10^{-7} (X - 175.347)^2 + 1.0 \qquad (2)$$

where X is the fuel rod edge position in pixels. The amplification factor, A, was given by

$$A = D_i / D_p \qquad (3)$$

where: D_i = nominal rod diameter (inches), and

D_p = average measured rod diameter (pixel) for each scan.

Rod edges were determined at approximately 60 positions along the length of each fuel rod. Processing of the video tape was done automatically. Display of the video "trigger" on the tape was used to initiate digitizing. The edge positions were written on a floppy disk for subsequent evaluation of in-bundle bow and gaps on a mainframe computer.

Gaps between adjacent rods were determined from the relationship

$$Gap = [X2L - X1R] A \qquad (4)$$

where X2L and X1R are adjacent rod edges and A was the amplification factor. Local fuel rod centers, as defined by the midpoint between the left and right edges of the fuel rod at each of the prescribed axial planes, were used to calculate fuel rod bow. As shown in Figure 12, measured rod bow could be divided into two components: (1) fuel rod bow due to module bow and (2) local fuel rod bow between grids.

Rod bow due to module bow is defined as the offset of the rod relative to a line through the ends of the rod. Rod bow due to module bow had little effect on rod-to-rod spacing.

For EOL examinations of LWBR fuel modules, local fuel rod bow was defined as the offset of the rod relative to a straight line through the fuel rod seating location in adjacent grids. Local fuel rod bow is similar to the bow calculated for LWBR design analysis using the ROBOT computer program, (Reference 20). Local rod bow can have a significant effect on rod spacing.

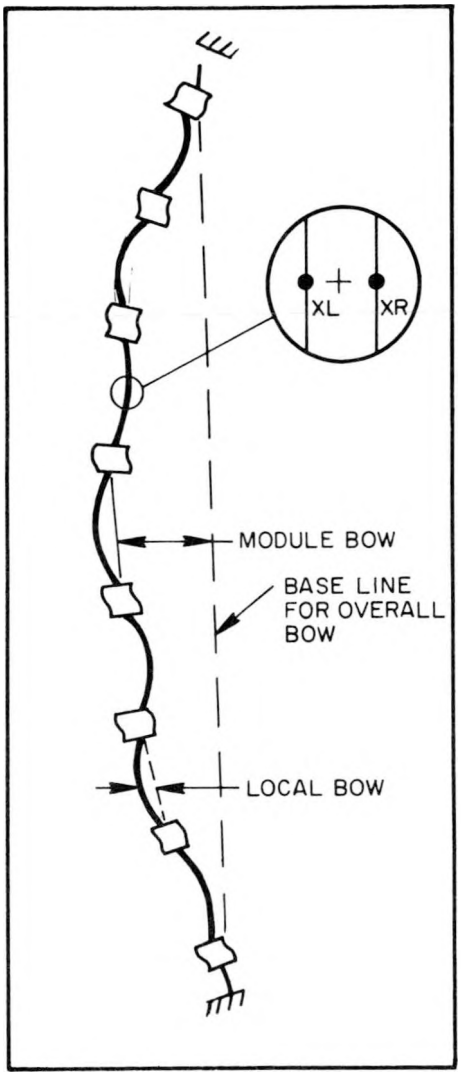

A. BOW MODEL

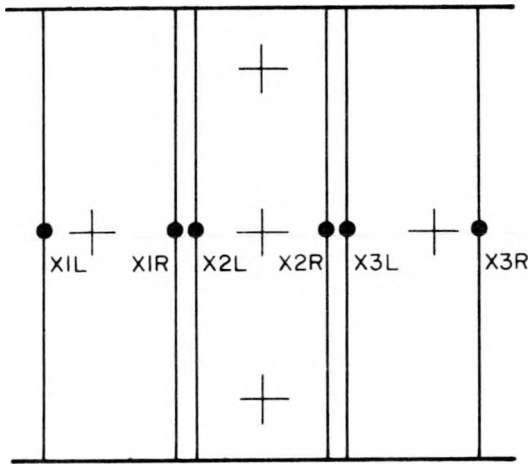

B. ROD TO ROD GAPS

Figure 12 - Definition of Fuel Rod In-Bundle Bow and Gaps

The seating surface at each grid was defined as the average of the local fuel rod centers for the inspection points immediately above and below the grid. Two criteria were used to determine the maximum local bow between two grids. First, the seating points at the grids adjacent to the span must be well defined; that is, points immediately above and below the grid could not differ by more than 0.015 inch. Secondly, the centerline for the maximum bow location could not differ by more than 0.010 inch on the average from its two adjacent points.

It should be noted that fuel rod bows calculated from the video tapes indicated the rod bow perpendicular to the "line of sight" for the video camera and therefore represented a lower bound on the actual fuel rod bow. Similarly, rod-to-rod gaps measured from the video tapes indicated the projected clearance along the "line of sight" for the camera and therefore provided a lower bound on actual fuel rod gaps. A true measure of the gaps is obtained when the line between the fuel rod centers for two adjacent rods is perpendicular to the line of sight for the camera. An underestimate of gap size is obtained when it is not perpendicular.

3.3 - Rod Length

Length measurement of LWBR fuel rods is important to fuel rod performance assessment and evaluation of the CYGRO computer analysis program (Reference 21). The incremental increase in rod length was limited in design evaluations to the clearance between the rods and baseplates less an allowance equivalent to one rod diameter to permit free coolant flow through baseplate flow holes. Other performance considerations affected by rod length increase included rod bow and cladding collapse. Assessment of length prediction accuracy is important to future rod design and is useful for evaluation of Zircaloy growth models.

EOL rod length of 19 LWBR fuel rods were measured with the rod examination gage (REX) to determine cladding elongation. Cross hairs on the REX rod visual camera were used to sight on the ends of a fuel rod, and the vertical inspection gage (VIG) axial encoder readout was used to determine the fuel rod end positions. Axial positions of the fixed end of the fuel rod were measured at 90- and

270-degree angular positions relative to the fuel rod serial number. Axial position for the free end of the rod was measured at 0-degree orientation only. EOL rod length was the difference between the average position at the fixed end and the axial position at the free end. To correct for temperature effects, a similar set of measurements was made on a standard bar of known length. The measured fuel rod length was adjusted to account for thermal expansion due to the difference between waterpit temperature (normally 53F) and the 70F reference temperature at which pre-irradiation length measurements were made.

3.4 - VISUAL INSPECTIONS

Detailed visual inspections for unusual conditions (e.g., cladding cracking, cladding collapse) were performed for 19 fuel rods using the high resolution EDO Western underwater camera on the REX. Each rod was viewed at 5X magnification along its entire length at 0, 90, 180, and 270-degree orientations. Scan rate for the inspection was 5 inches/minute. Video recordings of each fuel rod were reviewed by engineering personnel.

Less detailed visual inspections for unusual conditions were also performed for all rods removed using a camera on the vertical disassembly stand during rod removal with the RRS. The rods were viewed at only one orientation and 2X magnification.

3.5 - FREE HANGING BOW

EOL free hanging bows were determined for 13 fuel rods for comparison with similar measurements (Reference 22) obtained during rod fabrication and for calculation of in-bundle fuel rod bow. EOL free hanging bow of the rods was determined by using the REX to obtain 5X video recordings of the rod at 0, 45, 90, and 135-degree orientations. A video digitizer was used to determine fuel rod center positions at approximately 60 axial positions for each of the four orientations.

The fuel rods were suspended in the REX with a collet. A gimbal in the collet permitted the top end of the rod to translate freely along two orthogonal axes. A rod guide at the bottom of the REX prevented swaying of the lower end of the fuel rod during the free hanging bow inspection. A semi-circular white

background was placed behind the fuel rod, and REX lighting was adjusted to obtain a silhouette image of the fuel rod. Video recordings of the rod were obtained at four rod orientations. Axial position of the REX camera was monitored by a computer during scanning, and a character generator displayed a "trigger" on the video image at at prescribed elevations for automation of the analysis.

The video digitizing equipment used to determine fuel rod in-bundle bow and rod-to-rod spacing was also used to process fuel rod free hanging bow tapes. The digitizing equipment was used to determine the local fuel rod center positions at the approximately 60 inspection planes on the rod for each of the four orientations. Fuel rod center positions were then adjusted for offset and inclination of the fuel rod axis of rotation to the line of travel for the REX camera. A best fit radial position and best fit angular position for the local fuel rod center was then determined from a least squares method. Offset of the best fit local radius relative to a line through the top and bottom of the rod was used as the free hanging bow of the fuel rod.

Accuracy of the measurements was determined for each rod by comparing measured fuel rod centerline positions at 45-degree orientation with calculated center positions based on measured center position for 0 and 90-degree orientations and by comparing measured fuel rod centerline position at 90-degree orientation with calculated position based on measurements for 45 and 135-degree orientations.

3.6 - CLADDING DIAMETER AND IN-STACK OVALITY MEASUREMENTS

Cladding diameter and ovality over fuel pellets (in-stack) were measured for 19 fuel rods with the REX axial profilometer. Measured diameters were used for comparisons with predicted EOL diameters calculated with CYGRO and for evaluation of fuel rod ridging, grooving, and ovality. The REX axial profilometer used a pair of V-rollers and a backup roller to position the fuel rod in the gage and a Sony Magnescale probe to measure fuel rod diameter. Fuel rod diameters were measured at 0, 45, 90, and 135-degree orientations. Diameters at each orientation were measured during a continuous scan from the top to the bottom of the rod. For the first twelve rods examined the scanning

rate was approximately 0.67 inch/minute and diameters were measured and recorded at approximately 0.010-inch increments. Axial position for the probe was recorded for every fifth diameter measurement. After the first 12 rods, the scanning speed was doubled and rod diameters were measured at approximately 0.020-inch increments.

Local average diameter and local ovality at each plane were then calculated by (1) using linear interpolation to determine local diameters at common planes for each of the four scans, (2) averaging the four interpolated diameters to determine the local average diameter, and (3) subtracting the minimum interpolated diameter from the maximum interpolated diameter to determine the local ovality.

The axial profilometer was calibrated before each rod examination by measuring three step diameters on a gage bar. Accuracy of the rod measurements was ensured by checking calibration of the axial profilometer after each rod inspection. Deviations from known diameters were limited to 0.0001 inch average and 0.00026 inch maximum for pre-calibration measurements and to 0.00016 inch average and 0.00039 inch maximum for post-calibration measurements.

As shown in Table 8, data from qualification testing of the REX on dummy fuel rods indicates that the 2-sigma accuracy for axial profilometer diameter measurements was ±0.00012 inches. The 2-sigma accuracy for ovality was ±0.0002 inch.

Additional details on the design and operation of the axial profilometer are presented in Reference 1.

3.7 - PLENUM OVALITY

Plenum ovality was measured for 14 (four seed, seven standard blanket, and three power flattening blanket) fuel rods. Plenum ovality of seed rods was measured to confirm stability of the freestanding RXA cladding. Plenum ovality of blanket (standard and power flattening) fuel rods was measured to confirm predictions of cladding deformation for the nonfreestanding SRA

Table 8 - REX Measurement Accuracies

Gage	Attribute	Accuracy*
Axial Profilometer	Diameter (inch)	0.00012**
	Ovality (inch)	0.00020**
Orbiting Profilometer	Wear Depth (inch)	0.00016
Wear Volume (%)	14.2**	
Plenum Ovality (inch)	0.00010**	
EDCOT	Oxide Thickness (inch)	0.00015
----	Free Hanging Bow (inch)	0.0058
----	Rod Length (inch)	0.0082
Ultrasonic	Crack detection (length, inch)	$\geq$ 0.002***

*2σ variation between measured value during gage calibration check and known value.
**Based on results from REX qualification.
***Consistently able to detect cracks of 2 mils or greater on calibration standards.

cladding. Plenum ovality for reflector rods was not measured because little deformation was expected.

Plenum ovalities of LWBR fuel rods were obtained with the REX orbiting profilometer. The orbiting profilometer used a set of rollers to clamp the fuel rod in the center of the gage. A DC motor rotated a platform about the clamped fuel rod on a precision roller bearing, and an absolute encoder recorded the rotational orientation of the platform. A Sony Magnescale probe on the rotating platform, pointed toward the center of the gage, indicated the radial position of the rod surface relative to the center of the gage. Probe tip diameter for the gage was 0.040 inch. Radial position for the rod surface was measured and recorded at 0.5-degree increments.

Plenum ovality for bottom mounted seed and blanket fuel rods was measured at three planes located as shown in Figure 13. Relative position of inspection planes and fuel rod internals (i.e., plenum sleeve and pellets) were comparable for top mounted seed and blanket fuel rods. The ovality at each plane was determined by (1) determining the centroid for the 720 radial positions, and (2) determining the maximum and minimum rod radii relative to the calculated centroid. Planar ovality was then defined as twice the difference of the maximum radius and the minimum radius.

Accuracy of the gage was checked before and after each inspection by measuring three flats (2, 10, and 20 mils deep) on seed or blanket gage bars. Differences between measured flat depth and known flat depth were limited to a 0.00012-inch average difference and a 0.00029-inch difference range for pre-calibration and to a 0.00017-inch average and a 0.00044-inch difference range for post-calibration measurements.

Data from repeat measurement of ovality on a test rod during REX qualification indicated that the 2 sigma accuracy of fuel rod ovality measurements was ±0.0001 inches.

Additional details on the design and operation of the orbiting profilometer are presented in Reference 1.

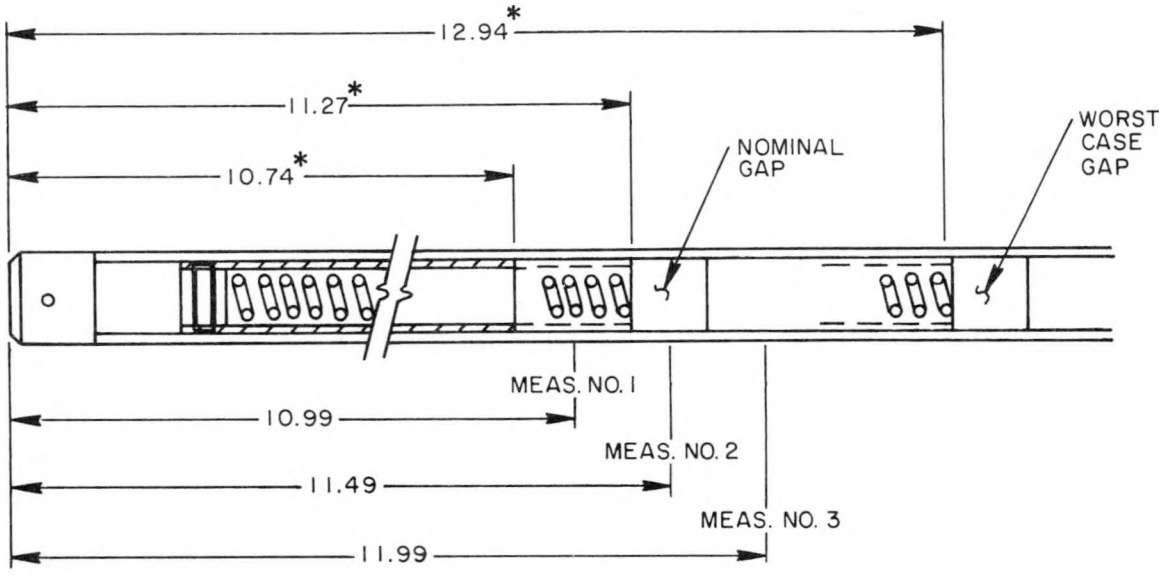

BLANKET RODS

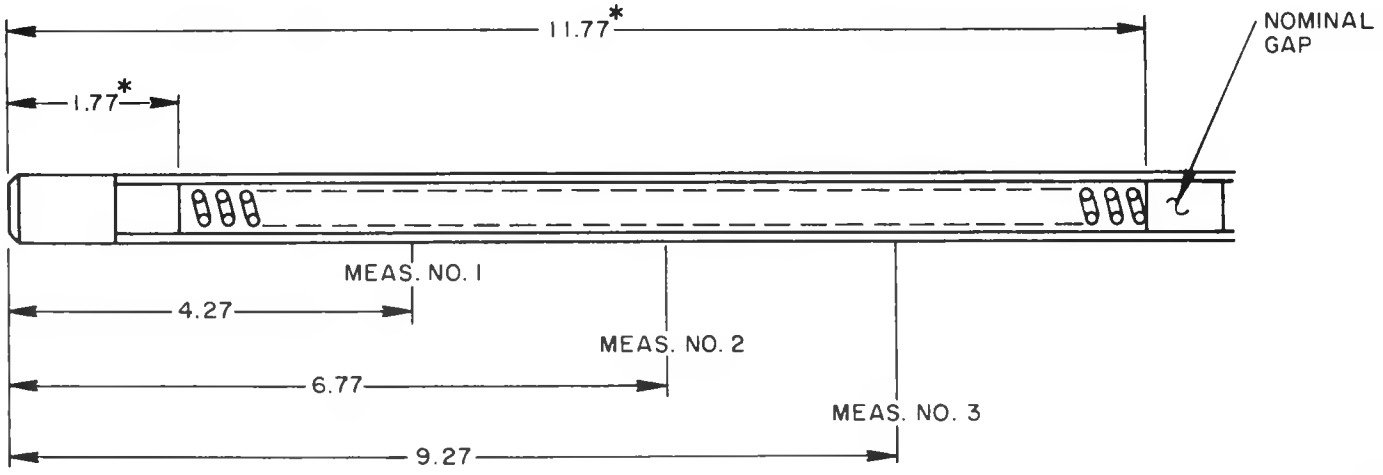

SEED RODS

* - Nominal as-built

Figure 13 - Bottom Mounted Fuel Rod Plenum Ovality Measurement Locations

3.8 Wear Mark Depth, Volume, and Location

Fuel rod wear mark depth, volume, and location were measured to confirm the LWBR fuel rod design analysis procedure for rod wear presented in Reference 23 and to provide an overall view of rod wear for the LWBR grid support system. Fuel rod wear depths and volumes were measured with the REX orbiting profilometer. Measurements were normally done after the plenum ovality measurements prior to any post-exam standard measurements. The orbiting profilometer was discussed in Section 3.7.

The orbiting profilometer was used to perform screening measurements at suspect elevations of a fuel rod to locate wear marks with significant depth (> 1.5 mils). Elevations for wear mark screening measurements were determined from rod visuals and ultrasonic examinations of the rods. Multiple inspections at 0.005 to 0.010-inch axial increments were then performed for the deep wear marks.

Wear mark screening depths were determined by

(1) obtaining orbiting profilometer data of cladding radial position at 0.5-degree increments around the entire rod circumference,

(2) using the data to determine local rod center and nominal radius for 50 different sets of cladding radial positions (three points per set) on the fuel rod,

(3) determining the average center and average rod radius for the 50 data sets, and

(4) determining the maximum difference between the average rod radius and minimum local rod radius at areas corresponding to grid contact locations.

Wear depth and volume for deep wear marks were calculated by determining the maximum local wear depth and summing the wear volumes for each of the inspection planes through a wear mark.

Wear depth at each plane was determined by

(1) measuring the cladding radial position at 0.5-degree increments for a 60-degree segment centered about the wear mark,

(2) using the measurement data for three points away from the wear mark to determine the local rod center and radius, and

(3) determining the maximum local difference between the local rod radius and radius in the wear region (local wear depth).

Planar wear volume was determined from the relationship:

$$\Delta V = \{ [R_w(i) + R_w(i+1)] / 2 - R \} \Delta\theta \, \Delta z(5)$$

where

R_w = local rod radius at wear mark relative to local rod center,

R = local rod radius,

$\Delta\theta$ = angle (radians) between inspection points,

Δz = axial spacing between inspection planes,

n = number of measurements per plane (120), and

i = inspection angle index.

Results for 10 calculations using different sets of points to determine local rod center and radius were averaged to determine maximum local planar wear depth and planar wear volume. Averaging was performed to minimize errors due to spurious measurements. Total volume for a wear mark was obtained by summing the planar wear volumes.

Accuracy of the orbiting profilometer was checked before and after wear mark measurements by measuring the flats on the appropriate seed, standard blanket, power flattening blanket, or reflector calibration standard. Based on the repeat measurements of these standards, the calculated 2-sigma accuracies for wear depth was ±0.00016 inch. Based on repeat measurement of wear volumes during REX qualification, the 2-sigma accuracies of wear volumes was ±14.2 percent.

3.9 - OXIDE THICKNESS

LWBR fuel rod cladding oxide thickness was measured non-destructively with a Nortec 5-MHz eddy current probe on the REX axial profilometer. In addition to providing a better statistical data base more readily and rapidly than standard destructive metallographic techniques, eddy current measurement allowed investigation of axial variations of oxide thickness.

Cladding oxide thickness was measured at 0, 90, 180 and 270-degree orientations. Oxide thicknesses for each orientation were measured by pausing at 0.5-inch intervals during a scan from the top to the bottom of the fuel rod. Measured oxide thicknesses along with the axial and angular position were recorded on floppy disk using the REX computer.

The eddy current oxide thickness (EDCOT) probe was calibrated prior to each inspection by measuring six known oxide thicknesses for fuel rod cladding segments on seed, standard and power flattening blanket, and reflector standard bars. Oxide thicknesses for the standard bar cladding segments were determined by repeat inspections during REX qualification. Instrumentation was adjusted to obtain an average deviation between known (average thickness for repeat EDCOT measurements during gage qualification) and measured oxide thickness of 0.08 mils or less and a maximum difference range of 0.34 mils or less.

A check point on the rod was established at the beginning of the first scan for in-process evaluation of thickness measurements. The gage was checked for drift after each scan by repeating the check point thickness measurement. The maximum allowable difference between repeat check point thicknesses was 0.28 mils. The average error after two scans was limited to 0.14 mils. The average error after three scans was limited to 0.12 mils. Failure of the in-process checks required a check of equipment calibration with the standard bar. Failure of the standard measurement required a recalibration and a repeat of the last scan.

The oxide thickness standards were measured after the last scan to check for drift. Average difference and maximum difference range between known oxide thicknesses were limited to 0.13 mils and 0.51 mils, respectively. Failure of the post-calibration measurements required a repeat inspection of the entire rod.

Measured fuel rod oxide thickness values were adjusted to accounted for differences in measured thickness for the oxide standards on the standard bar and metallographic measurement for oxide thickness for remnants of the cladding used for the standard bar.

Additional details on the design and operation of the REX eddy current gage are presented in Reference 1.

3.10 - CLADDING DEFECTS (UT)

The REX ultrasonic gage was used to evaluate fuel rod cladding and some weld areas to determine if cracks formed as a result of core operation and to locate defect indications as a guide for destructive metallographic examination.

The REX ultrasonic gage had two immersion-type transducers. One transducer was mounted perpendicular to the axis of the fuel rod and was offset horizontally so that the pulse entered the fuel rod surface 22.5 degrees off the tangent point. This transducer detected longitudinal cracks or defects. The second transducer was mounted so that the pulse entered the fuel rod surface on the tangent point (i.e., rod centerline), but inclined vertically 22.5 degrees to the fuel rod surface. This transducer detected circumferential cracks or defects. Both transducers operated at 700 pulses/sec and emitted 15-MHz sound waves. The ultrasonic beams were focused to provide 0.02-inch diameter detecting spots. A Sonic FTS MARK II Tester was used as the ultrasonic transmitter and receiver.

Each rod was scanned in a spiral from top to bottom of the rod. Rotational speed and axial translation were set to provide a 10 percent overlap of the beam spot to assure 100 percent inspection of the rod. Sensitivity and gate amplitude for the electronic equipment were adjusted to screen out small surface scratches and extraneous signals (<4 mils).

Both strip chart and digital data were obtained from the inspection. Digital data were collected with a MODICON 584 programmable controller which acquired the MARK II analog output and digitized it by summing 54 data points per revolution.

The equipment was calibrated before each rod inspection by measuring simulated cracks on a seed, blanket, or reflector standard bar. Calibration of the equipment was also checked after the inspection to check for drift.

3.11 - CRUD MEASUREMENTS

Crud measurements for LWBR fuel rods were performed to characterize crud deposits on the external surface of a seed, a standard blanket, and a reflector fuel rod. The examination included visual examination of the rods before and after decrudding, fuel rod diameter measurements before and after decrudding to determine crud thickness, incremental chemical decrudding of the rods, and quantitative chemical analysis of the descale solutions. The examination was performed by Argonne National Laboratory-West.

The purpose of the pre-descale visual examination was to observe and record the appearance of the specimen in the crudded condition prior to fuel rod diameter measurements and descale operations. The purpose of the post-descale visual examination was to determine the effectiveness of the descale operation and to record the appearance of the rod in the descaled condition prior to measurement of decrudded rod diameter. Differences in pre- and post-decrud diameter measurements were used to determine the axial variation of crud thickness. The quantitative analysis of the decrud solution was performed to determine concentrations of iron, nickel, chromium, cobalt, and copper and to determine the activities of selected isotopes (Fe-55, Ni-63, Co-60, Mn-54, and Sb-125). Quantitative analysis of the incremental decrud solutions was also used to study the axial variation of crud thickness.

Visual examinations of the rod were performed by four full-length scans of the rod separated azimuthally by 90 degrees. A minimum of 10 pre-descale and 10 post-descale photographs of representative and unusual surface conditions were obtained per rod. A full length montage at one orientation was obtained for each rod prior to and following descale operations. Photographs were obtained with an 8-foot long bellows camera which provided a 1:1 image on 4-inch x 5-inch fine-grain, black-and-white film.

Pre- and post-descale diameter measurements were obtained by laser profilometry along a full-rod-length track spiraling about the rod axis. A description of the equipment used to perform diameter measurements is presented in Reference 24. Axial and azimuthal positions of diameter measurements were recorded since they had to be duplicated during post-descale

diameter measurements. Accuracies for axial and azimuthal positions were ±0.003 inch and ±0.5 degrees, respectively. Pitch of the rod spiral during diameter measurement was selected so that guide rollers on the measuring equipment did not roll across the region of measurement. Diameter measurements were made at 15-degree azimuthal increments and 0.0833-inch axial increments. The diameter at each measurement location was determined with a laser-beam scan rate of 128 passes for each measurement. The diameter of a standard bar of certified diameter in a parallel orientation with the fuel rod was used to scale the measurements. Each spiral track was scanned three times, utilizing an independent and unbiased re-establishment of azimuthal and axial reference positions between scans, with the objective of obtaining diameter measurements at exactly the same axial and azimuthal position for each scan. Data for the three scans were averaged to obtain best estimate local diameters. Changes in pre- and post-descale average diameters were used to determine local crud thicknesses.

All three rods examined were decrudded in three axial increments. The axial increments were as follows:

	Axial Region (inches)		
Increment	Seed	Blanket	Reflector
1	0-25.5	0.0-23.3	0-22.3
2	0-94.1	0.0-91.5	0-87.6
3	0-114.9	0.0-116.2	0-109.9

These axial increments were chosen to correspond with expected variations in crud thickness in which crud is lighter in the central 60 percent of rod length versus the upper and lower 20 percent of the seed, blanket, and reflector fuel rods.

The rods were decrudded by placing them in a 10-foot vertical chamber constructed of zirconium metal with plastic inlet and outlet piping and with external heaters, thermocouples, and insulation. The rod was incrementally decrudded by filling the chamber to specified levels.

Four solutions were used to decrud the rods. The first descale solution, alkaline permanganate (AP-1), was added to the chamber, heated to near boiling, and maintained at this temperature for two hours. The solution was then drained into a plastic container. The second solution, hydrazine versenate (HV), was then added to the chamber, heated to near boiling and maintained for 1.75 hours. This solution was then drained into a separate plastic container. The third and fourth solutions, alkaline permanganate (AP-2) and mono-ammonium citrate hydroxyethylenediaminetriacetic acid (MAC/HEDTA), were then added in turn, heated, maintained for two hours, and drained into containers. Finally, water was added to the same level as the previous solutions to rinse the area of the rod and chamber involved in the descale operation. The rod was then removed from the chamber for visual inspection.

The four containers of solution were weighed on an electronic balance to establish the net amount of each solution. Proportional samples of each solution were combined to make a single sample. Two such samples were used for analysis by the ANL-W Analytical Laboratory. The remaining solution was then discarded and the containers were thoroughly rinsed. The above process was repeated for each incremental area of the rod.

3.12 - NEUTRON RADIOGRAPHY

Neutron radiography was performed on 12 fuel rods which were subsequently destructively examined. Radiographs were required for proper cutting of rods, for examining fuel pellet integrity, and for determining fuel stack and plenum dimensions in the intact fuel rods. Rods were cut preferentially at pellet interfaces for shipping, examination, and testing of fuel and cladding sections. For plenum gap analysis, a laser hole was drilled at a favorable cladding location as determined from radiograph examination. Parallel scales appearing in each radiograph enabled length and position measurements with 0.010-inch precision.

Radiography was conducted in the NRAD facility at ANL-W. The rod liner containing the fuel rod and stabilizer (to prevent the rod from rolling inside the liner) was lowered vertically by overhead crane into the radiograph specimen tube located on a positioning elevator. The elevator was used to position the specimen tube and its contents into the horizontal neutron beam, which passed

through the 46-foot long beam tube from a TRIGA-type reactor. The specimen tube was then shifted laterally against the beam tube between a pair of fixed axial scales. Approximately 18 inches of rod length were exposed to the neutron beam. Radiograph exposures were spaced every 15 inches along the rod length to provide overlaps. Eight exposures were therefore sufficient to cover the 10-foot length of an LWBR fuel rod.

Radiograph images were recorded on dysprosium foil sensitive to thermal neutrons. A 40-minute exposure time was required for clarity and definition of images. Initially, an indium foil was also used to provide an image of epithermal neutrons. This image proved to be much weaker than the thermal neutron image and provided no additional information. Accordingly, only the thermal neutron image on dysprosium foil was used for subsequent rods.

Two scales appeared in the exposures, one on each side of the outer container with the inch marks precisely aligned between the two scales. The scales remained stationary while the fuel rod and containers were moved approximately 15 inches between exposures. Therefore, the same scale markings appeared in all radiographs. To provide continuity in longitudinal measurements across the exposure boundaries, reference markings appeared at 15-inch intervals along the length of the outer container. The reference markings were 0.051-inch diameter holes filled with cadmium for contrast in the exposures. Distances between the cadmium markings were provided by ANL-W to the nearest 0.0001 inch.

3.13 - GAMMA SCAN

Gamma scanning with the PIFAG was conducted on 24 fuel rods indicated in Table 7. One of the 24 rods was also neutron radiographed and destructively examined. The other 23 rods received only non-destructive examinations. Gamma scans therefore provide the only means of detecting in-stack gaps and measuring stack lengths of this group of 23 rods.

Scanning of the fueled sections of the rods was conducted with the PIFAG gamma scan setup in the hot cells at ECF. The scanner was incremented in 0.1-inch steps with a detector window of 0.200 inch. A 6-second count time was used at each increment, and this resulted in a 100-minute scan time over the fuel length. Electronic stability of the measuring system was sufficient to provide consistent readings without drift over this time period.

SECTION 4 - NONDESTRUCTIVE EXAMINATION RESULTS

4.1 Rod Pull Force Measurements

Plots of measured pull force versus pull distance for 17 of the 19 fuel rods examined with the REX are presented in Appendix A3. (Data for rods 0604555 and 1606710 were lost due to disk problems.) These forces include rod weight and grapple drag forces. Similar data were obtained for all rods removed from LWBR modules during the end-of-life (EOL) examination program. Maximum measured pull force and average pull forces for decreasing numbers of grids engaged are also presented on the plots. These forces do not include rod weight and grapple drag force. The vertical dashed lines on the plots represent best estimate positions for each of the grids in the modules. Histograms of maximum pull forces and average pull forces for decreasing numbers of grids engaged for nearly all the rods pulled (data for some rods was lost due to disk problems) are also presented in Appendix A3.

Rod pull force was expected to increase until rod motion was initiated and then to decrease when static friction was overcome. Pull force was then expected to decrease in steps as the rod end passed through each grid. Beginning-of-life (BOL) rod-grid contact force (sum of the reactions at all rod-grid contact points) was in the 80 to 140-pound range for seed rods, 160 to 330-pound range for blanket rods, and the 125 to 420-pound range for reflector fuel rods. Allowing for a 50 percent reduction of contact force due to AM-350 grid spring thermal and irradiation induced relaxation and assuming a coefficients of friction in the range of 0.1 to 0.4, the expected EOL pull forces with all grids engaged ranged from 4 to 28 pounds for seed rods, 8 to 66 pounds for blanket rods, and 6 to 84 pounds for reflector rods.

In general, measured pull forces acted as expected. Pull force fluctuations of approximately 5 pounds during intervals between passage of a fuel rod end through a grid were frequently observed. A large portion of the fluctuation can be attributed to flexing of the grapple housing during rod pull. The remainder of the fluctuation was probably due to variations in sliding

friction for the fuel rod on the AM-350 grid contact points. For numerous rods (e.g., rod 1605629 in BI-3), pull forces increased slightly just before the rod end passed through a grid. This was probably due to lateral forces which resulted when a bowed rod was pulled through each grid.

Figure 14 presents a comparison of average pull forces and upper and lower 95/95 tolerance interval pull forces for 254 rods removed from seed modules I-1, II-3, III-1, and III-2. Average pull forces ranged from 14 to 19 pounds for nine grids engaged, to 0 to 7 pounds for one grid engaged. The upper 95/95 tolerance interval for measured pull force ranged from 23 to 29 pounds for nine grids engaged, to 3 to 10 pounds for one grid engaged. Measured pull forces for all nine grids engaged were comparable to the expected range of 4 to 28 pounds. Pull forces for seed modules I-1 and III-2 were comparable. Pull forces for seed modules II-3 and III-1 were on the average about 4 pounds less than forces for the other seed modules. The lower forces for these modules were probably due to a force measurement bias. This bias frequently resulted in a negative pull force when only the top grid was engaged.

Figure 15 presents a comparison of average pull forces and upper and lower 95/95 tolerance interval pull forces for 590 rods removed from blanket modules I-3, II-2, III-2 and III-6. Average pull force ranged from 24 to 36 pounds for eight grids engaged and decreased to a range of 0 to 11 pounds for one grid engaged. The upper 95/95 tolerance intervals for measured blanket fuel rod (standard and power flattening) pull forces ranged from 33 to 52 pounds for eight grids engaged, to 5 to 20 pounds for one grid engaged. The measured pull forces for eight grids engaged were within the expected range of 8 to 66 pounds. Average pull forces for BIII-2 and BIII-6 were approximately equal. Pull forces for BI-3 were on the average about 5 pounds greater than pull forces for BIII-2 and BIII-6. Pull forces for BII-2 were on the average about 4 pounds lower than pull forces for BIII-2 and BIII-6. These differences in average pull force were also probably due to biases in pull force measurements.

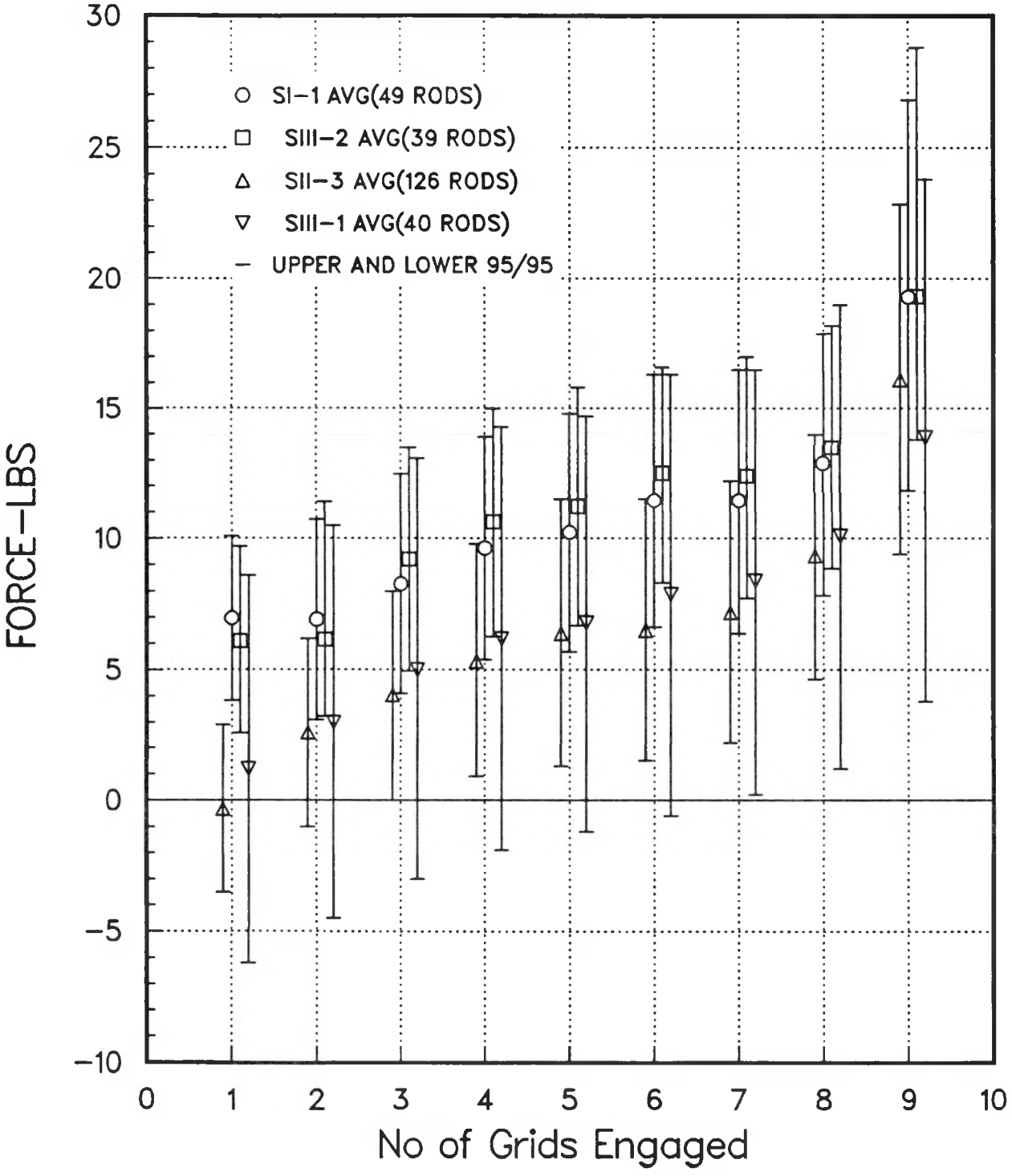

Figure 14 - Seed Fuel Rod Pull Forces
(Average and Range)

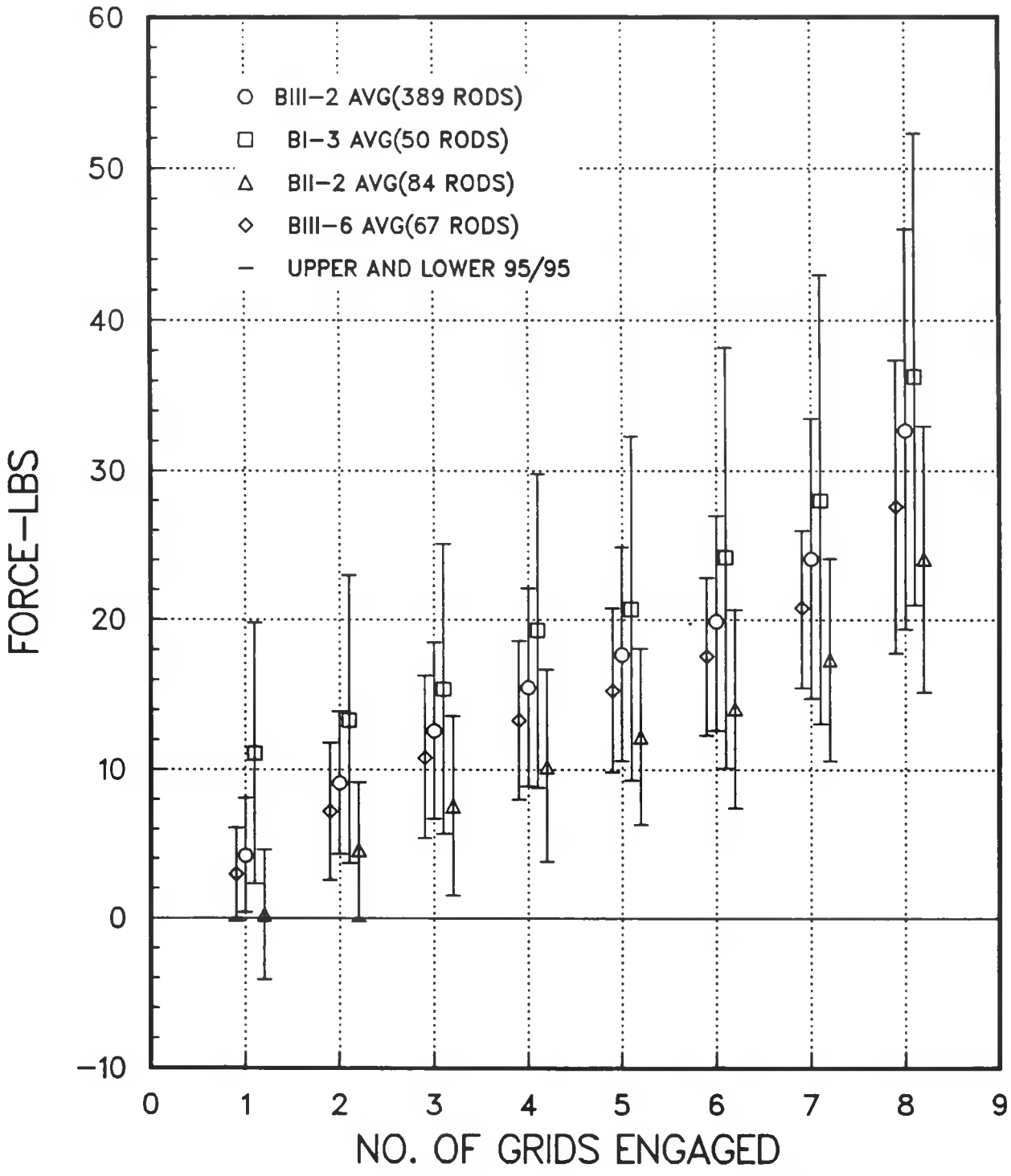

Figure 15 - Blanket Fuel Rod Pull Forces
(Average and Range)

Figure 16 presents a comparison of pull forces for 194 rods removed from reflector modules IV-3, IV-4, IV-9, and V-4. Average pull force for the reflector rods removed ranged from 28 to 35 pounds for six grids engaged and decreased to a range of 4 to 7 pounds for one grid engaged. The upper 95/95 tolerance interval for measured pull forces ranged from 39 to 56 pounds for six grids engaged, to a range of 7 to 14 pounds for one grid engaged. Again, measured pull forces for six grids engaged were within the expected range of 19 to 84 pounds.

Table 9 compares maximum measured pull force for each of the seed, blanket, and reflector modules with the control limits built into the RRS system. These limits were used to prevent overstressing of a fuel rod during rod removal. As shown, maximum measured pull forces were well below the RRS limits, thereby indicating that the rods were not subjected to any binding forces due to broken or deformed grid springs or dimples and rod-to-grid panel interference.

Figures 17, 18, and 19 present comparisons of average sliding friction forces for rods removed from seed, blanket, and reflector modules respectively. Except for the top grid, the change in average pull force for decreasing numbers of grids engaged was used to determine the friction force for each grid. Friction forces for the top grid were determined by subtracting the rod weight and grapple drag force from the average measured pull force. Calculated friction forces for the top grids in seed modules II-3 and III-1 and blanket module II-2 were increased 4 pounds to correct for the suspected bias in pull force measurements.

In general, average sliding friction forces for rods in seed, blanket, and reflector modules were large at or near the end grids and decreased to a minimum for the central grids. This is consistent with the residual spring force profile that was expected for these modules.

For seed modules, average friction force varied from about 7 pounds at the end grids to about 1 pound for the central grids. Assuming a 0.4 coefficient of friction, the corresponding grid spring force is in the 0.8 to 5.8-pound range. BOL design spring force for seed grids were in the 3.0 to 5.1-pound

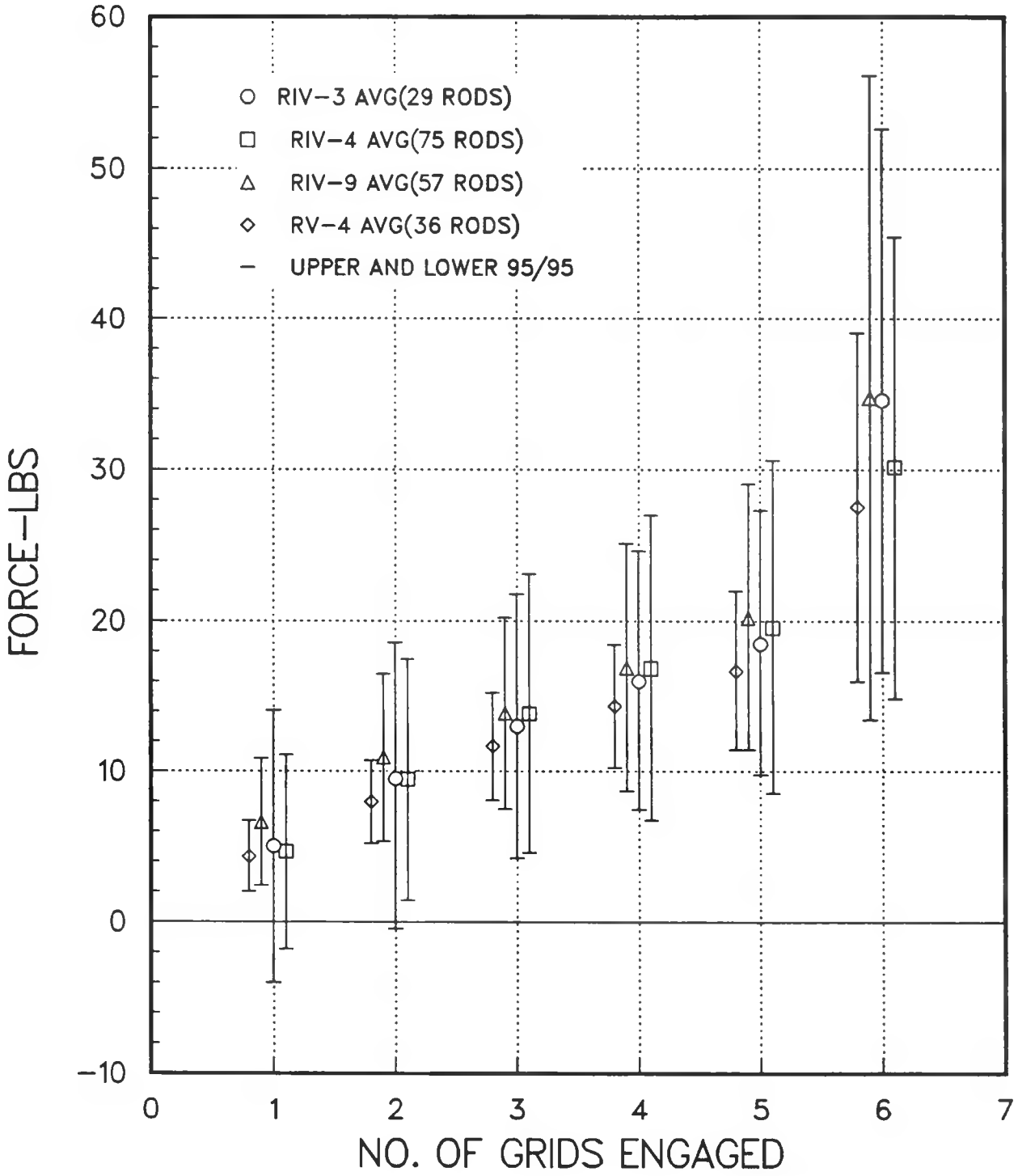

Figure 16 - Reflector Fuel Rod Pull Forces
(Average and Range)

Table 9 - Comparison of Maximum Measured Pull Forces With RRS Limits

Seed Fuel Rods

No. of Grids Engaged	Limit (lb)	SI-1	SII-3	SIII-2	SIII-1
Initiate	200	36	90	28	35
9	138	26	23	27	25
8	122	15	14	16	17
7	107	14	11	15	15
6	92	14	12	15	14
5	77	13	11	15	13
4	61	12	10	13	12
3	46	11	7	12	11
2	31	9	7	9	9
1	16	8	3	8	8

Blanket Fuel Rods

No. of Grids Engaged	Limit (lb)*	BI-3	BII-2	BIII-2	BIII-6
Initiate	500/500	79	64	96	80
8	331/220	67	35	70	49
7	290/220	49	27	45	29
6	248/220	43	23	33	25
5	207/207	35	21	30	25
4	166/166	30	20	25	22
3	124/124	25	16	26	20
2	83/83	22	12	17	13
1	42/42	18	6	9	7

Reflector Fuel Rods

No. of Grids Engaged	Limit (lb)**	RIV-3	RIV-4	RIV-9	RV-4
Initiate	500/500	115	128	145	100
6	329/418	54	52	66	43
5	275/348	24	36	32	21
4	220/278	20	33	28	16
3	165/209	17	30	22	14
2	110/139	15	21	17	9
1	55/70	9	11	10	4

*Standard Blanket Fuel Rods / Power Flattening Blanket Fuel Rods
**Rods in grid cells with normal springs / rods in grid cells with wide springs

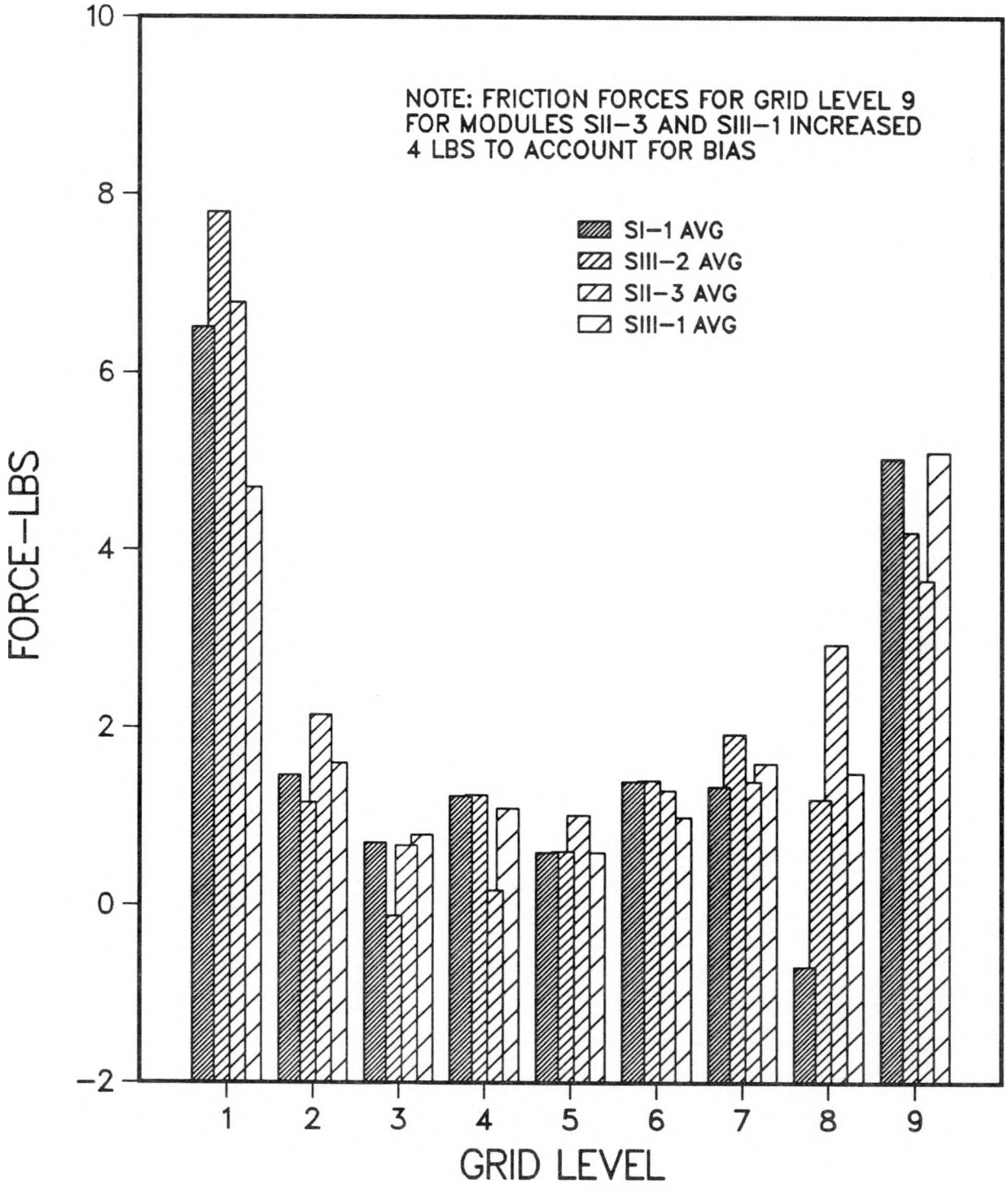

Figure 17 - Seed Fuel Rod-Grid Average Friction Forces

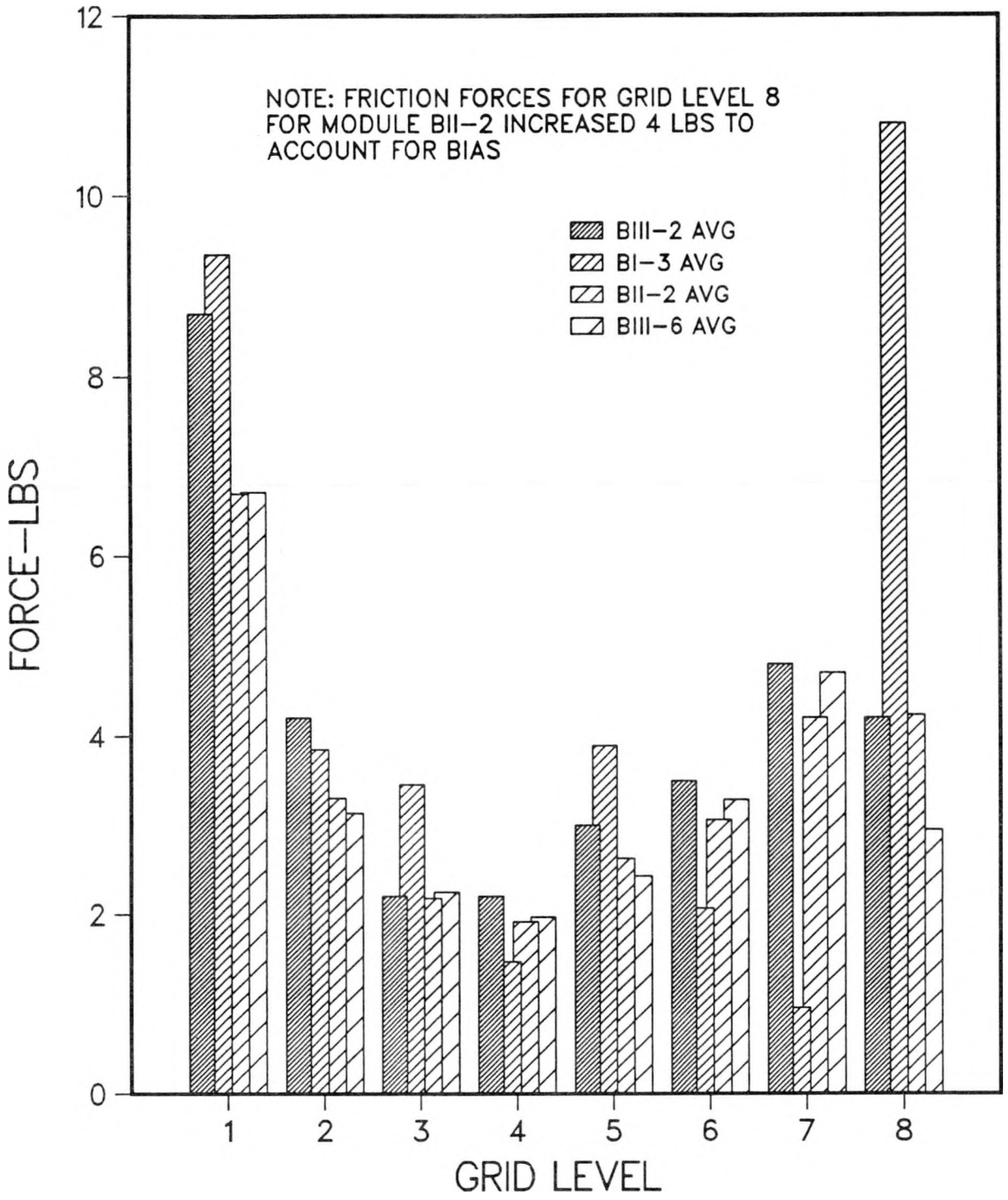

Figure 18 - Blanket Fuel Rod-Grid Friction Forces

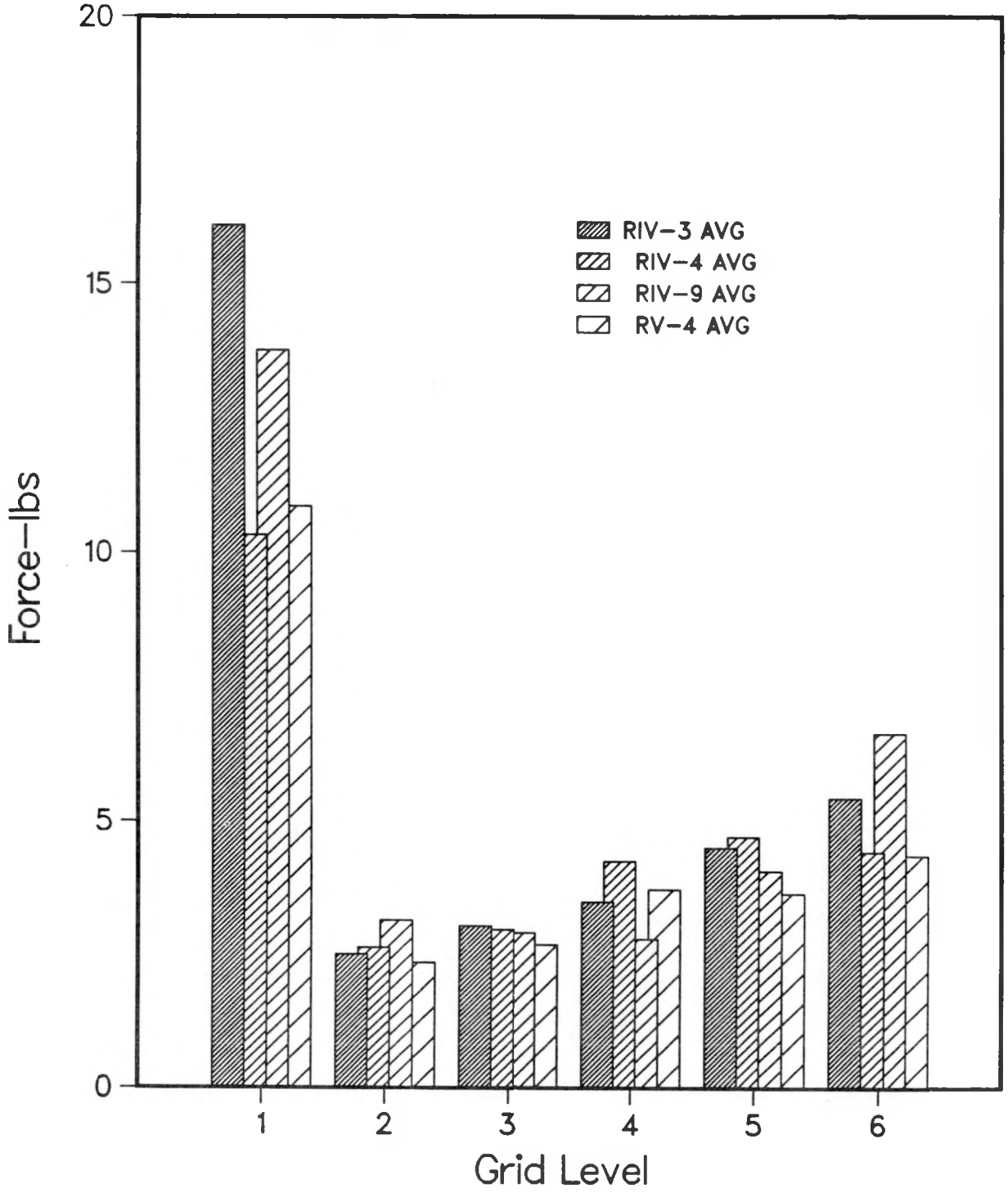

Figure 19 - Reflector Fuel Rod-Grid Friction Forces

range. Near zero and negative friction forces (an increase in average pull force after passage of a rod through a grid) were obtained for several inner grids in seed module I-1. Although this indicates low seating forces at these locations, fuel rod visual and orbiting profilometer examination results indicate that this did not result in significant wear for rods in these modules.

For blanket modules, average friction force varied from about 7 pounds at the bottom grid (level 1) to about 2 pounds at grid level 4 and then increase to about 4.0 pounds for grid level 8. Assuming a 0.4 coefficient of friction, the corresponding grid spring force for grid levels 1 to 8 was in the 1.5 to 5.8-pound range. Measured BOL spring forces for blanket grids were in the 6.7 to 13.8-pound range. For blanket module I-3, the average friction force was about 11 pounds at the top grid level. This corresponds to a 9.2-pound average residual grid spring force.

For reflector modules, average friction forces ranged from about 13 pounds at the bottom grid to about 2.5 pounds at grids 3 and 4 and then increased to about 5 pounds at the top grid. Assuming a 0.4 coefficient of friction, the corresponding grid residual spring force is in the 2.1 to 10.8-pound range. Design BOL spring forces for reflector grids were in the 6.9 to 23.2-pound range.

Figure 20 presents histograms of the ratio of module disassembly pull force to assembly pull force for 25 rods removed from blanket module I-3 and 25 rods removed from seed module III-2. The ratios are for all grids engaged (i.e., eight blanket grids and nine seed grids). Differences in grids engaged for insertion of a rod into a module versus removal from a module prevent comparison of pull forces with fewer grids engaged. As shown, disassembly forces for blanket module I-3 were on the average a factor of 1.85 greater than assembly forces. The force ratio ranged from 1.26 to 3.19. Disassembly forces for seed module III-2 were on the average a factor of 1.91 greater than assembly forces. The force ratio ranged from 1.2 to 3.2. Therefore, grid spring relaxation during reactor operation was more than offset by increases in sliding friction for the rods. During installation, LWBR fuel rods were liberally lubricated with neolube to keep assembly forces low and to minimize rod scratching.

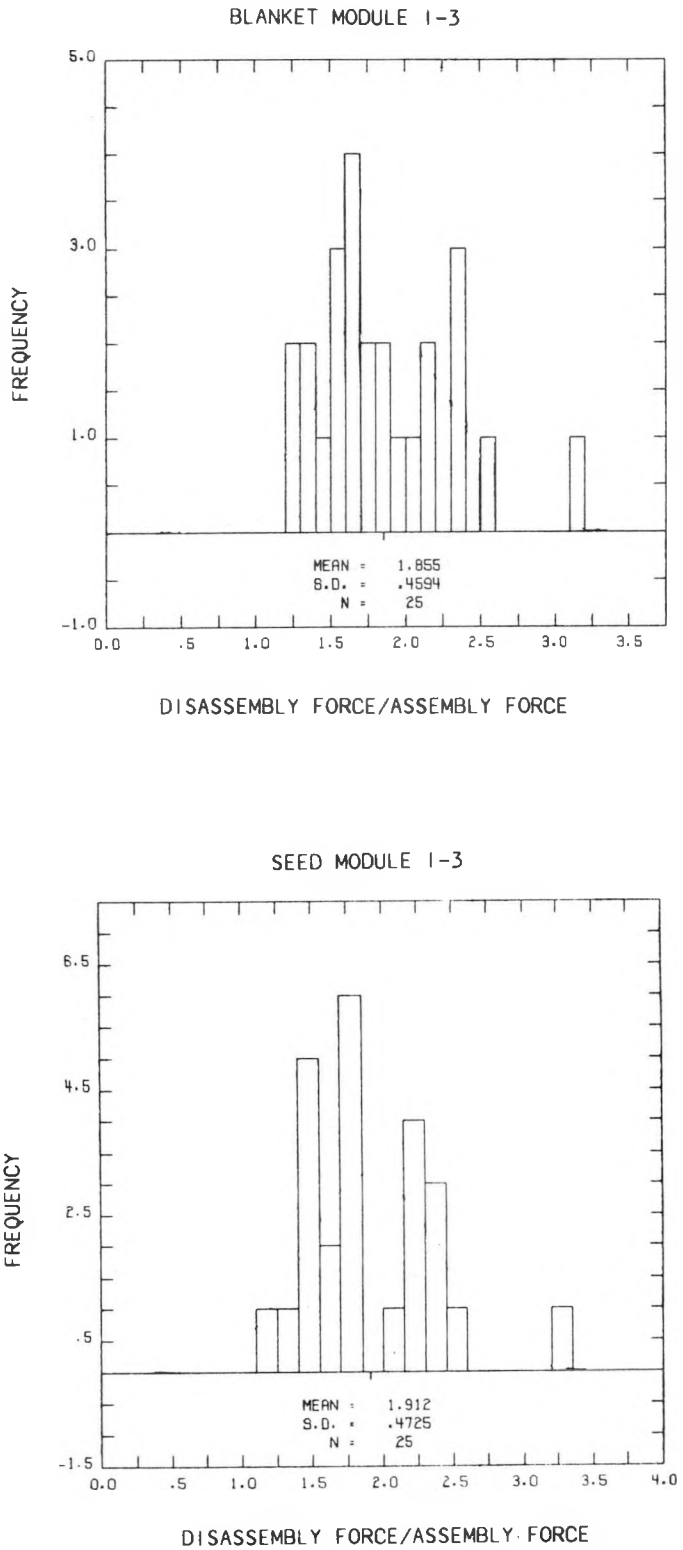

Figure 20 - Comparison of Assembly and Disassembly Pull Forces

4.2 - IN-BUNDLE BOW AND GAP MEASUREMENTS

Appendices A4 and A5 present plots of rod centerline positions and rod-to-rod gaps for 50 to 60 axial positions along the length of peripheral rods on sides 4 and 5 of seed module II-3, sides 5 and 6 of blanket module III-2, and sides 1 and 5 of reflector module IV-4. Rod centerline positions and rod-to-rod gaps were determined by digitizing 5X to 6X video recordings of the module. The horizontal broken lines on the plots represent best estimate grid locations. Location of the rods in their modules can be determined from the rod cell maps presented in Appendix A1. Fuel rod in-bundle bow and gap data were obtained from one seed module, five blanket modules, and one reflector module.

Data for seed module II-3 and reflector module IV-4 were obtained following removal of the Zircaloy shells. Except for reflector module IV-4, data for all peripheral fuel rods were obtained prior to severing of the top and bottom baseplates for rod removal. Data for all reflector IV-4 rods and all internal fuel rods were obtained following severing of the baseplate. Because of potential rod movements during the severing operation, data for the two rod spans near the fixed end of fuel rods in these modules may be significantly different from actual in-reactor rod bow and spacing. Comparison of measured bow and rod-to-rod spacing of nine peripheral rods in blanket module III-2 prior to and following baseplate severing indicated that the severing operation may change rod spacing by up to 0.04 inch for the two spans nearest the fixed end. Removal of the Zircaloy shells for seed module II-2 and reflector module IV-4 may also have affected measurements by relieving stresses due to flux gradient induced bow of these modules.

In general, rod edges (and therefore rod centerlines) for the central 70 percent of peripheral fuel rods were well defined with the video digitizing equipment. Crud buildup on the upper and lower 15 percent of the modules made edge detection in these areas more difficult.

Support structure in the vertical disassembly stand prevented examination of the upper 11 to 12 inches of seed module II-3 and reflector module IV-4.

As would be expected, proper illumination of the module was crucial in determining rod edges. Difficulty in illuminating internal fuel rods for blanket module III-2 made edge detection particularly difficult. Poor lighting generally resulted in shadows next to the rod. Results were monitored for errors due to shadows by checking the rod-to-rod gap to rod diameter ratio. For a large number of rod and gap pairs, the average ratio of gap to rod diameter should be approximately equal to the nominal as-fabricated gap to diameter ratio. Where necessary, measured rod-to-rod gaps were corrected to account for detected biases. No adjustment of measured fuel rod bow was required.

Comparison of bow data for peripheral fuel rods on adjacent sides of seed module II-3, blanket module III-2, and reflector module IV-4 shows the effect of the flux gradient on fuel rod bow. Rods on sides near or parallel to radial lines from the core center had large bow components due to module bow. Rods on sides perpendicular (or nearly so) to radial lines from the core center had little rod bow due to module bow.

Plots of rod centerline positions for seed module II-3 indicated that rod bow due to module bow was small. This was confirmed by module bow measurements presented in Reference 4 that indicated that bow for this seed module was approximately 0.03 inch.

Plots of rod centerline position for blanket module III-2 and reflector module IV-4 indicated that the rods in these modules had large bow components due to module bow. Comparison of rod profiles for sides 5 and 6 of blanket module III-2 indicated that the module had a bow of approximately 0.095 inch toward the core center. This is comparable to the 0.098-inch bow obtained during module bow inspections (Reference 4). Similiar bow profiles were obtained for blanket modules I-3, II-2, and III-3. Rod profiles for sides 1 and 6 of reflector module IV-4 indicate that the module had a bow of approximately 0.160 inch toward the core center. This was approximately 0.080 inch less than the bow measured for reflector module IV-4 prior to shell removal (Reference 4).

Figure 21 presents a comparison of the average measured, maximum measured, and the upper 95/95 tolerance interval for measured local bow for the top and bottom mounted fuel rods in seed module II-3 with predicted local bow for the most limiting seed fuel rod (5L31 in seed module I-1). Measured bow for the two spans immediately adjacent to the fixed end of rods inspected after baseplate severing were not included in this comparison. Predicted local bows were determined using the ROBOT and CYGRO computer programs. Local bow predictions were only obtained for the four spans near the fixed end of seed rods. The "avg + 1.64 sigma" predictions presented in Figure 21 were calculated using propagation of error techniques assuming the fuel rod bow due to various as-fabricated fuel rod and environmental characteristics (e.g., initial rod non-straightness, flux gradient, grid cell alignment, etc.) were additive. Standard deviations of bow for each of the factors were assigned assuming that the difference between best estimate and worst case bow for each of the bow contributors was equal to 2 or 3 standard deviations. Ninety-five percent of the rods would be expected to have in-bundle local bows less than the "avg + 1.64 sigma" predictions.

Measurements indicate that both top and bottom mounted peripheral fuel rods in seed module II-3 had average local bows in the range of 4 to 9 mils. The maximum measured bows ranged from 7 to 20 mils for bottom mounted rods and from 7 to 18 mils for top mounted rods. These bows are significantly smaller than worst case predicted bows, thereby confirming statistical analysis which indicated that worst case seed fuel rod bow was highly unlikely. The upper 95/95 tolerance interval of measured bow for these rods ranged from 6 mils to approximately 17 mils for both top and bottom mounted fuel rods. This was slightly less than the "avg + 1.64 sigma" fuel rod bow determined by propagation of error techniques.

Figure 22 presents a similar comparison of bow for standard and power flattening blanket fuel rods from blanket modules I-1, I-3, II-2, III-2, and III-3. Bow for the two spans immediately adjacent to the fixed ends of rods measured after baseplate severing were not included in this comparison. Since all blanket peripheral rods were bottom mounted, data for top mounted rods was

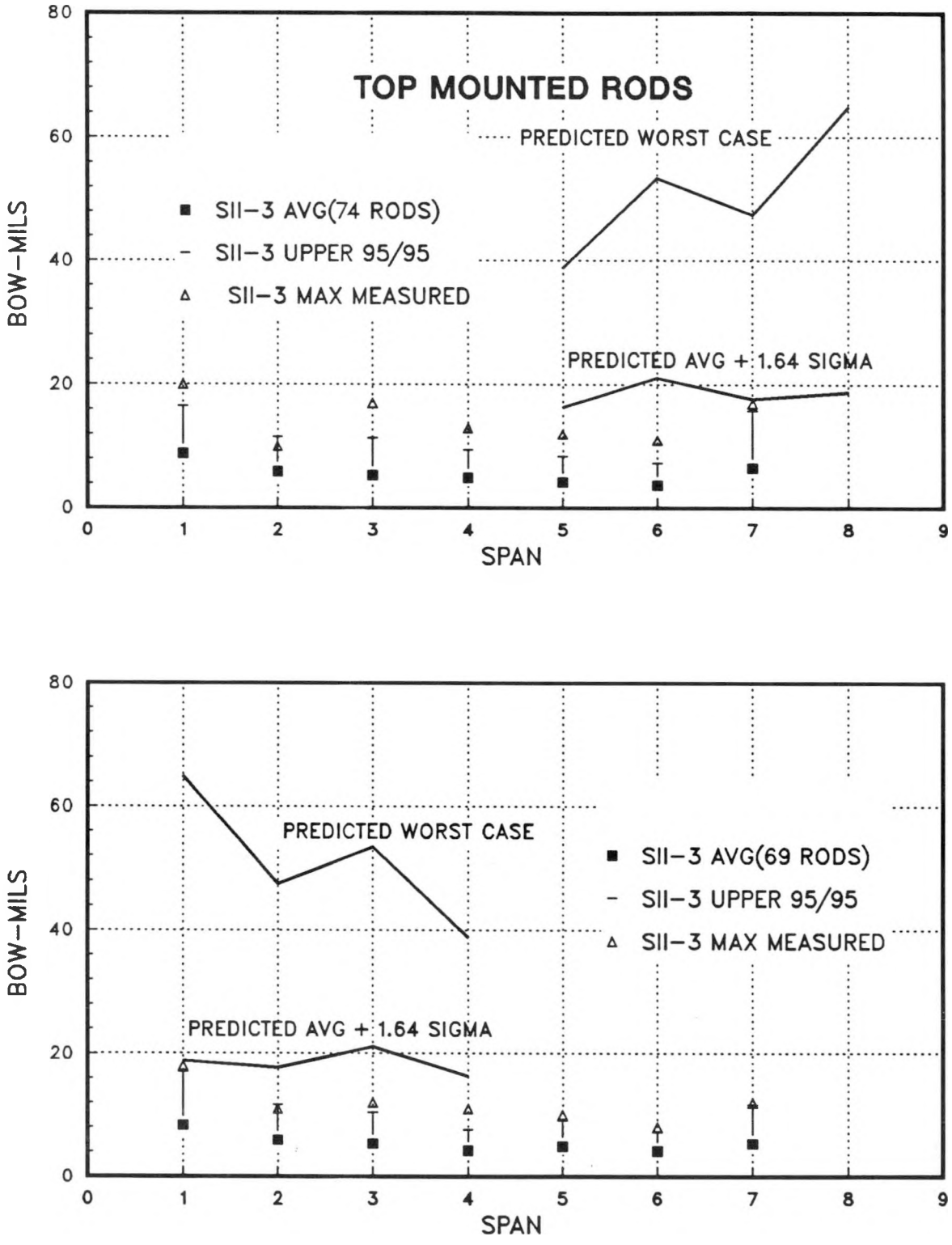

Figure 21 - Seed Fuel Rod In-Bundle Bow

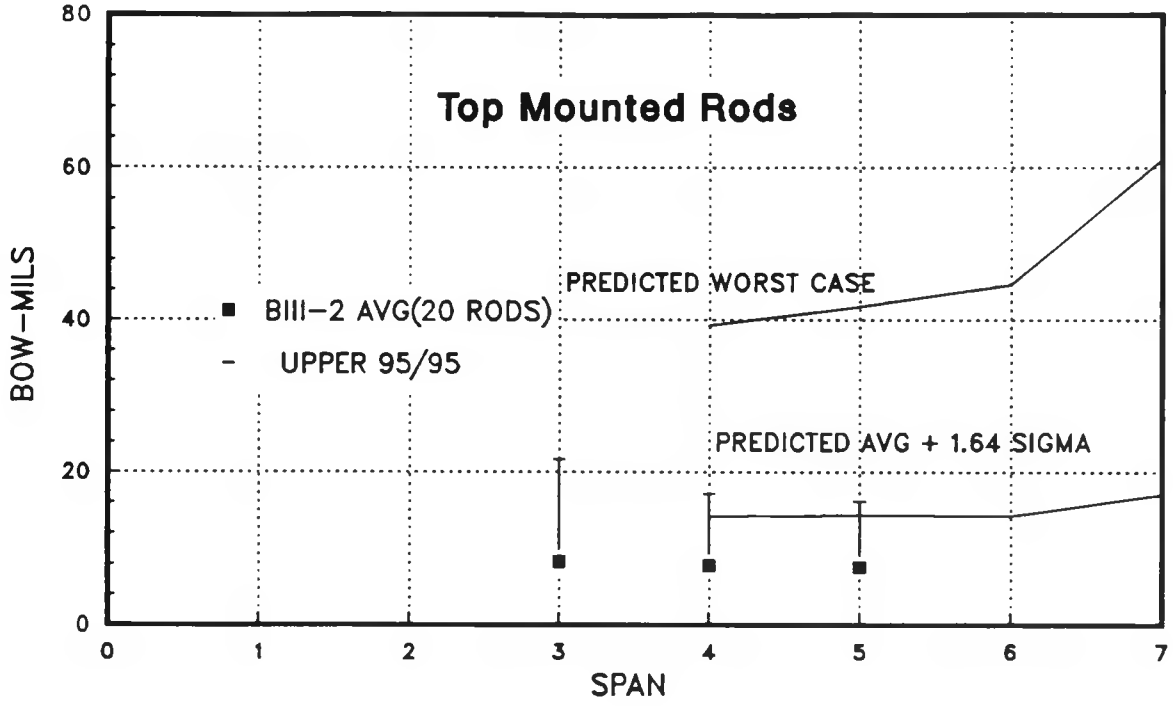

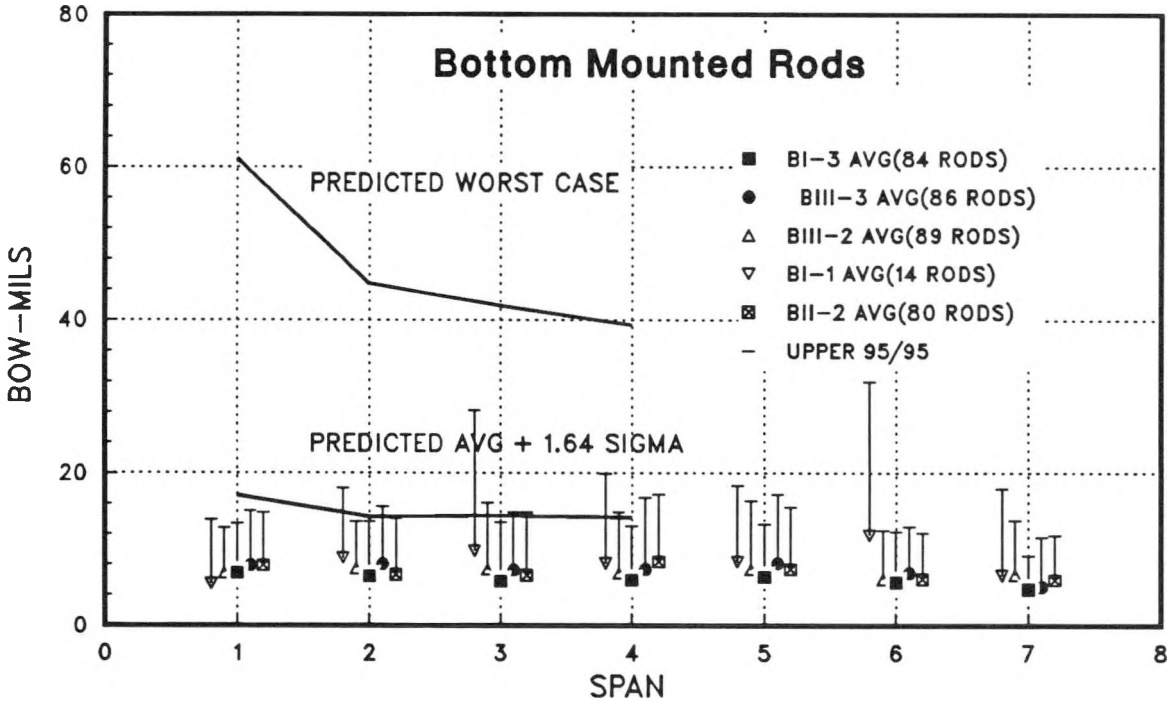

Figure 22 - Blanket Fuel Rod In-Bundle Bow

not obtained prior to baseplate severing. Only peripheral bottom mounted fuel rods were examined for blanket modules I-1, I-3, II-2, and III-3. All data for these modules was obtained prior to baseplate severing. Bow predictions on Figure 22 are for the limiting standard blanket fuel rod (15F56 in blanket module I-3).

Average measured fuel rod bow for all 5 blanket modules examined was comparable. It ranged from about 5 mils for span 7 to about 8 mils for span 1. Maximum measured bow ranged from 19 mils for span 1 to 27 mils for the third span from the fixed end. Worst case predicted bow ranged from 39 mils for span 4 to 61 mils for span 1. The large difference between worst case predicted bow and maximum measured bow supports statistical calculations which indicated that worst case bow of a blanket fuel rod was highly unlikely. Contrary to predictions that bow was greater near the fixed end of fuel rods, measured bow was independent of span. Except for blanket module I-1, the upper 95/95 tolerance interval for measured bow for bottom mounted fuel rods ranged from 9 to 17 mils and was comparable to bow calculated using propagation of error techniques. Although the upper 95/95 tolerance interval for bow of fuel rods in blanket module I-1 was greater than the statistical limits, this is not considered significant because the upper 95/95 tolerance limit was based on a sample size of only 14 rods. The upper 95/95 tolerance interval of measured bow for top mounted fuel rods was slightly greater than statistical limits. This is also not considered significant because the 95/95 tolerance limit was based on only 20 measurements.

Figure 23 presents a summary of measured fuel rod in-bundle bow for fuel rods from reflector module IV-4. Because all reflector measurements were performed after baseplate severing, measured bows for the two spans adjacent to the fixed end were included in the comparison. Predictions of bow for reflector rods for operation to 30,000 EFPH are not available. Touching of reflector fuel rods was shown to be acceptable throughout core life, and therefore rod bow was not evaluated for operation beyond 18,000 EFPH. Average measured bow of reflector fuel rods ranged from 9 to 14 mils for top mounted rods and from 8 to 13 mils for bottom mounted rods. The upper 95/95 tolerance

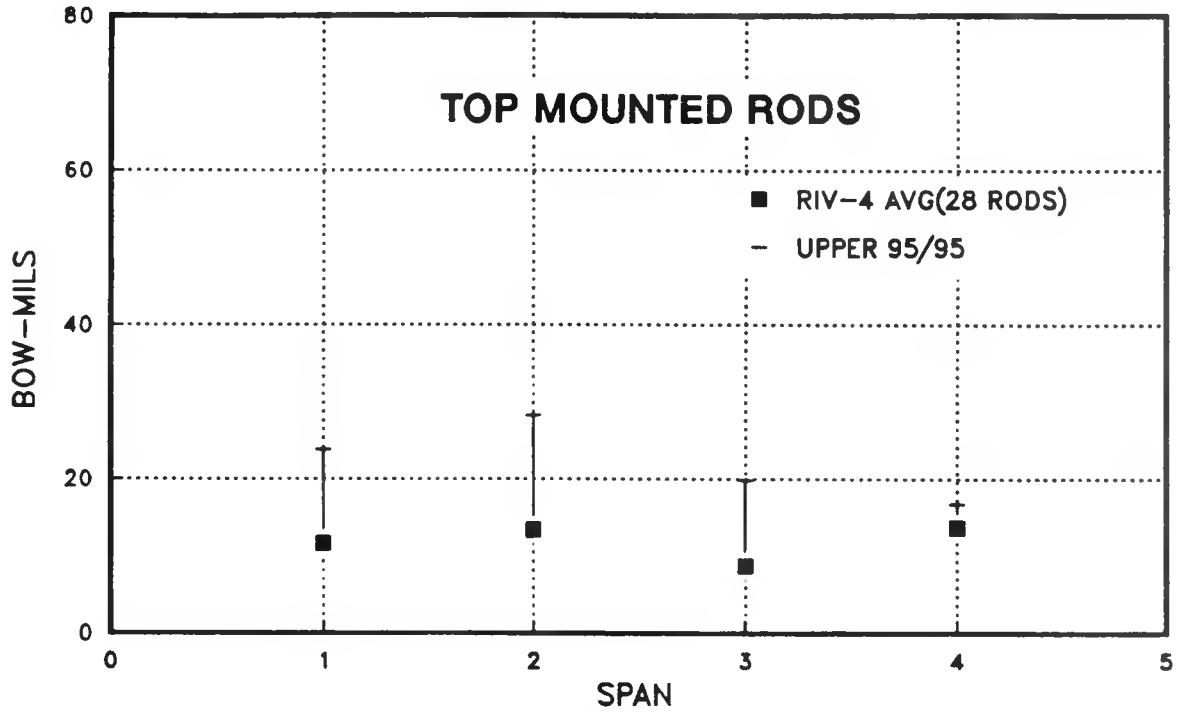

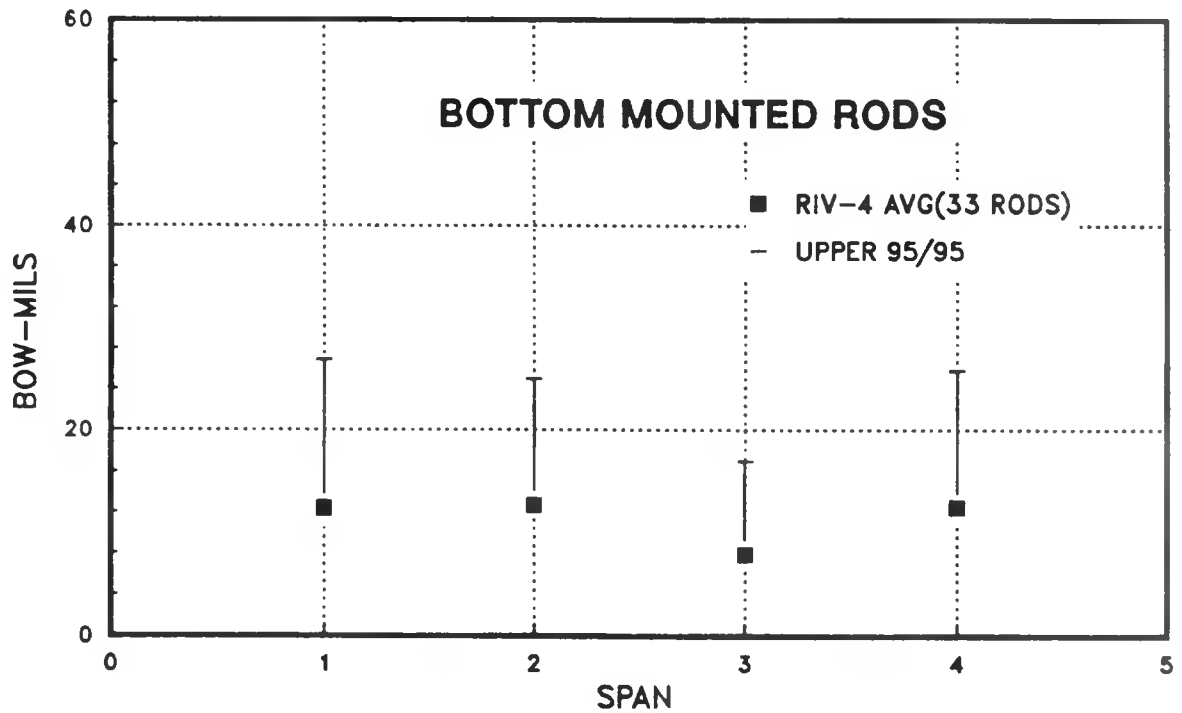

Figure 23 - Reflector Fuel Rod In-Bundle Bow

interval for measured bow ranged from 17 to 28 mils for top mounted fuel rods and from 17 to 26 mils for bottom mounted rods. Measured bow was independent of span. The maximum measured bow for reflector rods was 29 mils.

Figure 24 presents a comparison of measured rod-to-rod spacing for seed module II-3 and predicted rod-to-rod spacing at the limiting seed location. Nominal assembled and minimum assembled rod-to-rod spacing are also presented. As was the case for fuel rod bow, data associated with the two spans nearest the fixed end of the rod obtained after baseplate severing were excluded from the comparison. The measured gap reported represent the minimum gap for an entire span. For rods bowing toward one another, the minimum gap was near the midspan. For rods bowing away from one another, the minimum gap was near either the grid above or below the span.

Average measured gaps for SII-3 were in the range of 53 to 58 mils for all spans. The minimum measured gap was 10.0 mils at span 7. The minimum predicted gap was zero for all spans. The lower 95/95 tolerance interval for minimum measured gaps ranged from 45 mils for span 4 to about 32 mils for span 7. Except for span 7, the lower 95/95 tolerance interval for minimum rod spacing was comparable to the corresponding "avg - 1.64 sigma" predicted spacing. The lower 95/95 tolerance intervals for minimum measured gap for span 7 was 7 mils less than predicted "avg - 1.64 sigma" values. The variability of measured minimum gap was particularly large for span 7.

Figure 25 presents comparisons of average measured and the lower 95/95 tolerance intervals of measured minimum rod-to-rod spacing for standard blanket fuel rods from blanket modules I-1, I-3, II-2, III-2, and III-3 with predicted spacing. This comparison indicates that minimum blanket fuel rod spacing were well defined by statistical methods. Except for span 2 of blanket module I-3 and span 4 of blanket module III-3, the lower 95/95 tolerance interval for minimum measured gaps were comparable to or less than the corresponding "avg - 1.64 sigma" predicted spacing. For span 2 of blanket module I-3 and span 4 of blanket module III-3, the lower 95/95 tolerance intervals for minimum measured gaps were 3 to 4 mils less than predicted values.

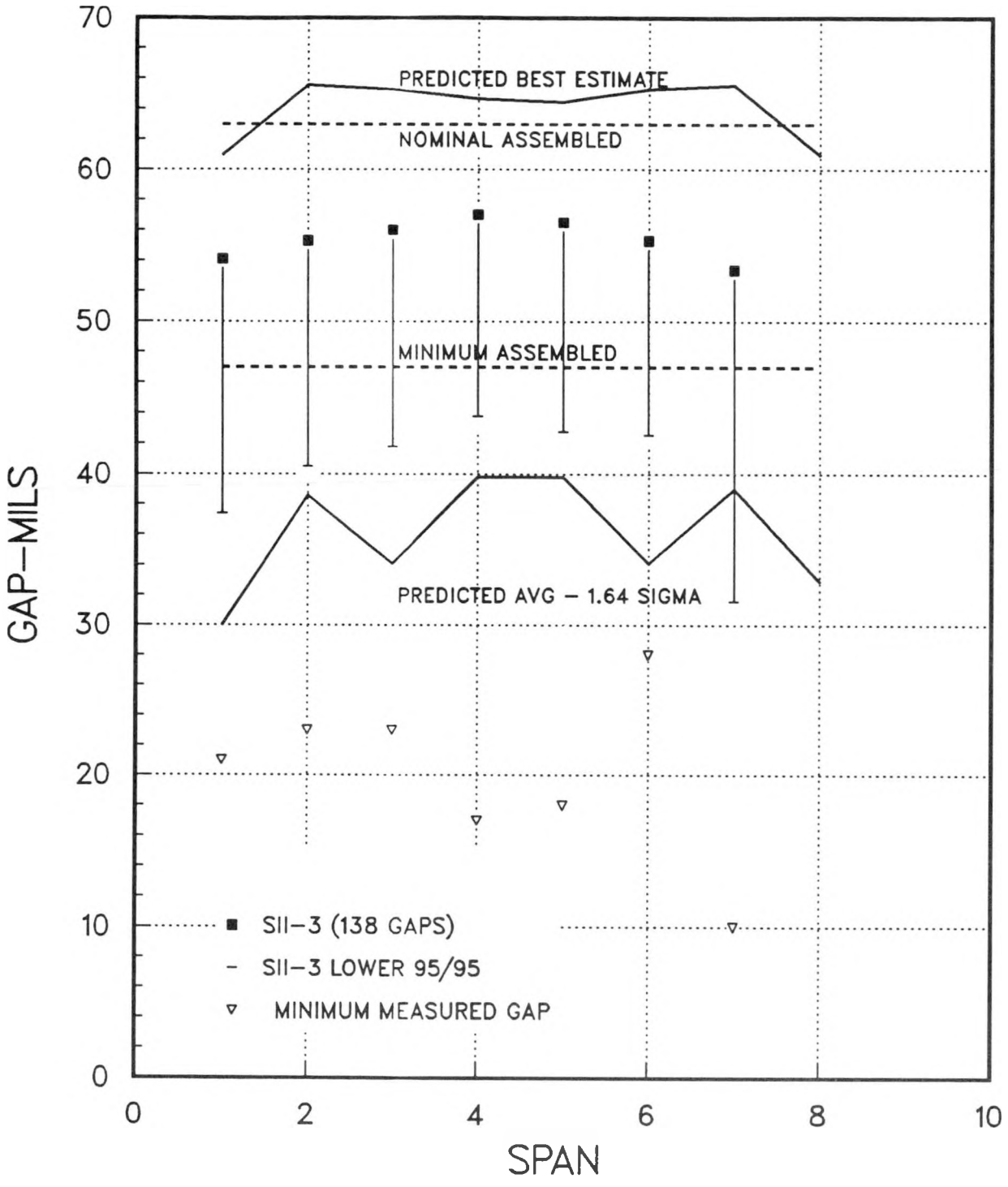

Figure 24 - Seed Fuel Rod In-Bundle Spacing

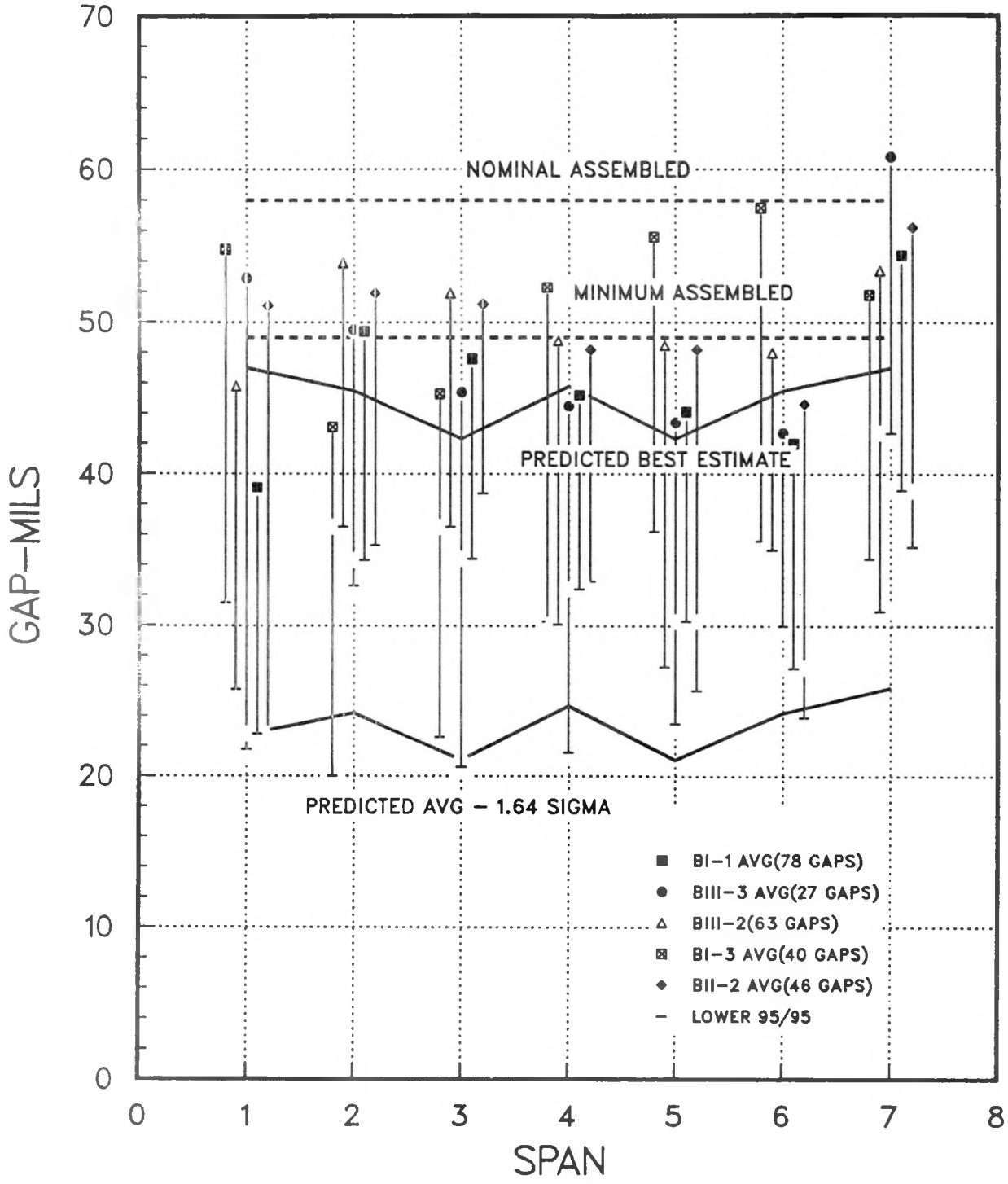

Figure 25 - Standard Blanket Fuel Rod In-Bundle Spacing

Rod-to-rod spacing measurements for standard blanket rods revealed one near contact condition. A minimum rod-to-rod spacing of 2 mils was measured at span 3 for the rods in cells 15F43 and 15F44 of blanket module III-3 (Figure 26). Figure 27 presents a plot of gap along the entire length of the module for the rods in cells involved in the near contact condition and for the rod in the adjacent cell 15F42. As shown, closure in the gap at the 48-inch level for the rods in cells 15F43 and 15F44 is confirmed by a corresponding increase in spacing between the rods in cells 15F43 and 15F42.

Figure 28 presents comparisons of measured rod-to-rod spacing for the power flattening blanket rods in blanket modules II-2, III-2, and III-3. The data also indicated that spacing for power flattening blanket fuel rods was well defined by statistical estimates. Average minimum measured gaps were comparable to best estimate minimum gaps for the limiting power flattening blanket fuel rod. Except for span 1, the lower 95/95 tolerance intervals for minimum measured rod spacing were comparable to design predictions. For span 1, the lower 95/95 tolerance interval for minimum measured gap was approximately 10 mils less than predicted "avg - 1.64 sigma" gaps. Diffusion of light in these regions made detection of rod edges particularly difficult.

Figure 29 presents a summary of minimum measured gaps for reflector module IV-4. As discussed above, predictions of minimum reflector rod-to-rod spacing were not made for operation beyond 18,000 EFPH. Average minimum measured rod-to-rod spacing ranged from 62 to 70 mils. The lower 95/95 tolerance interval for minimum measured spacing ranged from about 35 mils at spans 1 and 5 to about 55 mils for span 2.

Figure 30 presents an evaluation of one-sided 95/95 percent channel closure for seed, standard blanket, power flattening blanket, and reflector

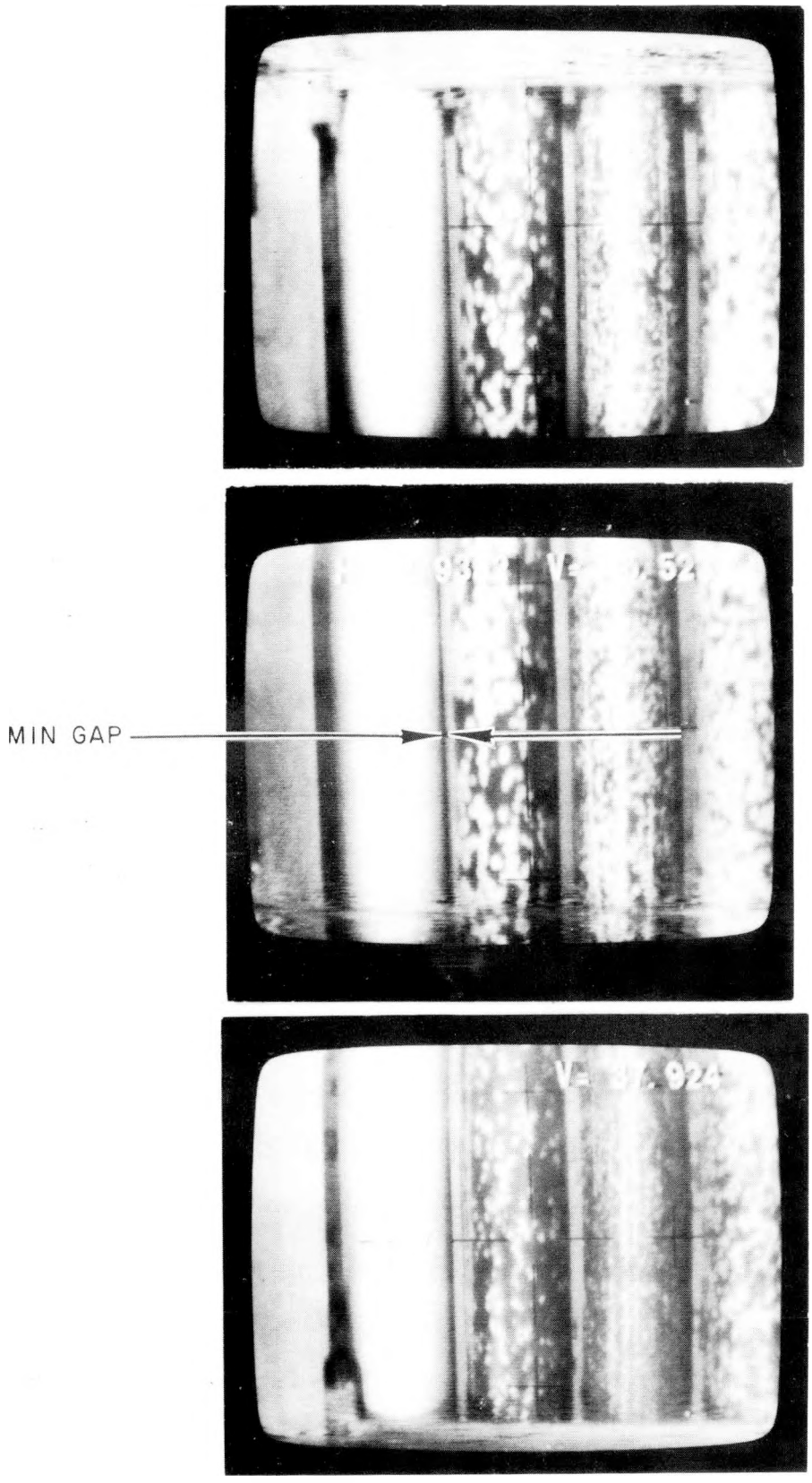

Figure 26 - Blanket Module III-3 Near
Contact Condition 15F43-15F44

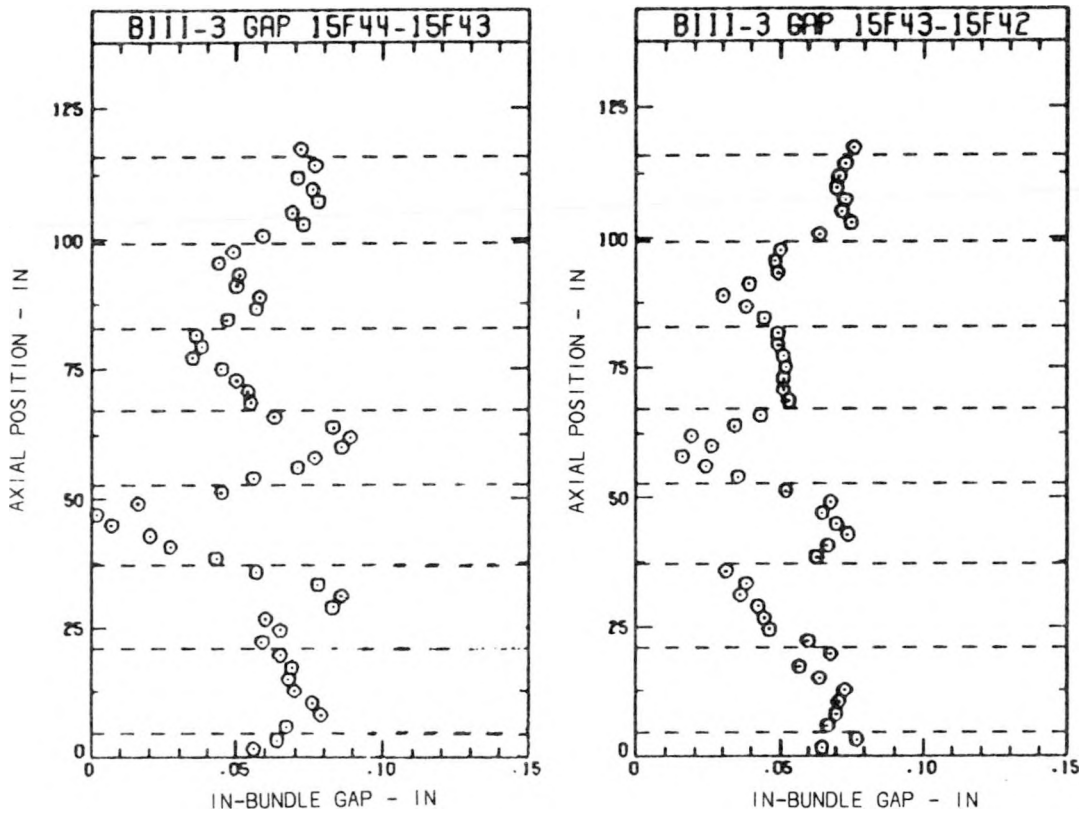

Figure 27 - Rod-to-Rod Gap Profile for
Near Contact Condition

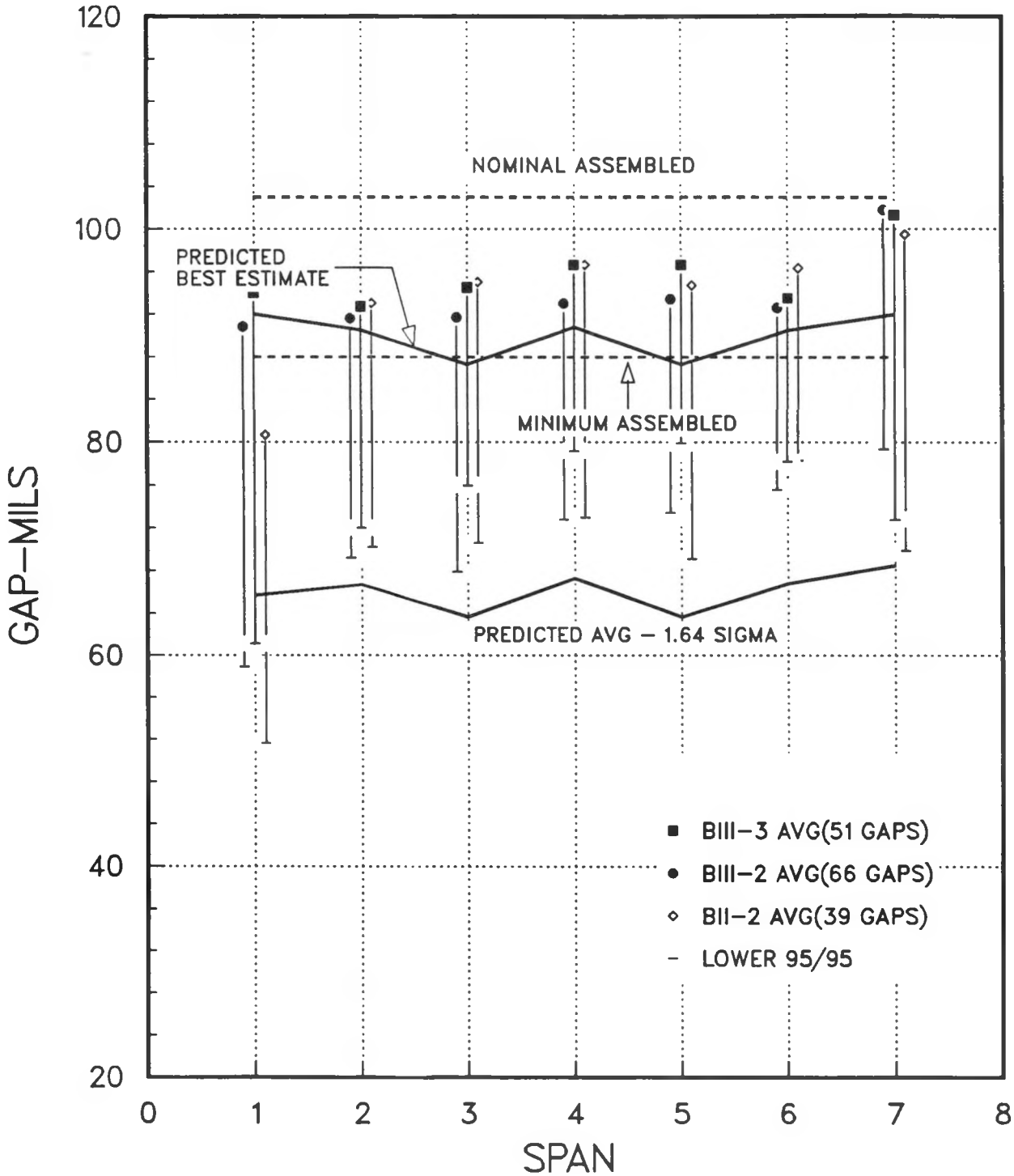

Figure 28 - Power Flattening Blanket
Fuel Rod In-Bundle Spacing

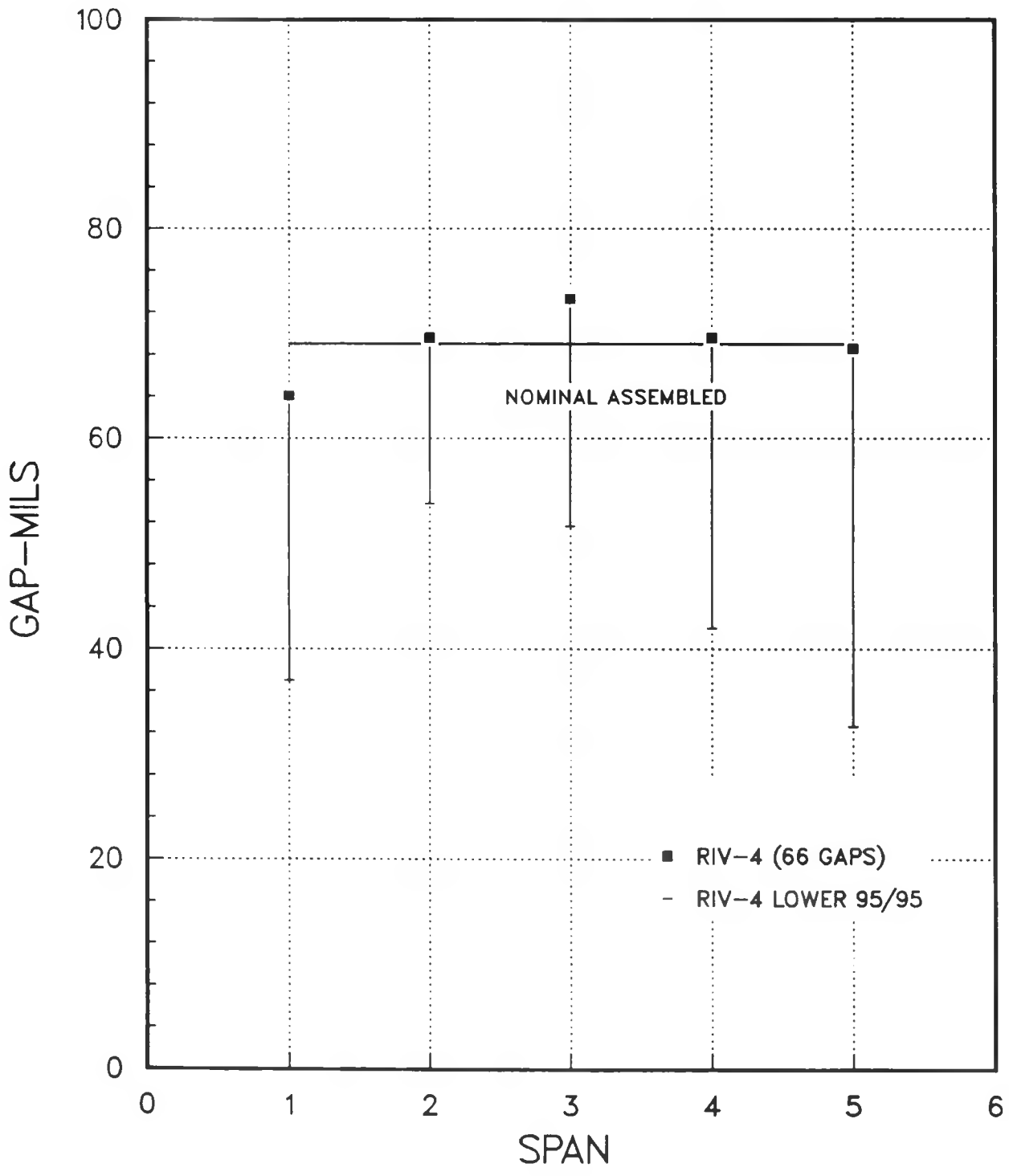

Figure 29 - Reflector Fuel Rod In-Bundle Spacing

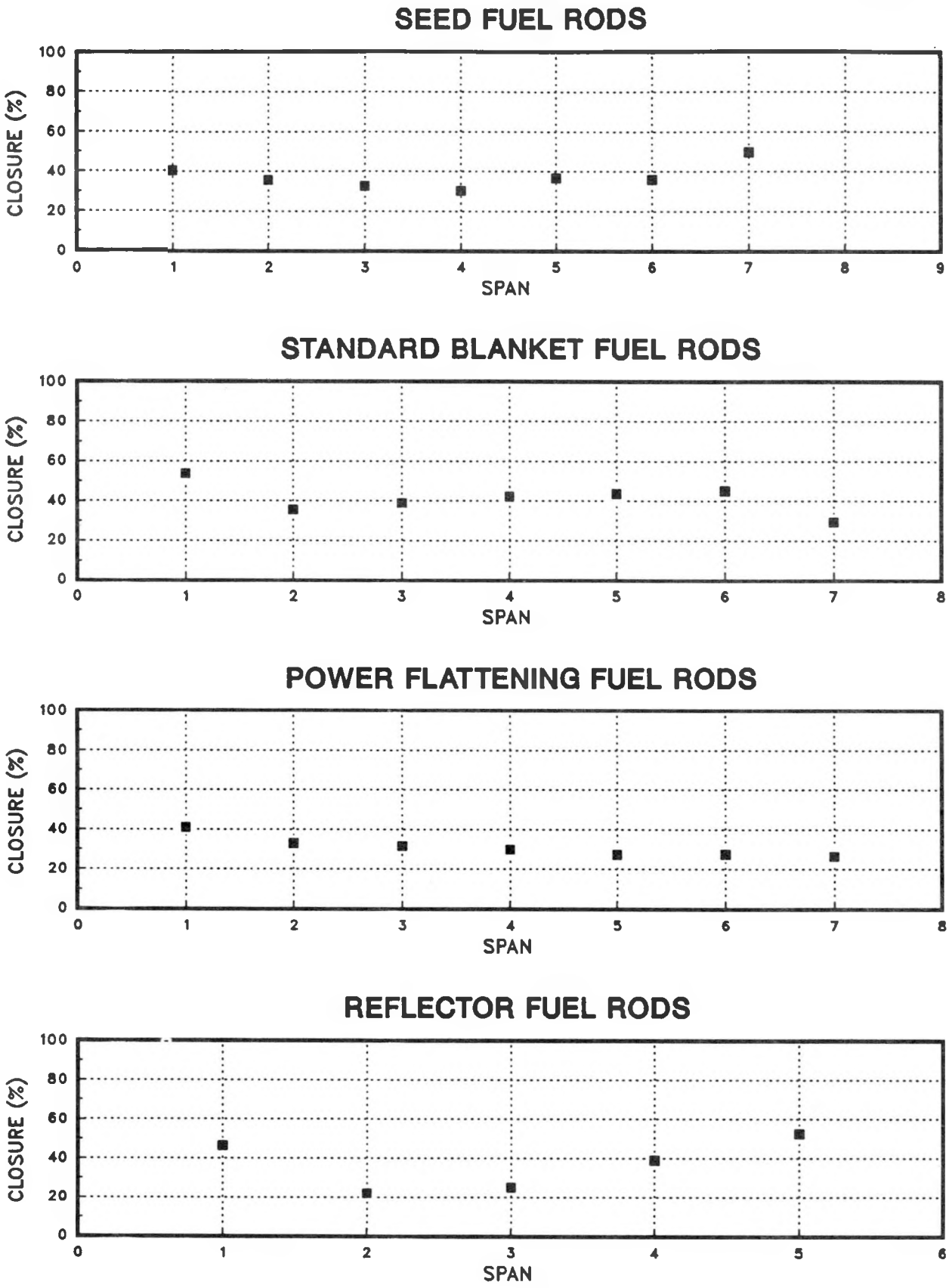

Figure 30 - LWBR Fuel Rod Channel Closure

fuel rods. Data for the 5 blanket modules examined have been pooled for this evaluation. The percent channel closure was calculated using the relationship

$$\% \text{ Closure} = 100.0 \, [G_n - (G_a - K\sigma)] \, / \, G_n \qquad (6)$$

where

G_n = nominal design gap
G_a = average measured minimum gap
K = factor for one-sided 95/95 tolerance interval
σ = standard deviation for measured minimum gap.

For the seed, calculated channel closure ranged from 30 to 50 percent and was larger at the top and bottom spans and decrease to a minimum at span 4. Calculated channel closure for standard blanket rods ranged from 34 percent for span 7 to 59 percent for span 1. Channel closure for the peak power spans (4, 5 and 6) ranged from 43 to 48 percent. For power flattening blanket fuel rods, the one-sided 95/95 percent channel closure ranged from about 31 percent for spans 5, 6, and 7 to about 48 percent for span 1. For reflector rods, the calculated channel closure was in the range of 22 to 39 percent and was largest at the top and bottom spans decreasing to a minimum at span 2.

4.3 - ROD LENGTH MEASUREMENTS

Rod in-reactor length increase results from the combined effects of thermal expansion, system pressure, irradiation growth of the Zircaloy cladding, and pellet-cladding interaction. Measured length increase, from room temperature conditions at BOL to the same temperature at EOL, includes only the permanent effects. Increases due to thermal expansion were recovered on cooldown.

Length increases of the measured rods are listed in Table 10 along with predicted increases. Plots of measured and predicted data (straight-line fit) against peak fluence levels are shown by fuel region in Figures 31 through 34. Included in these plots are results of other measurements on these and other LWBR fuel rods. Each of the twelve DE rods, for example, were also measured from neutron radiographs. The average difference between REX length

Table 10 - Fuel Rod Length Change

Sequence	Rod S/N	Cell No.	Module	As-Built Length (in.)	Post-Irrad.* Length (in.)	Length Increase (in.)	Predicted Increase (in.)	Increase from Radiographs (in.)
1	0400736	4M33	SI-1	116.636	116.934	0.298	0.438	0.32
2	0606773	6B4	SI-1	116.649	116.975	0.326	0.439	0.35
3	0205071	2Q41	SI-1	116.654	116.886	0.232	0.324	0.23
4	0507672	5L31	SI-1	116.645	116.986	0.341	0.505	0.36
5	1606710	16E57	BI-3	117.689	118.229	0.540	0.927	0.56
6	3102657	1A1	RIV-3	110.892	111.218	0.326	0.343	0.30
7	1208823	12A12	BII-2	117.683	118.141	0.458	0.667	0.48
8	2610746	26E68	BII-2	117.700	118.135	0.435	0.817	0.47
9	1105717	11A46	BI-3	117.685	118.129	0.444	0.834	0.43
10	1504272	15F11	BI-3	117.686	118.181	0.495	0.830	0.48
11	2514164	25K13	BII-2	117.688	118.069	0.381	0.611	0.38
12	2607600	26E19	BII-2	117.695	118.188	0.493	0.828	0.55
13	3107082	1A1	RIV-4	110.885	111.169	0.284	0.374	NM**
14	3206304	2D10	RIV-4	110.883	111.000	0.117	0.116	NM**
15	1601036	16E71	BI-3	117.651	118.159	0.508	0.912	NM**
16	1612146	16E20	BII-2	117.663	118.125	0.462	0.780	NM**
17	0604555	6B3	SI-1	116.633	116.949	0.316	0.454	NM**
18	0504502	5L32	SI-1	116.649	116.990	0.341	0.508	0.349***
19	1605629	16E58	BI-3	117.677	118.192	0.515	0.941	0.526***

*Measured in ECF waterpit by the REX and adjusted to 68F.
**NM Not Measured
***ANL-W Measurements (decrud rods)

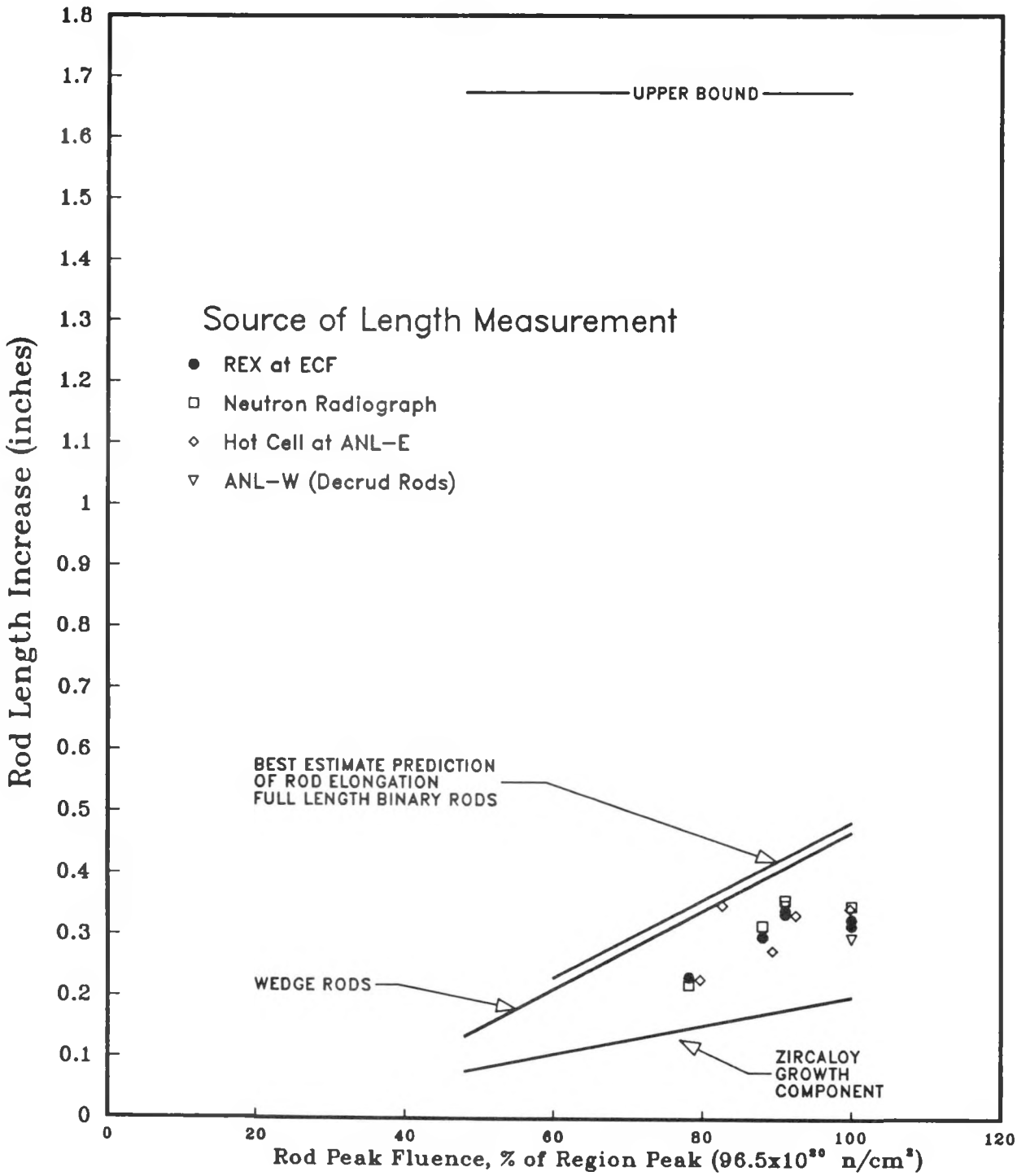

Figure 31 - Seed Fuel Rod Length Increase (RXA Cladding)

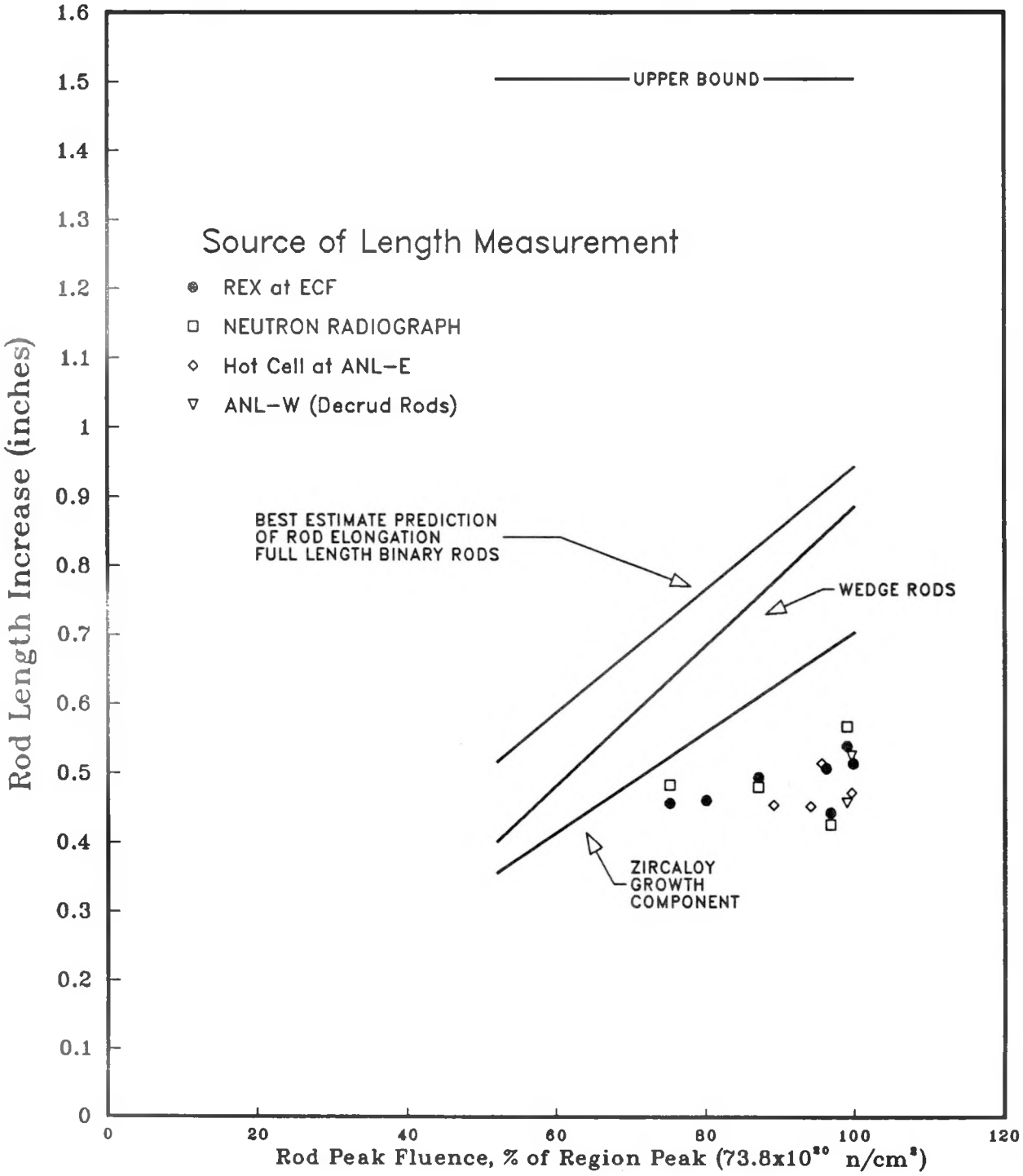

Figure 32 - Standard Blanket Fuel Rod
Length Increase (SRA Cladding)

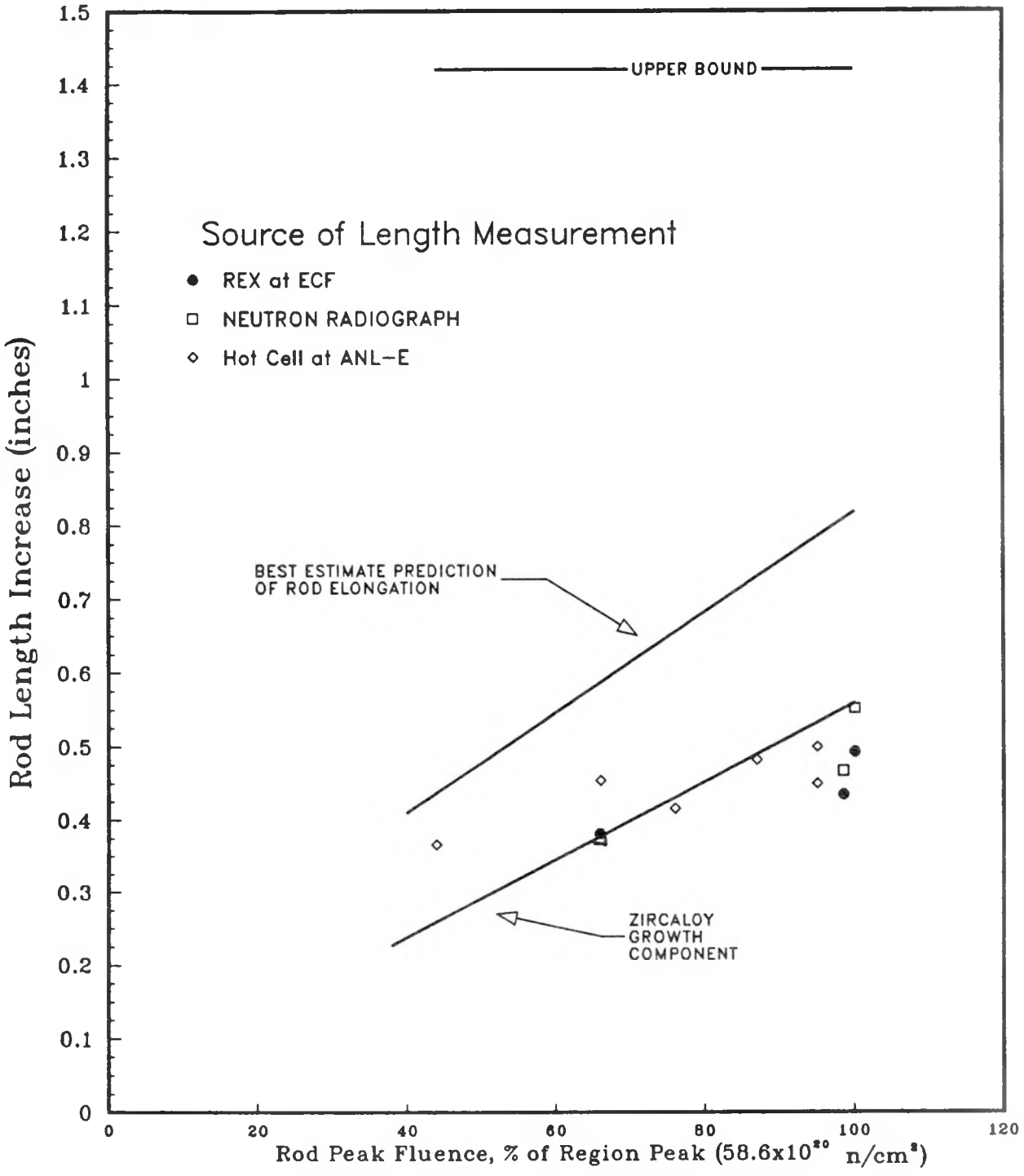

Figure 33 - Power Flattening Blanket Fuel
Rod Length Increase (SRA Cladding)

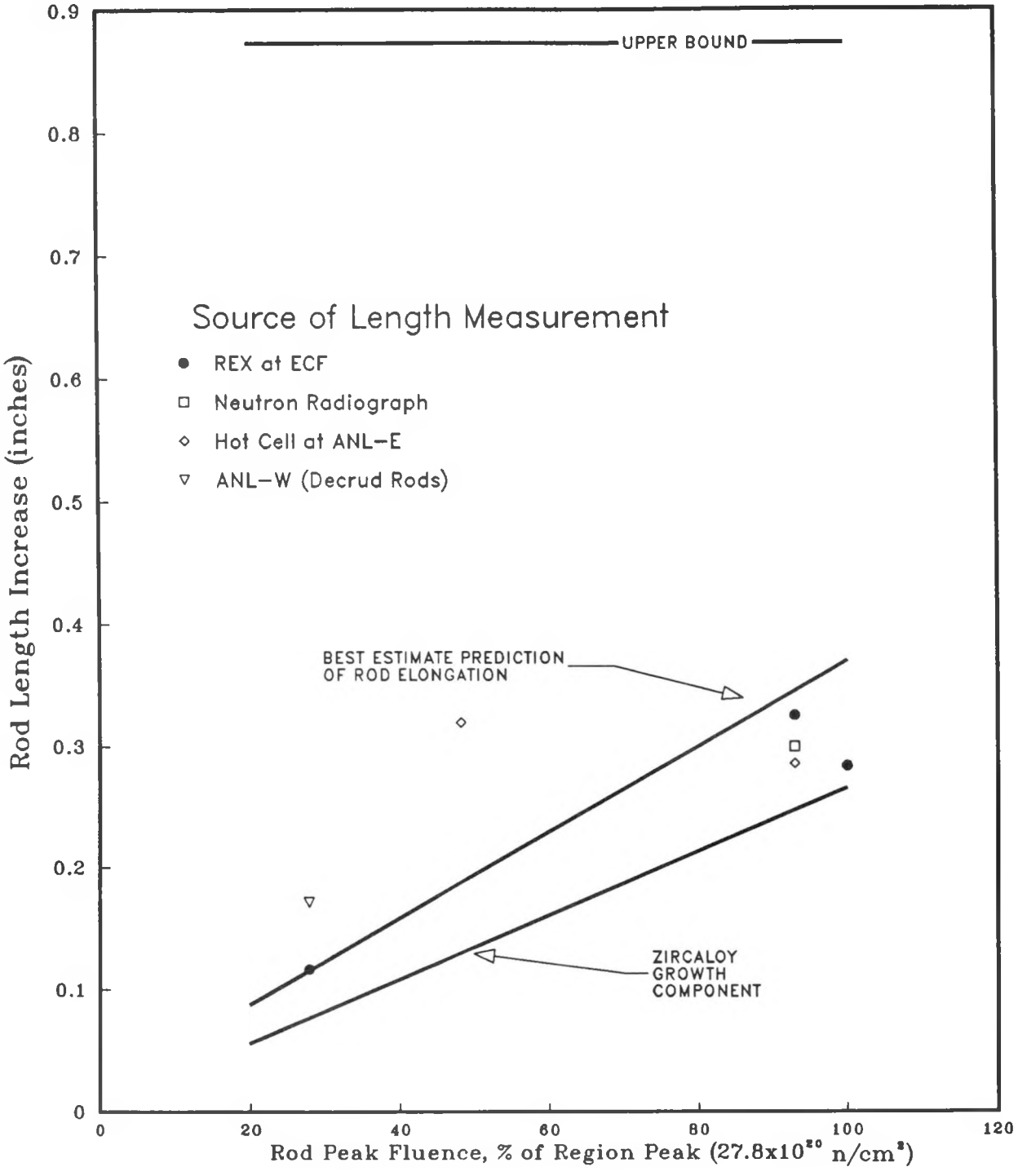

Figure 34 - Reflector Fuel Rod Length Increase (SRA Cladding)

measurements and rod lengths determined from neutron radiographs was 0.011 inch and the maximum difference was 0.057 inch. Other rods from LWBR modules were measured by ANL-W in preparation for crud analysis and by ANL-E in preparation for destructive assay in the proof-of-breeding program.

Prediction lines are shown based on CYGRO analysis of fuel rod length changes in Figures 31 through 34. The line representing Zircaloy growth is the expected minimum. The upper bound line is a worst case prediction for each fuel region that includes all biases, peaking factors, and conservative parameters aimed toward prediction of maximum rod elongation. All measured length changes were well below the upper bounds. Most points were below the best estimate lines, and some points fell below the Zircaloy growth lines. These elongations at lower than predicted levels were favorable for fuel rod performance and indicate some conservatism, even in the best estimate analysis model.

As shown in Figure 31, length changes of the seed rods (RXA cladding) were more than the Zircaloy growth component (as expected), but less than the best estimate predicted total elongation. Apparently, the amount of pellet-cladding interaction (PCI) built into the seed rod analysis model, and based on irradiation test rod experience, did not occur in the LWBR rods. A major cause of PCI in the seed rod model was the effect of postulated loose fuel chips lodged in the fuel-cladding gap. The reduced elongations indicate that the chip effect was not as extensive as assumed in the best estimate model.

Measured length changes of standard blanket and power flattening blanket fuel rods (Figures 32 and 33) indicate that the Zircaloy growth component for SRA cladding is overpredicted at the higher fluence levels. Length increases of rods from the two blanket regions, plus data from the SRA cladding of reflector rods, are combined in Figure 35 to provide a comparison with predicted Zircaloy growth. Saturation appears to occur above a peak fluence of about 50×10^{20} n/cm^2, at which level the rod elongation slows significantly and is not appreciably affected by increased exposure. This effect was not included in the prediction model.

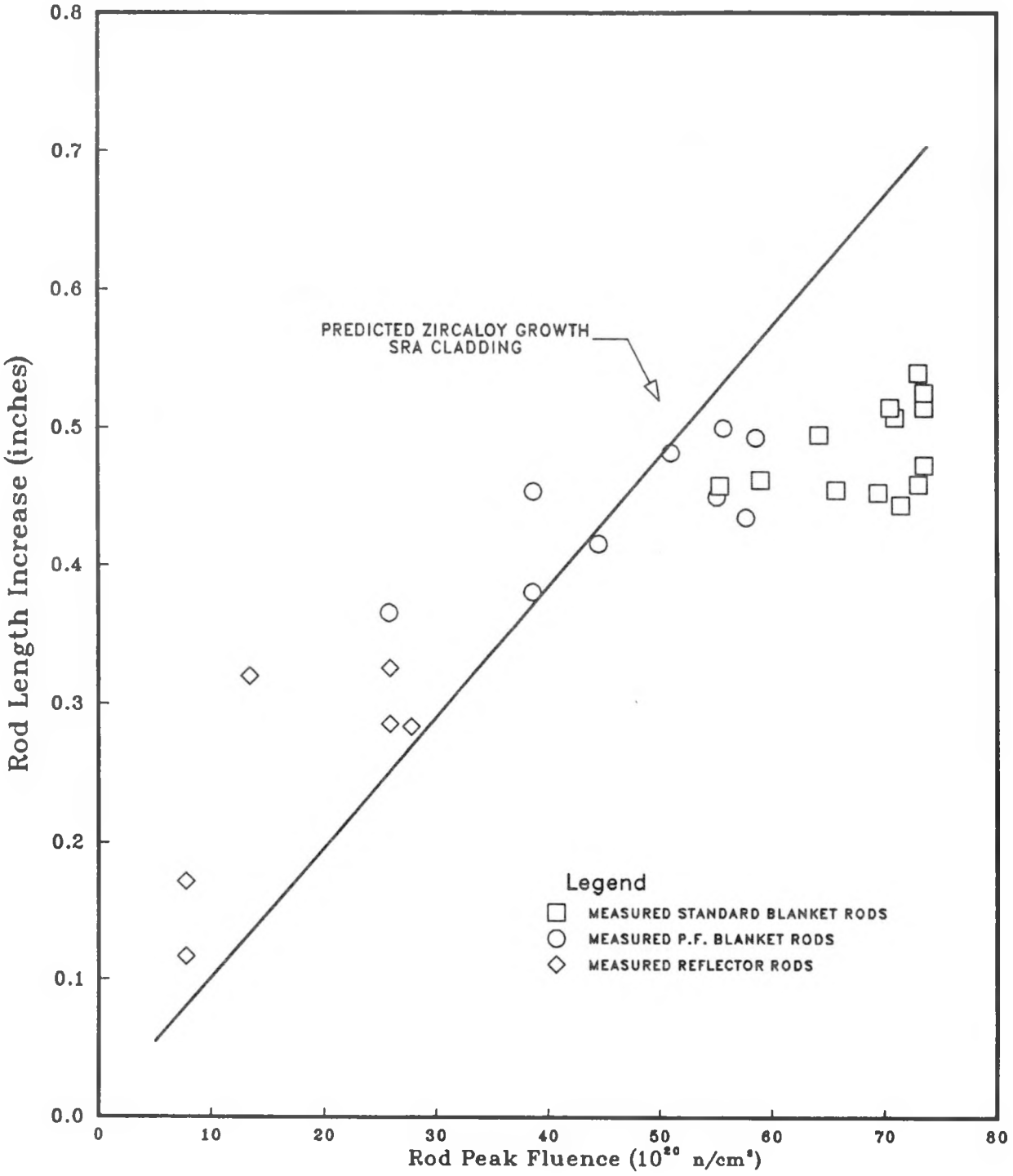

Figure 35 - Combined Standard, Power Flattening Blanket, and Reflector Fuel Rod Length Increases (SRA Cladding)

Pellet-cladding interaction effects on rod elongation were over-estimated for blanket rods also. A pellet-cladding ratchetting mechanism was included in the blanket rod analysis to account for the alternate gripping and releasing of the cladding and fuel stack during the 10 pressure cycles of LWBR (Reference 23). A pressure cycle begins at operating temperature and pressure, includes the plant shutdown and depressurization, and is completed with the return to operating temperature and pressure.

In the CYGRO calculations for a worst case blanket rod, the coolant pressure cycle imposed rod length increase ranged from 0.082 inch per cycle early in life to 0.042 inch per cycle in extended lifetime, when fuel temperatures and system temperature and pressure were lower. The net increase following each cycle was less due to stress relaxation, so that the accumulated length increase attributed to pressure cycling was 0.23 inch calculated. Since the measured increase of 0.49 inch was less than the predicted Zircaloy growth of 0.56 inch for this rod, it is concluded that the major portion was Zircaloy growth and that pressure cycling did not contribute significantly to the measured rod length increase.

To convert the measured rod lengths at end-of-life to rod lengths in-reactor and at power, the effects of temperature reduction and system depressurization were added back into the length data. This is shown in Table 11 for the worst case rod in each fuel region to estimate the minimum rod-to-baseplate clearance that existed during power operations. As shown in Table 11, all clearances were greater than the equivalent of one rod diameter, ranging from 1.9 diameters in reflector modules to 5.6 diameters in seed modules. Thus, the design objective of no interference with coolant flow at the baseplates was met.

4.4 - VISUAL OBSERVATIONS

Almost 1100 LWBR fuel rods* were visually examined and videotaped at one orientation as they were removed from the 12 modules listed in Table 12. Rod surfaces exhibited the same range of conditions observed during the module

*At beginning of core life, the rods were black. As in-service life and corrosion oxidation progressed, the rod surface color changed from black to white.

Table 11 - Minimum Rod-to-Baseplate Clearances (Inches)

Fuel Region	Seed	Standard Blanket	Power Flattening Blanket	Reflector
Minimum As-built Clearance	1.81	2.93	2.93	1.93
Module Post or Shell Growth	0.42	0.27	0.27	0.11
Maximum Rod Length Change:				
Measured Cold	0.35	0.54	0.50	0.33
Cold to Hot, Calculated	0.13	0.13	0.13	0.12
Net Changes, Hot	0.48	0.67	0.63	0.45
Clearance, Hot	1.75	2.53	2.57	1.59
Design Limit on Hot Clearance*	0.31	0.57	0.53	0.83
Ratio of Hot Clearance to Design Limit	5.6	4.4	4.8	1.9

*Equivalent to one rod diameter.

Table 12 - Fuel Rod Visual Examinations During Rod Removal

Module	Rods Examined
SI-1	50
SII-3	127
SIII-1	42
SIII-2	39
BI-3	52
BII-2	84
BIII-2	391
BIII-6	84
RIV-3	33
RIV-4	76
RIV-9	57
RV-4	37
Total	1072

visual examinations at the Shippingport reactor site (Reference 4). The upper and lower portions of the rods appeared smooth and uniformly dark gray or black with some occasional scratches and minor color variations. Mottled and speckled areas were generally associated with the high power, binary fueled, higher-cladding-temperature regions near the middle of the seed and blanket rods. A range of speckled intensity appeared on the outer row of blanket rods (Figure 36). Several rods showed dark circumferential bands at locations corresponding to fuel pellet interfaces. Flow pattern indications of wear marks from grid contact points were observed in expected locations (e.g., free end grid level) near the top of bottom-mounted rods and at the bottom of top-mounted rods. There was no evidence of gross cladding deformation, cracked cladding, excessive wear, or any other unusual conditions.

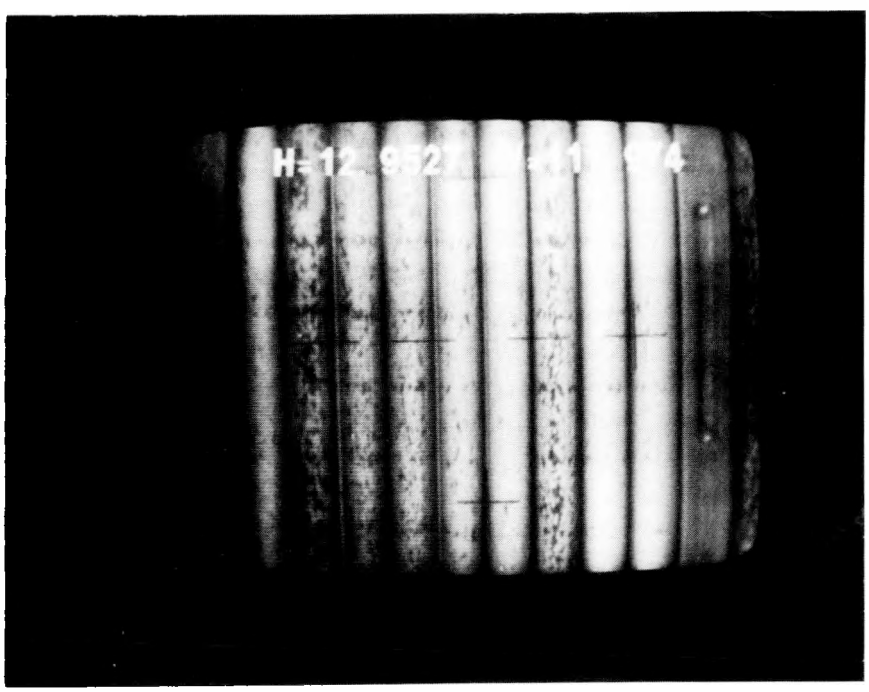

Figure 36 - Outer Row of Fuel Rods in Blanket Module II-2

The REX performed closer examination of individual fuel rods with an underwater black-and-white video camera. The entire outer surface of each rod was examined at approximately 4X magnification. Locations of unusual conditions and suspected wear marks were then examined further with other REX instrumentation. Rod surface appearances of shades of gray and speckled transition regions correlated with measured profiles of surface oxide thickness. However, occasionally, adjacent rods were of different color.

Typical rod surface appearance for seed rods is shown in Figure 37. Vertical lines at the top and bottom of the seed rod, although appearing as cladding wrinkles, showed no indication of cladding deformation when measured by the orbiting profilometer. From about 34 inches to 42 inches from the top of the rod, the surface became uniformly gray. Below 42 inches, white speckling appeared and became more dense over the high power segment of the rod (peak depletion, a measure of lifetime-average peak power, occurred near the 63-inch level). Below 83 inches, widely scattered dark spots appeared on a light background. Toward the rod bottom, the surface darkened, indicating negligible post-transition oxide.

Figure 38 shows the surface appearance for a typical blanket rod. The rod shown was a thoria wedge rod, with binary fuel in the top half and thoria fuel in the bottom half. The surface was dark at the top, with vertical surface lines, then uniformly gray down to the 30-inch level where dark speckles appeared. Occasionally, a solid black area appeared (such as at 35 inches) which coincided with a grid level. Speckling continued across the binary-thoria interface at 61.7 inches, becoming darker below the interface. The surface was uniformly dark below 92 inches, and vertical lines reappeared at the bottom.

Surface speckling appeared when oxide growth was in transition between uniformly dark segments (where oxide was minimal), and uniformly light gray areas (where oxide formation was in more advanced stages). Fuel rods that were located in high fast flux regions (such as seed rod 0606773 or standard blanket rod 1606710) had surfaces of uniform light gray over most of the fuel length. On blanket rods, dark bands appeared (Figures 36 and 39) at pellet

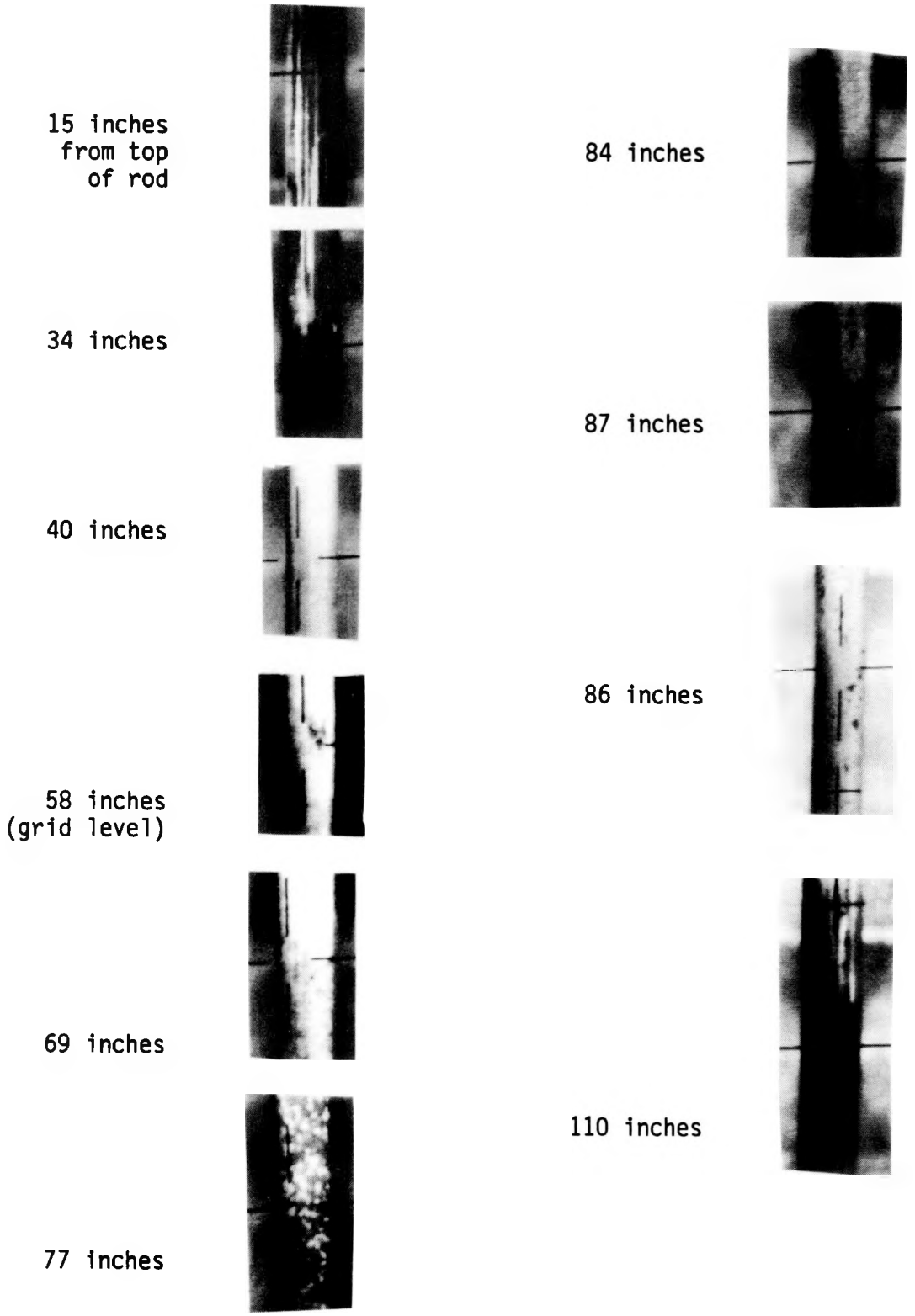

Figure 37 - Visual Examination of Seed Rod 0507672

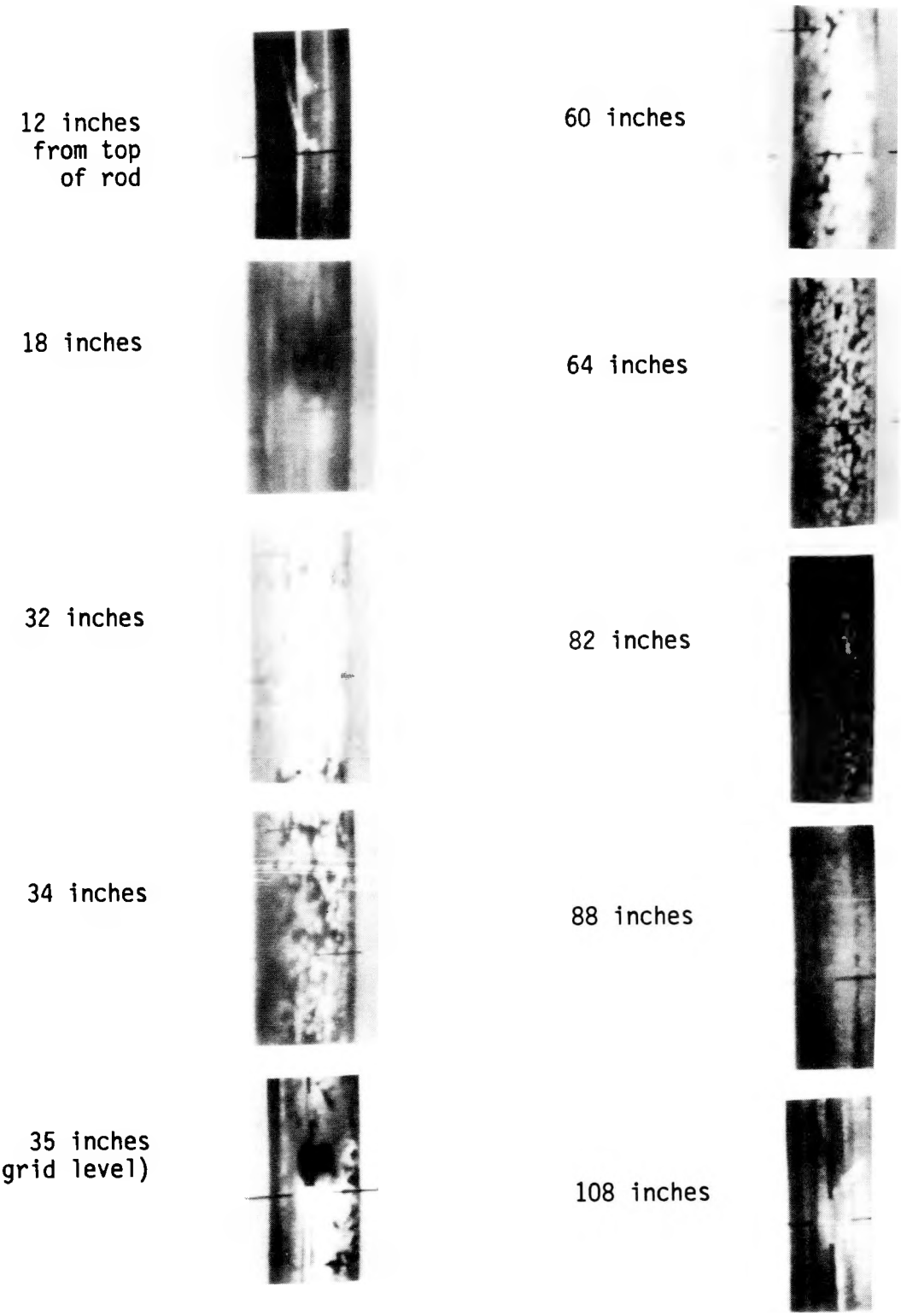

Figure 38 - Visual Examination of Standard Blanket Rod 1105717

27 inches
from rod top

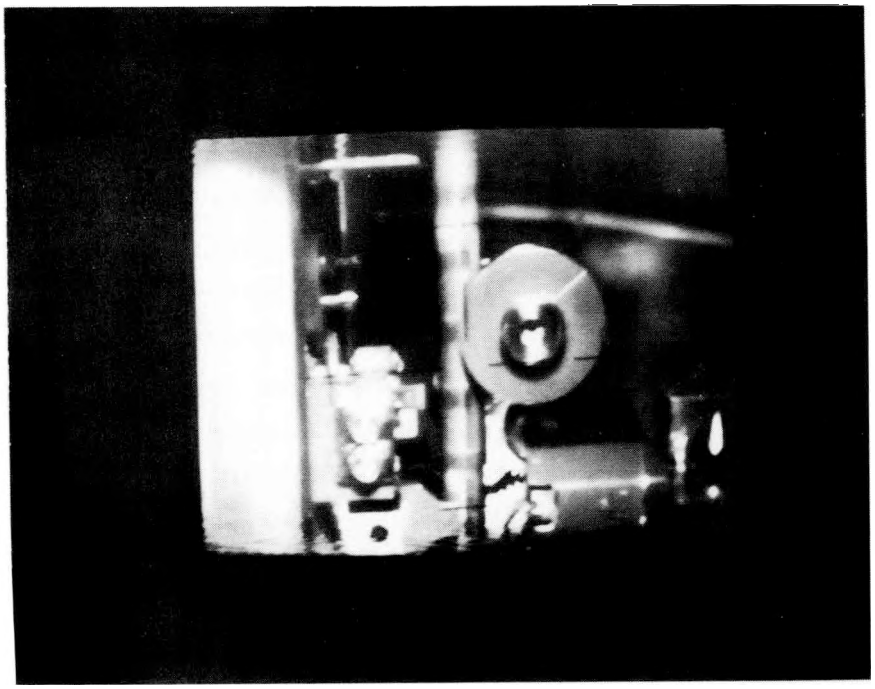

37 inches
from rod top

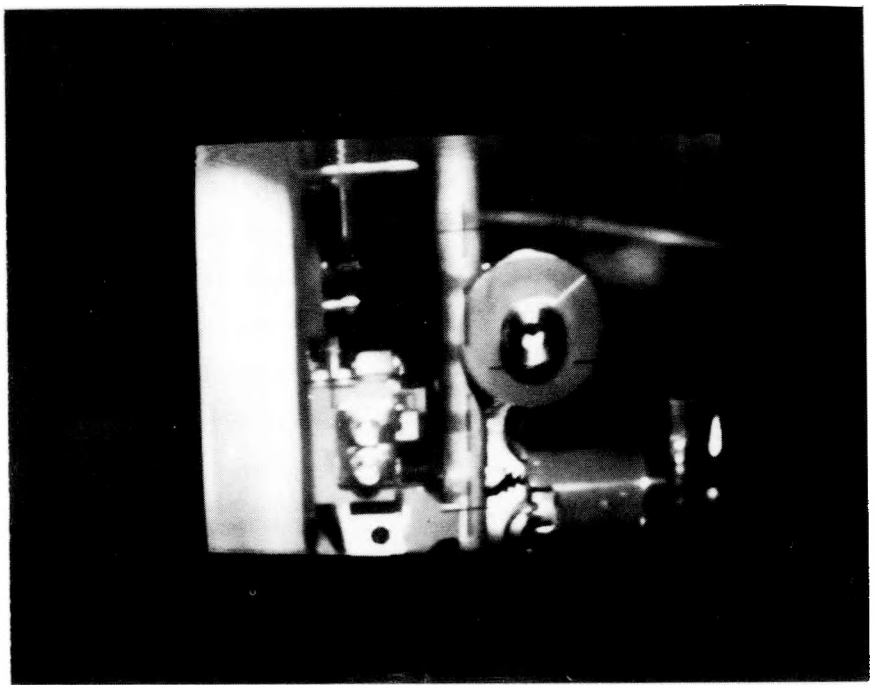

Figure 39 - Standard Blanket Rod 1606710 Mounted in REX with Axial Profilometer Engaged

interfaces, indicating reduced oxide at these lower temperature locations. (The blanket rod in Figure 39 is shown mounted in the REX with the axial profilometer instrument and rollers in place.)

Locations of grid spring and dimple contact with the fuel rod surface were identified by flow patterns such as those shown in Figure 40 for seed, blanket, and reflector rods. The marks on reflector rod 3102657 were the only marks to have wear depths of any significance.

In general, visual exams of fuel rods both in-bundle and individually provided a record of rod surface condition and indicated areas requiring further examination. Axial variations in surface oxide are evident in the shades of gray and in speckle density. Flow patterns provide the only indication of grid contact and possible wear mark locations. Results of surface probes with the axial and orbiting profilometers gave no indications of unexpected surface conditions as discussed in Section 4.6 and 4.8.

4.5 - FREE HANGING BOW

Fuel rod free hanging bow measurements were used during rod fabrication to determine fuel rod straightness. Results from the examination were used to calculate seating force and BOL bow of each rod in a "perfectly aligned" support system. Rods requiring seating forces beyond the support system capability and rods with large calculated in-bundle bows were not used in LWBR.

Free hanging bow at EOL was measured for five seed rods, four standard blanket fuel rods, three power flattening blanket fuel rods, and three reflector fuel rods to determine the effects of irradiation on the free hanging bow of the rods and to determine EOL in-bundle bow of the rods.

Figures 41, 42, and 43 present typical seed, blanket (standard and power flattening), and reflector EOL free hanging bow data. The top frame (frame 1) in these figures shows the measured rod centerlines for three or four tracks along the fuel rod. Frame 2 presents the best fit radial position (free hanging bow) for the rod center positions shown in frame 1. As-fabricated free hanging bow is also presented on frame 2 for the seed and reflector

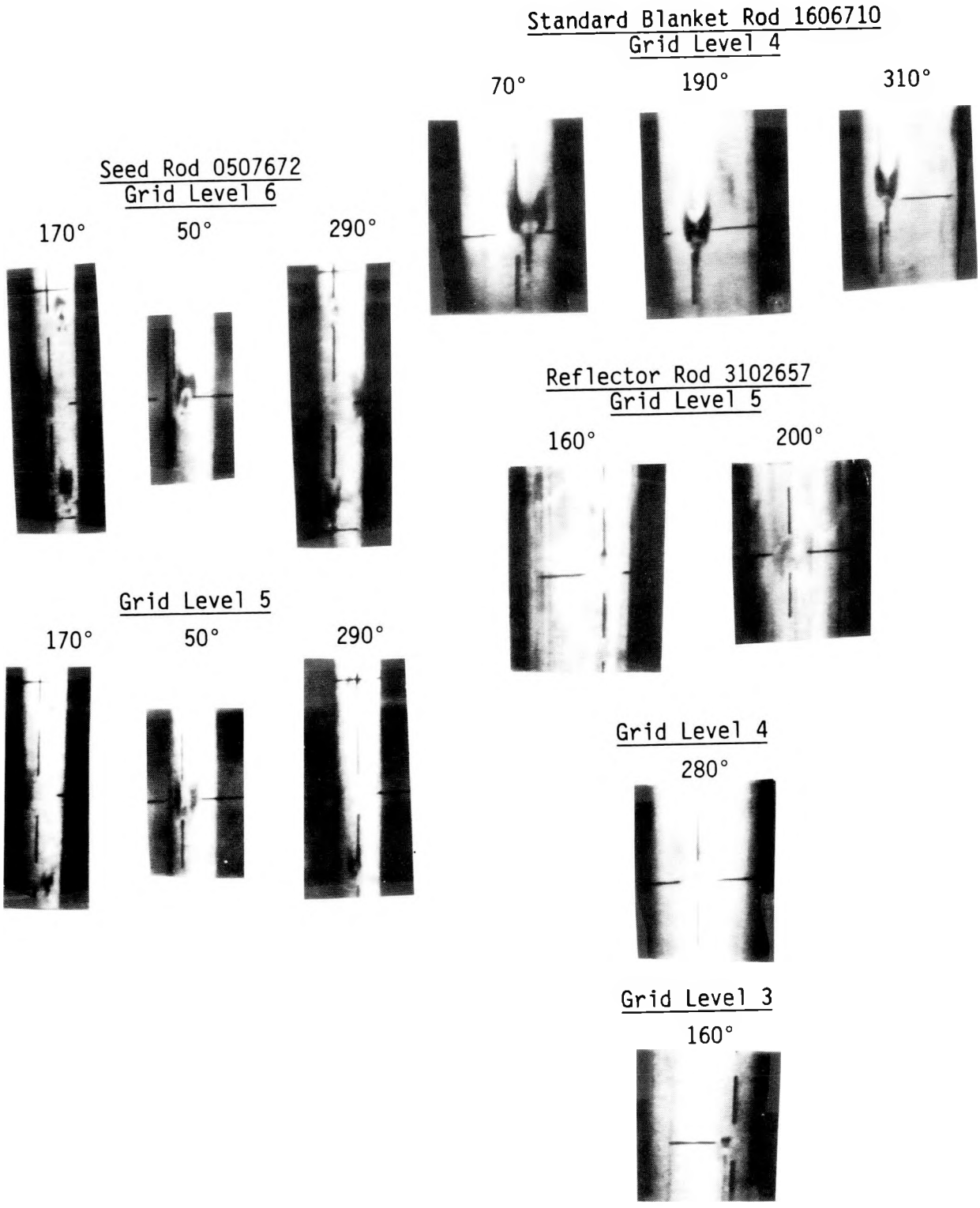

Figure 40 - Flow Patterns at Grid Locations

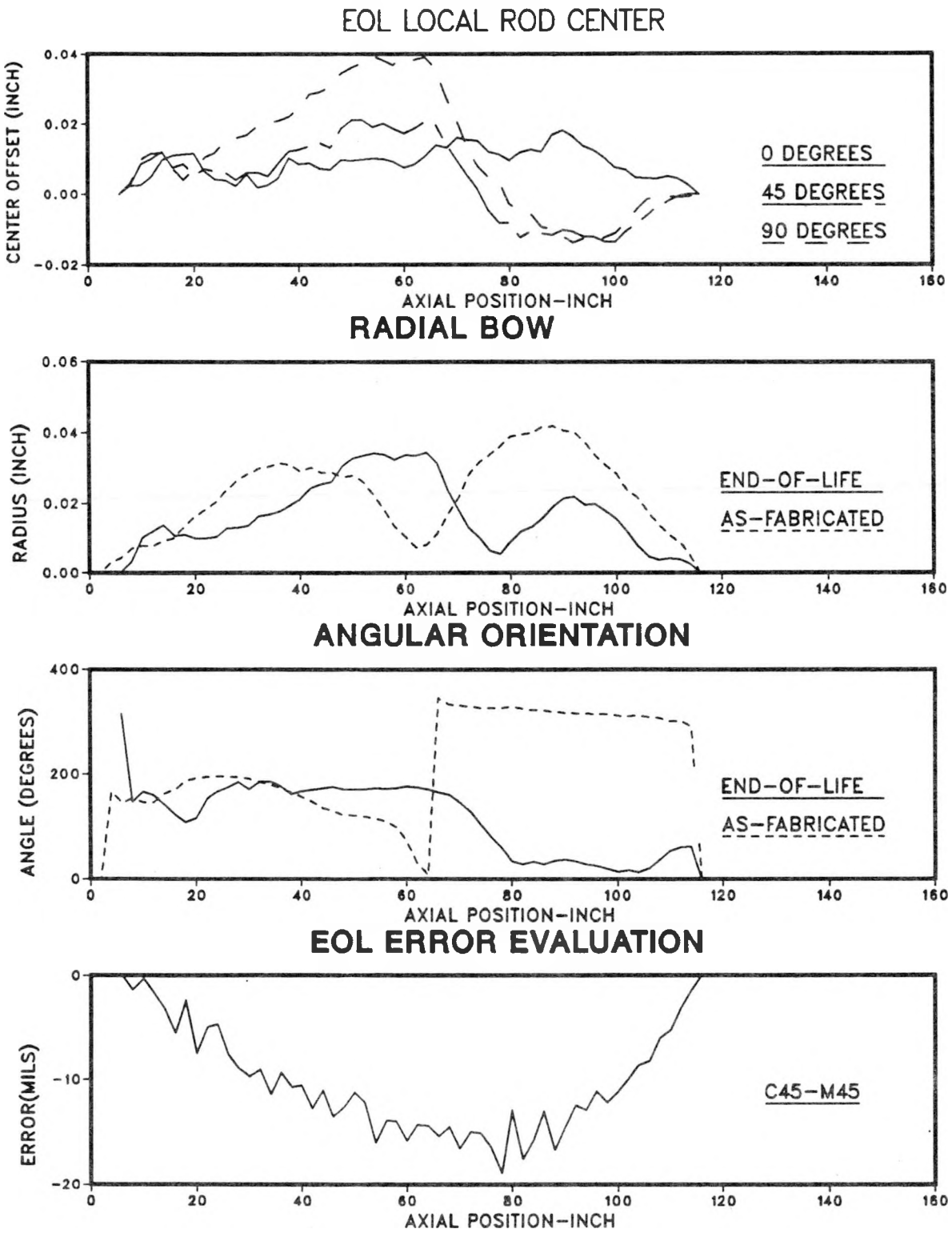

Figure 41 - Seed Rod 0507672 Free Hanging Bow

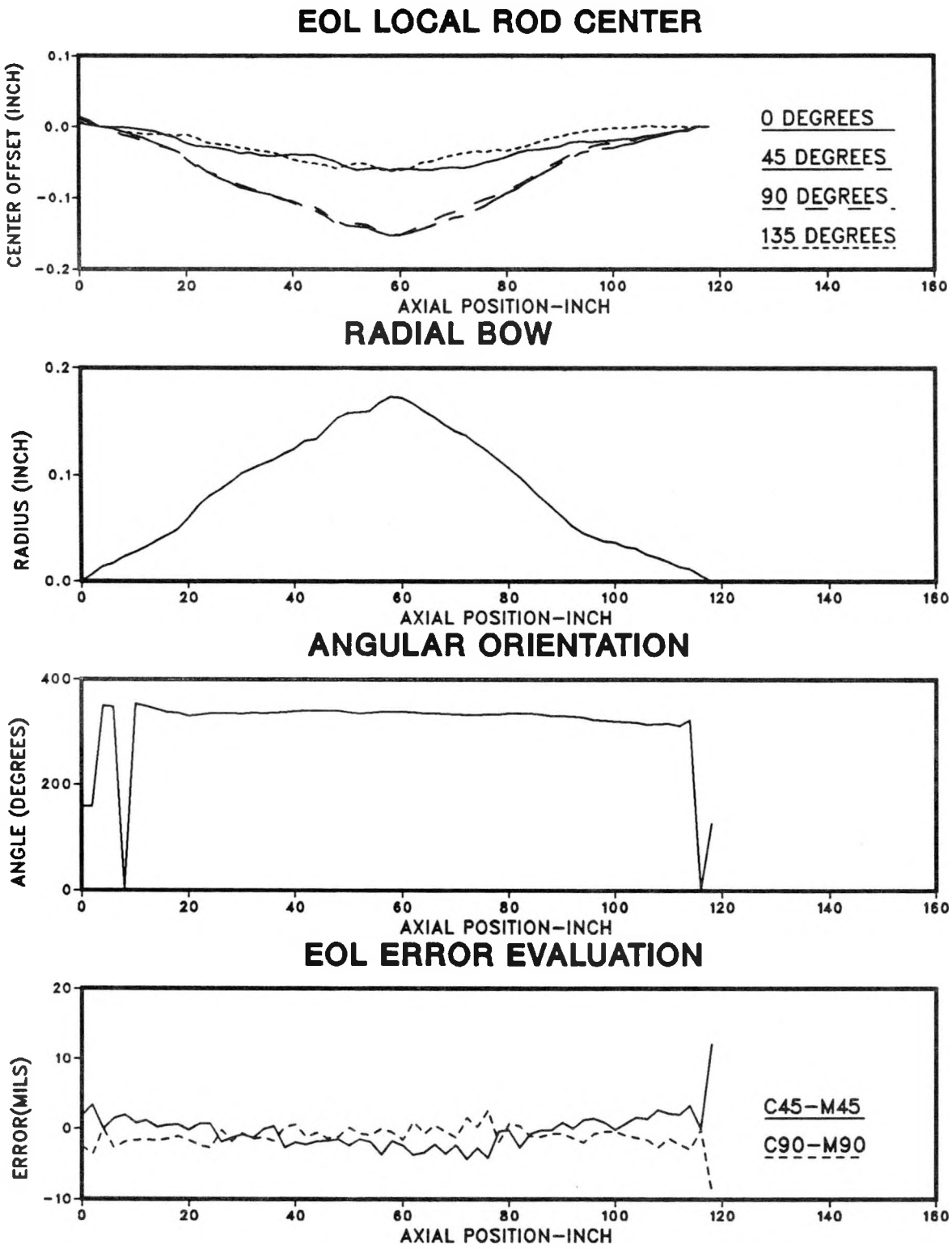

Figure 42 - Blanket Rod 1105717 Free Hanging Bow

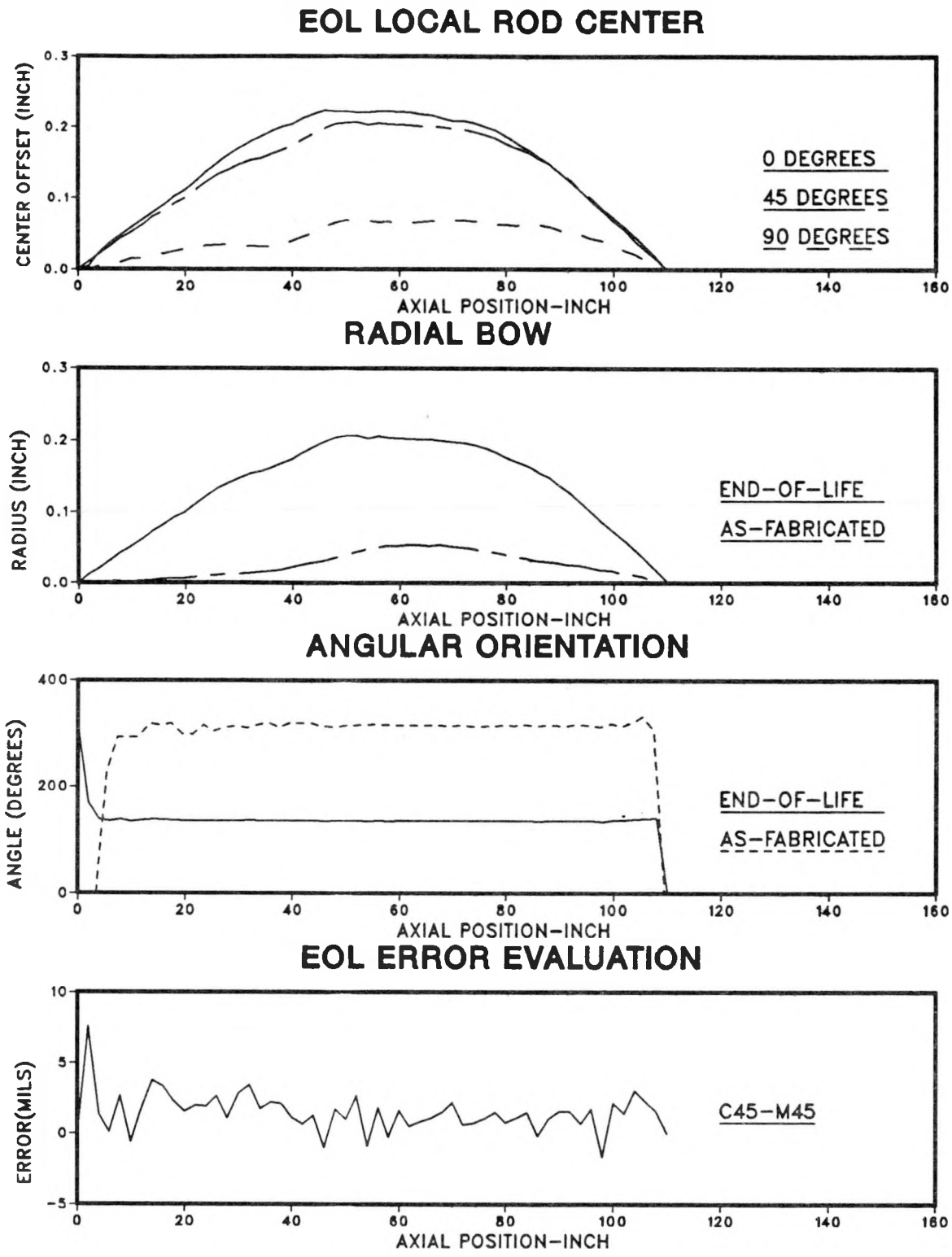

Figure 43 - Reflector Rod 3102657 Free Hanging Bow

rod. As-fabricated free hanging bow data were not available for all blanket fuel rods and for some seed rods. Frame 3 of the figures show "best fit" angular orientation for the measured rod centers. The bottom frame (frame 4) shows the difference between measured and calculated bow at 45 and 90-degree orientations for the EOL free hanging bow measurements. Differences between measured and calculated bow at 45 degrees and 90 degrees were used to monitor accuracy of the measurements.

As shown in Figure 41, comparison of the as-fabricated and EOL free hanging bow for seed rod 0507672 from seed module SI-1 indicated that the peak decreased slightly during reactor operation. The maximum chordal bow at BOL was approximately 0.040 inch at BOL and decreased to about 0.030 inch at EOL. The rod had a multi-peaked as-fabricated and EOL free hanging bow. Loads on the rod from the support system apparently shifted the peaks slightly toward the top of the rod during reactor operation. Angular orientation of the free hanging bow did not change significantly during operation. Measurements of bow for SI-1 (Reference 4) indicate that the module bowed only 0.03 inch during core life. Peak chordal bows for all seed rods examined for free hanging bow are summarized in Table 13. Available BOL data are also presented for comparison.

As shown in Figure 42, the peak EOL chordal bow for the blanket rod 1105717 from blanket module BI-3 was 0.16 inch at the middle of the rod. Measured EOL bow for blanket module I-3 was 0.033 inch. Angular orientation of free hanging bow of the rod was nearly constant along the entire length of the rod. As indicated above, BOL free hanging bow data for blanket rods were not available for comparison with EOL data. Peak chordal bows for all standard and power flattening fuel rods examined for free hanging bow are also presented in Table 13.

As shown in Figure 43, comparison of the as-fabricated and EOL free hanging bow for reflector rod 3102657 from module RIV-4 indicated that the free hanging bow changed significantly. The peak chordal bow increased from 0.040 inch at BOL to 0.200 inch at EOL. The angular orientation for the bow

Table 13 - Fuel Rod Free Hanging Bow Measurement Summary

		BOL		EOL	
Rod Type	Rod S/N	Bow (in.)	Angle	Bow (in.)	Angle
Seed	0400736	N/A	N/A	0.060	12.1
	0606773	N/A	N/A	0.083	18.3
	0205071	0.043	55.3	0.089	354.3
	0507672	0.042	317.9	0.039	167.3
Standard Blanket	1606710	N/A	N/A	0.077	351.7
	1208823	N/A	N/A	0.128	358.1
	1105717	N/A	N/A	0.162	337.5
	1504272	N/A	N/A	0.056	74.2
Power Flattening Blanket	2610746	N/A	N/A	0.136	125.4
	2514164	N/A	N/A	0.242	190.9
	2607600	N/A	N/A	0.083	169.0
Reflector	3102657	0.053	314.9	0.206	135.5
	3206304	0.042	106.7	0.242	133.1
	3107082	0.074	287.6	0.291	67.4

changed from a 150-degree angle relative to the fuel rod serial number at BOL to a 300-degree orientation at EOL. The large change in free hanging bow of reflector rod 3102657 was most likely due to flux-gradient induced bow of the module. Module bow measurements indicate that module RIV-4 had an EOL bow of 0.24 inch. Results of free hanging bow measurements of other reflector rods are presented in Table 13.

Table 14 presents calculated in-bundle span bows for all of the rods evaluated for free hanging bow at EOL. Table 14 also presents for comparison worst case EOL bows predicted with the ROBOT computer program (Reference 20). The calculated in-bundle bows were determined using a plane frame finite-element computer program in which 50 to 60 straight beam elements were used to

model the free hanging bow of the rod at 0-degree and 90-degree orientations. Displacements were then imposed on the rod to seat it at each of its grid contact points. Restrained shapes of the rods at 0-degree and 90-degree orientations were then combined vectorially to obtain the EOL in-bundle bow. For rods from seed and Type I blanket modules where EOL module bow was small (0.01 to 0.03 inch), the grid contact points were assumed to be aligned along a straight line. For rods from Type II blanket modules and reflector modules where measured EOL module bow was large (0.10 to 0.24 inch), the grid contact points were assumed to follow the module bow shape. It was also assumed that the angular orientation for fuel rod free hanging bow and module bow coincided. In either case, the in-bundle bows reported represent the peak bow relative to a line through the seating points in adjacent grids.

Except for span 7 of rod 1606710, calculated EOL in-bundle span bows from free hanging bow data were significantly smaller than worst case bow predictions. They were slightly (0.004 inch or less) greater than statistical in-bundle bows calculated using propagation of error techniques. This is consistent with in-bundle bow measurements presented in Section 4.2. A 0.025-inch bow was calculated for the span near the free end of rod 1606710. This bow is larger than expected.

4.6 - CLADDING DIAMETER AND IN-STACK OVALITY MEASUREMENTS

Cladding outside diameter was measured with the REX axial profilometer at 0.010-inch intervals on four axial tracks on the surface of each fuel rod. After the first 12 rods, measuring increments were increased from 0.010 inch to 0.020 inch without significant loss of information. Measurements were made over more than 90 percent of a rod length. (Several inches were missed at each end to accommodate rod positioning devices.) Diameters from the four tracks, taken at 45-degree intervals, were combined to form axial profiles of average diameter and cladding ovality over the measured length. Additional in-stack ovality measurements were made with the orbiting profilometer to confirm that the ovalled surface had a smooth geometry and was not subject to local bending or wrinkling.

Table 14 - Calculated In-Bundle Fuel Rod Bow
Based on Free Hanging Bow Measurements

Seed Fuel Rods

Rod S/N	Module ID	Module Bow (in.)	Span Bow (mils) 1	2	3	4	5	6	7	8
0400736	SI-1	0.010	4.6	8.4	2.2	5.7	5.7	4.4	2.0	3.8
0606773	SI-1	0.010	8.5	7.4	6.1	14.8	5.6	4.4	2.5	4.1
0205071	SI-1	0.010	11.9	5.4	2.7	2.8	8.6	3.6	5.6	6.6
0507672	SI-1	0.010	4.9	1.8	2.6	2.8	4.2	3.0	2.7	2.0
W.C. Predicted Bow			64.9	47.4	53.4	38.9	--	--	--	--
Statistical Limit			18.8	17.7	21.1	16.3	--	--	--	--

Standard Blanket Fuel Rods

Rod S/N	Module ID	Module Bow (in.)	Span Bow (mils) 1	2	3	4	5	6	7
1606710	BI-3	0.033	3.5	15.9	17.3	6.3	5.0	10.4	24.8
1208823	BII-2	0.098	1.8	7.4	6.7	18.3	6.6	2.5	2.0
1105717	BI-3	0.033	8.0	5.5	10.0	14.3	4.7	5.8	3.4
1504272	BI-3	0.033	1.4	11.3	12.1	1.9	5.2	11.1	1.8
W.C. Predicted Bow			61.1	44.7	41.8	39.3	--	--	--
Statistical Limit			17.1	14.3	14.4	14.2	--	--	--

Power Flattening Blanket Fuel Rods

Rod S/N	Module ID	Module Bow (in.)	Span Bow (mils) 1	2	3	4	5	6	7
2610746	BII-2	0.098	4.2	11.5	8.9	7.7	10.7	2.9	6.0
2514164	BII-2	0.098	5.4	6.6	2.6	9.9	7.4	5.9	2.2
2607600	BII-2	0.098	2.3	5.1	5.9	7.6	4.2	8.1	4.6
W.C. Predicted Bow			61.1	44.7	41.8	39.3	--	--	--
Statistical Limit			17.1	14.3	14.4	14.2	--	--	--

Reflector Fuel Rods

Rod S/N	Module ID	Module Bow (in.)	Span Bow (mils) 1	2	3	4	5
3102657	RIV-3	0.239*	5.1	14.9	9.7	12.5	3.7
3206304	RIV-4	0.239	7.2	2.8	7.4	15.1	2.9
3107082	RIV-4	0.239	6.7	3.6	9.6	6.3	13.7

*Module bow not measured; bow assumed to be equal to bow for reflector module IV-4.

Diameter shrinkage was less than predicted for all types of fuel rods. This comparison is consistent with those of rod and fuel stack length increases which indicated that pellet-cladding interaction in the axial direction did not reach predicted levels. Cladding ovality also was less than predicted due to the absence of significant gaps in the fuel stack and shorter-than-expected plenum gaps. The decreased amount of cladding shrinkage and ovality was beneficial to rod performance concerns of cladding strain, power ramping capability, and residual grid spring force.

Axial profiles of measured cladding diameter are shown in Figures 44, 45, and 46 for the first 12 rods examined. Included in these plots are the as-built average diameter, from measurements at four locations along the rod, and the predicted diameter profile based on the CYGRO cladding shrinkage model with best estimate rod parameters, physics peaking factors, and power history. A summary of measured and predicted maximum diameter shrinkages is given in Table 15.

Seed rod diameter profiles are shown in Figure 44. The profile for rod 0606773 shows diameter depressions of about 0.0005 inch caused by the decreased surface oxide thickness at grid levels. Oxide thickness constituted part of the measured diameter but was not included in the predicted diameter. The remaining three seed rods had diameter profiles that varied cyclically every 6 inches over the rod length. Diameter cycling resulted from the tubing manufacture process and can be correlated with cycling in strip chart recordings of cladding thickness measurements of the fabricated fuel rod. Cycling was also evident in post-irradiation diameter measurements made by ANL-W during rod crud examination.

Comparative plots (Figure 44) indicate that seed diameter shrinkage was overpredicted by approximately 0.001 inch, which is a significant part of the 0.0023 maximum shrinkage predicted for seed rods. When oxide thicknesses from Section 4.9 are considered, however, the difference between measured and predicted shrinkage is within approximately 0.0005 inch. It is also apparent from the measured diameter profiles that no fuel-cladding contact occurred, as

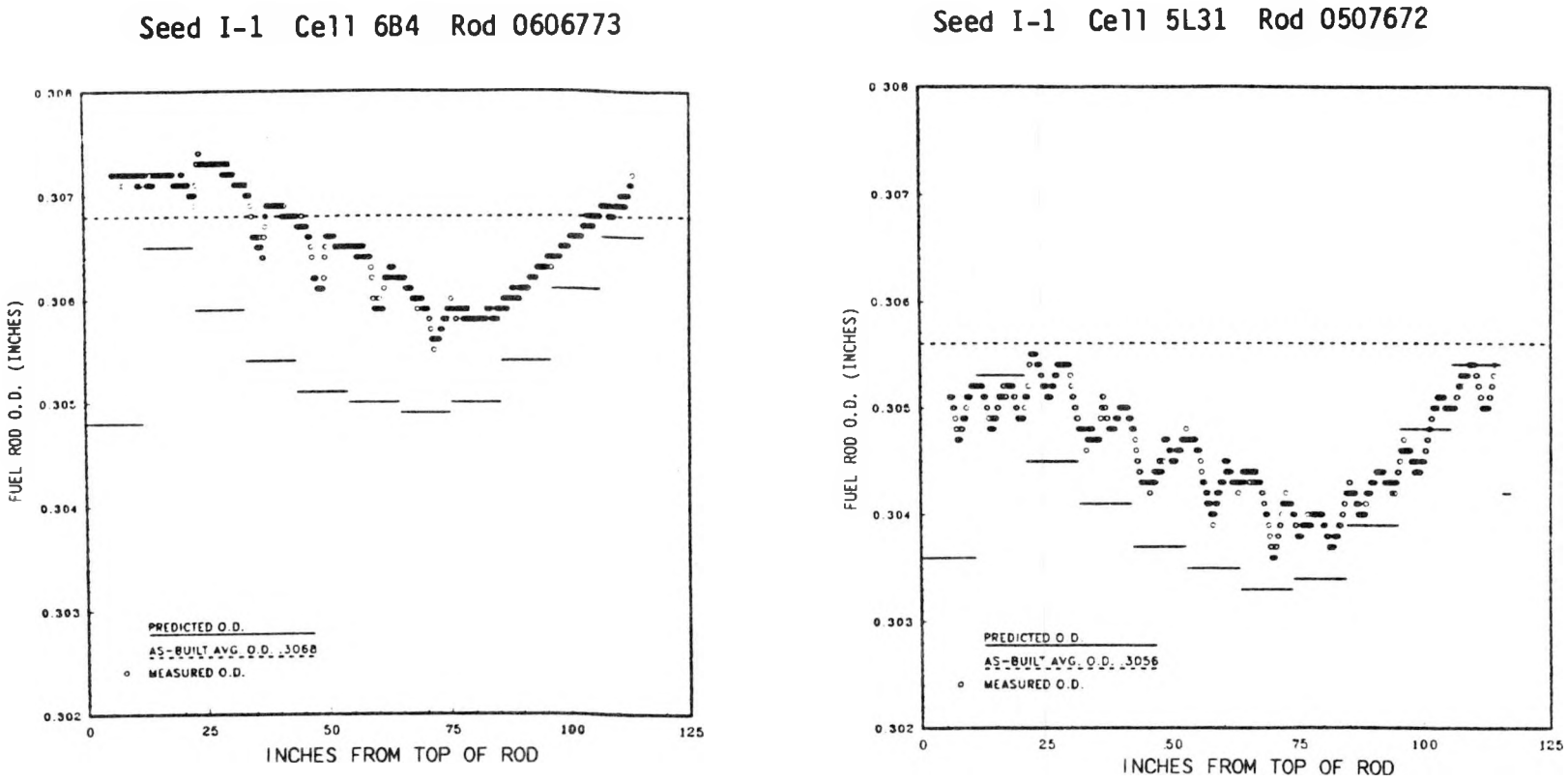

Figure 44 - Seed Rod Diameter Profiles

Seed I-1 Cell 4M33 Rod 0400736

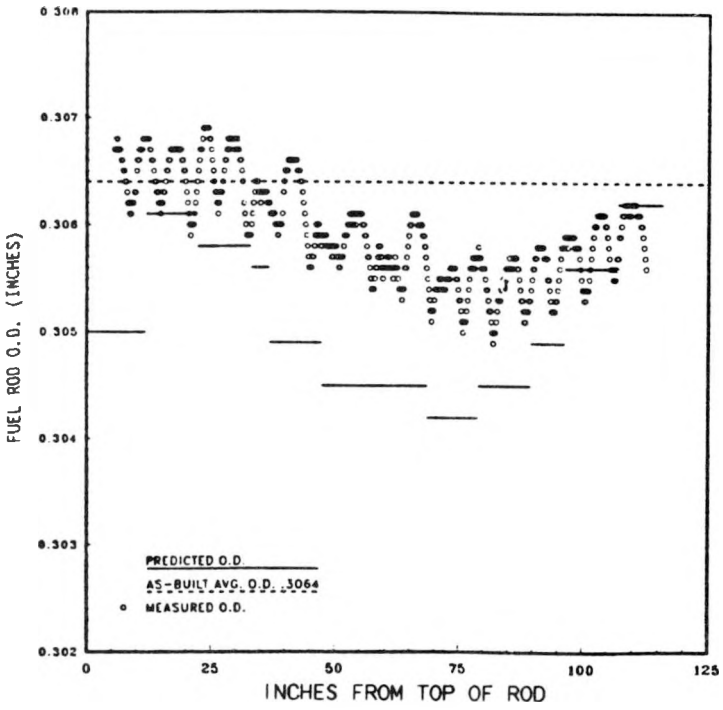

Seed I-1 Cell 2Q41 Rod 0205071

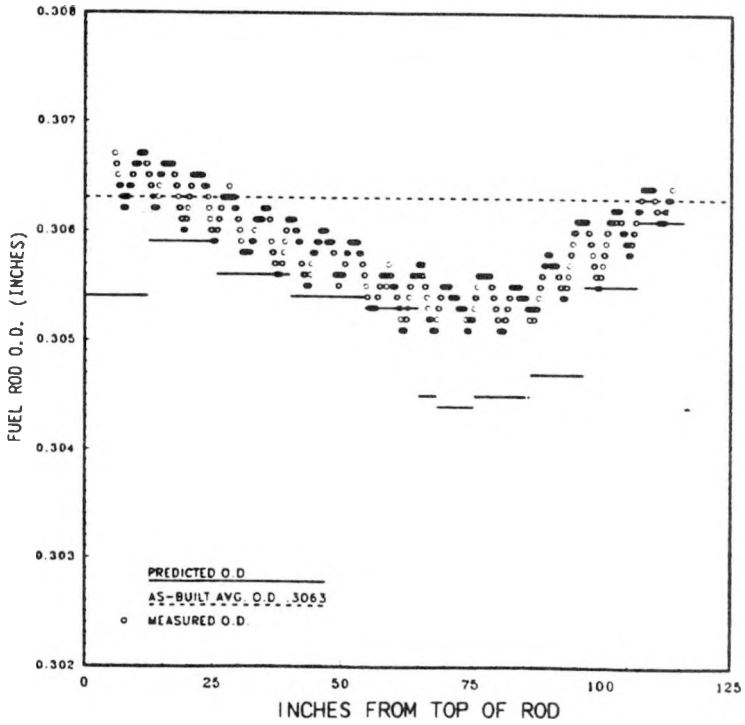

Figure 44 - Seed Rod Diameter Profiles (Cont)

Blanket I-3 Cell 16E57 Rod 1606710

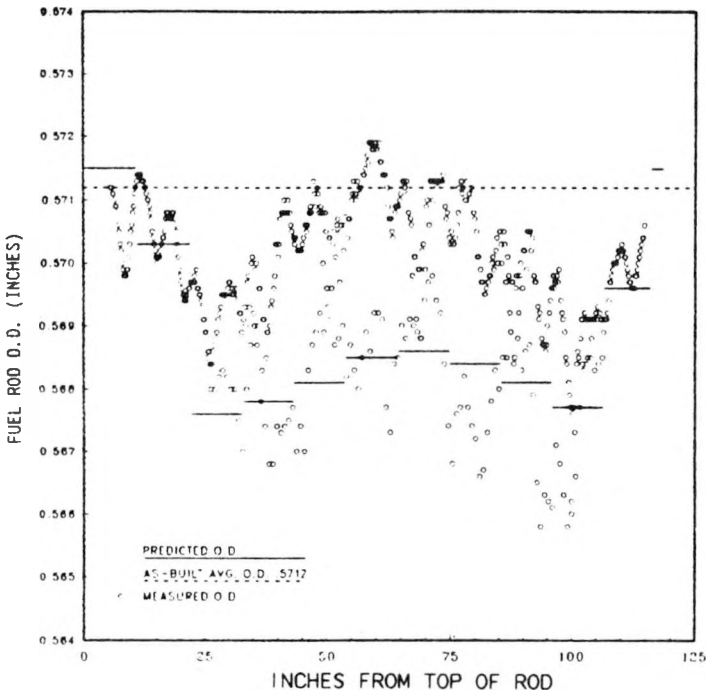

Blanket I-3 Cell 15F11 Rod 1504272

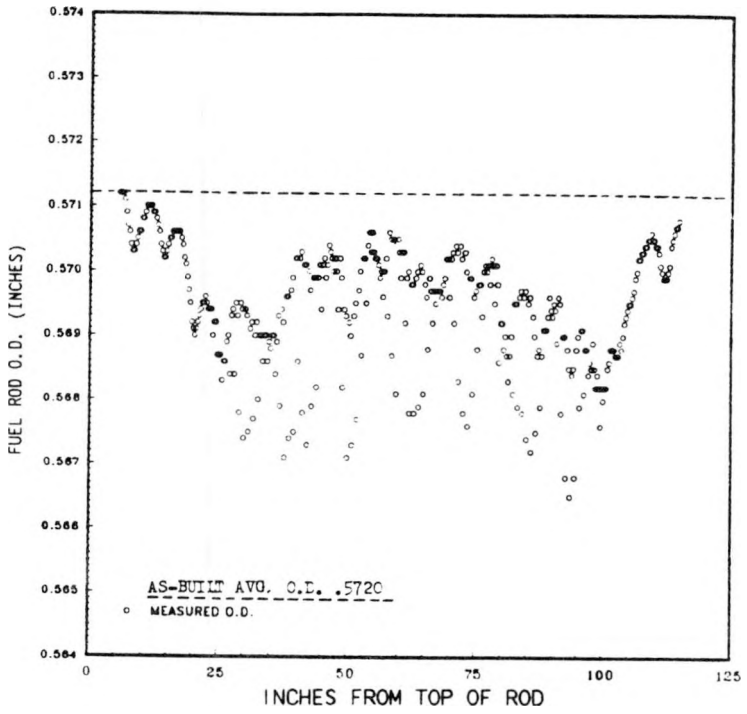

Figure 45 - Standard Blanket Rod Diameter Profiles

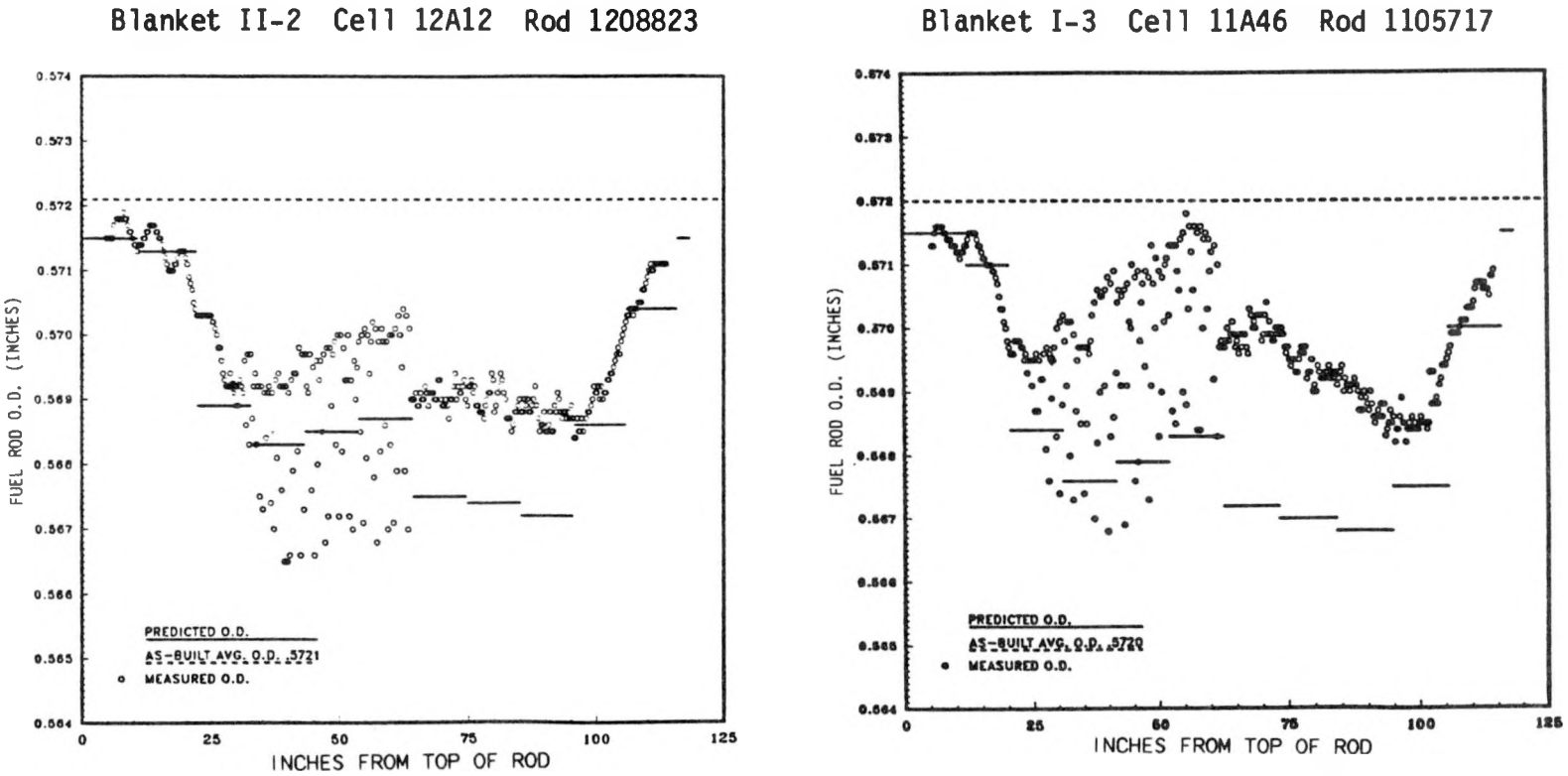

Figure 45 - Standard Blanket Rod Diameter Profiles (Cont)

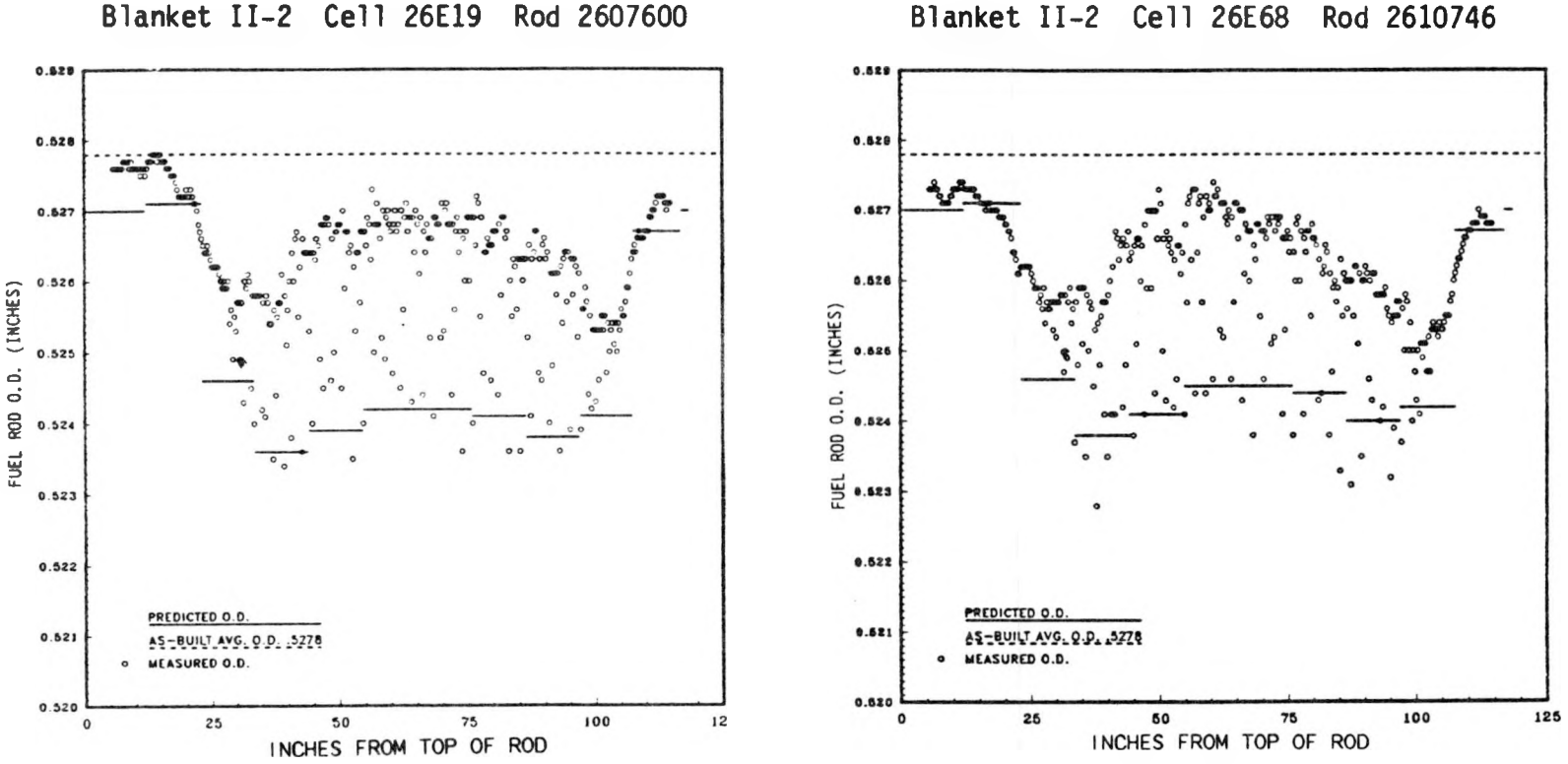

Figure 46 - Power Flattening Blanket and
Reflector Rod Diameter Profiles

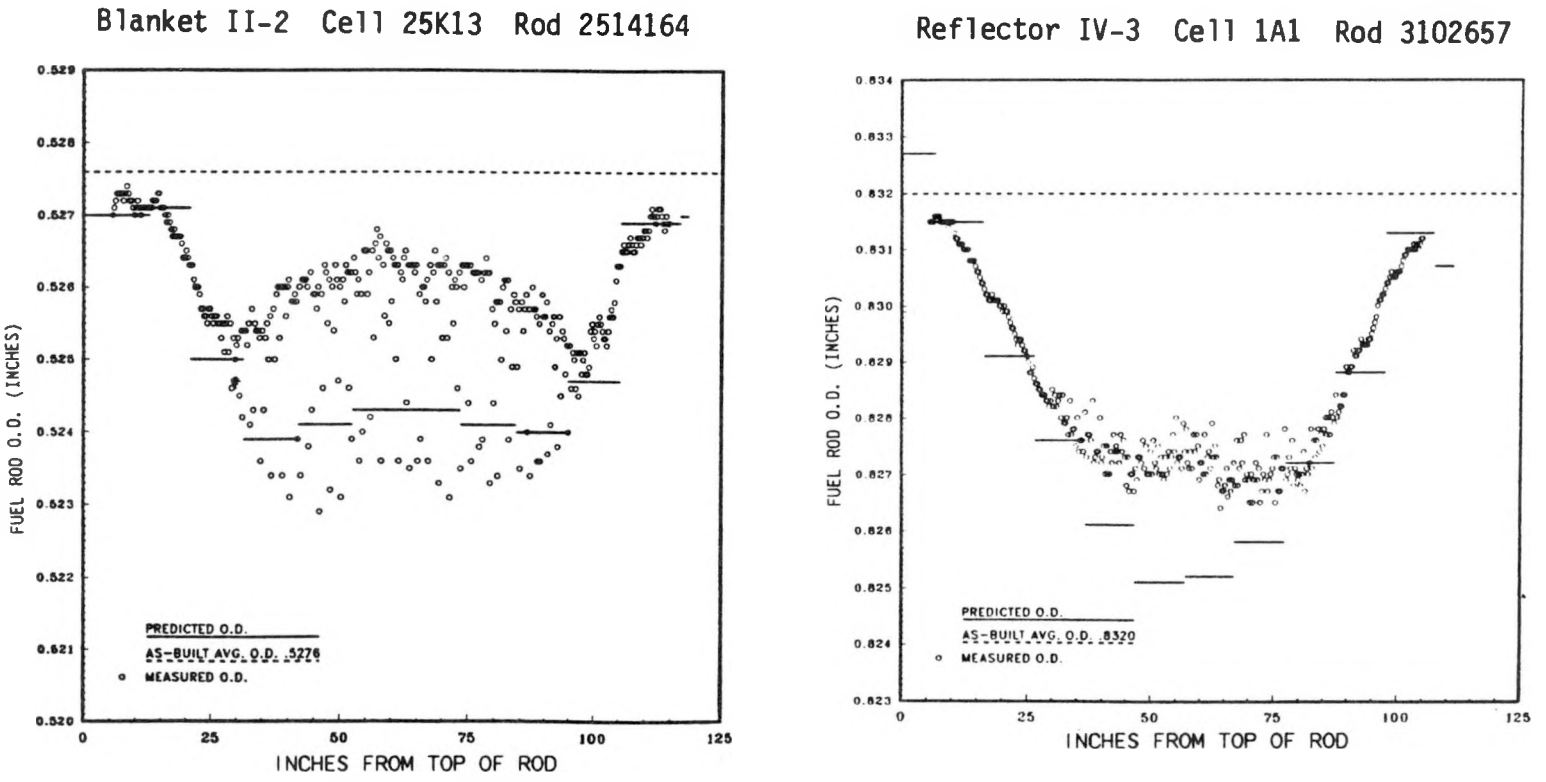

Figure 46 - Power Flattening Blanket and
Reflector Rod Diameter Profiles (Cont)

Table 15 - Rod Diameter Shrinkage

Fuel Region	Rod S/N	Cell	Module	Max. Diameter Shrinkage Measured* (mils)	Max. Diameter Shrinkage Predicted (mils)
Seed	0606773	6B4	SI-1	1.3	1.9
	0507672	5L31	SI-1	2.0	2.3
	0400736	4M33	SI-1	1.5	2.2
	0205071	2Q41	SI-1	1.2	1.9
	0604555	6B3	SI-1	2.5	2.0
	0504502	5L32	SI-1	1.8	**
Standard Blanket	1606710	16E57	BI-3	3.6	3.6
	1504272	15F11	BI-3	3.8	**
	1208823	12A12	BII-2	3.5	4.8
	1105717	11A46	BI-3	3.6	5.3
	1601036	16E71	BI-3	3.2	4.1
	1612146	16E20	BI-3	2.9	4.2
	1605629	16E58	BI-3	3.2	**
Power Flattening Blanket	2607600	26E19	BII-2	2.4	4.2
	2610746	26E68	BII-2	2.8	4.0
	2514164	25K13	BII-2	2.4	3.7
Reflector	3102657	1A1	RIV-3	5.5	6.9
	3107082	1A1	RIV-4	5.5	7.0
	3206304	2D10	RIV-4	2.9	3.3

*Not including groove depths (0.004 inch maximum) in blanket rods and ridge heights (0.001 inch maximum) in reflector rods.

**These rods had no predicted diameter profiles because they were selected for examination after individual rod dimensional changes were calculated. Standard Blanket Rod 1504272 was designated following module examination at ECF, in which it appeared to have bowed toward an adjacent rod in the outer row. Seed Rod 0504502 and Standard Blanket Rod 1605629 were chemically decrudded prior to REX examinations.

predicted. Radial contact would have appeared in the profiles as cladding ridging and reversal of cladding shrinkage at the high power locations at the center of the fuel stack lengths.

Diameter profiles for blanket rods (shown in Figures 45 and 46) are more difficult to compare with predictions. In addition to oxide thickness, grooving of blanket cladding at binary pellet interfaces also confounds the diameter profiles. This results in a large scatter of diameter data in the binary fuel regions of blanket rods. A more detailed plot showing the cladding grooves is given for standard blanket rods 1208823 and 1606710 in Figure 47. (Detailed diameter profiles of the first 12 rods examined are given in Appendix A6.) The mid-rod interface between tapered binary pellets and untapered thoria pellets is obvious in the diameter profile for rod 1208823. From the detailed plots, a minimum diameter disregarding grooving was determined for each rod. The resulting uniform shrinkage is listed in Table 15. Maximum shrinkage occurred in the lower quarter of all seven blanket rods examined (four standard blanket and three power flattening blanket). Measured and predicted shrinkages are in good agreement at the ungrooved segments near the rod ends. The major differences occurred in the central section of each rod, whether grooved or ungrooved. Reversal of cladding shrinkage (due to expanding pellets in the central section) was underpredicted by as much as 0.003 inch. This increased reversal at the higher power locations resulted from overprediction of fuel densification and possibly from underprediction of fuel swelling in the best estimate model. The resulting reduction in cladding shrinkage was beneficial to residual grid spring forces and, because in most cases shrinkage reversal did not return diameters to original dimensions, coolant flow channels and rod-to-rod clearances were not jeopardized.

The three reflector rods examined showed good agreement with predicted diameter shrinkage (Figure 46 and Table 16). The central region of two reflector rods, however, showed more radial pellet-cladding interaction than predicted. In that region, cladding reversal occurred and the hourglassed pellets caused ridging of the cladding. Ridges as high as 0.001 inch were measured from the diameter profile shown in Appendix A6. Ridge height of up

Rod 1208823
Average Diameter

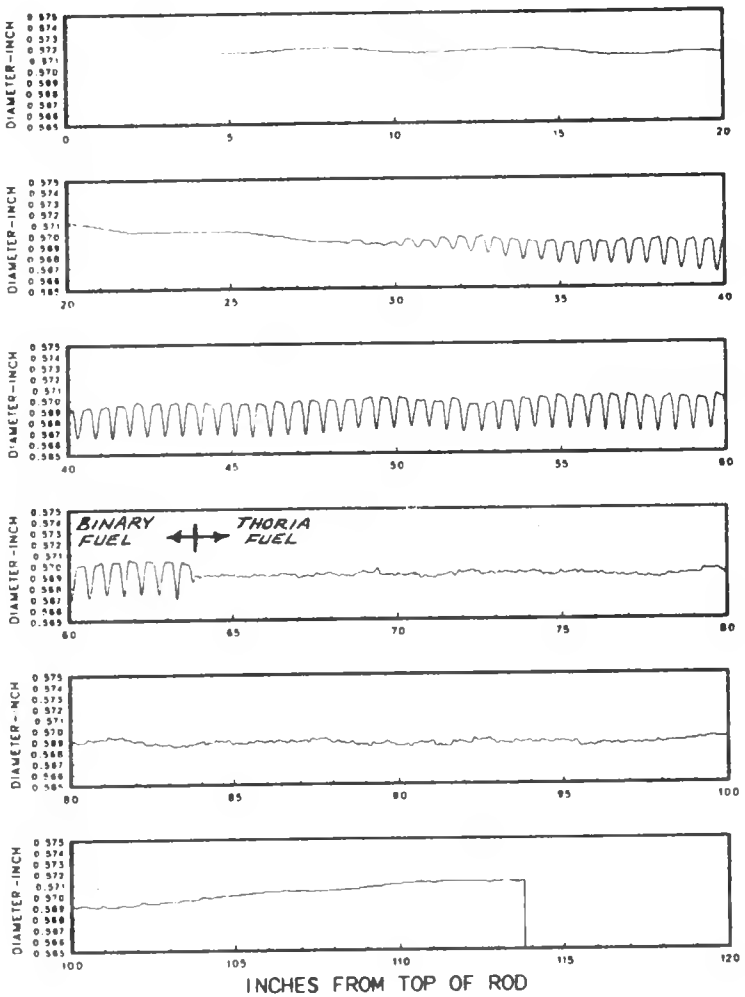

Rod 1606710
Average Diameter

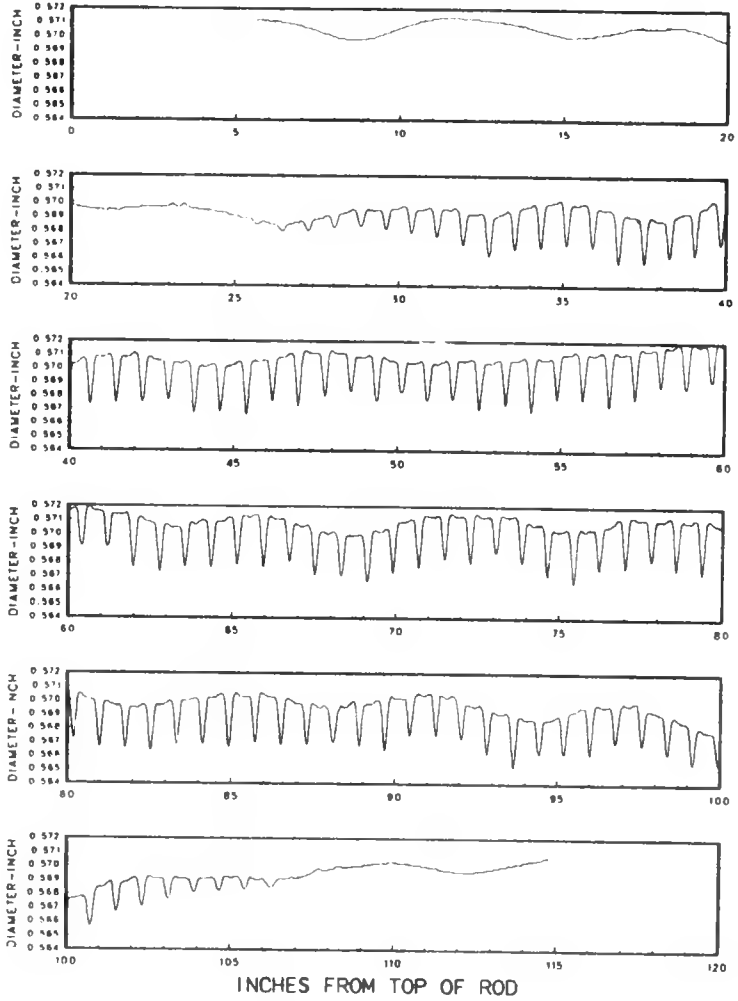

Figure 47 - Rod Average Diameter Profiles

Table 16 - In-Stack Cladding Ovality

Fuel Region	Rod S/N	Cell	Module	Maximum In-Stack Ovality (in.) Measured	Predicted (B.E.)	Design Limit*
Seed	0606773	6B4	SI-1	0.0044**	0.00067	0.0271
	0507672	5L31	SI-1	0.0016		
	0400736	4M33	SI-1	0.0015		
	0205071	2Q41	SI-1	0.0018		
	0604555	6B3	SI-1	0.0016		
	0504502	5L32	SI-1	0.0030		
Standard Blanket	1606710	16E57	BI-3	0.0048**	0.0243	0.0602
	1504272	15F11	BI-3	0.0043**		
	1105717	11A46	BI-3	0.0020		
	1208823	12A12	BII-2	0.0039**		
	1601036	16E71	BI-3	0.0035		
	1612146	16E20	BI-3	0.0025		
	1605629	16E58	BI-3	0.0028		
Power Flattening Blanket	2610746	26E68	BII-2	0.0032**	0.0243	0.0602
	2607600	26E19	BII-2	0.0025		
	2514164	25K13	BII-2	0.0025		
Reflector	3102657	1A1	RIV-3	0.0039**	<0.0243	>0.0602
	3107082	1A1	RIV-4	0.0028		
	3206304	2D10	RIV-4	0.0022		

*Design limit is the ovality beyond which cladding collapse could occur at unsupported (axial gap) locations.

**Measured by orbiting profilometer; all others are from 4-track diameter data of the axial profilometer.

to 1.4 mils was measured for rod 3107082. Expected ridge height was 0.0011 inch (Reference 23). No reversal of cladding shrinkage was expected, however, as shown by the prediction profile in Figure 46. This difference is consistent with blanket rod results and indicates overprediction of fuel densification and underprediction of fuel swelling in the radial direction.

Cladding ovality was calculated from the maximum and minimum diameters at each axial position. The four-track diameter profiles were used for the calculation. The resulting profile of cladding ovality is shown for each of the first twelve rods in Appendix A6. Examples of ovality profiles for a seed and blanket rod are shown in Figure 48. Ovality in seed rods was consistently low (less than 0.005 inch) over the rod length, as expected for freestanding cladding. The maximum ovality among the seed rods examined was 0.0044 inch located over a 2-inch segment near the middle of the fuel stack in rod 0606773. This was at the maximum fluence location in the core, at the center of the fuel stack in a rod from the center of a Type I seed module. A correlation of ovality with fluence level, however, was not confirmed by diameter data from an adjacent rod. Seed rod 0604555 from an adjacent cell had a maximum ovality of 0.002 inch, consistent with all other seed rods examined. Ovality in blanket rods was most prominent near the rod ends, where the lower temperatures and lower fluence levels resulted in incomplete shrinkage of the cladding onto the fuel.

The maximum ovality calculated from track diameters is listed in Table 16 for the 19 rods examined with the axial profilometer. Backup measurements using the orbiting profilometer at selected axial locations are shown for five rods. Measured in-stack cladding ovalities of seed rods were greater than the 0.00067 inch best estimate predicted but were no more than one-fifth the design limit at which cladding collapse would occur. Blanket rod in-stack cladding ovalities were below predictions by a factor of five and below the design limit by a factor of 13. Cladding collapse predictions were based on the probability of axial gaps of 1.0 inch or greater forming in the pellet stack. However, no gaps greater than 0.030 inch formed in the twelve rods examined by neutron radiography. Therefore, in-stack ovality was acceptable in all fuel regions.

Seed
Rod 0507672
Ovality

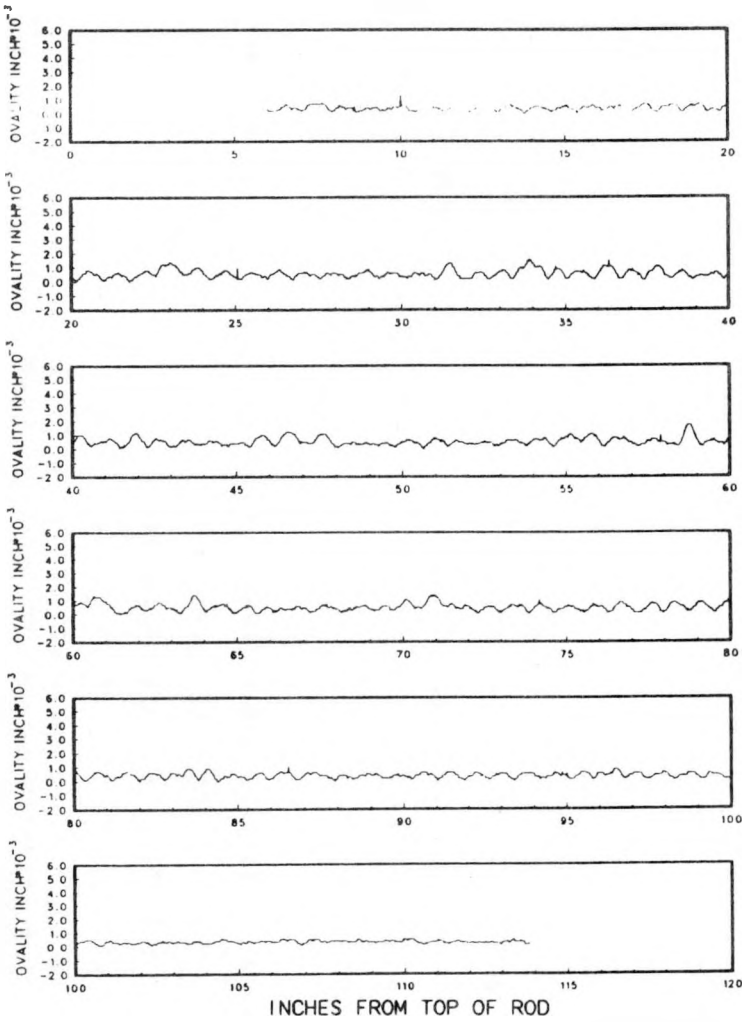

Standard Blanket
Rod 1504272
Ovality

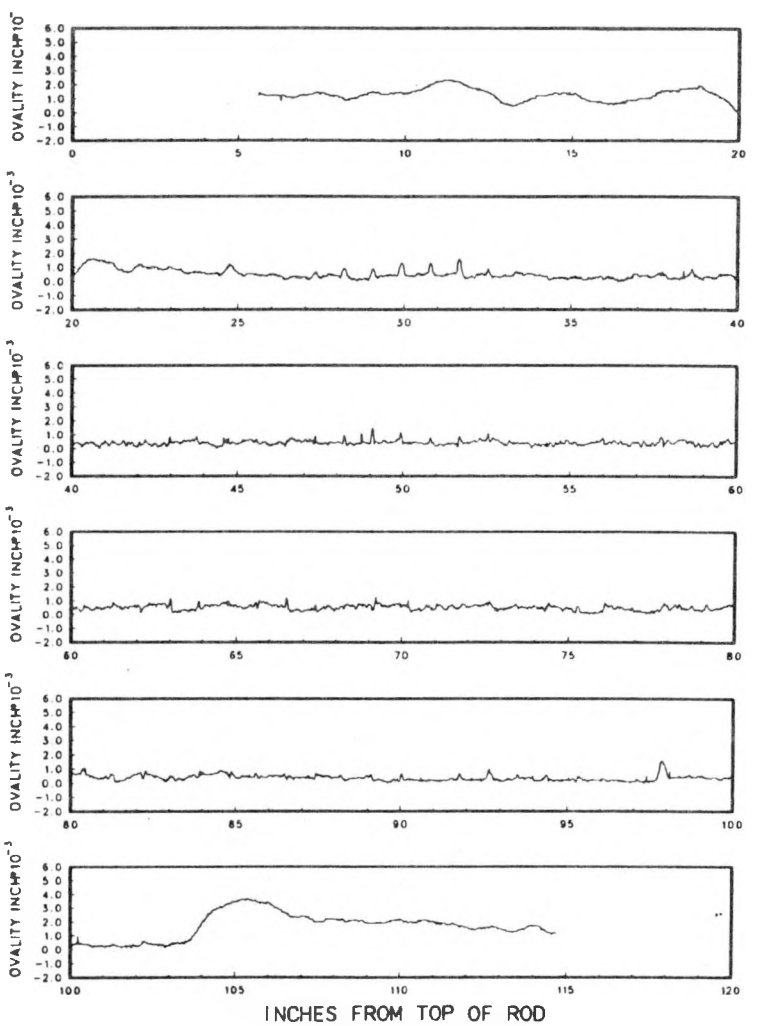

Figure 48 - Cladding Ovality

4.7 - PLENUM OVALITY

Ovality of cladding in the plenum was measured for four seed fuel rods, six standard blanket fuel rods, and three power flattening blanket fuel rods. The measurements were performed to confirm stability of the freestanding RXA seed cladding and to confirm predictions of cladding deformation for the nonfreestanding blanket cladding.

Measured plenum ovalities are presented in Table 17. Measured EOL unsupported cladding lengths (EOL Gap) for blanket fuel rods are also presented in Table 17. The recorded EOL cladding ovality is the maximum for the three inspection planes. Figure 49 presents plots of typical seed and typical blanket plenum ovality profiles.

Measured ovalities confirmed the stability of seed cladding in the plenum region. The maximum measured ovality for the 10-inch plenum was only 0.0018 inch. This was less than the 0.0036-inch worst case EOL ovality predicted by finite element analysis with the ACCEPT computer program. The average measured ovality was 0.0014 inch. This is comparable to the best estimate 0.001-inch EOL ovality predicted with ACCEPT.

Measured ovalities for the nine standard and power flattening blanket plena were also very small. The average measured ovality was 0.0028 inch. This was less than the predicted best estimate ovality of 0.006 inch for the limiting blanket fuel rod. The maximum measured plenum ovality was only 0.0038 inch. This is significantly smaller than the worst case predicted ovality of 0.040 inch for the most limiting blanket fuel rod.

The large difference between measured and worst case predicted plenum ovalities for blanket fuel rods is largely due to overprediction of unsupported cladding. The maximum measured unsupported cladding length for the blanket rods examined was only 0.58 inch. Allowing for 0.065-inch gap increase due to differential expansion of the fuel and Zircaloy cladding, the resulting unsupporting cladding length is well below both the best estimate (1.5 inches) and the worst case predicted (2.2 inches) axial gap for the limiting blanket fuel rod. ACCEPT studies have indicated that cladding ovality is a strong function of axial gap length.

Table 17 - LWBR Fuel Rod Plenum Ovalities

Seed Fuel Rods

Rod S/N	Cell	Module S/N	EOL Gap (inch)	Ovality (mils)
0606773	6B4	SI-1	~10.0	1.18
0507672	5L31	SI-1	~10.0	1.18
0400736	4M33	SI-1	~10.0	1.77
0205071	2Q41	SI-1	~10.0	1.64
			Average =	1.45
			Best Est. Predicted =	1.0
			Worst Case Predicted =	3.6

Standard and Power Flattening Blanket Fuel Rods

Rod S/N	Cell	Module S/N	EOL Gap (inch)	Ovality (mils)
1606710	16E57	BI-3	0.54	3.79
1504272	15F11	BI-3	0.54	3.41
1105717	11A46	BI-3	0.50	2.48
1601036	16E71	BI-3	NM	3.14
1605629	16E58	BI-3	NM	3.29
1612146	16E20	BI-3	NM	1.77
2610746	26E68	BII-2	0.48	2.77
2607600	26E19	BII-2	0.53	2.13
2514164	25K13	BII-2	0.50	2.54
			Average =	2.81
			Best Est. Predicted =	6.0
			Worst Case Predicted =	40.0

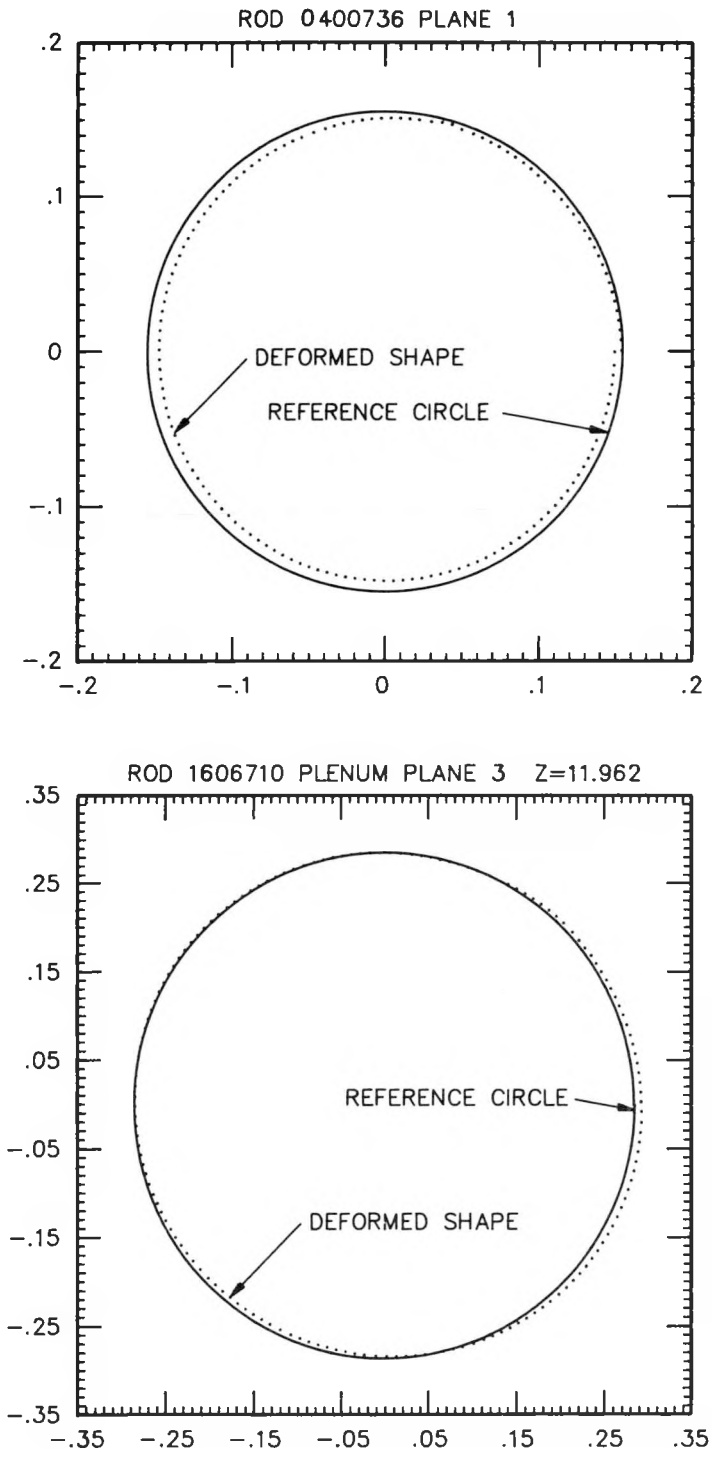

Figure 49 - Typical LWBR Fuel Rod Plenum Ovalities

4.8 - WEAR MARKS

Wear marks on LWBR fuel rods were virtually nonexistent. Two marks were detected on reflector rod 3102657 at the fifth grid level from the bottom, the second grid from the free end of this bottom mounted rod. No wear marks of depth greater than 1 mil were detected on any other core examination fuel rod.

Wear marks were selected during REX visual examinations of rod surfaces recorded on video tapes. All visual indications of wear mark locations were screened by the orbiting profilometer Magnescale probe. In addition, the grid location at the free end of the rod was screened. All screened locations that gave indications of mark depths greater than 1 mil were then scanned in detail by the Magnescale probe.

For the first 12 rods examined, there were 366 total grid contact locations. Forty-five percent (165) of these exhibited images typical of wear mark locations (Table 18) and were screened to determine if significant depths existed. Eight screenings indicated depths greater than 1 mil and were therefore probed for detailed characterization of the wear mark size. Some were narrow scratches (Figure 50) and others revealed no noticeable indentation when plotted (Figure 51). Only two marks were of sufficient size to be considered wear marks (Figure 52). These both occurred at the same grid level on reflector rod 3102657, the highest duty in reflector module IV-3. The two marks were 1.2 and 1.4 mil deep. Later examination of a rod from the same location in reflector module IV-4 revealed one mark of 0.9 mil depth (Figure 53).

Among the first 12 rods examined, the two wear marks with depths greater than 1 mil were only 0.5 percent of the total grid contact locations. Predicted wear depths were 2.8 mil on seed rods, 4.5 mil on blanket rods, and 2.1 mil on reflector rods, with best estimate parameters but assuming low spring forces at all interior grid levels and normal spring force at the free end grid level (Reference 23). In reality, all grid levels associated with the 12 examined rods apparently had springs that maintained forces sufficient to prevent excessive vibratory wear. Reference 6 presents an evaluation of residual spring forces for a grid from seed module II-3.

Table 18 - Orbiting Profilometer Measurements at Suspected Wear Mark Locations

Rod S/N	Number of Grid Contacts	Locations Screened	Number of Areas Scanned	Area Scan Results Max. Depth(mil)	Volume(mil^3)
0606773	45	11	1	0.3	1
0507672	45	8	0	--	--
0400736	45	13	2	0.3	10
				0.1	0
0205071	45	10	0	0	--
1606710	24	6	0	--	--
1504272	24	18	1	0.4	700
1105717	24	18	0	--	--
1208823	24	21	1	0.6	80
2610746	24	18	0	--	--
2607600	24	15	1	0.9	0
2514164	24	15	0	--	--
3102657	18	12	2	1.4	3000
				1.2	2700
Total	366	165 (45.1%)	8 (2.2%)		

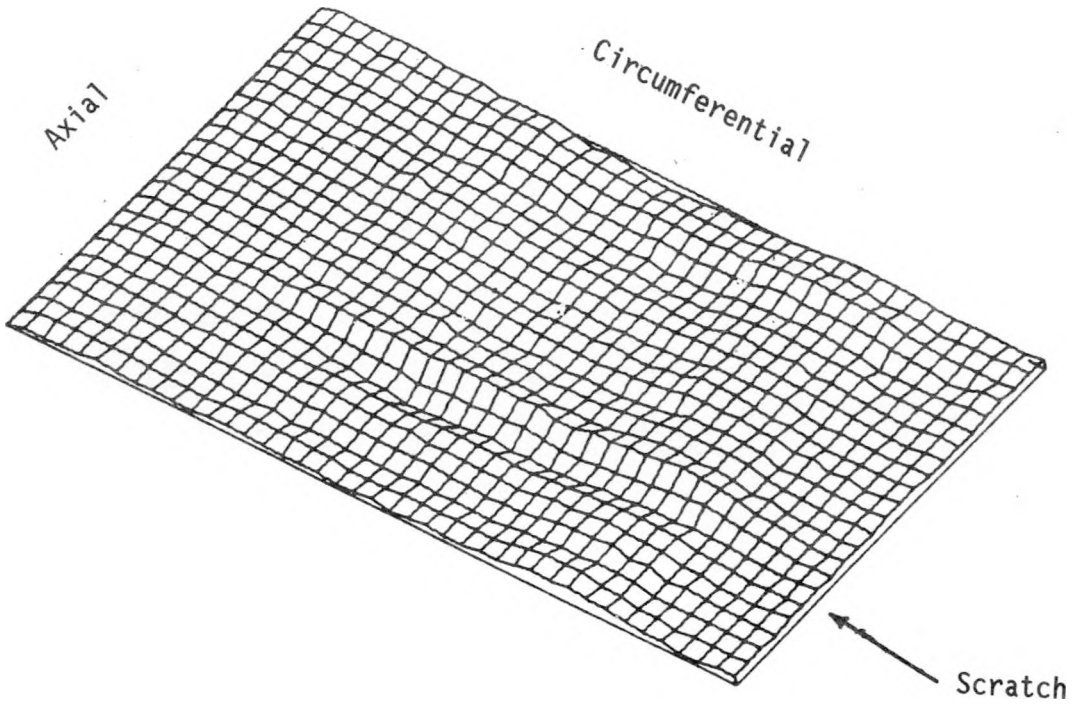

Figure 50 - Orbiting Profilometer Scan of Narrow Scratch

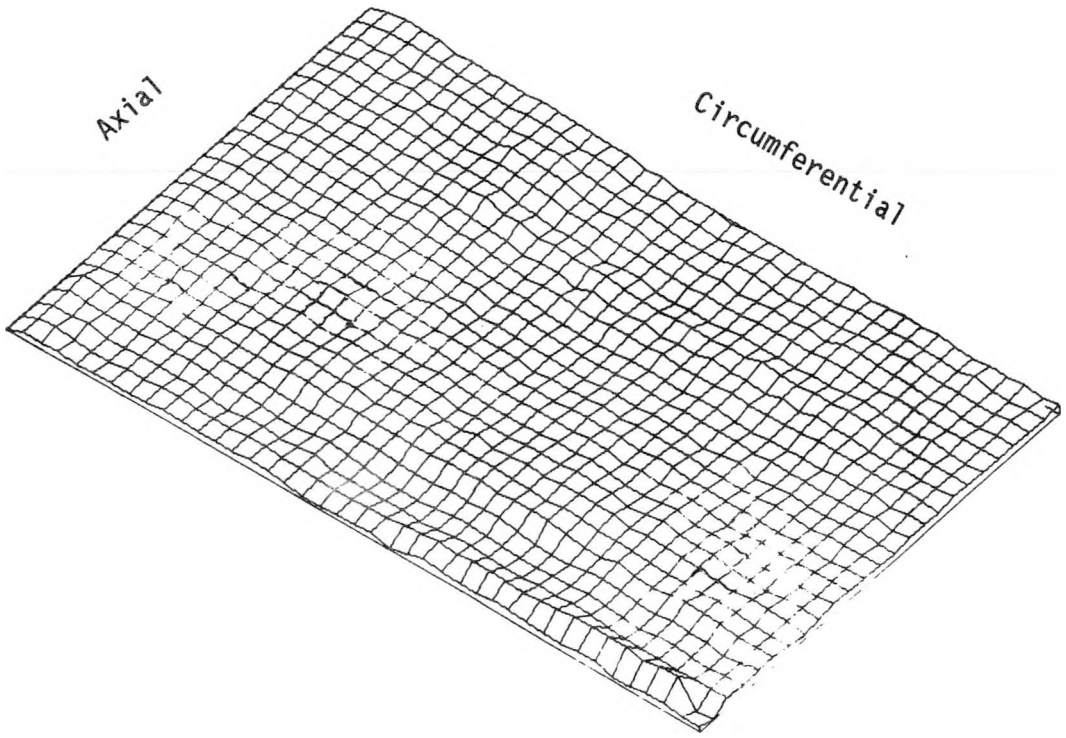

Figure 51 - Scan of Location with No Indentation

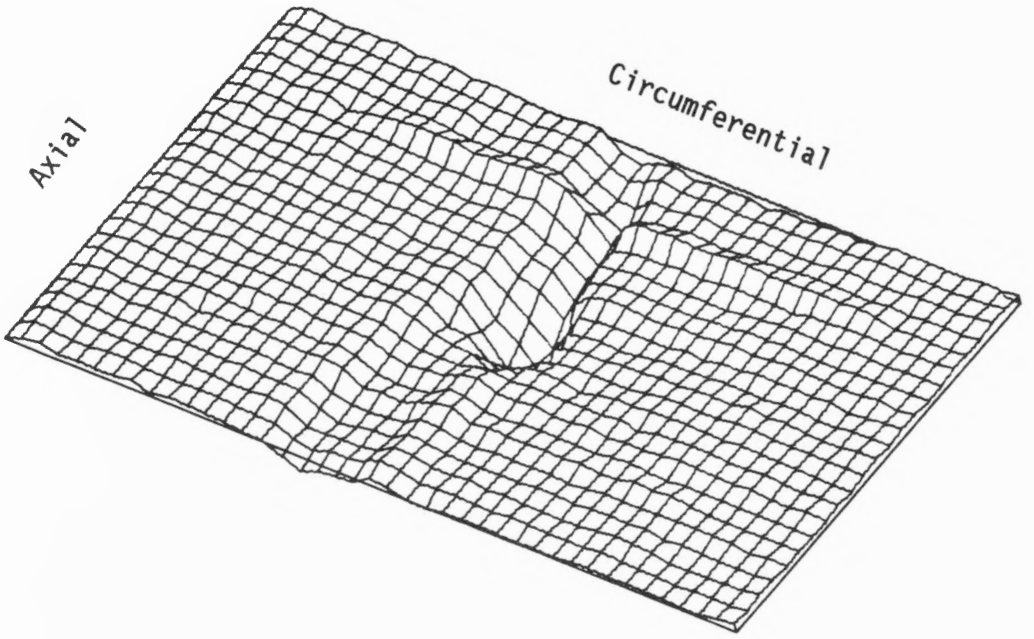

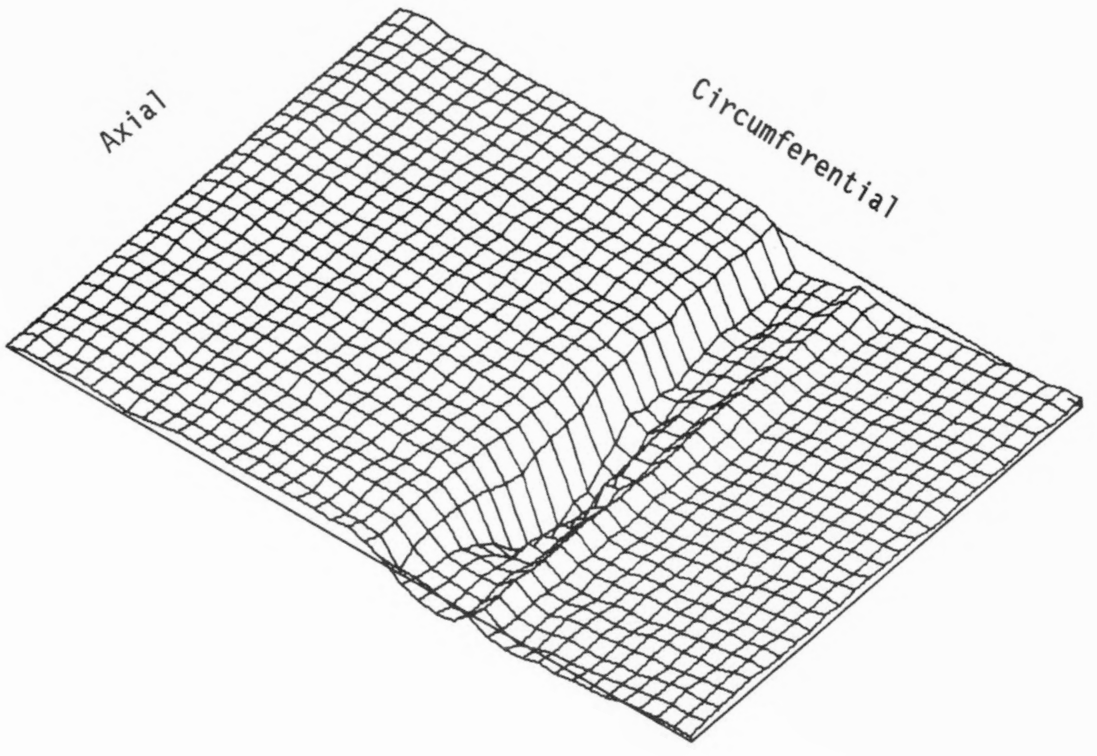

Figure 52 - Scan of Wear Marks on Reflector Rod 3102657 at Grid Level 5

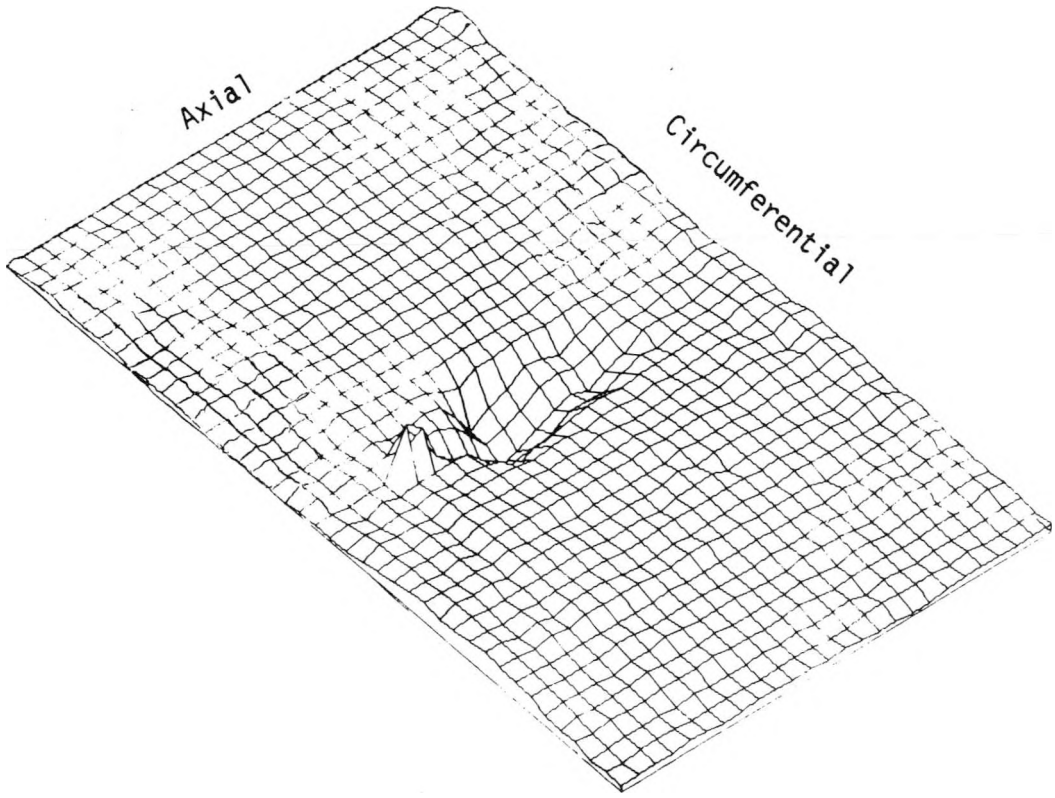

Figure 53 - Scan of Wear Mark on Reflector Rod 3107082

Post-descale visuals of the rods examined for crud by ANL-W revealed several clear wear marks on blanket rod 1605629 and on reflector rod 3220018. Figure 54 presents photographs of two wear marks observed at the free end of blanket rod 1605629. Figure 55 presents a photograph of a wear mark at an inner grid location. All three wear marks were long, showing the effect of rod growth. Figure 56 presents photographs of two wear marks on reflector rod 3220018. Both of these wear marks were short.

Screening measurements were performed for blanket rod 1605629. Multiscan orbiting profilometer inspections were performed for the deepest wear mark. Figure 57 presents a contour plot for the lower 0.05 inch of the wear mark at the 116-inch level and 270-degree orientation (Figure 54). The maximum depth for the area examined was only 0.0002 inch.

4.9 - OXIDE THICKNESS

Fuel rod outer surface corrosion oxide film thicknesses were measured with the eddy current oxide thickness (EDCOT) gage on the 12 rods chosen for destructive examination and on four other selected rods. Plots of the planar average oxide thickness and the separate track measurements are shown in Figures 58 and 59 for seed rod 0400736 and in Figures 60 and 61 for seed rod 0606773. Calculated fuel depletion and integrated fast flux (fluence) profiles are shown with the planar average plots. These are average levels over 3.5-inch axial segments. The effect of local flux depressions at grid levels do not appear in these curves, but are shown from flux wire data in Reference 18. Approximate grid positions are indicated on the oxide plots.

The oxide thickness is less than 0.2 mil over the bottom 30 inches of each rod (up to about 85 inches from the top). It rises to a peak of 1.46 mils near the seventh grid level in rod 0400736, which coincides with the top of the binary (ThO_2-UO_2) fuel stack, and to a peak of 1.56 mils between the sixth and seventh levels in rod 0606773. Oxide thinning is evident at the support grid levels due to the lower cladding temperature and fluence at these locations of local heat flux and fast neutron flux depression. In addition, hydraulic disturbances, such as local coolant turbulence within and downstream of the grids, increase the local heat transfer coefficient between the coolant

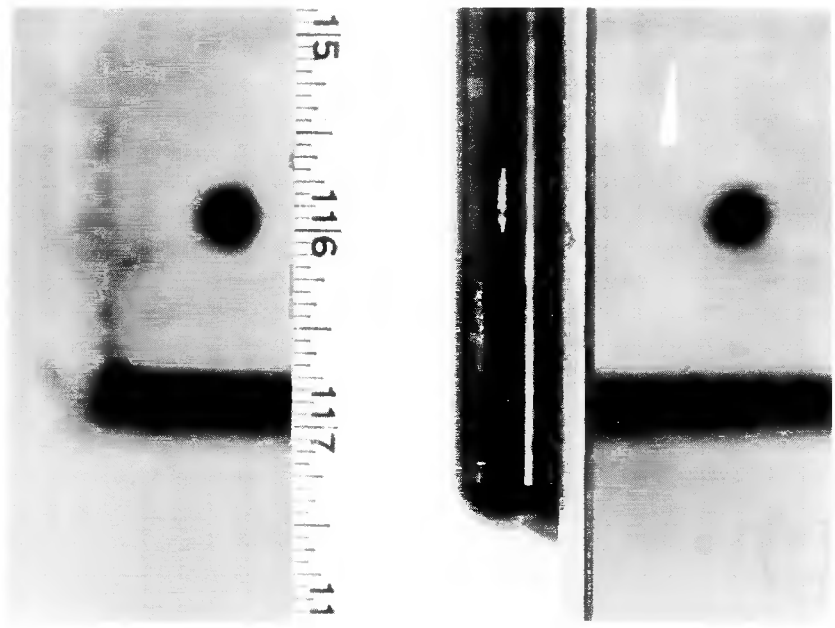

270 degrees

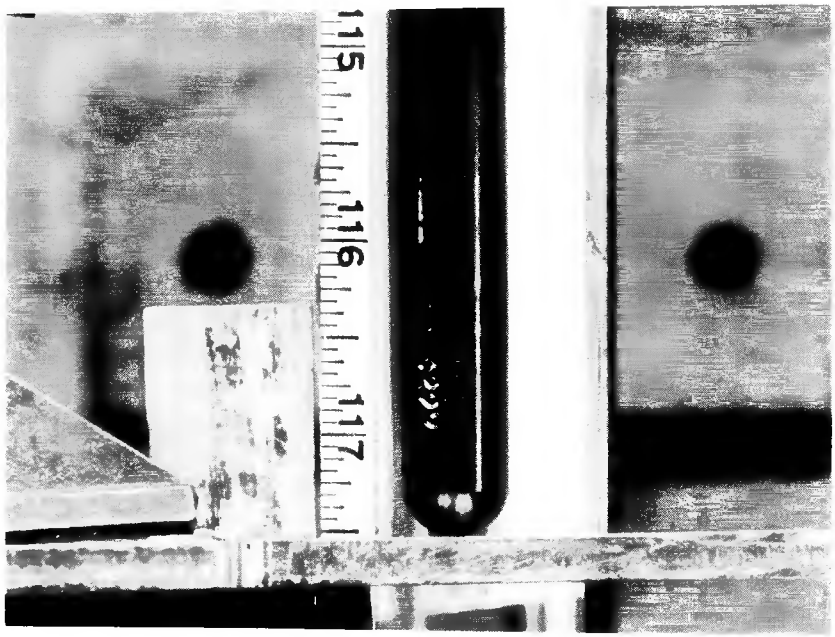

30 degrees

Figure 54 - Blanket Rod 1605629 Wear Marks at Free End
(Post-Descale Visual)

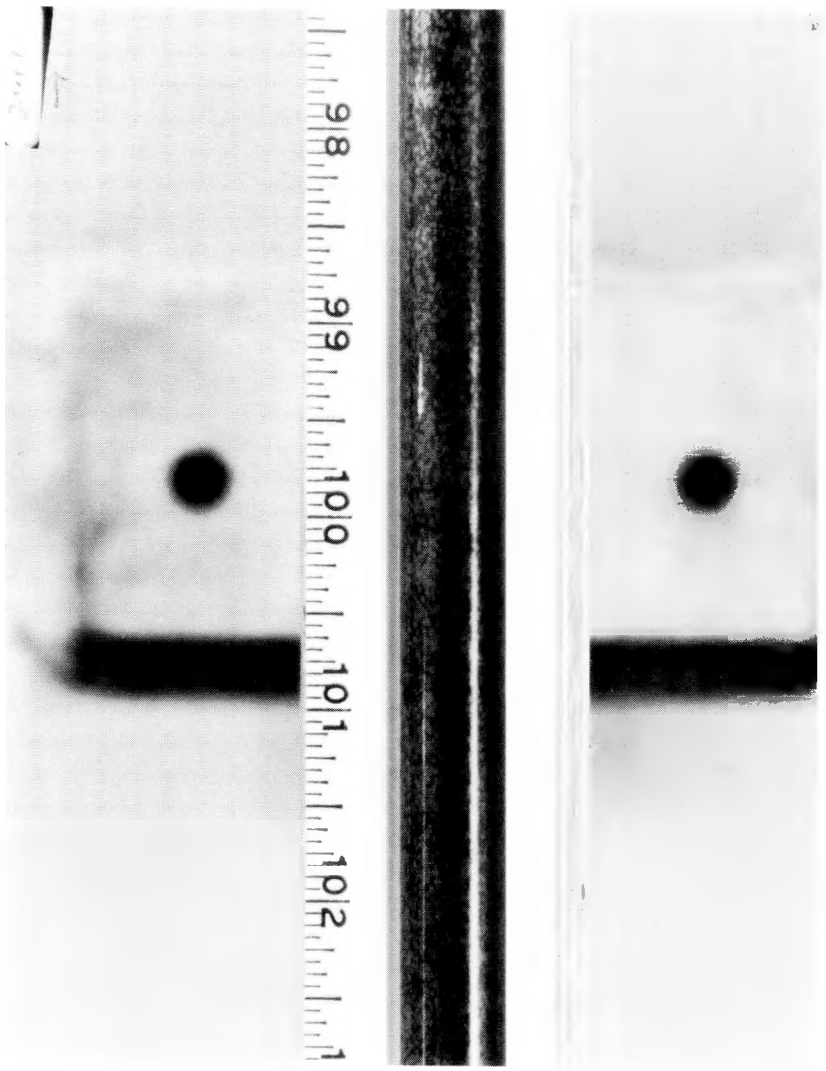

Figure 55 - Blanket Rod 1605629 Wear Mark at Inner Grid
(Post-Descale Visual)

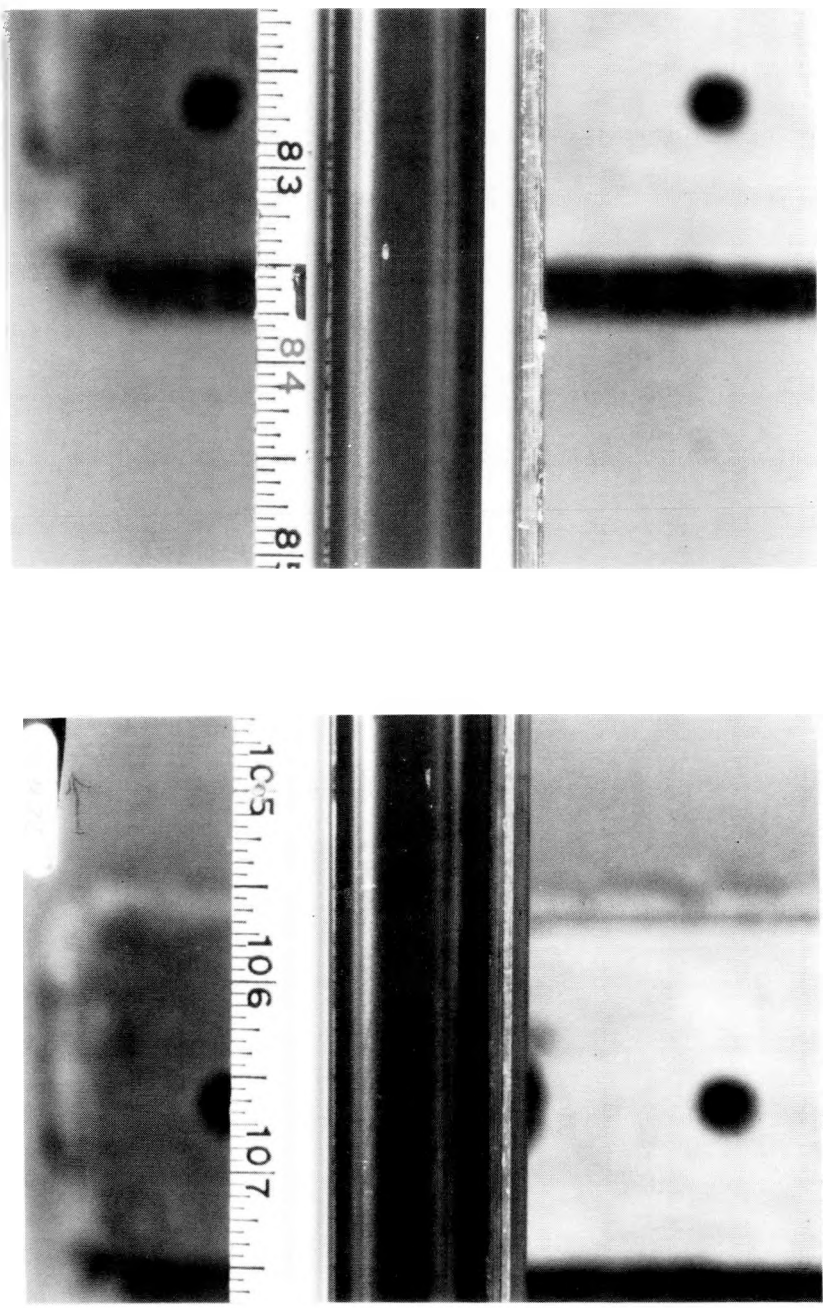

Figure 56 - Reflector Rod 3220018 Wear Marks
(Post-Descale Visual)

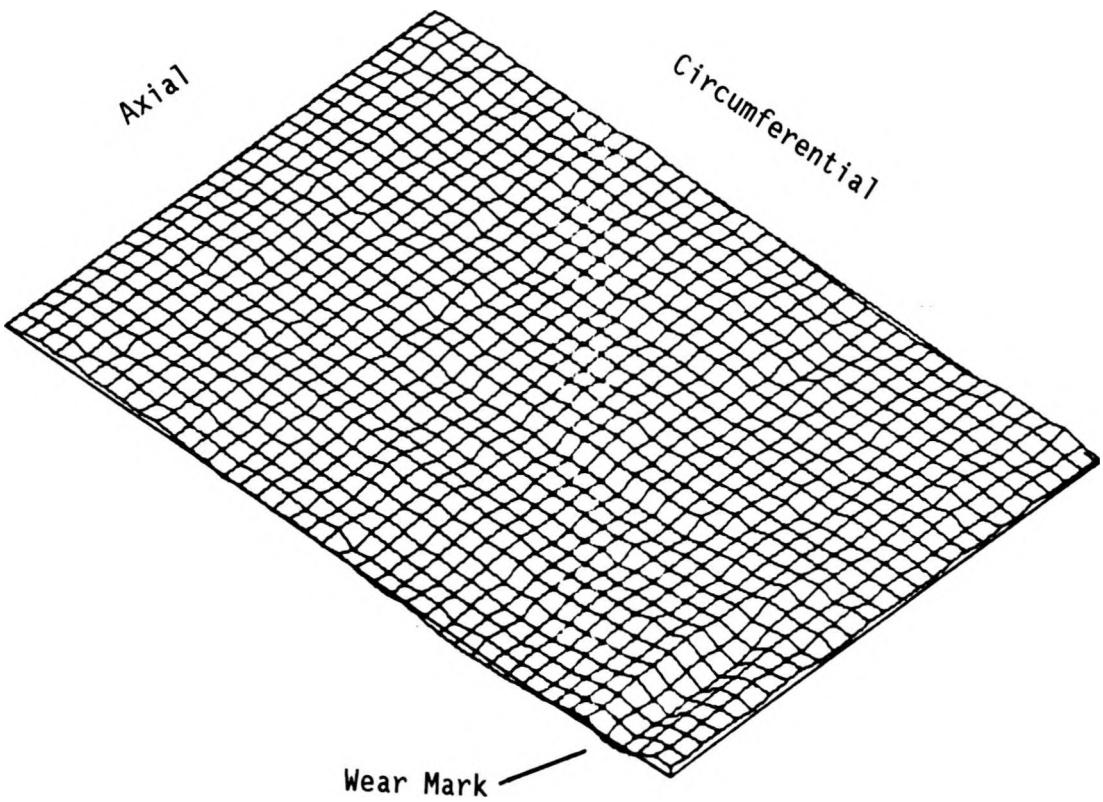

Figure 57 - Scan of Wear Mark on Blanket Rod 1605629
(Z = 116 inch, θ = 270 degrees)

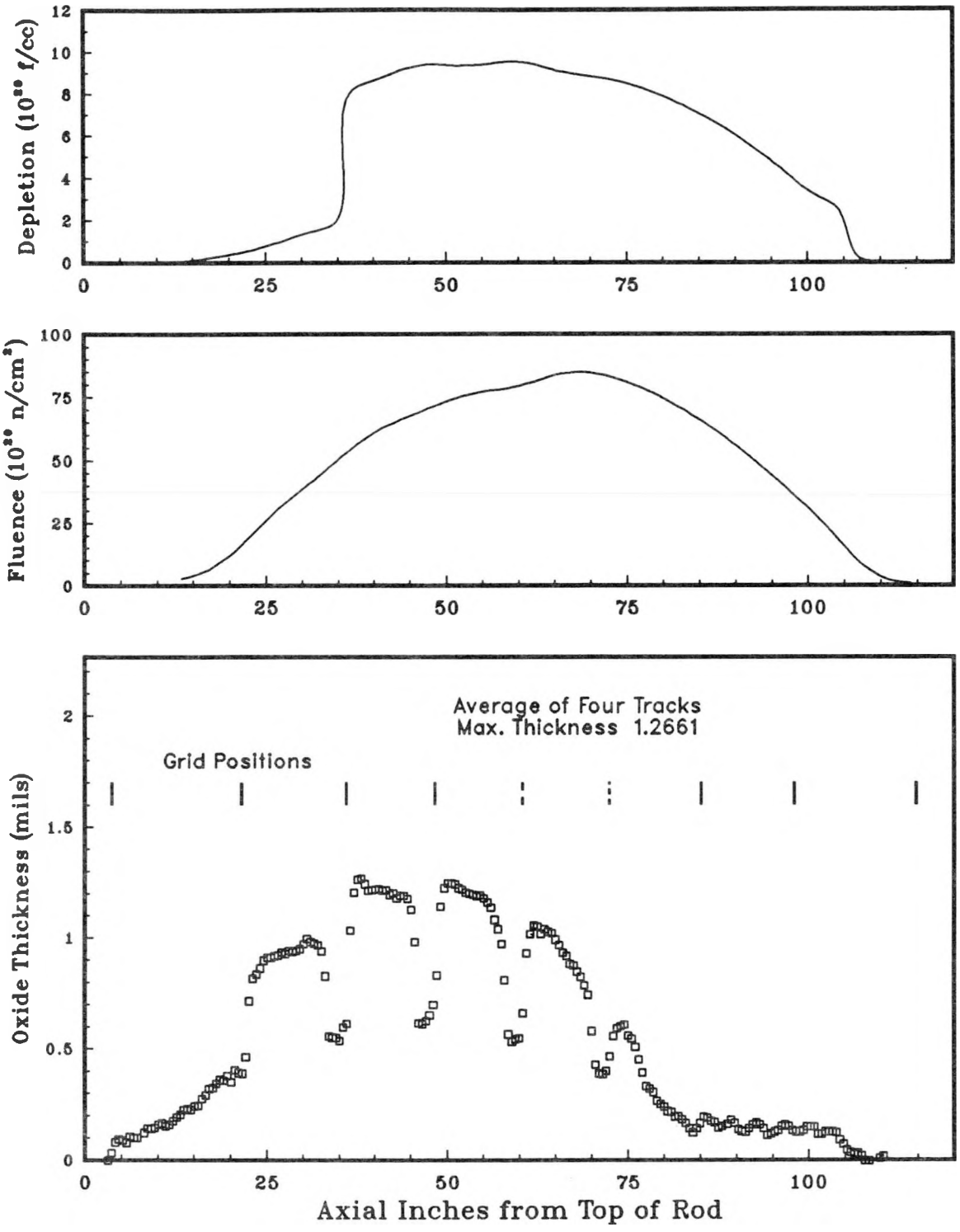

Figure 58 - Axial Profile of Measured Oxide Thickness
Seed Rod 0400736 (Cell 4M33 SI-1)

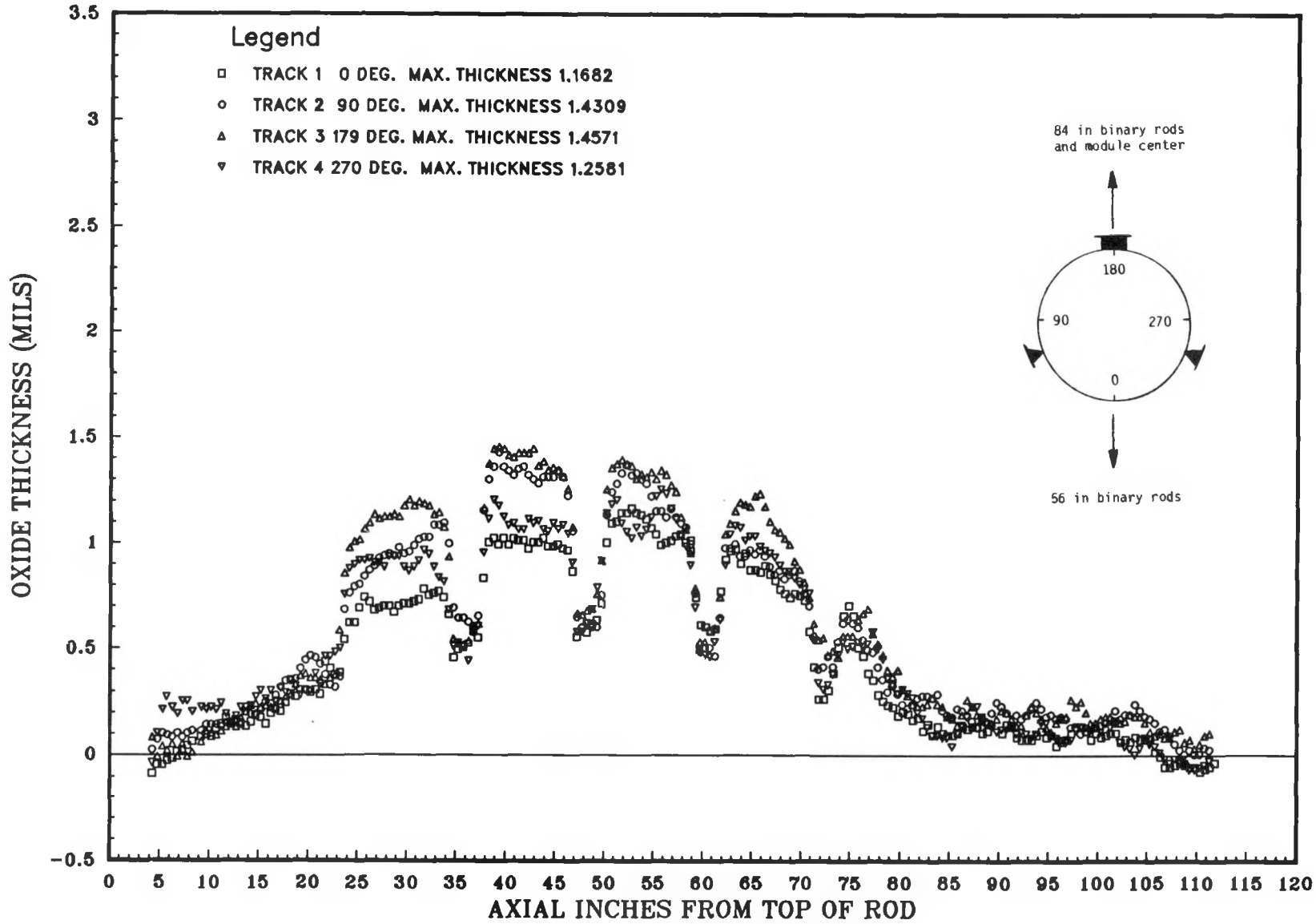

Figure 59 - Oxide Thickness Measurements on Four Tracks
Seed Rod 0400736 (Cell 4M33 SI-1)

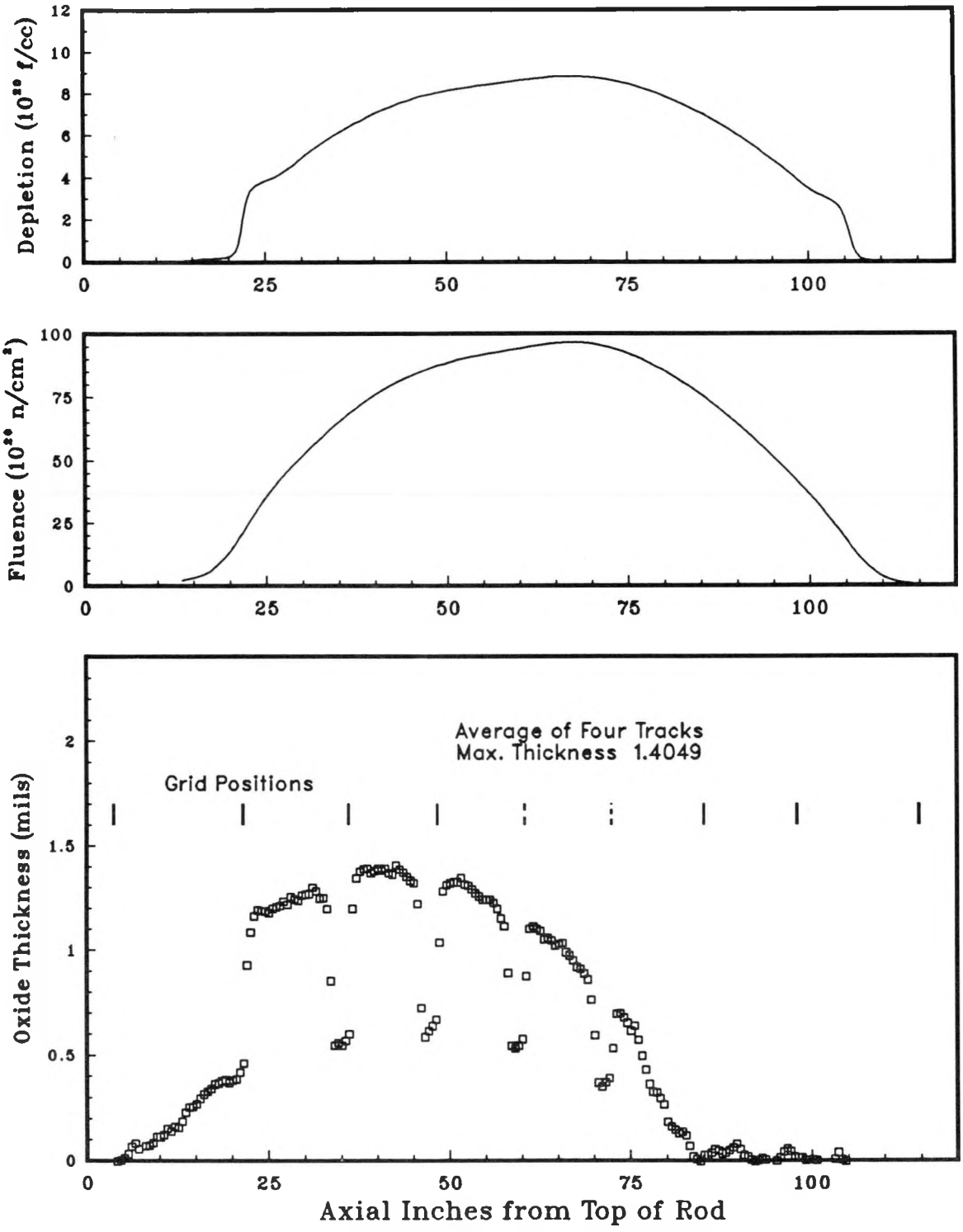

Figure 60 - Axial Profile of Measured Oxide Thickness
Seed Rod 0606773 (Cell 6B4 SI-1)

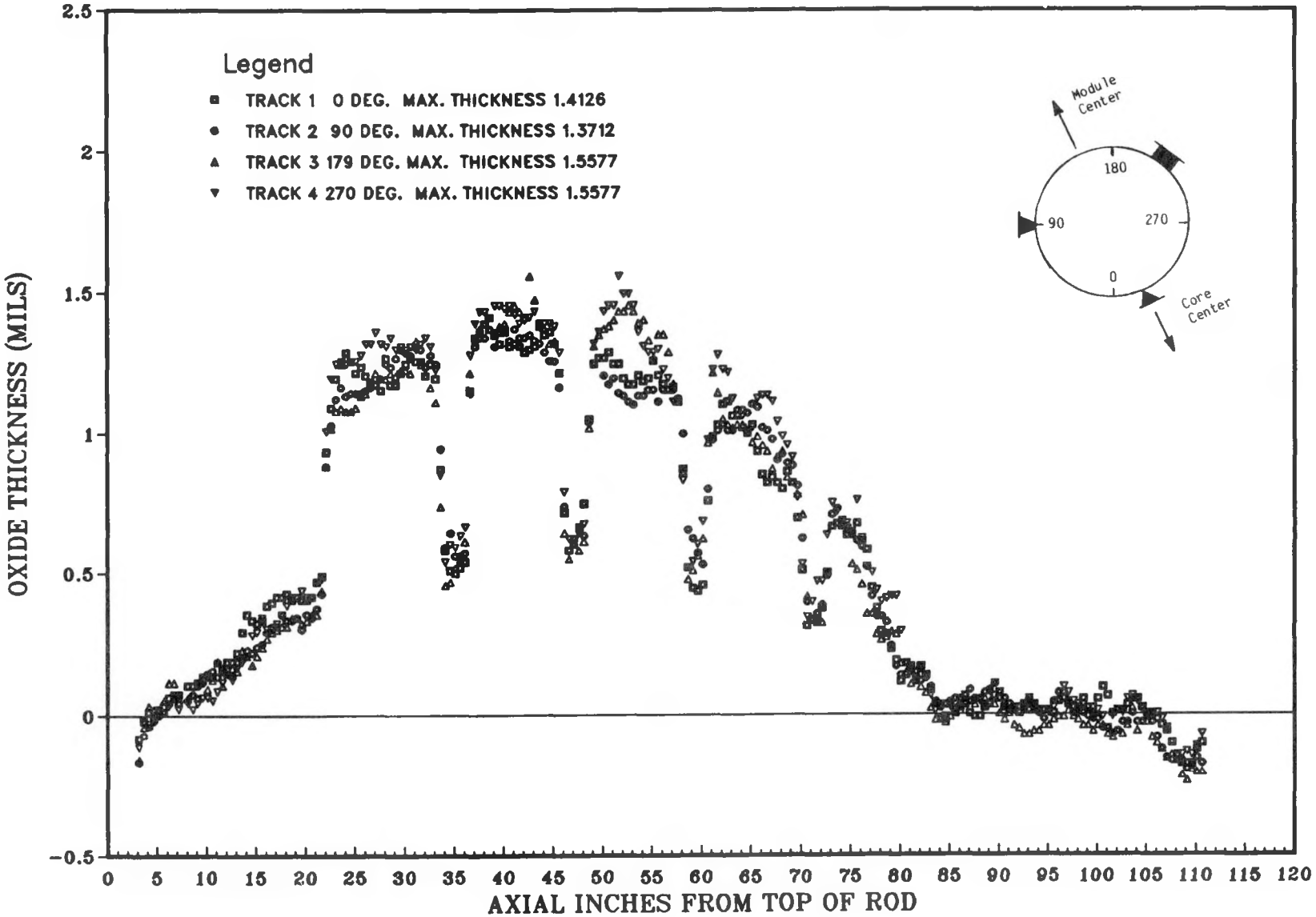

Figure 61 - Oxide Thickness Measurements on Four Tracks
Seed Rod 0606773 (Cell 6B4 SI-1)

and fuel rod surface and contribute to lowering the cladding surface temperature (Reference 25). Similar sawtooth corrosion oxide film patterns have been observed on commercial pressurized water reactor (PWR) fuel rods (References 25, 26, and 27).

An interesting correlation between radial heat flux gradient and oxide thickness differential on opposite sides of rod 0400736 was noted from the plots in Figure 59. The diagram at the top right of the figure shows the measuring track orientation relative to the grid spring and dimple locations (based on visual examinations) and relative to adjacent rod rows (based on the grid cell diagram for seed module I-1). Like all other rods in the same row, rod 0400736 contained binary fuel beginning at 36 inches from the top of the rod. The next row outward had binary fuel below the 50-inch level. The adjacent row inward and all remaining rod rows to the center of the module had binary fuel below 22 inches. Thus, the top portion of rod 0400736 was located in a region of high radial flux gradient with the flux being higher on the side facing the module center. This side was the 180-degree track. The lower flux was at the 0-degree track. The corrosion profiles between 22 and 50-inch levels on these tracks are consistent with the flux gradient. Lower on the rod, the 0 and 180-degree profiles are closer, which is consistent with the reduced magnitude of the flux gradient below the 50-inch level.

Rod 0606773 was located near the module center and was surrounded by full-length (84-inch) binary fuel rods. Therefore, the radial heat flux was level across the rod. Consistent with this level flux gradient, the corrosion profiles have a greatly reduced spread as shown in Figure 61.

Oxide thickness plots for the remaining 14 fuel rods are given in Appendix A7. The EDCOT data are summarized in Table 19. Circumferential variations in oxide film thickness were observed in all of the fuel rods and have been reported for commercial PWR rods (References 25 and 27). Grooving was detected in the cladding diameter measurement of the blanket rods at the higher power locations (Section 4.6). This resulted in considerable scatter in the blanket EDCOT data due to the poor probe-rod contact when instrument probe bridged the grooves.

Table 19 - EDCOT Corrosion Oxide Film Thickness Measurements

Rod Type	Peak Fluence (10^{20} n/cm^2)	Peak Power (Mw/ft)	Peak Depletion (10^{20} n/cm^2)	Peak Burnup (MWD/MTM)	Maximum Oxide Thickness (mils) 0°	90°	180°	270°
Seed Rods								
0400736	85.0	6.7	9.5	44,500	1.17	1.43	1.46	1.26
0606773	96.5	4.4	8.8	41,200	1.41	1.37	1.56	1.56
0205071	75.5	5.5	11.4	53,400	0.84	0.83	0.69	0.67
0507672	87.9	4.2	10.1	43,300	1.36	1.26	1.12	1.31
0504502*	87.9	4.2	10.1	43,300	0.92	1.20	1.55	1.56
Standard Blanket Rods								
1606710	73.0	8.7	5.1	22,300	1.05	1.50	1.95	1.80
1208823	55.4	6.9	4.3	18,700	0.72	0.75	0.50	0.60
1105717	71.4	8.6	5.2	22,800	0.70	1.45	1.50	0.75
1504272	51.0	7.4	4.4	19,200	1.30	1.25	0.95	0.84
1605629*	74.1	8.9	5.2	22,800	1.05	1.30	1.55	1.10
Power Flattening Blanket Rods								
2610746	57.7	8.7	5.7	25,200	1.16	1.10	1.18	1.20
2514164	38.6	8.3	5.1	22,300	0.60	0.41	0.40	0.40
2607600	58.6	8.4	5.5	24,400	0.95	0.93	0.85	0.90
Reflector Rods								
3102657	25.9	3.4	0.9	4,100	0.50	0.75	0.50	0.56
3107082	27.8	3.6	1.0	4,500	0.46	0.63	0.37	0.37
3206304	7.8	0.9	0.2	900	0.35	0.29	0.46	0.56

*Chemically decrudded

In general, the corrosion oxide film thickness increased with cladding surface temperature, as indicated by rod power, fluence, and to a lesser extent with burnup/fuel depletion. This is in agreement with much of the visual examination results for the seed and blanket rods. The upper and lower portions of the rods appeared uniformly dark gray or black, indicating a thin (<0.2 mil) substoichiometric zirconium oxide. Mottled, speckled, and spotted transition zones (0.2-0.4 mil) were often observed associated with the high power, binary fueled, high cladding temperature regions near the middle of the fuel rods. Oxide layers with thicknesses greater than 0.4 mil had a light gray or white coloration, indicating a stoichiometric zirconium oxide (Reference 27). Locations at support grid levels (which were characterized by reduced cladding corrosion) were black in color.

The measured maximum corrosion oxide thicknesses determined with both eddy current and metallographic techniques (Reference 5) are compared in Table 20 with values calculated in Reference 23 by a corrosion model designated CHORT (corrosion and hydriding of reactor tubing). The major variables in the CHORT model are Zircaloy cladding surface temperature, fast neutron flux (>1 Mev), and exposure time (References 17, 28, and 29). The measured thicknesses are in reasonable agreement with CHORT predictions. The measured maximum thickness values of <2 mils are comparable to those of commercial PWRs (References 25 through 27). Oxide layers of >4 mils thickness have been reached in experimental high burnup rods without adverse effects (Reference 25). The EDCOT measurements are considered an upper limit since they include any residual crud coating. The fuel rods were brushed before examination to remove loosely adherent crud, but they were not chemically decrudded. Crud thickness studies (Section 4.11) in which a seed, blanket, and reflector rod were chemically descaled indicated that the average diametral crud thickness were approximately 0.2 mil for LWBR fuel rods. Peak local average diametral thicknesses (5-inch segments) of approximately 0.5 mil were obtained. Crud on rods brushed before oxide thickness measured would be less than that measured by ANL-W.

Table 20 - Measured and CHORT-Calculated Maximum Corrosion Oxide Film Thickness of LWBR Fuel Rods

Rod Type	Corrosion Oxide Film Thickness (mils)			
	Measured		CHORT-Calculated*	
	EDCOT	Metallography**	Best-Estimate	Design
Seed	1.56	1.0	1.08	1.62
Standard Blanket	1.95	1.75	1.10	1.65
Power Flattening Blanket	1.20	1.10	1.03	1.55
Reflector	0.75	0.25	0.86	1.29

*from Reference 23
**from Reference 5

In summary, corrosion oxide film thickness on fuel rod cladding at end-of-life:

(1) increased with cladding surface temperature along the axial length of a rod,
(2) varied along rod circumference with highest values in the regions of highest heat flux,
(3) exhibited a marked decrease at support grid levels,
(4) decreased sharply at the top and bottom of the binary fuel stack, and
(5) was in reasonable agreement with a model based on cladding surface temperature, fast neutron flux, and exposure time.

4.10 - CLADDING DEFECTS

Ultrasonic examinations were performed on all 12 fuel rods selected for destructive examination. The equipment was adjusted to screen out minor surface defects (scratches, pits, etc.) that were less than four mils in depth. The maximum UT responses are plotted in Figure 62. The ultrasonic inspections showed no indications of significant defects, through-cladding cracks, or other unusual conditions in nine of these rods. However, one standard blanket rod (1105717) and two power flattening blanket rods (2514164 and 2607600) had strong UT indications (>10 mils) which were not surface marks. Metallographic samples at a single plane were obtained at the location of peak UT signal on two of the rods. The metallographic examinations showed no indications of defects. However, since the metallographic examinations were limited to a single plane for each of the two rods examined, absence of a defect did not preclude the possibility of defects in adjacent planes. Time constraints prevented a more intensive (i.e., multiplane) metallographic examination of the rods.

4.11 - CRUD MEASUREMENTS

4.11.1 Pre- and Post-Descale Visuals

Figures 63, 64, and 65 present photographs of selected portions of seed rod 0504502, blanket rod 1605629, and reflector rod 3220018 before and after chemical descaling of the rods. Comparison of the photographs illustrates the effectiveness of the descale process in removing crud. The post-descale photographs provide a view of the fuel rod cladding without crud. (It should be noted that some crud could have been removed by extensive rod handling prior to pre-descale examination.) Results of visual examinations of LWBR rods in the REX after mechanical (brushing) decrudding are presented in Section 4.4.

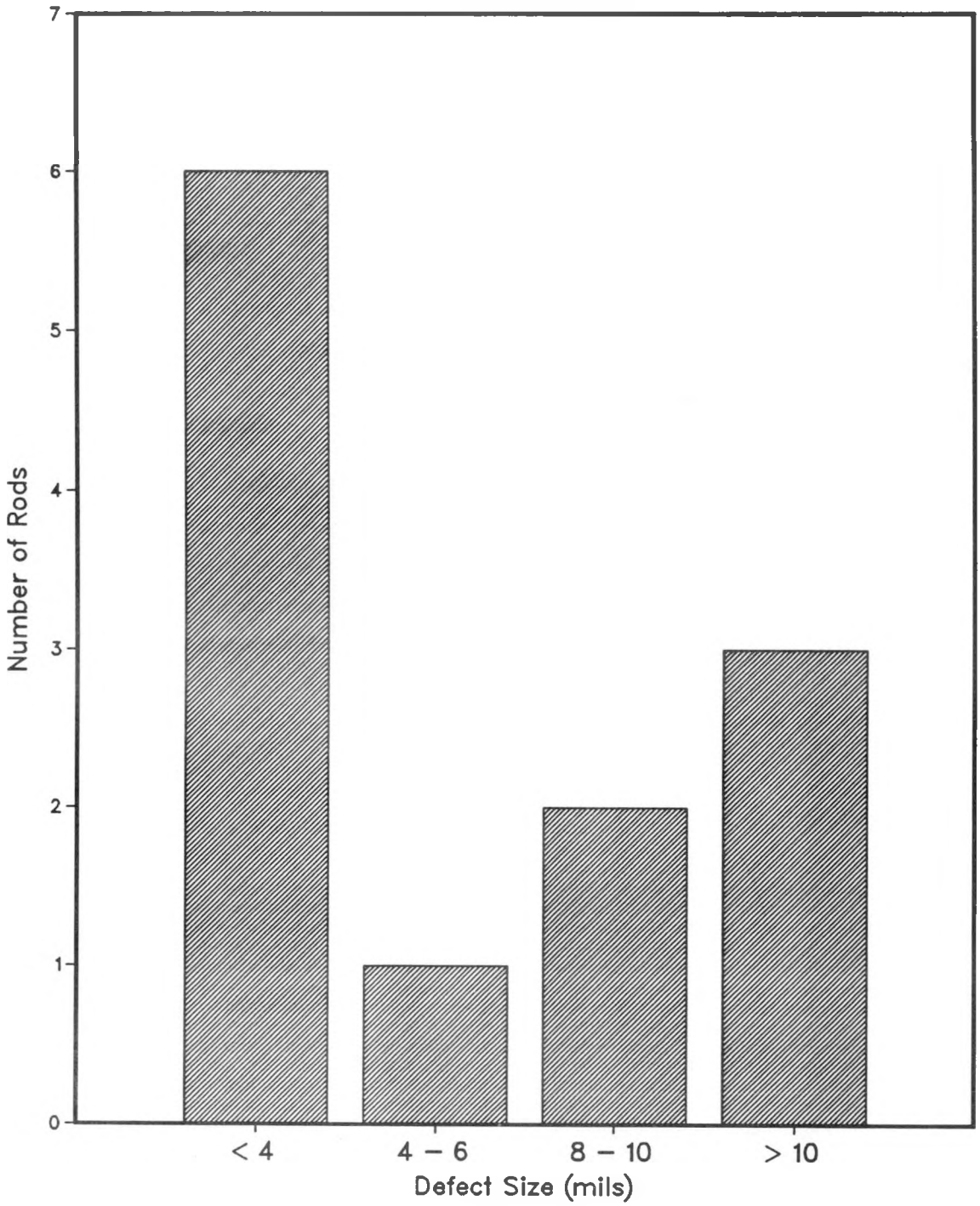

Figure 62 - Summary of UT Indications

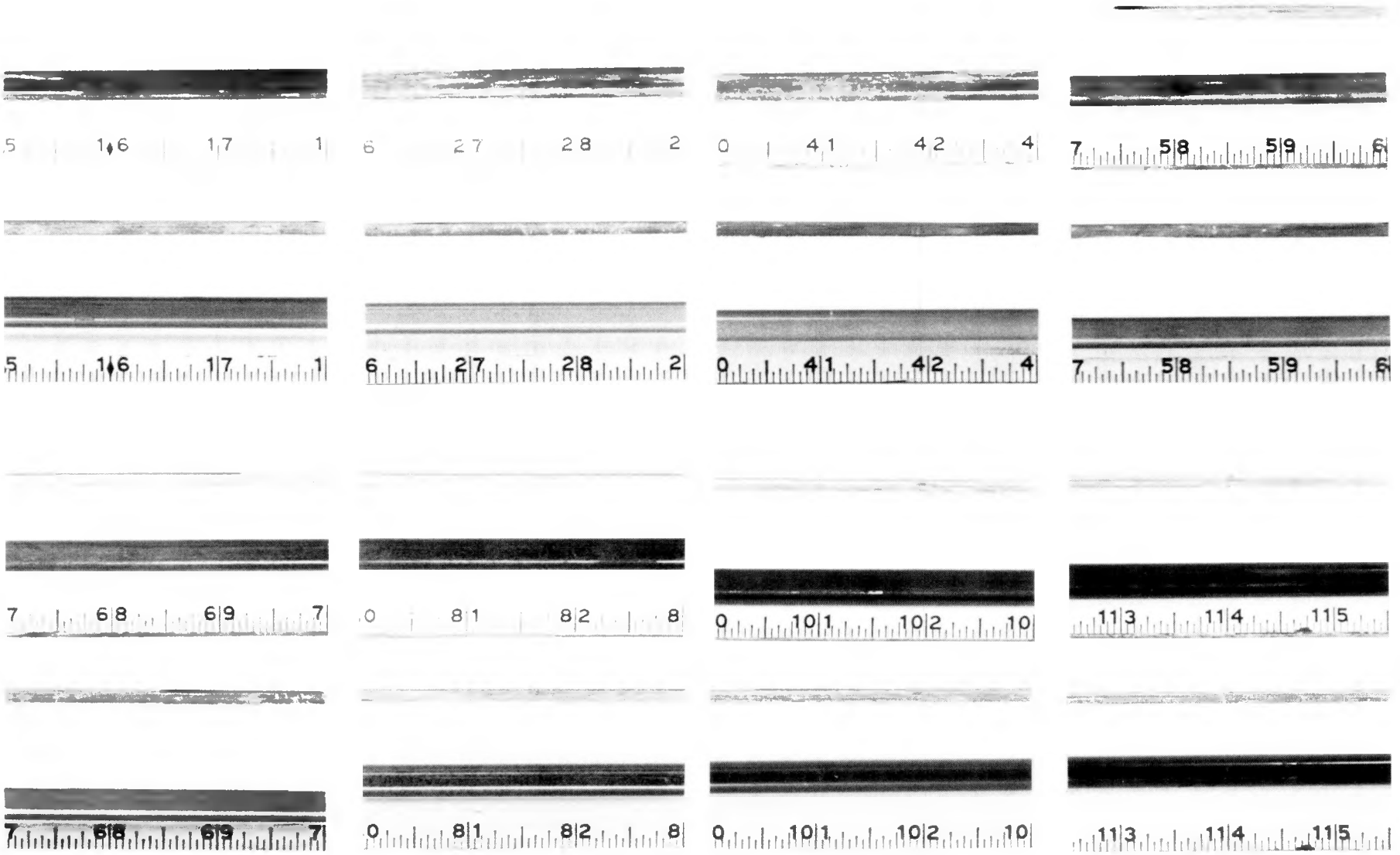

Figure 63 - Seed Rod 0504502 Pre- and Post-Descale Photographs

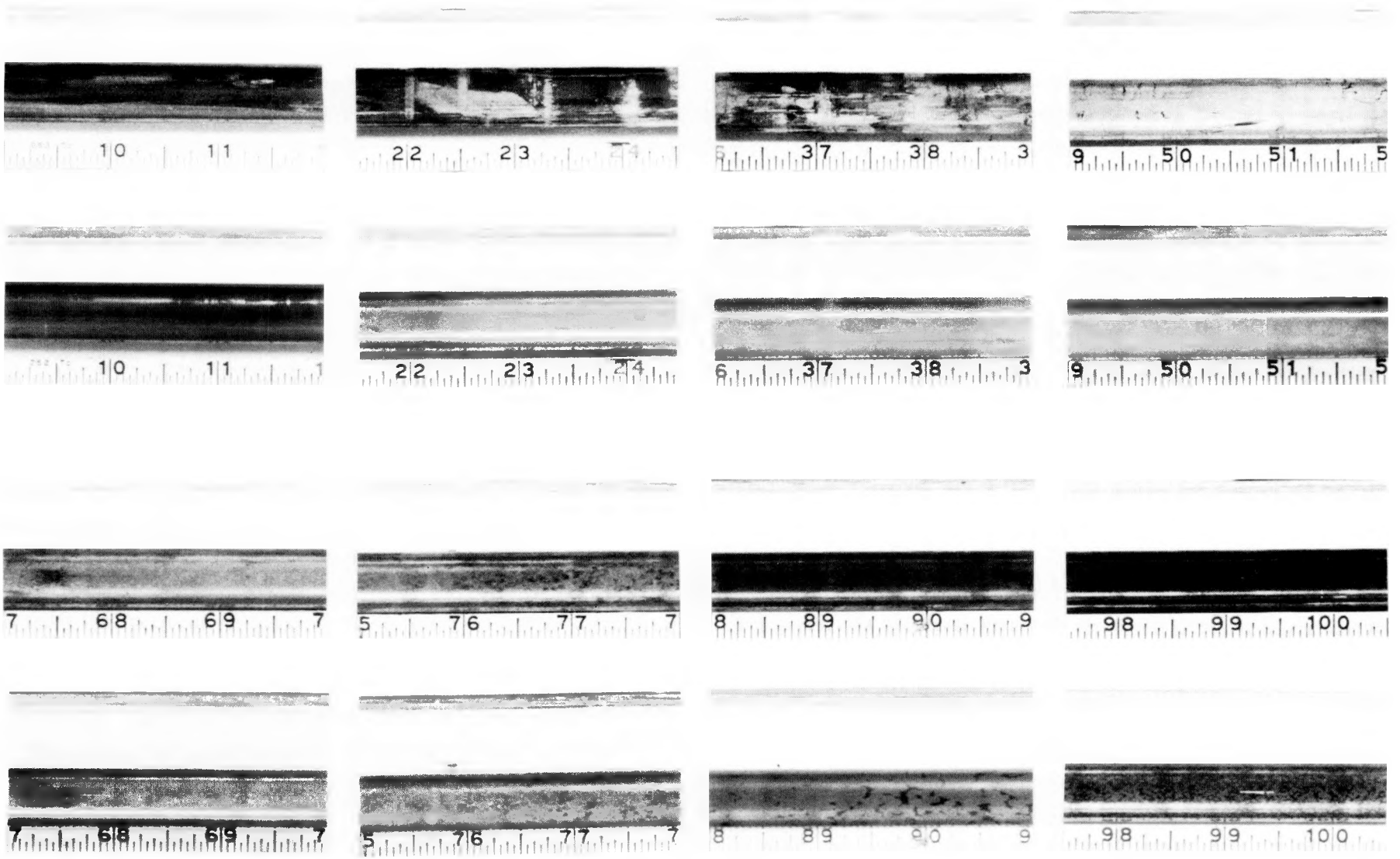

Figure 64 - Blanket Rod 1605629 Pre- and Post-Descale Photographs

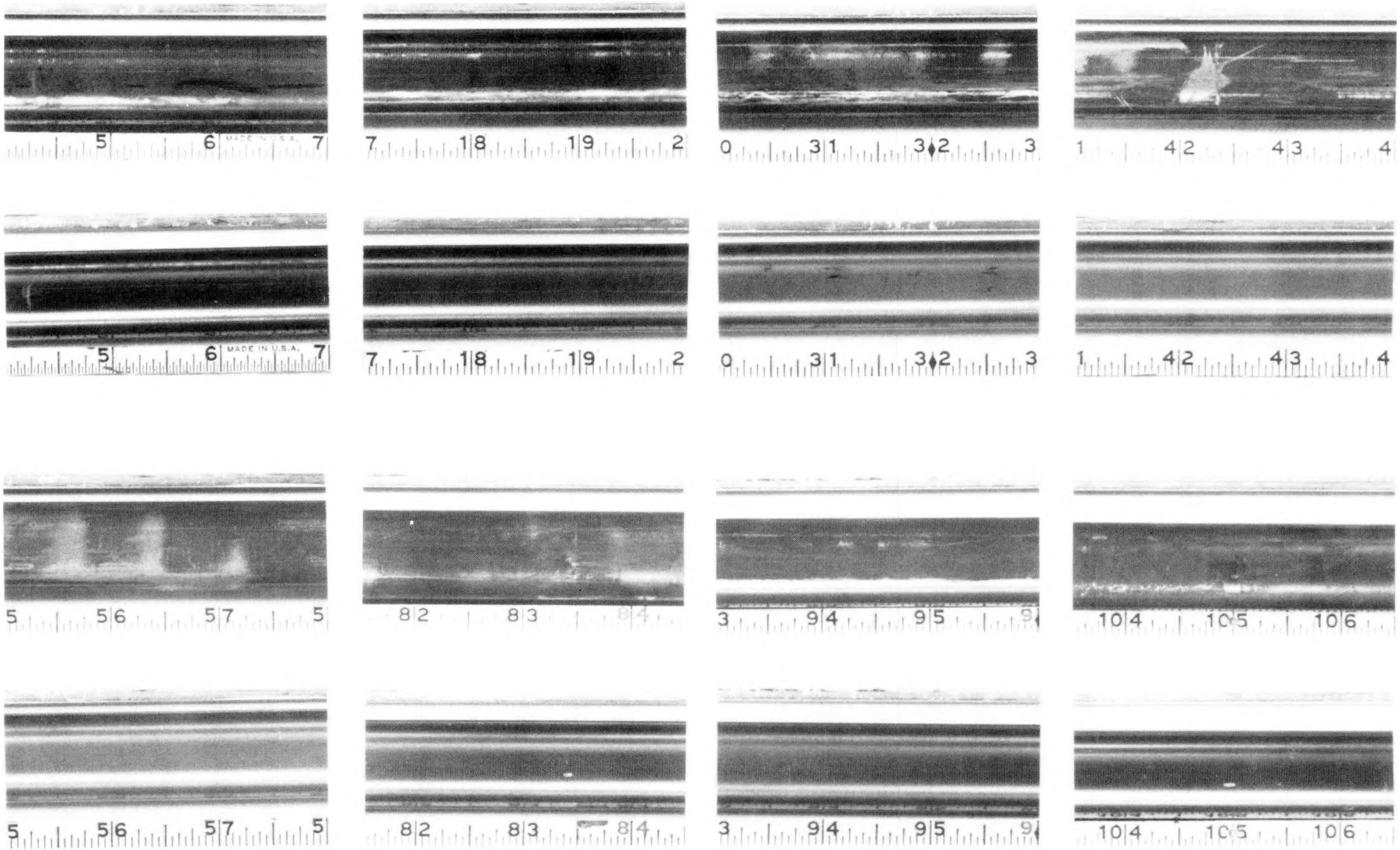

Figure 65 - Reflector Rod 3220018 Pre- and Post-Descale Photographs

As shown in the figures, chemical descaling was very effective in removing crud from fuel rods. This is particularly evident at the 23 and 38-inch levels of blanket rod 1605629, where the dark areas with gray smudges before descaling became uniform gray after chemical descaling. Similar changes in fuel rod appearance can be observed at the 27 and 42-inch levels of seed rod 0504502 and at the 42 and 56-inch levels on reflector rod 3220018. Comparison of the pre- and post-descale photographs also indicates that crud deposition was not uniform around the rods. Local smudge-like areas of crud were frequently observed on the fuel rods. As can be seen at the 99-inch level of blanket rod 1605629 and 82-inch level of seed rod 0504502, the mottled appearance on portions of the rod was not significantly changed by descaling, indicating that mottling of the rod was probably due to variations in corrosion oxidation of the fuel rod Zircaloy clad.

4.11.2 - Descale Solution Quantitative Analysis

Table 21 presents results of the quantitative analysis of the descale solutions for the incremental decrudding of rod 0504502 from seed module SI-1, rod 1605629 from blanket module BI-3, and rod 3220018 from reflector module IV-4. As shown, the descale solutions were examined for five elements (iron, nickel, chromium, cobalt, and copper). Activities were also determined for five isotopes (Fe-55, Ni-63, Co-60, Mn-54, and Sb-125). The values represent the deposition per unit area of rod surface and are based on the average for quantitative analysis of two decrud solution samples for each of the descale increments. Relative errors for the results as determined by ANL-W are presented in Table 22.

As shown in Figure 66, crud on the seed, blanket, and reflector fuel rods was predominantly made up of iron and nickel with a small amount (3 to 7 percent) of chromium. Levels of cobalt and copper were not measurable. Crud on the blanket fuel rod had a slightly higher percentage of iron than crud on the seed rod.

As shown in Figure 67, crud for all three rods had high Co-60 activities. Co-60 accounted for 44 to 68 percent of the radioactivity. Ni-63, Fe-55, and Mn-54 accounted for the remainder of the radioactivity. Traces of

Table 21 - Fuel Rod Crud Characterization

Seed Rod 0504502

	Elements (mg/dm^2)				
Increment	Fe	Ni	Cr	Co	Cu
First	0.38	0.45	0.10	nd*	nd*
Second	0.26	0.26	0.03	nd*	nd*
Third	0.54	0.88	0.08	nd*	nd*

	Radioisotopes ($\mu Ci/dm^2$)				
Increment	^{55}Fe	^{63}Ni	^{60}Co	^{54}Mn	^{125}Sb
First	3.87	3.45	10.21	7.74	nd*
Second	3.54	1.70	15.21	5.76	nd*
Third	5.23	1.95	26.87	6.54	trace

Blanket Rod 1605629

	Elements (mg/dm^2)				
Increment	Fe	Ni	Cr	Co	Cu
First	0.48	0.39	0.08	nd*	nd*
Second	0.73	0.56	0.04	nd*	nd*
Third	2.02	0.86	0.09	nd*	nd*

	Radioisotopes ($\mu Ci/dm^2$)				
Increment	^{55}Fe	^{63}Ni	^{60}Co	^{54}Mn	^{125}Sb
First	3.02	1.91	12.68	3.30	nd*
Second	8.52	5.57	42.61	7.10	nd*
Third	13.83	4.18	62.76	5.81	trace

Reflector Rod 3220018

	Elements (mg/dm^2)				
Increment	Fe	Ni	Cr	Co	Cu
First	0.49	0.47	0.04	nd*	nd*
Second	0.34	0.86	0.04	nd*	nd*
Third	0.40	0.04	0.04	nd*	nd*

	Radioisotopes ($\mu Ci/dm^2$)				
Increment	^{55}Fe	^{63}Ni	^{60}Co	^{54}Mn	^{125}Sb
First	2.03	1.48	2.61	3.47	nd*
Second	4.58	5.08	9.66	2.69	nd*
Third	2.16	0.73	5.13	nd*	nd*

*nd - not discernible

Table 22 - Fuel Rod Crud Characterization - Relative Errors

Seed Rod 0504502

	Elements (%)				
Increment	Fe	Ni	Cr	Co	Cu
First	8	5	7	na*	na*
Second	15	12	30	na*	na*
Third	29	14	45	na*	na*

	Radioisotopes (%)				
Increment	^{55}Fe	^{63}Ni	^{60}Co	^{54}Mn	^{125}Sb
First	4	5	4	6	na*
Second	4	5	4	8	na*
Third	4	5	4	16	na*

Blanket Rod 1605629

	Elements (%)				
Increment	Fe	Ni	Cr	Co	Cu
First	9	5	14	na*	na*
Second	7	5	18	na*	na*
Third	10	10	20	na*	na*

	Radioisotopes (%)				
Increment	^{55}Fe	^{63}Ni	^{60}Co	^{54}Mn	^{125}Sb
First	4	5	4	8	na*
Second	4	5	4	9	na*
Third	4	5	4	20	na*

Reflector Rod 3220018

	Elements (%)				
Increment	Fe	Ni	Cr	Co	Cu
First	2	3	4	na*	na*
Second	3	2	5	na*	na*
Third	11	153	24	na*	na*

	Radioisotopes (%)				
Increment	^{55}Fe	^{63}Ni	^{60}Co	^{54}Mn	^{125}Sb
First	4	5	4	19	na*
Second	4	5	4	31	na*
Third	4	5	5	na*	na*

*na - not applicable

Seed Rod 0504502

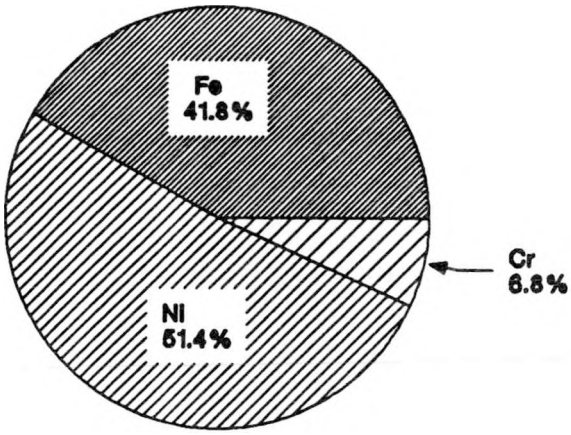

Blanket Rod 1605629

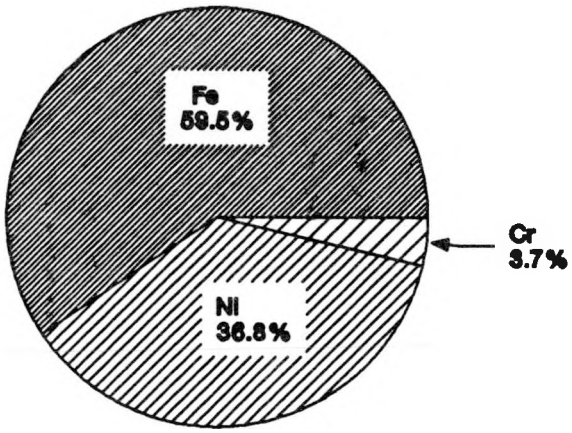

Reflector Rod 3220018

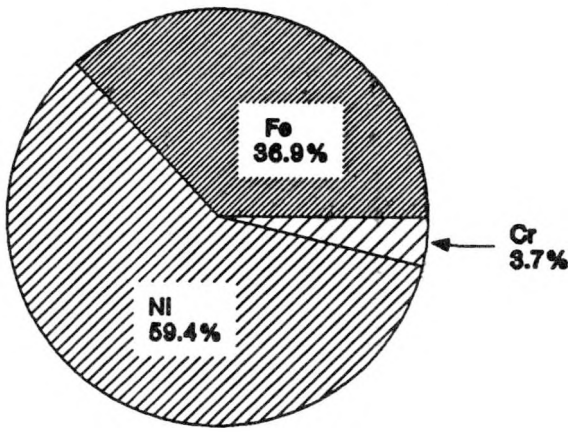

Figure 66 - Rod Total Crud Composition

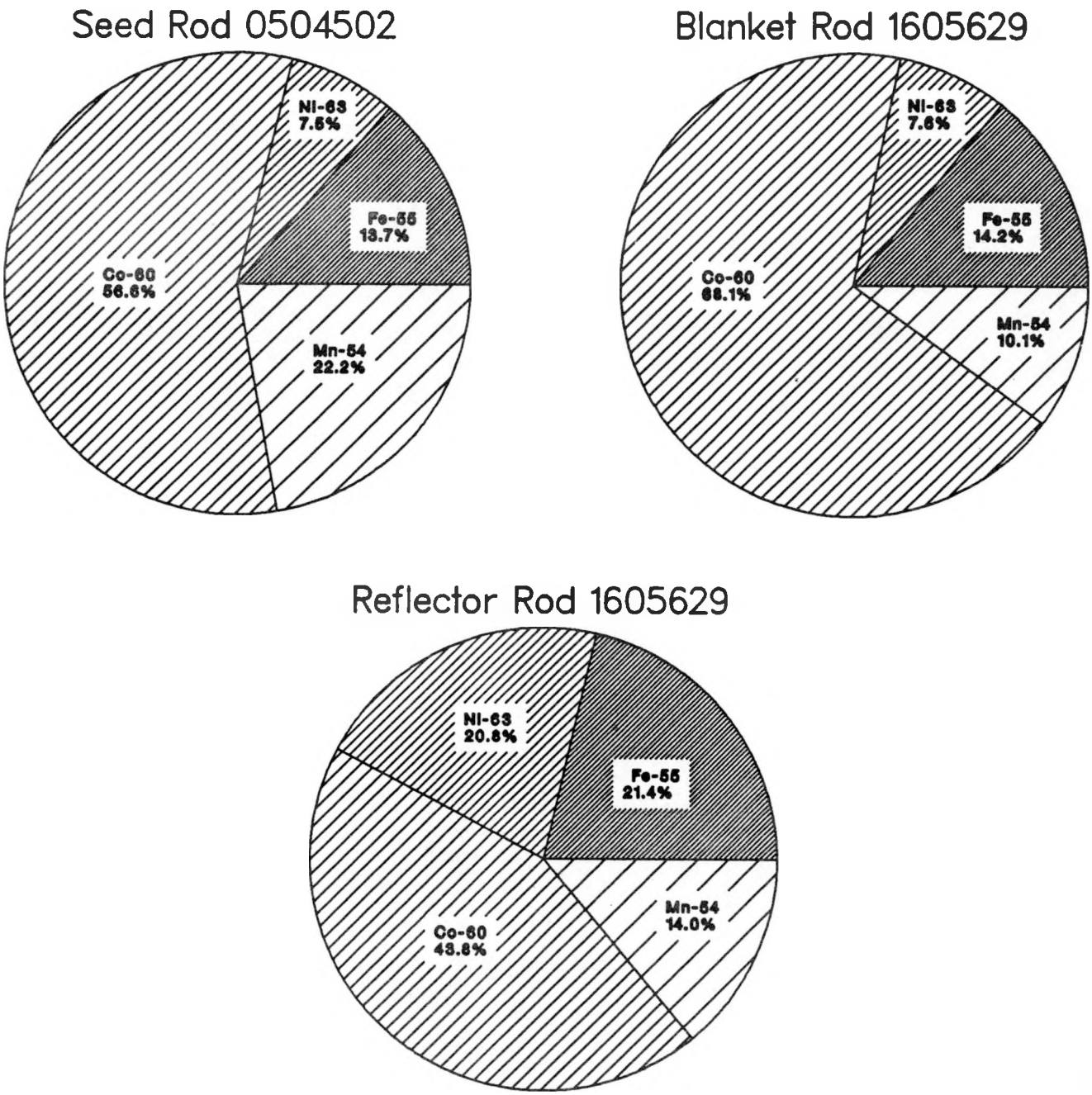

Figure 67 - Rod Total Isotopic Distribution

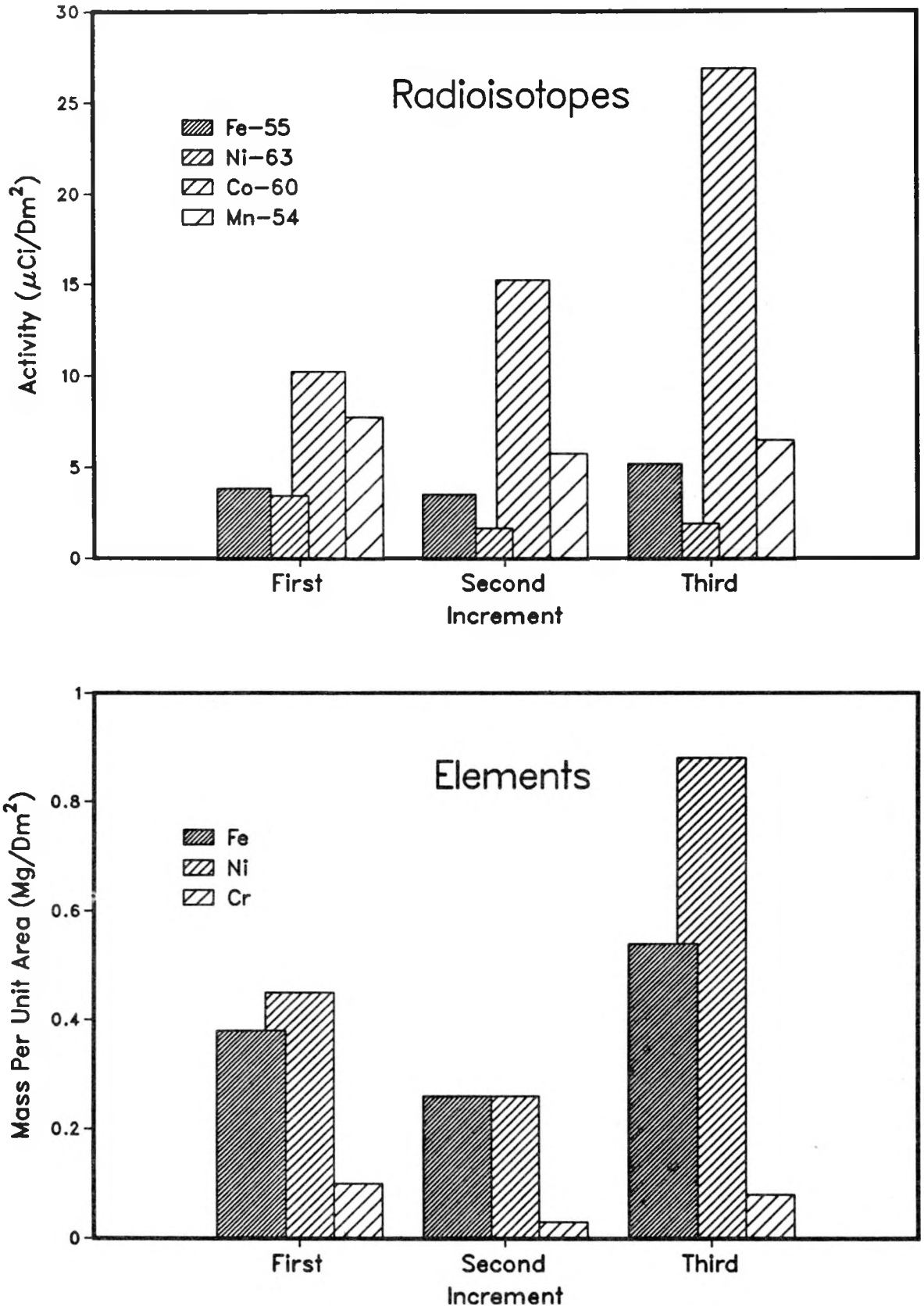

Figure 68 - Seed Rod 0504502 Crud Axial Variation
(Descale Solution Analysis)

Sb-125 were detected only at the top of the seed and blanket fuel rod. Radioactivity was highest for the blanket rod and lowest for the reflector rod.

Figure 68 shows the axial variation of the elemental and isotopic composition of crud on seed rod 0504502. Crud deposition as determined by elemental mass per unit surface area was lower for central 60 percent of the rod (second increment) than for the bottom (first increment) and top (third increment) 20 percent of the fuel rod. This is consistent with the distribution obtained during LWBR developmental testing and with crud thickness predictions. Crud deposition was greater at the top than at the bottom. Activities for Co-60 increased monotonically from the bottom to top of the rod. Activities for the other isotopes were slightly lower for the middle 60 percent of the rod versus the top and bottom 20 percent of the rod.

Figure 69 shows the axial variation of the elemental and isotopic composition of crud on blanket rod 1605629. Crud deposition increased from the bottom to the top of the rod. Crud deposition was four times greater for the top 20 percent of the rod versus the lower 20 percent of the rod. Crud deposition for the central 60 percent of the rod was approximately half of that for the top 20 percent of the rod. This distribution was inconsistent with the distribution obtained during LWBR developmental testing and with crud thickness predictions. Fe-55 and Co-64 also increased from bottom to top of the rod. Activities for Ni-63 and Mn-54 were slightly greater in the middle of the rod.

Figure 70 shows the axial variation of the elemental and isotopic composition of crud on reflector rod 3220018. Except for Fe concentrations, both elemental and isotopic measurements indicate that crud deposition was greater in the central 60 percent of the rod versus the upper and lower 20 percent of the rod. This distribution is also inconsistent with test results and predictions. Fe concentrations were slightly lower for the central 60 percent of the rods versus the ends.

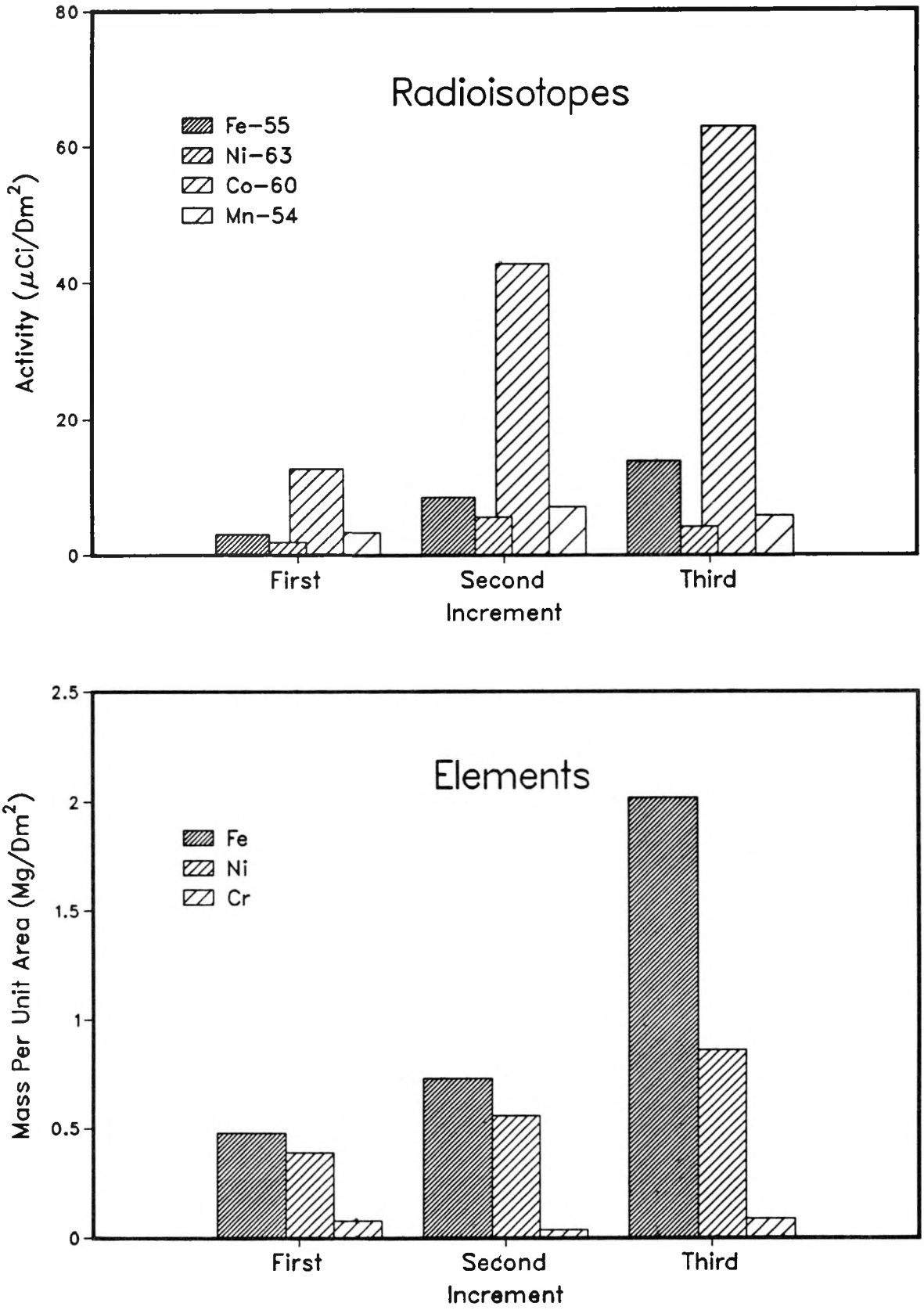

Figure 69 - Blanket Rod 1605629 Crud Axial Variation
(Descale Solution Analysis)

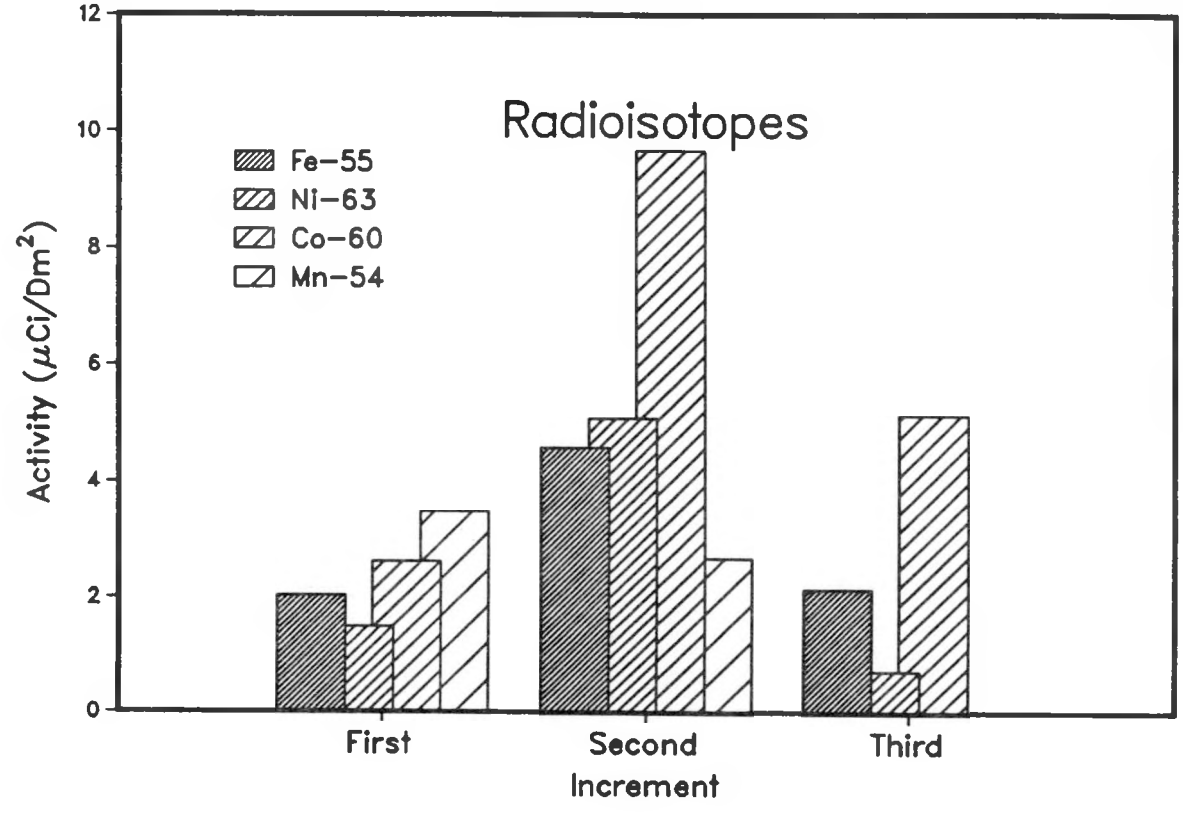

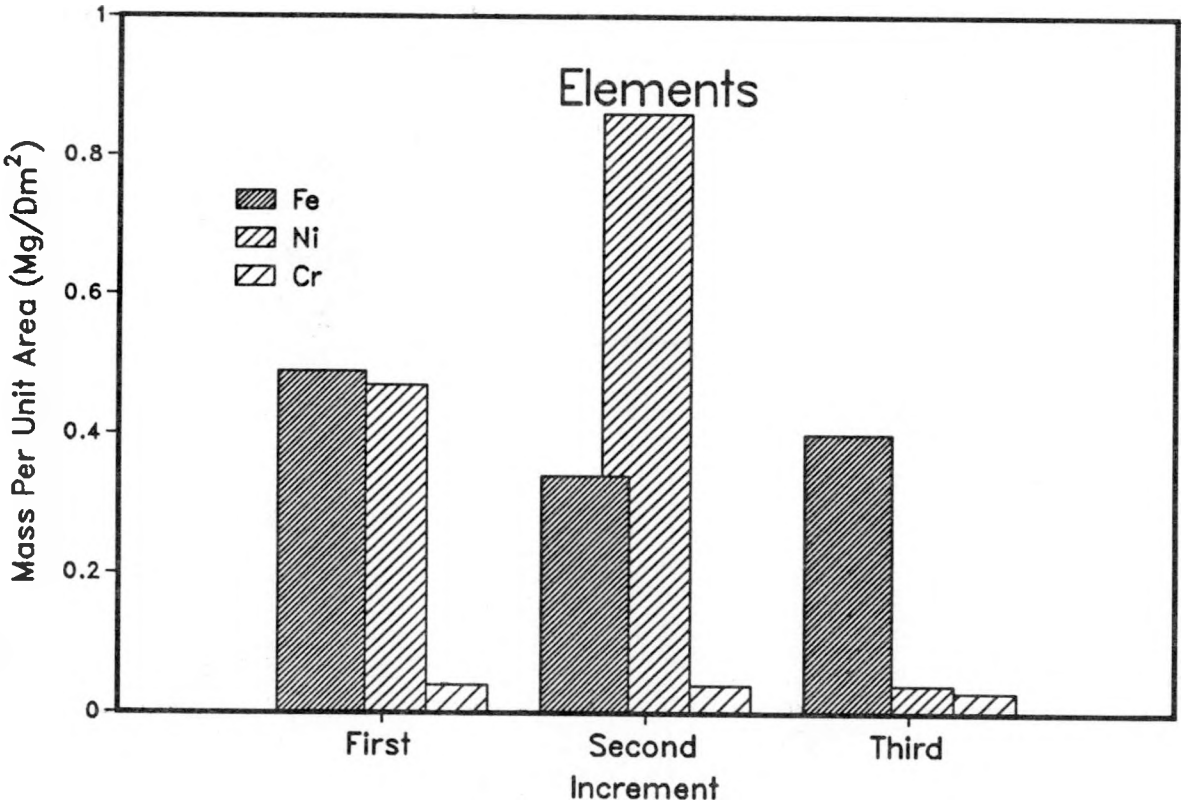

Figure 70 - Reflector Rod 3220018 Crud Axial Variation
(Descale Solution Analysis)

4.11.3 - Crud Diametral Thickness Measurements

Figure 71 presents crud diametral thickness axial profiles for the three rods examined by ANL-W. Crud thicknesses were determined from laser profilometer measurements of fuel rod diameter before and after chemical descaling. The thicknesses presented on these figures represent the average thickness for 5-inch increments along the length of the rod. They have been adjusted to account for suspected biases in diameter measurements. Local crud thicknesses (as determined by the difference between average diameters for three repeat predescale and three post-descale diameter measurements) for each of the rods examined are presented in Appendix A8.

Based on raw data, calculated local average diametral crud thickness for seed rod 0504502 varied from about 0.0001 inch at the ends of the rods to about -0.0015 inch near the middle of the rod. This thickness profile is relatively consistent with the crud deposition profile obtained from quantitative analysis of the descale solutions (Section 4.11.1) and the expected profile based on irradiation test results. The maximum local average thickness was 0.00030 inch at the top of the rod. The minimum local average thickness was -0.00018 inch near the middle of the rod. The average crud thickness for the entire rod was 0.00002 inch. The negative crud thicknesses (i.e., an increase in rod diameter after descaling) calculated for the central portion of the rod are believed to be due to a bias in the pre-descale diameter measurements. There is no reason to expect an increase in rod diameter by descaling. If the data is adjusted so that the minimum local average diametral crud thickness is 0.000 inch (Figure 71), crud thickness would vary from about 0.00028 inch at ends of the rods to about 0.0003 inch near the middle of the rod. The maximum local average crud thickness would be 0.00048 inch, with a rod average thickness of 0.00020 inch. These adjusted crud thicknesses are less than the 0.0030-inch end crud thicknesses and 0.0004-inch central crud thickness used for design calculations.

Based on raw data, calculated local average diametral crud thickness for blanket rod 1605629 was less than zero for most of the rod. It varied from about 0.00005 inch at the bottom of the rod to about -0.0003 inch at the middle

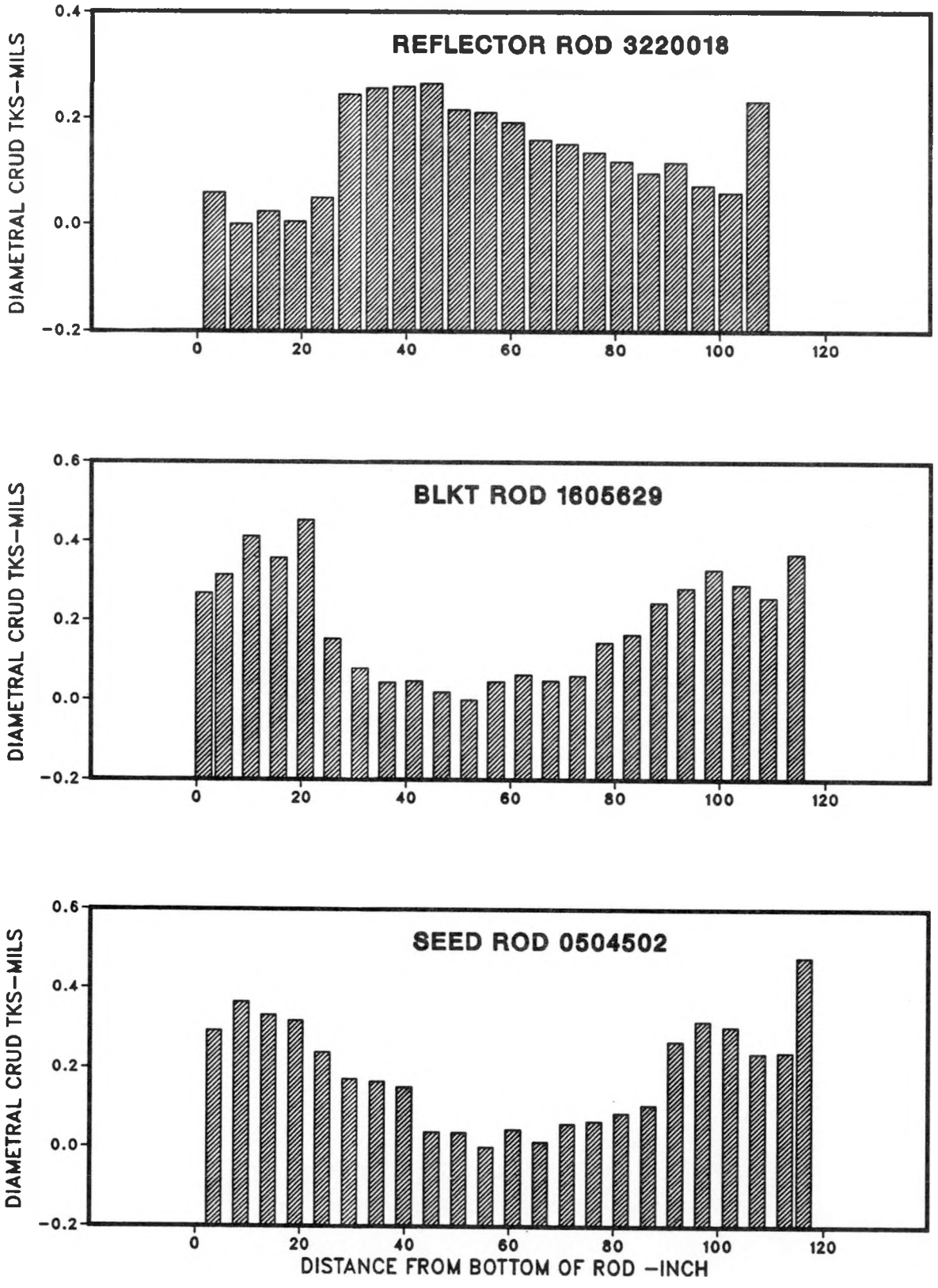

Figure 71 - Crud Thickness Variation (Adjusted)
from Diameter Measurements

of the rod to about -0.00005 inch at the top of the rod. This profile (i.e., large at the ends and small in the middle) is consistent with the crud profile obtained for irradiation test rods. It is inconsistent with the profile obtained from analysis of the decrud solutions. The maximum local average crud thickness was 0.00011 inch. The minimum local average crud thickness was -0.00034 inch. The rod average crud thickness was -0.00013 inch. If the blanket data is also adjusted so that the minimum local average crud thickness is 0.000 inch (Figure 71), calculated crud thickness would vary from about 0.00034 inch at the ends of the rods to about 0.00004 inch in the middle of the rod. The maximum local crud thickness would be 0.00045 inch, with an average thickness of 0.00021 inch. Crud thicknesses used for design calculations were 0.0034 inch for the top and bottom 20 percent of the rod and 0.00048 inch for the central 60 percent of the rod.

Based on raw data, calculated local average diametral crud thickness for reflector rod 3220018 varied from about -0.0001 inch near the ends of the rods to about 0.00015 inch at the 80-inch level of the rod. This profile is inconsistent with those obtained for seed rod 0504592 and blanket rod 1605629 examined by ANL-W and profile obtained for irradiation test rods. The profile is consistent with the crud deposition profile obtained from quantitative analysis of the descale solutions. The maximum local average diametral crud thickness was 0.00013 inch. The minimum local average diametral crud thickness was -0.00013 inch. The average diametral crud thickness was 0.00004 inch. Like the seed and blanket rods examined by ANL-W, there appears to be a bias of at least 0.00013 inch in the predecrud diameter measurements. If the calculated local average diametral crud thicknesses are adjusted for this bias (Figure 71), calculated crud thickness would vary from about 0.00003 inch at the ends to about 0.00028 inch at the 80-inch level. The maximum local average would be 0.00026 inch, with an average of 0.00017 inch. Crud thickness used for design calculations were 0.014 inch for the top and bottom 20 percent of the rod and 0.00053 inch for the central 60 percent of the rod.

4.12 - NEUTRON RADIOGRAPHIC EXAMINATIONS

Neutron radiographs of the 12 fuel rods scheduled for destructive examination provided information on fuel and cladding integrity, on fuel stack and upper plenum dimensions, and on plenum spring and sleeve conditions after five years of power operations. The radiographed rods are the first 12 listed in Table 6, which gives the ranges of peak power experience and accumulated depletion and fluence. Four radiographed rods were from seed modules, four were standard blanket rods, three were power flattening blanket rods, and one rod represented the reflector region. The 12 rods are grouped by fuel region in Tables 23 through 25.

With the exception of a slight separation between turns in the plenum spring of one rod, nothing unusual was observed in the radiographs. None of the radiographs of the 12 rods examined gave an indication of defected cladding or of massive hydriding, which would have appeared as white spots in the radiograph negatives. Except for several rods which had small in-stack gaps between pellets, pellet stacks were stable and continuous. No cocked pellets or crumbled pellets were observed. Pellet end dishes were still clear-cut and circular, indicating that no extreme pellet centerline expansion had occurred. Fuel pellets remained intact except for some cracking which was expected from experiences with irradiation test rods. Most pellet cracks appeared in the radiographs as hairline cracks; only a few were sufficiently wide to indicate fuel separation. Some pellet surfaces had scuff marks, probably due to spalling or to missing surface chips. End voids appeared on many pellets, some of which could be correlated with observations in pre-irradiation x-rays. No end void had an axial dimension greater than 0.2 inch and, although the radial and circumferential dimensions cannot be determined from radiographs, the observed voids were not considered detrimental to support of the cladding. None of the observed irregularities in pellet geometry or axial gaps would have led to loss of cladding integrity during power operations.

Table 23 - Binary Fuel Length Changes from Neutron Radiographs

Rod S/N	Cell	Module	Measured Binary Fuel Length (in.) As-Built	Post-Irradiation	Change	Predicted Change (in.)
0606773	6B4	SI-1	83.686	84.28	0.59	0.252
0507672	5L31	SI-1	84.143	84.93	0.79	0.284
0400736	4M33	SI-1	69.913	70.47	0.56	0.138
0205071	2Q41	SI-1	41.886	42.25	0.36	0.086
1606710	16E57	BI-3	84.073	84.52	0.45	0.119
1504272	15F11	BI-3	84.091	84.50	0.41	-0.011
1105717	11A46	BI-3	41.969	42.17	0.20	0.042
1208823	12A12	BII-2	42.017	42.18	0.16	0.043
2610746	26E68	BII-2	84.312	84.73	0.42	0.099
2607600	26E19	BII-2	84.260	84.71	0.45	0.092
2514164	25K13	BII-2	84.307	84.71	0.40	0.024

Table 24 - Thoria Fuel Length Changes from Neutron Radiographs

			Measured Top Thoria Fuel Length (in.)				Measured Bottom Thoria Fuel Length (in.)			
Rod S/N	Cell No.	Module	As-Built	Post Irradiation	Change	Predicted Change (in.)	As Built	Post Irradiation	Change	Predicted Change (in.)
0606773	6B4	SI-1	10.909	10.909	-0.01	-0.030	9.253	9.29	0.04	-0.030
0507672	5L31	SI-1	10.042	10.040	0.00	-0.029	9.661	9.69	0.03	-0.030
0400736	4M33	SI-1	24.928	24.930	0.00	-0.064	9.004	9.04	0.04	-0.030
0205071	2Q41	SI-1	52.940	52.960	0.02	-0.064	9.038	9.05	0.01	-0.027
1606710	16E57	BI-3	11.288	11.280	-0.01	-0.031	9.493	9.52	0.03	-0.026
1504272	15F11	BI-3	8.211	8.200	-0.01	-0.023	11.508	11.51	0.00	-0.031
1105717	11A46	BI-3	8.312	8.300	-0.01	-0.023	53.520	53.74	0.22	-0.031
1208823	12A12	BII-2	11.319	11.310	-0.01	-0.031	51.510	51.71	0.19	-0.079
2610746	26E68	BII-2	11.072	11.070	0.00	-0.031	9.488	9.52	0.03	-0.026
2607600	26E19	BII-2	11.087	11.093	0.01	-0.031	9.519	9.55	0.04	-0.026
2514164	25K13	BII-2	8.008	7.998	-0.01	-0.022	11.495	11.494	0.00	-0.032
3102657	1A1	RIV-3	101.075	100.990	-0.09	-0.296				

Table 25 - Plenum Gap Measurements from Neutron Radiographs

Rod S/N	Measured Gap Length (in.) As-Built	Post-Irradiation	Change	Predicted Change (in.)
1606710	0.501	0.54	+0.04	+0.86
1504272	0.485	0.54	+0.06	No Pred.
1105717	0.483	0.50	+0.02	+0.88
1208823	0.485	0.58	+0.10	+0.73
2610746	0.499	0.48	-0.02	+0.77
2607600	0.509	0.53	+0.02	+0.79
2514164	0.512	0.50	-0.01	+0.64
3102657	0.220	0.58	+0.36	+0.64

A compilation of pellet irregularities observed from radiographs of the 12 rods examined is given in Table 26. No in-stack gaps were found in seed or reflector rods. Gaps of 0.03 inch or less occurred in standard blanket rods. Pellets in blanket rods were not free to move independently of the cladding due to cladding shrinkage onto the pellets and into the end tapers. Seed and reflector pellets (except for those near mid-elevation in the high-duty reflector rods) were free of the cladding and apparently had no other interacting mechanisms (such as cocked pellets and lodged fuel chips) to cause a pellet to hang up and thereby leave a gap. The small gaps in the blanket fuel stacks were not detrimental to cladding support, and the increased stack length caused by accumulated gaps (maximum of 0.11 inch among the four rods) was accommodated by the plenum gap.

Pellet end voids were prevalent in the reflector rod (on 30.4 percent of the pellets) and one standard blanket rod (on 32.6 percent of the pellets). Other blanket rods had a maximum of 16.1 percent. Seed rods had a maximum of 3.4 percent. All voids were less than 0.2 inch on the side and most were less

Table 26 - Fuel Pellet Irregularities Observed in Neutron Radiographs

Rod S/N	Number of Axial Gaps (Total Gap, in.)	Percent of Pellets with Irregularities					
		End Voids	Transverse Cracks	Axial Cracks	Transverse & Axial Cracks	Total Cracked	Spalled Surface
0606773	0	2.8	0.6	4.0	0	4.6	0
0506762	0	3.4	0	4.5**	0	4.5	0.6
0400736	0	0	0	5.9**	0	5.9	0
0205071	0	1.4	2.4	4.7**	4.2	11.3	1.9
1606710	5(.05)	16.1	26.6	6.3	14.7	47.6	1.4
1504272	3(.03)	32.6	23.5**	3.8	0	27.3	0.8
1105717	6(.11*)	6.1	21.7**	1.1	2.8	25.6	0.6
1208823	5(.07)	12.5	10.9	9.8	4.3	25.0	0
2610746	1(.02)	3.0	21.6	7.8	11.4	40.7	0.6
2607600	4(.04)	8.4	15.6	3.6	9.6	28.7	0
2514164	2(.02)	8.4	12.6	14.4	3.0	30.0	0
3102657	0	30.4	0	4.3	0	4.3	1.4

*Maximum axial gap in-stack was 0.03 inch.
**At least one crack was sufficiently wide to indicate fuel separation.

than 0.1 inch. No void extended circumferentially as much as 90 degrees. With these maximum dimensions, no void was large enough to jeopardize pellet end land support or cladding support.

Pellet cracks were classified as transverse or axial; some pellets contained both in a cruciform shape. The percentages of each are listed in Table 26, with the understanding that many more axial cracks not aligned with the neutron beam most likely escaped detection. The total number of cracked pellets was greatest in blanket rods, probably due to the forces resulting from pellet-cladding interaction. Transverse cracks predominated in blanket rods. Two standard blanket rods each contained one pellet with fuel separation at the transverse crack. The separations were less than 0.02 inch and not detrimental to cladding support. Three seed rods contained pellets with fuel separation at axial cracks. No axial shifting of the fuel pieces resulted, however, and no detrimental fuel-cladding interaction was evident in rod diameter measurements at those locations. Two locations of axially cracked pellets in seed rods were designated for metallographic samples, (Reference 5).

Spalled pellet surfaces were the only remaining irregularity observed on fuel pellets. Their frequency (less than 2 percent of the pellets in any rod) and their size (less than 0.1-inch diameter) were not sufficient to affect the cladding.

In the plenum regions, one spring irregularity was observed from the radiographs. The spring of standard blanket rod 2504272 had a separation in the spring at 5.8 inch from the top. The radiographs showed a 0.02-inch spacing between turns. Removal of the spring for examination revealed the sharp bend in the coil. This spring irregularity was not detrimental to fuel rod integrity. No other irregularities to the plenum hardware or endclosures were observed in the neutron radiographs.

Fuel stack dimensions were determined from the scales and reference marks appearing in each radiographic segment. Measured binary and thoria stack lengths are listed with as-built dimensions and the resulting length change in Tables 24 and 25. Predicted and measured stack length changes for stack

lengths greater than 12 inches are plotted in Figure 72. Both binary and thoria length changes were greater than predicted, which is consistent with those fuel stacks measured from gamma scans (Section 4.13).

Plenum gap lengths were measured from radiographs; results are given in Table 25. Gaps increased in standard blanket rods, but far less than expected (approximately 0.8 inch less) due to the less-than-predicted cladding length changes. Plenum gap data are used to evaluate cladding deformation as measured by cladding ovality in the plenum gap area.

Rod lengths measured from radiographs were consistent with lengths measured on the REX. Comparisons of measured and predicted length changes are included in Figures 31 through 34.

4.13 - GAMMA SCANS OF FUEL RODS

Gamma scans of 24 core examination fuel rods were performed at ECF using the PIFAG gamma scan facility. Results of gamma scans provided data for axial profiles of fuel depletion, for measurement of fuel stack lengths, and for indications of in-stack gaps. The fuel rods scanned were not scheduled for neutron radiography. Therefore, gamma scans provided the only means of detecting in-stack gaps and of measuring fuel stack lengths for these rods. One rod, however, was later used as a replacement DE rod and thereby received both gamma scan and radiographic examinations.

Scans of the full stack lengths of reflector rods were obtained, and in seed and blanket rods the binary fuel section and the upper thoria section were scanned. The lower thoria section of a seed or blanket rod was not fully scanned due to length restrictions in the measuring facility. Measurement precision was improved in the low-power thoria regions by removal of lead shielding that was normally in place to prevent detector saturation at peak power locations. The plotted gamma ray counts showed no indication of in-stack gaps over the lengths scanned, and fuel stack length increases were greater than predicted.

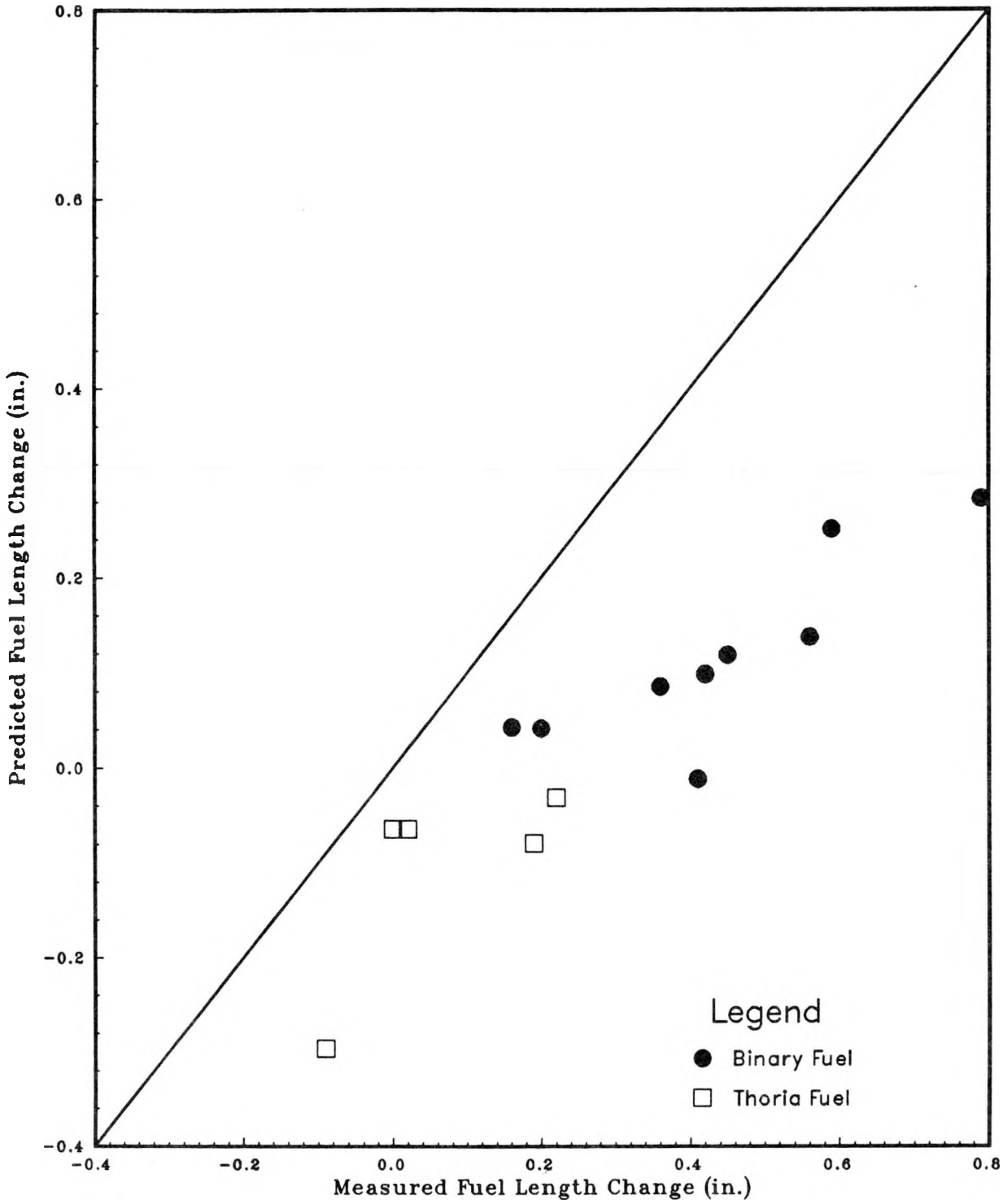

Figure 72 - Fuel Stack Length Changes Based on Neutron Radiographs

4.13.1 - Axial Profiles

Gamma ray counts from Cs-137 provided the basis for the typical axial profile plots shown in Figures 73 through 77. Figures 73 and 74 show scan results from seed rods, one scan of a full-length binary rod and one of a half-length binary (thoria wedge) rod. Figures 75 and 76 show scan results from standard blanket rods, a full-length binary and a wedge rod. The axial profiles from gamma scan of a typical reflector rod are shown in Figure 77.

Binary-thoria fuel interfaces can be discerned in the plots, and the results of flux depressions at grid levels are evident at the higher power locations on the profiles. Repeat scans near the tops of the fuel stacks, with shielding removed to improve detection, are shown for each rod. The reflector rod plot also had a repeat scan at the lower end. Confirmation of CINDER calculations (Reference 30) is provided by the profile of Cs-137 counts for a reflector rod in Figure 78. The major differences between gamma counts and CINDER-calculated counts occur at the grid-induced flux depression locations, but in general, the gamma scan coincides with the CINDER calculations. Thus, gamma scan profiles support the CINDER-calculated axial depletion profiles of the fuel rods.

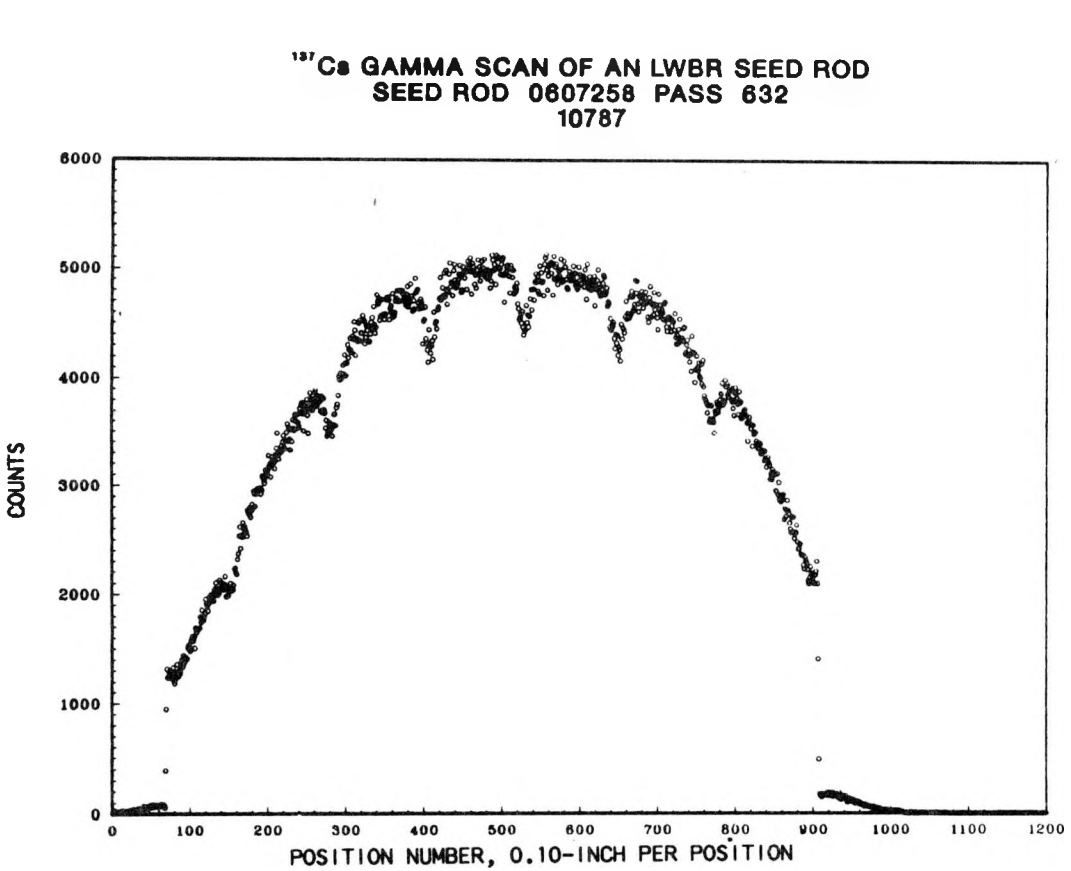

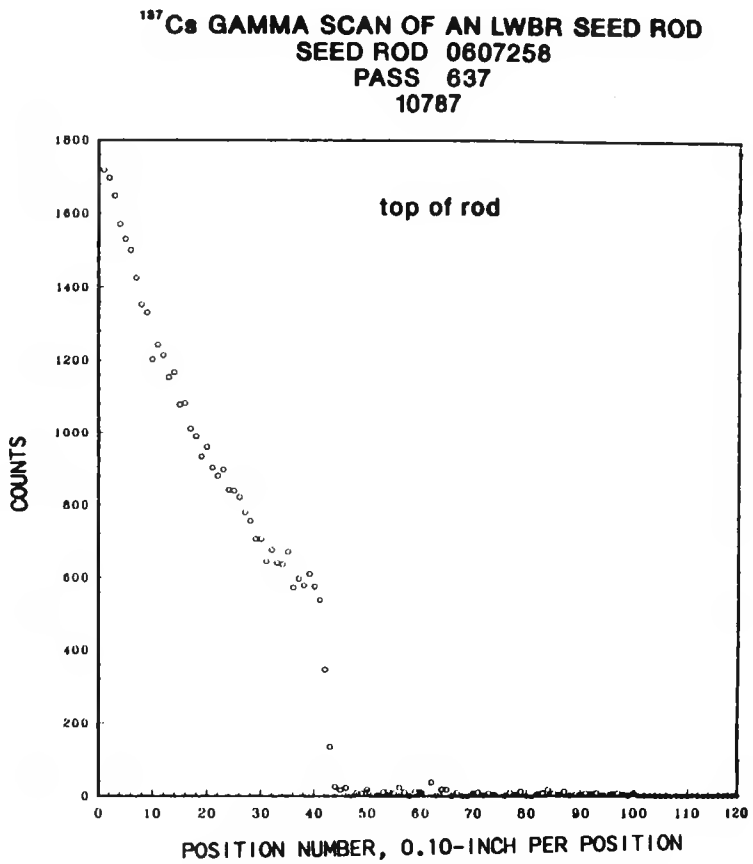

Figure 73 - Gamma Scan of Seed Rod with Full-Length Binary Fuel

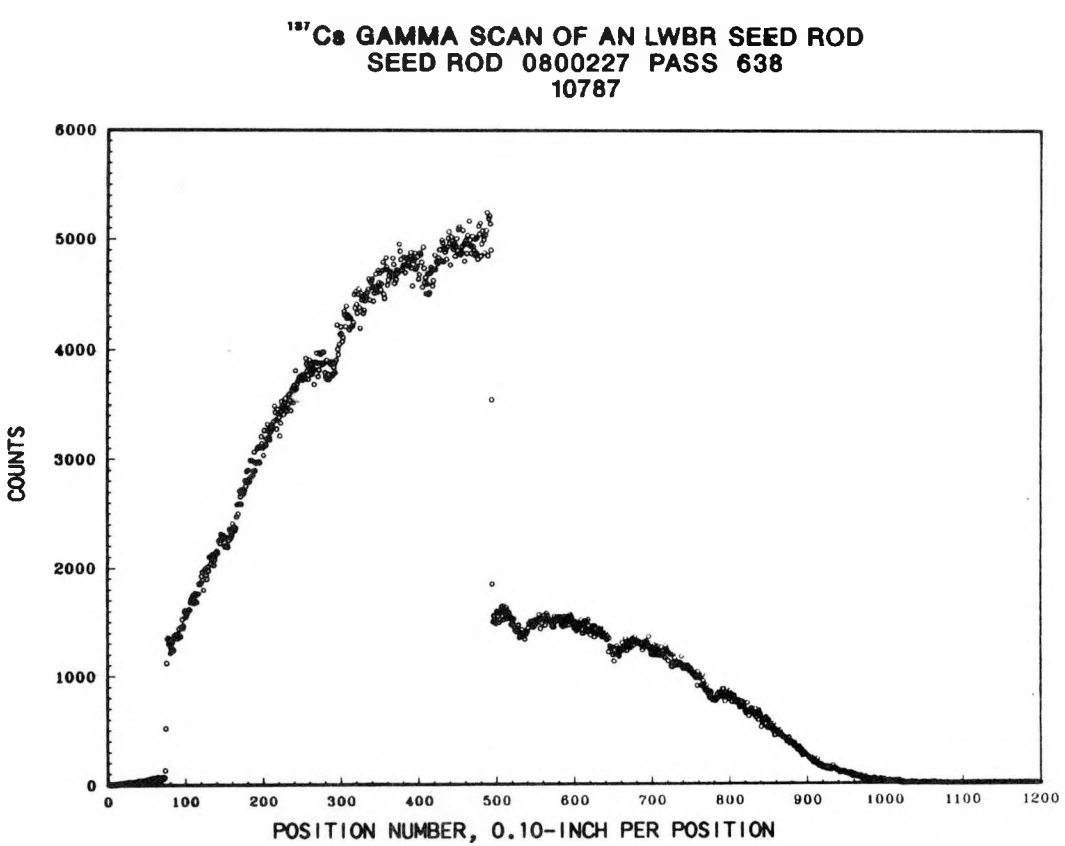

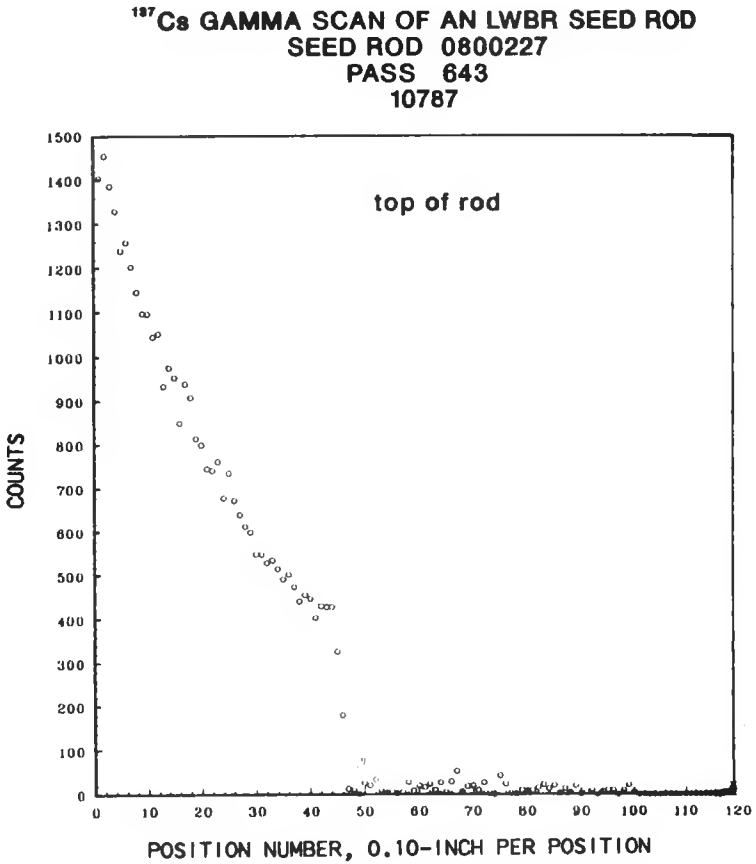

Figure 74 - Gamma Scan of Seed Rod with Thoria Wedge

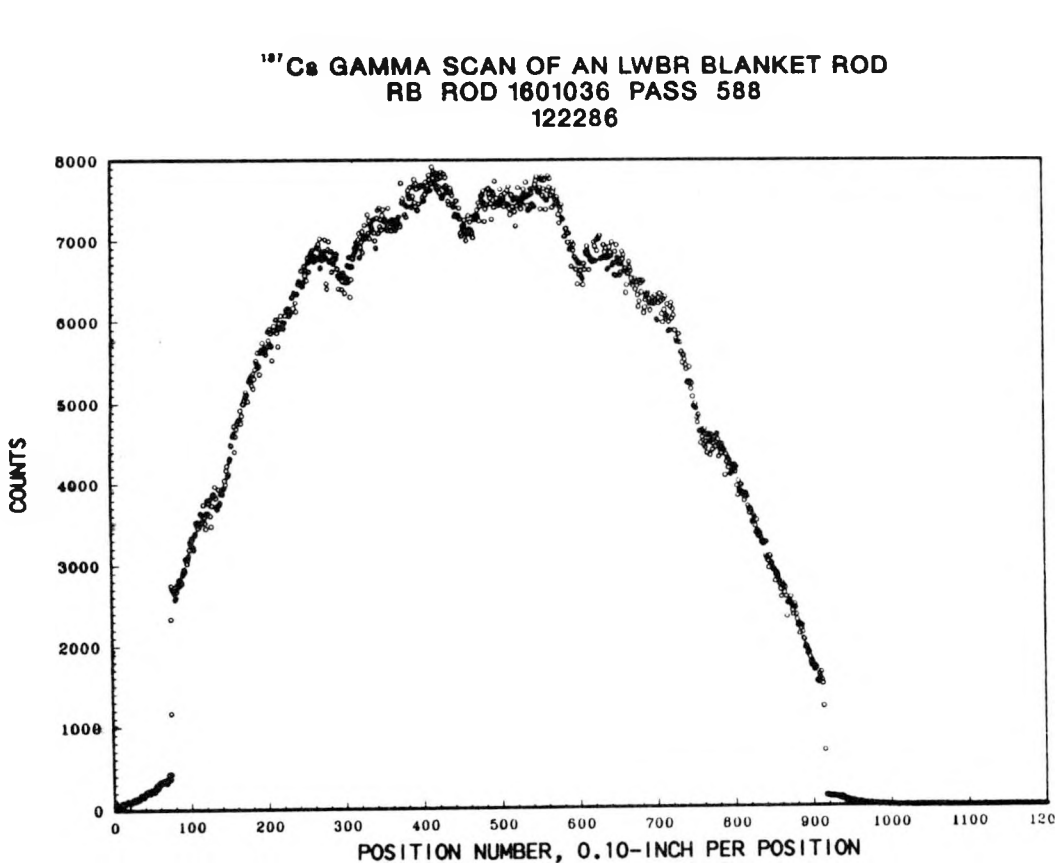

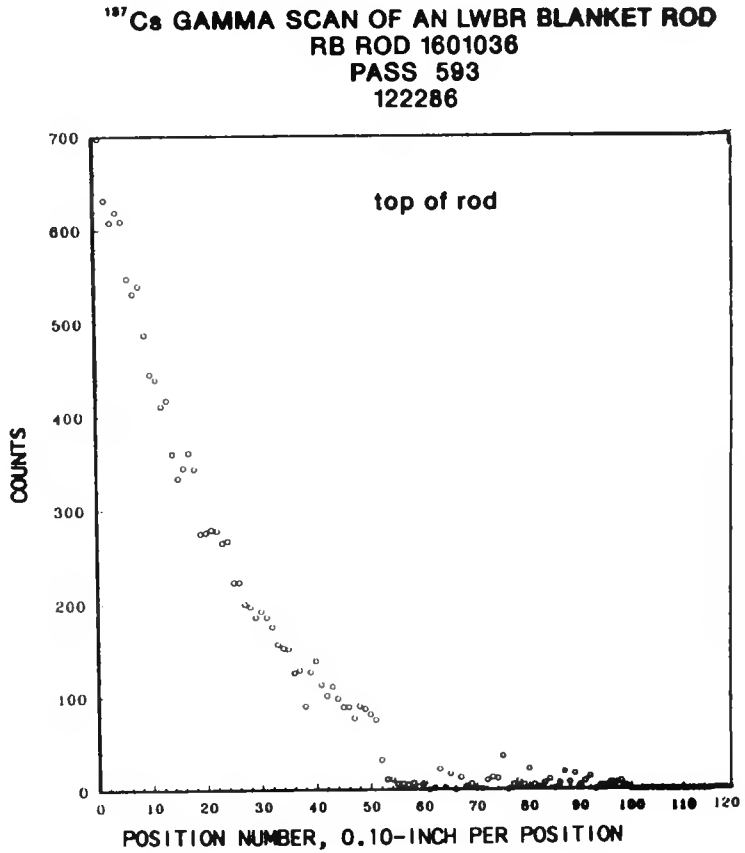

Figure 75 - Gamma Scan of Standard Blanket Rod
with Full-Length Binary Fuel

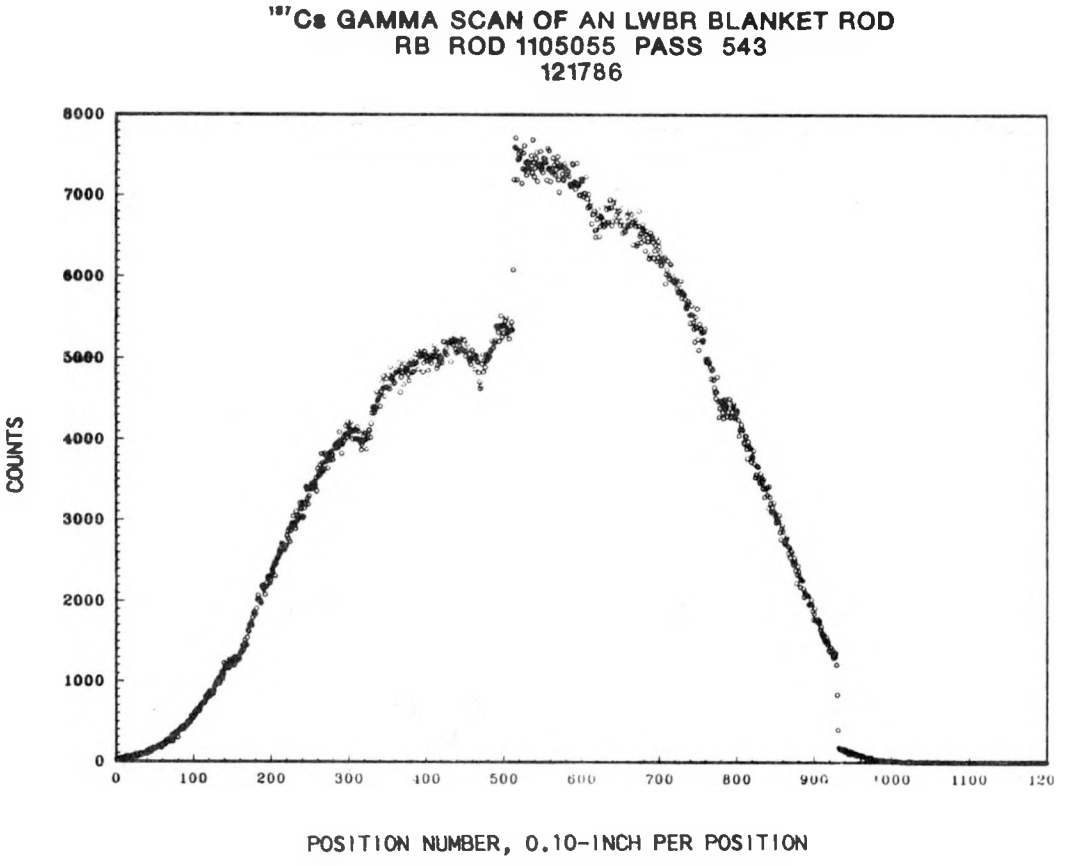

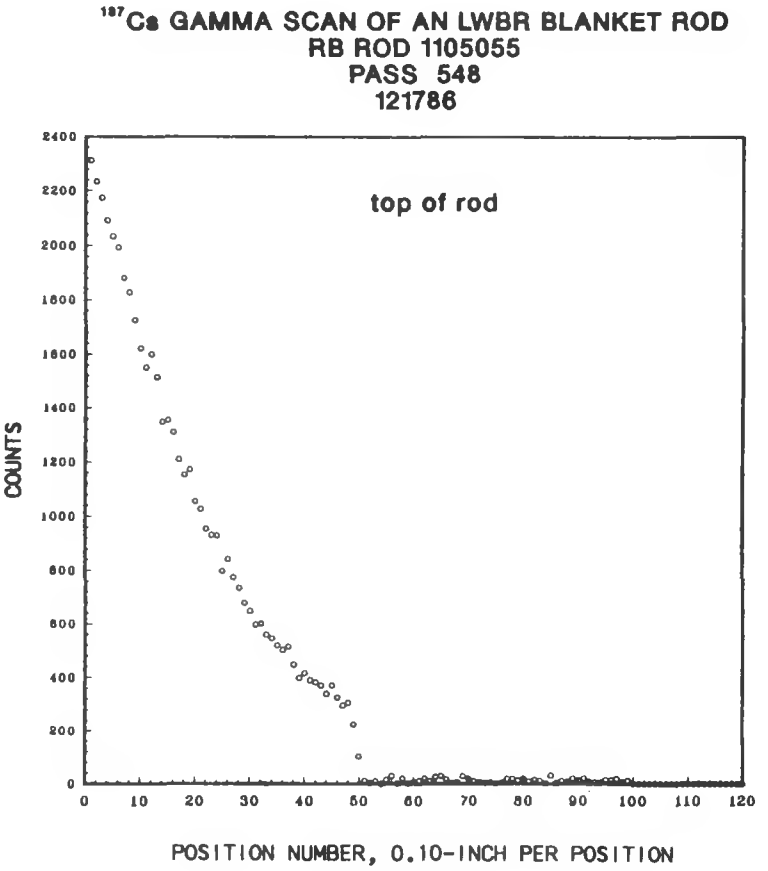

Figure 76 - Gamma Scan of Standard Blanket Rod with Thoria Wedge

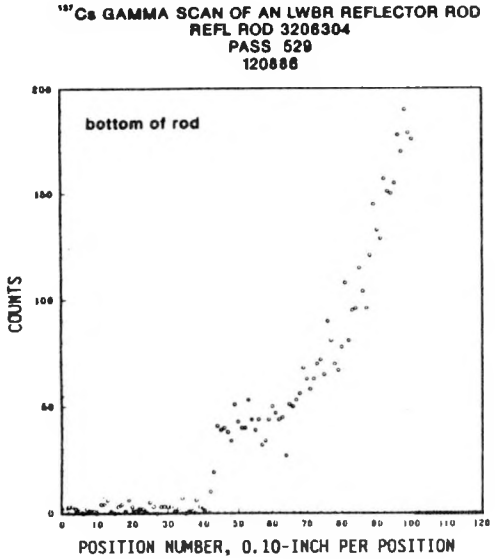

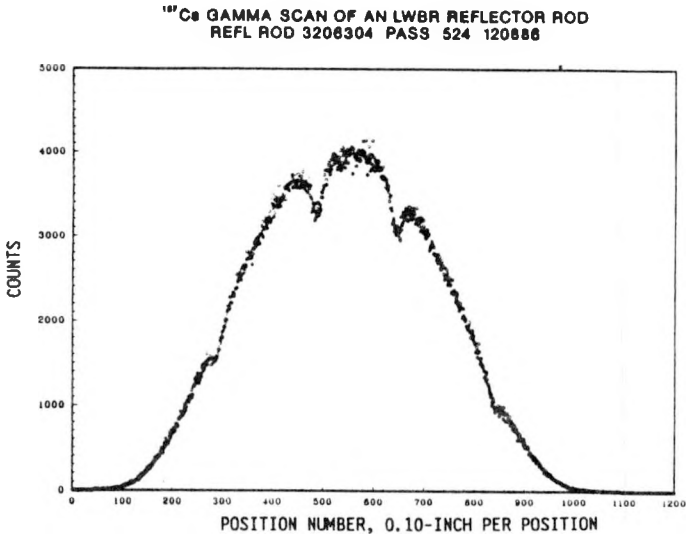

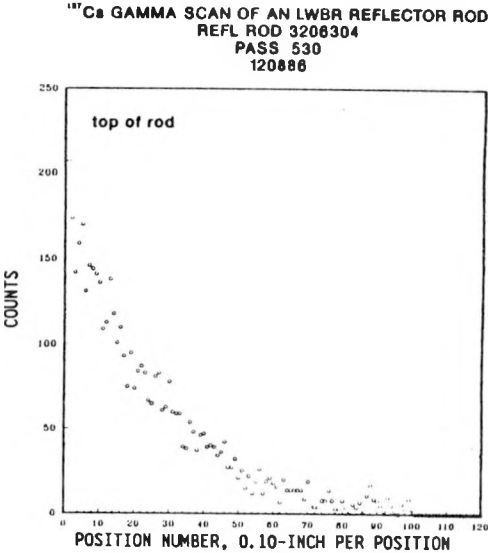

Figure 77 - Gamma Scan of Reflector Rod

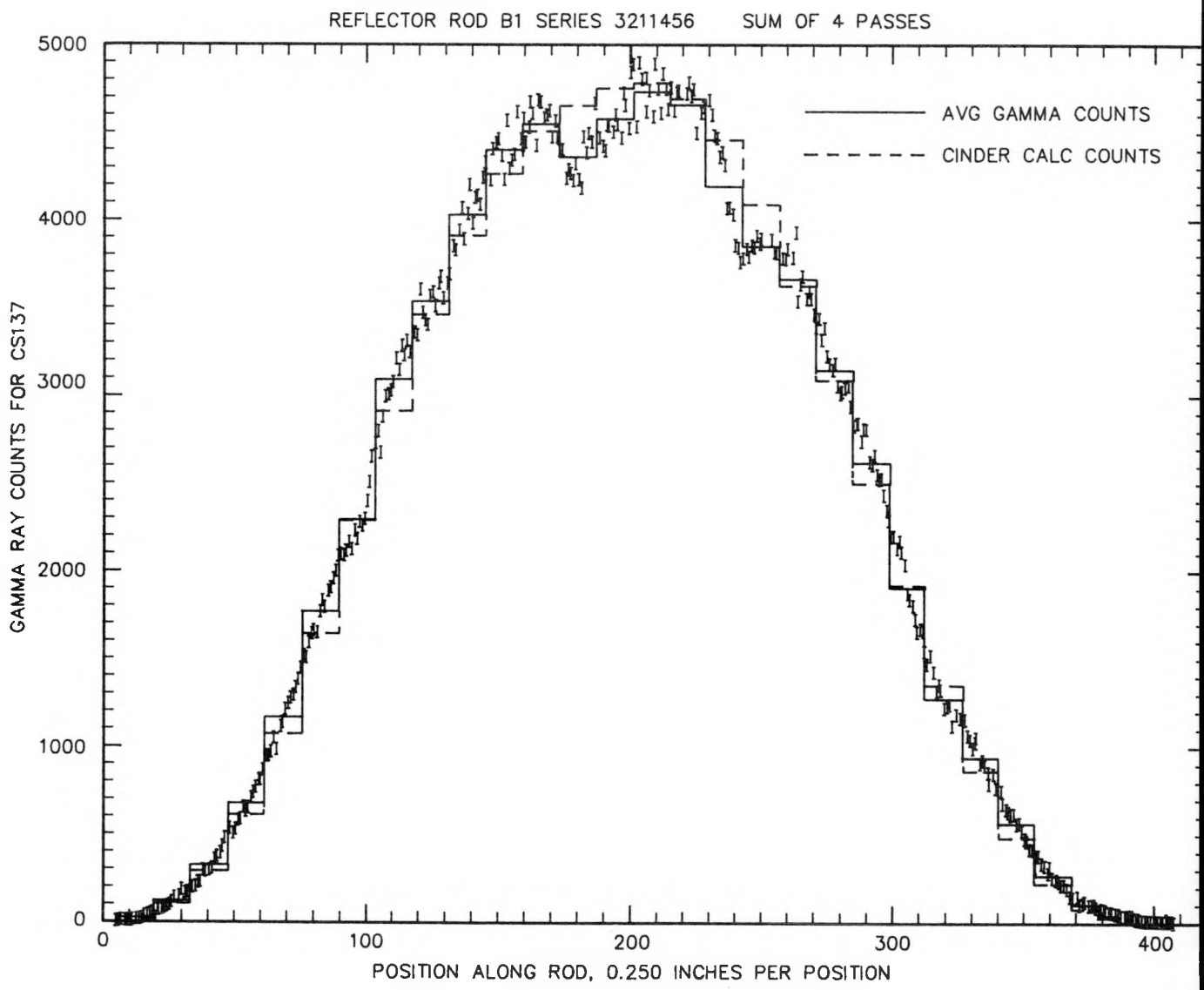

Figure 78 - Gamma Count Compared with CINDER-Calculated Count on Reflector Fuel Rod

4.13.2 - Fuel Stack Lengths

The sharp changes in gamma counts at the binary-thoria fuel interfaces provide a measurement of the binary fuel length in seed and blanket rods. Top thoria lengths and reflector stack lengths can also be obtained from the repeat scans of thoria regions with shielding removed. Fuel lengths of binary and top thoria sections so measured are listed in Table 27. From this measurement data and pre-irradiation length data, the fuel length change was calculated as shown for the binary and thoria sections.

Predicted fuel length changes are plotted against measured changes in Figure 79 for all binary lengths listed in Table 27 and for those thoria lengths greater than 12 inches. Length predictions and measurements of the shorter thoria lengths were subject to greater error, as shown in Table 27. The plotted comparison in Figure 79 shows that measured fuel length increases are greater than predicted.

A comparison of binary length measurement of rod 2607600 from both gamma scan and radiograph gives an indication of gamma scan accuracy. From the gamma scan, the binary length at EOL was 84.46 inches, and from the radiograph 84.71 inches, a difference of 0.25 inch. This error is appropriate for measurements where gamma counts are taken at 0.10-inch increments with a 0.20-inch window, and the length is a difference of two readings.

Fuel length changes are believed to result from the following mechanisms built into the LWBR analysis model:

a. Fuel densification by elimination of small pores early in life at high fuel temperatures.
b. Fuel swelling caused by fission gas generation and from irradiation-induced solids swelling.
c. Fuel cracking, creating small gaps at the crack locations.
d. Fuel-cladding interaction in which the fuel is restrained from length increase by the cladding and the cladding elongation is increased by fuel stack expansions.
e. Creation of in-stack gaps between pellets.

Table 27 - Gamma Scan Results

			Measured Binary Fuel Length (in.)				Measured Thoria Fuel Length (in.)				
Rod S/N	Cell No.	Module	As-Built	Post-Irradiation	Change	Predicted Change(in.)	As-Built	Post-Irradiation	Change	Predicted Change(in.)	In-Stack Gaps
0604555	6B3	SI-1	84.154	84.789	0.635	0.199	10.879	11.683	0.804	-0.032	None
0602209	6K27	SI-1	84.185	84.907	0.722	0.215	10.896	10.872	0.008	-0.032	None
0800117	8Q37	SI-1	41.827	42.205	0.378	0.125	52.889	52.983	0.094	-0.064	None
0702069	7P46	SI-1	41.849	42.204	0.355	0.126	52.063	52.156	0.093	-0.076	None
0301340	3N38	SI-1	56.179	56.710	0.531	0.165	38.048	37.955	-0.093	-0.073	None
0205154	2Q32	SI-1	41.827	42.299	0.472	--	52.926	52.981	0.055	--	None
0800227	8Q49	SIII-1	41.952	42.199	0.247	--	52.897	52.884	-0.013	--	None
0607258	6K14	SIII-1	83.866	84.494	0.628	0.275	10.916	10.886	-0.030	-0.033	None
0618561	6B1	SIII-2	83.800	84.496	0.696	0.239	10.923	11.084	0.161	-0.032	None
1503329	15F56	BI-3	84.213	84.705	0.492	0.112	8.089	8.042	-0.047	-0.022	None
1601036	16E71	BI-3	84.174	84.602	0.428	0.082	11.166	11.074	-0.092	-0.031	None
1104478	11A27	BI-3	41.963	42.207	0.244	0.031	8.314	8.257	-0.057	-0.023	None
1402762	14C48	BI-3	56.367	56.592	0.225	0.068	10.954	11.068	0.114	-0.030	None
1600616	16E43	BII-2	84.064	84.517	0.453	0.022	11.267	11.161	-0.106	-0.031	None
1612146	16E20	BII-2	84.172	84.713	0.541	-0.011	11.177	11.163	-0.014	-0.030	None
1105055	11A36	BII-2	41.978	42.193	0.215	0.017	8.324	8.269	-0.055	-0.022	None
1203626	12B27	BII-2	41.946	42.197	0.251	-0.015	11.401	11.379	-0.022	-0.031	None
2607600	26E19	BII-2	84.260	84.46	0.20	0.091	11.087	--	--	-0.030	None
2621223	26J15	BII-2	84.105	84.416	0.311	0.053	11.241	11.161	-0.080	-0.031	None
2104416	21A6	BII-2	41.828	41.95	0.12	0.030	8.487	--	--	-0.024	None
2620628	26G1	BIII-2	84.084	84.303	0.219	-0.049	11.264	11.476	0.212	-0.028	None
3107082	1A1	RIV-4					101.059	100.889	-0.170	-0.298	None
3116856	1D9	RIV-4					101.072	100.890	-0.182	-0.311	None
3206304	2D10	RIV-4					103.052	102.814	-0.238	-0.318	None

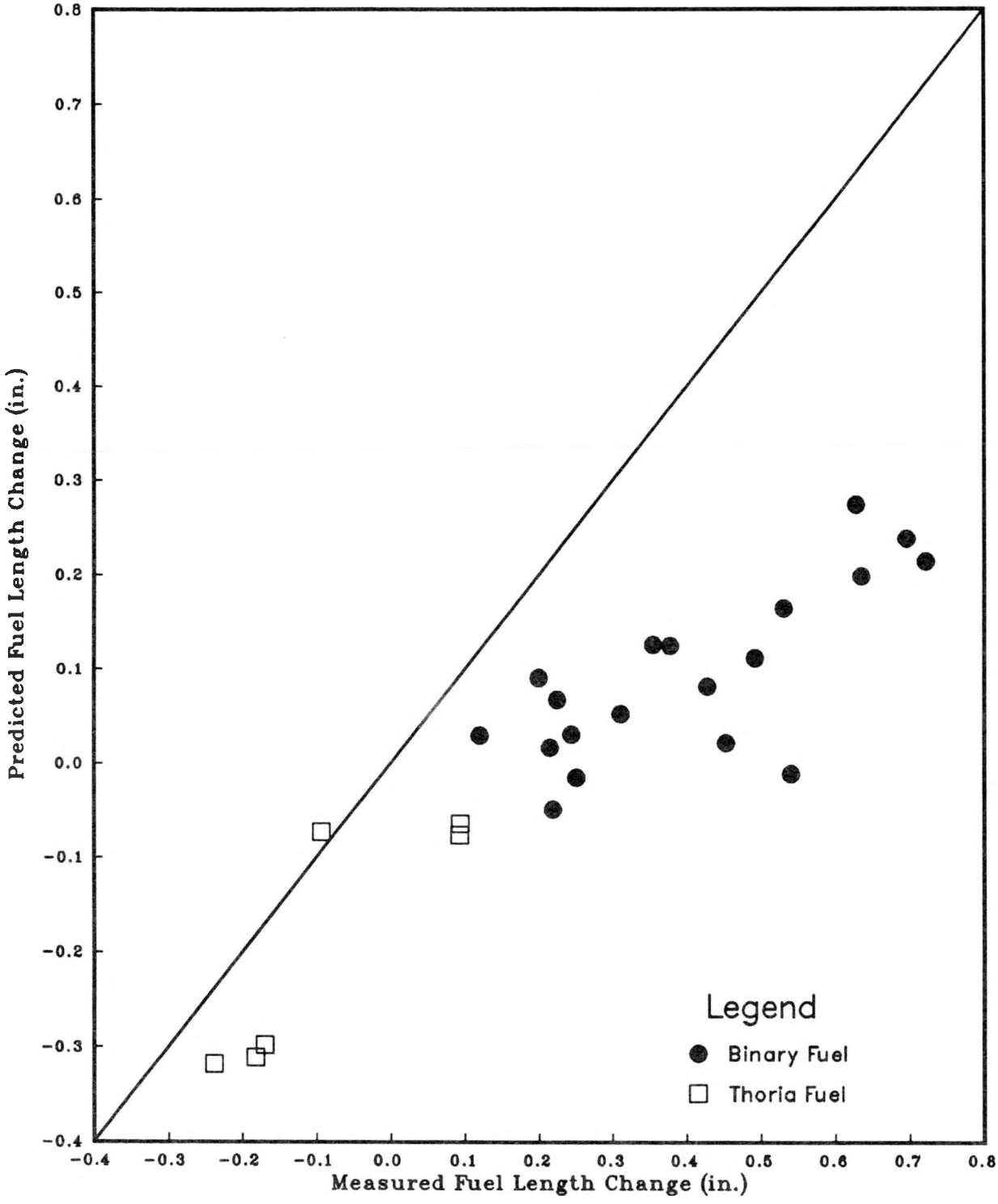

Figure 79 - Fuel Length from Gamma Scan

The last two mechanisms were minor effects in LWBR fuel rods, as indicated by less-than-predicted cladding elongations and by the relatively few and small in-stack gaps noted in neutron radiographs of representative rods. Fuel cracking can also be eliminated as a significant mechanism based on the lack of fuel separation at circumferential crack locations of the representative rods. This leaves fuel densification and fuel swelling as the major length-change mechanisms in LWBR fuel. Reflector fuel provides an indication that fuel shrinkage due to densification was not as great as the model predicted. The major difference in reflector fuel length change (0.2 inch measured versus 0.3 inch predicted) was due to densification rather than swelling because of the low fuel depletion. The same difference between predicted and measured changes in reflector rods (the three lower points in Figure 79) is also evident in the smaller binary length changes. The higher length changes in Figure 79 are associated with the higher depleted (and higher power) rods in which fuel swelling and fuel-cladding interaction would be more significant. The greater difference between predicted and measured changes in these rods indicates that either the fuel swelling component was underpredicted or the fuel-cladding interaction was overpredicted, or both. A strong case for overprediction of fuel-cladding interaction was apparent in the results of cladding elongation.

Thus, the underprediction of fuel length change shown in Figure 79 is attributed to less fuel densification and less fuel-cladding interaction than modeled. The increased length change is beneficial to fuel rod integrity because it reduces the size of the plenum gap in blanket and reflector rods and improves cladding support.

4.13.3 - In-Stack Gaps

As indicated in Table 27, no in-stack gaps between pellets were detected in the gamma scan data. This method could resolve gaps of approximately 0.2 inch or larger, since that was the size of the instrument window exposed to gamma rays at each increment along the rod. This evidence of no significant in-stack gaps is consistent with observations in other LWBR fuel rods from neutron radiographs, in which the maximum gap was 0.030 inch.

4.13.4 - Conclusions

Gamma scan results were useful in assessment of the LWBR fuel rod model. Gamma count profiles confirm the axial profiles of fuel depletion used in fuel rod analysis. Measured fuel stack length changes are greater than predicted, which is consistent with measurements from neutron radiographs of other rods. The major differences are attributed to less-than-predicted fuel densification and fuel-cladding interaction. The differences, in conjunction with smaller cladding elongations, resulted in a smaller plenum gap length than predicted. This was beneficial to cladding support in the plenum region of blanket and reflector rods, and did not degrade fuel rod integrity.

No in-stack gaps were detected by the gamma scans, which was consistent with results of neutron radiography of other representative LWBR fuel rods.

(Intentionally Blank)

SECTION 5 - SUMMARY AND CONCLUSIONS

Extensive non-destructive exams of LWBR fuel rods were undertaken to assess rod performance and to provide a data base for evaluating design procedure adequacy. The exams were performed in the Expended Core Facility (ECF) at the Naval Reactors Facility and Argonne National Laboratory-West (ANL-W) in Idaho Falls, Idaho. The exams included visual exams of fuel rods in modules for determination of spacing and shape by video digitizing techniques, visual examination and measurement of pull forces during removal of rods from modules, and examinations of single rods in the rod examination gage (REX), production irradiated fuel assay gage (PIFAG), and ANL-W facilities.

Individual exams in the REX included detailed visuals for rod appearance and wear mark identification, rod length measurement, free hanging bow measurement, rod diameter measurement, oxide thickness measurement, plenum ovality measurement, ultrasonic screening of cladding for defects, and wear mark depth and volume measurements. The PIFAG was used for gamma scanning of the rod for determination of axial depletion profiles, measurement of fuel stack length, and measurement of in-stack pellet-to-pellet gaps. Examinations at ANL-W included neutron radiography for evaluation of fuel and cladding integrity and measurement and characterization of crud on LWBR fuel rods.

Conclusions drawn from these examinations can be summarized as follows:

1. Rod length and diameter change measurements and fuel stack length measurements indicate that pellet-cladding interaction for seed and blanket fuel rods was less than anticipated based on irradiation test results and CYGRO analyses. Rod length increases were less than best estimate predictions. Fuel stack length was greater than best estimate predicted values. Cladding diameter shrinkage was less than CYGRO best estimate predictions. The smaller length increases resulted in greater than predicted rod end to baseplate clearances, thereby permitting coolant free flow through the baseplate holes.
2. Fuel geometry indicated that fuel pellet temperatures were less than expected. Fuel pellet end faces were still clearly dished after

30,000 EFPH operation. Blanket pellet end tapers were not distorted by pellet hourglassing at peak power locations. This conclusion is supported by results of fission gas measurements presented in Reference 5.

3. LWBR fuel pellets were dimensionally stable. Gamma scan and neutron radiography of 35 rods revealed no axial gaps greater than 0.030 inch. Cracks were observed in as many as 41 percent of pellets in a rod. Some cracks were wide enough to indicate fuel separation, but all pieces remained in place. No pellets were crumbled or gave any indication of risk to cladding integrity.
4. Cladding wear was low. A maximum wear depth of only 0.0014 inch was measured. Only 2.2 percent of the rod-to-grid contact points visually examined for wear had an appearance warranting examination with the orbiting profilometer. Half of the locations examined had depths less than 0.0005 inch. The absence of large cladding wear indicates that fuel rods were adequately restrained by the AM-350 support grids. Low cladding wear substantiates statistical evaluations of cladding wear, which indicated excessive wear of LWBR fuel rods was unlikely.
5. As expected, RXA seed cladding was freestanding. The maximum measured ovality for cladding was only 0.0017 inch over the plenum and 0.0044 inch over the fuel stack. Fuel-cladding clearances remained in seed rods throughout lifetime. Diameter profiles gave no indications of ridging or restricted shrinkage.
6. Deformation of unsupported, nonfreestanding cladding in the plenum region of blanket rods was small. Less than expected cladding elongation and fuel stack shrinkage resulted in smaller unsupported cladding lengths in fuel rod plena. The maximum measured plenum ovality was only 0.0038 inch. This ovality was comparable to best estimate predicted plenum ovality of 0.006 inch for the limiting blanket fuel rod with a 1.5-inch best estimate unsupported cladding length. Low blanket plenum ovalities supported statistical evaluations of blanket cladding ovality, which indicated that collapse of unsupported cladding was unlikely.
7. Nonfreestanding cladding in blanket and reflector rods shrank onto the pellets and assumed pellet shapes as predicted. Diameter profiles of

blanket rods showed grooves at pellet end tapers and reflector rod profiles showed ridges caused by the untapered pellets. All grooves were within predicted maximums. The maximum measured ridge for a reflector rod was 1.4 mils compared to a worst case predicted value of 1.1 mils.

8. Cladding ovality over the fuel stack was less than 0.005 inch for all rods. Ovality was most common at the end thoria fuel locations in blanket rods. The cladding apparently had not fully crept onto the fuel at these low power, low fluence locations.
9. Power depression at grid elevations was evident in measured profiles of rod diameter and surface oxide thickness. Variations in rod surface color occurred on some rods at grid levels and at pellet interfaces, caused by temperature-sensitive formation of oxide.
10. Examination of rod-to-rod spacing for one seed module indicated that the 95/95 tolerance interval for seed fuel rod channel closure was 50 percent or less for the central spans. No indications of rod-to-rod contact were observed. This was consistent with statistical analyses of rod-to-rod spacing. The minimum measured rod-to-rod spacing was 0.010 inch.
11. Examination of rod-to-rod spacings in 5 blanket modules indicated that the 95/95 tolerance interval for standard blanket channel closure was 48 percent or less for the peak power spans and 59 percent or less at all other spans. The 95/95 tolerance interval for power flattening fuel rod closure was 48 percent or less. One near contact condition (0.002 inch rod-to-rod spacing) was observed. Examination of the rods involved did not reveal any degradation in performance.
12. Examination of rod-to-rod spacing in one reflector module after baseplate severing indicated that the 95/95 tolerance interval for reflector channel closure was 39 percent or less. No near contact conditions were observed.
13. Measurement of fuel rod in-bundle bow indicated that module bow was the primary contributor to fuel rod bow. The maximum bow between grids measured was 0.020 inch, 0.027 inch, and 0.029 inch for seed, blanket, and reflector rods, respectively. These bows are well below worst case estimates of fuel rod bow. Calculations of in-bundle bow for the four spans near the fixed ends of rods from free hanging bow data yielded peak bows of 0.0148 inch,

0.0183 inch, and 0.015 inch for seed, blanket, and reflector rods. These calculated bows are well below worst case estimates of fuel rod bow. A 0.0248-inch bow was calculated for the span nearest the free end of one blanket rod. This bow was larger than expected.

14. There was no evidence of fuel rod binding in the AM-350 support grids. Pull forces for all rods removed were well below disassembly limits. Residual grid spring force was generally high at the end grid and low for the central grids.
15. Although there was no evidence of fuel rod defects, ultrasonic inspection of 12 fuel rods indicated that some LWBR fuel rods may have had significant cladding flaws. Three of the twelve rods examined had internal crack indications in excess of 0.010 inch. Metallographic examination of two of these indications showed no indication of cladding cracks.
16. Crud measurements on 3 rods indicate that crud buildup was low, although some crud could have been removed by rod handling. The maximum measured diametral crud thickness was only 0.00048 inch. As expected, crud for the seed rod and blanket fuel rod examined was heavier near the ends versus the central 60 percent of the rod. Contrary to expectations, crud for the reflector rod examined was heavier in the middle of the rod. Crud thicknesses on the reflector rod were less than for the seed and blanket rod.
17. Detailed visual examination of 19 fuel rods in the REX and cursory examination of about 1100 rods during rod removal did not reveal any indications of fuel rod failure or other unusual conditions (e.g., collapsed sections, etc.). A wide variation in rod surface appearance was observed. Appearance (from black-and-white video pictures) of rods in close proximity to one another varied from uniform white to speckled to uniform gray.
18. Corrosion oxide film thickness profiles were as expected for PWR fuel rods, i.e., highest at the high power, binary fueled regions with pronounced thinning at the support grid levels and at the top and bottom of the binary fuel stack. Measured thicknesses were in reasonable agreement with values calculated with a model based on cladding surface temperature, fast flux, and exposure time.

Overall, LWBR fuel rod performance was excellent. Examinations indicated that the rods sustained no defects (i.e., breached cladding), no major cladding deformations, and little wear during operation for 29,047 EFPH. Models for predicting fuel rod performance were found to be slightly over-conservative. Limiting observations were generally well below worst case predictions. In many instances, average observations were less than best estimate predictions. For the most part, the model conservatism can be attributed to an overestimate of pellet-cladding interaction. These examinations confirm the expected excellent performance behavior of the thorium-uranium^{233} fuel system.

(Intentionally Blank)

SECTION 6 - ACKNOWLEDGMENTS

The authors gratefully acknowledge the contributions of the following persons who played important roles in the work reported herein:

Messrs. W. J. Bacvinskas, G. Fodor, T. J. Kikta, R. M. Matchett, R. J. Nilsen, R. Wilczynski, B. C. Smith, and W. W. Davis for their efforts in the design, assembly, and testing of the REX.

Messrs. S. R. Crow, R. M. Brown, S. R. Brown, D. S. Duncan, D. D. Streett, K. D. Henderson, and P. E. Ireland for overseeing examination of LWBR fuel rods at ECF and ANL-W and operation of the REX.

Ms. S. J. Rhodes for her efforts in digitizing fuel module and single rod video tapes.

Ms. M. O. Malinchak for her assistance in evaluation of REX examination data and preparing figures for this report.

Mr. K. D. Richardson for his efforts in developing the LWBR End-of-Life examination program and coordinating work between Bettis, ECF, and ANL-W.

Mr. R. Winkler from Engineering Publications for his assistance in preparing this report.

The authors are also indebted to Messrs. W. J. Babyak, R. A. Frederickson, I. Goldberg, and Drs. P. L. Pfennigwerth and W. E. Franzen for their careful review and helpful suggestions.

(Intentionally Blank)

SECTION 7 - REFERENCES

1. W. S. Bacvinskas, "LWBR Module and Rod Examination Systems," WAPD-TM-1610, October, 1987.

2. A. C. Kahler, G. Tessler, "Testing of a Production Irradiated Fuel Assay Gauge," WAPD-TM-1555, July 1986.

3. G. Tessler, B. R. Beaudoin, W. J. Beggs, L. B. Freeman, W. C. Schick, Jr., "Non-destructive Assay of Spent Fuel Rods from a Light Water Breeder Reactor," WAPD-TM-1614, October 1987.

4. J. E. Wargo, "End-of-Life LWBR Component Examinations at Shippingport and Module Visual and Dimensional Examinations at ECF," WAPD-TM-1602, October 1987.

5. K. D. Richardson, "End-of-Life Destructive Examination of LWBR Fuel Rods," WAPD-TM-1606, October 1987.

6. B. C. Smith, "End-of-Life Examinations of LWBR Grids and Other Module Structural Components," WAPD-TM-1607, October 1987.

7. W. C. Schick, Jr., B. R. Beaudoin, W. J. Beggs, L. B. Freeman, G. Tessler, "Proof of Breeding in the Light Water Breeder Reactor," WAPD-TM-1612, October 1987.

8. J. T. Williams, "LWBR Core Evaluation Operations at ECF," WAPD-TM-1611, October 1987.

9. K. D. Richardson, "Summary of the Fuel Rod Support System (Grids) Design for LWBR," WAPD-TM-1331, February, 1979.

10. J. H. Eyler, "The Characteristics of the Zircaloy-4 Tubing for LWBR Fuel Rods," WAPD-TM-869, November, 1979.

11. J. H. Eyler, "Development and Control of the Process for the Manufacture of Zircaloy-4 Tubing for LWBR Fuel Rods," WAPD-TM-1289, January 1981.

12. J. Belle and R. M. Berman, editors, "Thorium Dioxide: Properties and Nuclear Applications," DOE/NE-0060, Government Printing Office, Washington, D.C., 1984.

13. H. R. Warner, "Release of Fission Gases from Oxide Fuels," WAPD-TM-805, July 1969.

14. I. Goldberg, et. al., "Fission Gas Release from ThO_2 and ThO_2-UO_2 Fuels (LWBR Development Program), "WAPD-TM-1350, August 1978.

15. J. M. Markowitz, J. C. Clayton, "Corrosion of Oxide Nuclear Fuels in High Temperature Water," WAPD-TM-909, February 1970.

16. J. C. Clayton, "In-Pile and Out-of-Pile Corrosion Behavior of Thoria-Urania Pellets," WAPD-TM-1548, January 1987.

17. G. P. Marino and R. L. Fischer, "Corrosion of Zircaloy-4 Tubing in 680 F Water," WAPD-TM-1322, December 1978.

18. W. A. Budd, "Shippingport Operations with the Light Water Breeder Reactor Core," WAPD-TM-1542, March 1986.

19. R. L. Matchett, "LWBR Rod Removal System," WAPD-TM-1609, October 1987.

20. J. J. Urbaniak, "ROBOT - A Computer Program to Solve the Bowing Problem in Rod-Type Fuel Elements," WAPD-TM-847, July 1969.

21. J. B. Newman, J. F. Giovengo, L. Comden, "The CYGRO-4 Fuel Rod Analysis Computer Program," WAPD-TM-1300, July, 1977.

22. A. J. Caffarel, et. al., "Free-Hanging Bow Measurements of LWBR Fuel Rods," WAPD-TM-1270, March 1979.

23. J. F. Giovengo, W. R. Campbell, "Summary of Fuel Element Design for LWBR," WAPD-TM-1387, October 1987.

24. R. W. Keyes, "The Element Laser Profilometer System in Hot Fuel Examination Facility/North," Proc. 29th Conference Remote Systems Technology, Vol. 2, pp. 21-25, 1981.

25. F. Garzarolli, R. P. Bodner, H. Stehle, and S. Trapp-Pritching, "Progress in Understanding PWR Fuel Rod Waterside Corrosion," pp 3.55-3.72, Proc. ANS Topical Meeting on Light Water Reactor Fuel Performance, Orlando, Florida (1985).

26. F. Garzarolli, P. Suchy, and P. G. Smerd, "Observations and Analysis of the Corrosion Behavior of PWR Fuel," pp 4.71-4.87, Proc. ANS Topical Meeting on LWR Extended Burnup-Fuel Performance and Utilization, Williamsburg, Virginia (1982).

27. F. Garzarolli, D. Jorde, R. Manzel, G. W. Parry, and P. G. Smerd, "Review of PWR Fuel Rod Waterside Corrosion Behavior," CE/KWU/EPRI NPSD79 (June 1979).

28. J. C. Clayton, "Corrosion and Hydriding of Irradiated Zircaloy Fuel Rod Cladding," WAPD-TM-1440, September 1982.

29. J. C. Clayton and R. L. Fischer, "Corrosion and Hydriding of Zircaloy Fuel Rod Cladding in 633 K Water and Reactor Environments," pp. 3.1-3.16 Proc. ANS Topical Meeting on Light Water Reactor Fuel Performance, Orlando, Florida, 1985.

30. T. R. England, "CINDER - A One-Point Depletion and Fission Product Program", WAPD-TM-334 (Revised), June 1964. Also, T. R. England, R. Wilczynski, and N. L. Whittemore, "CINDER-7: An Interim Report for Users," Los Alamos Scientific Laboratory report LA-5885-MS, April 1975.

APPENDIX A1 - LWBR MODULE FUEL ROD CELL DESIGNATIONS

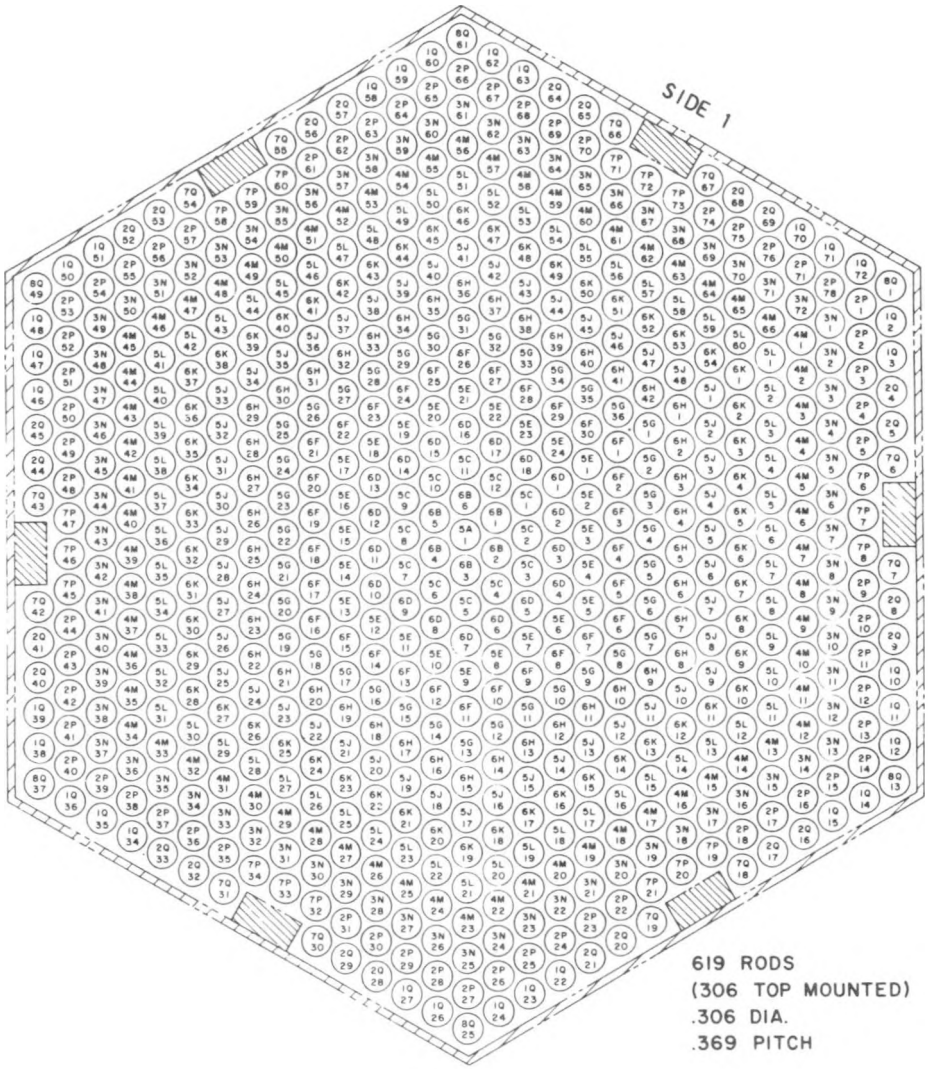

DESCRIPTION OF CELL IDENTIFICATION

ROD TYPE NUMBER EVEN NUMBERS ARE TOP MOUNTED - ODD NUMBERS ARE BOTTOM MOUNTED.

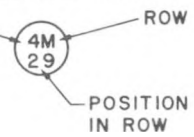

Figure A1-1 - LWBR Movable Seed Module
Rod and Cell Identification

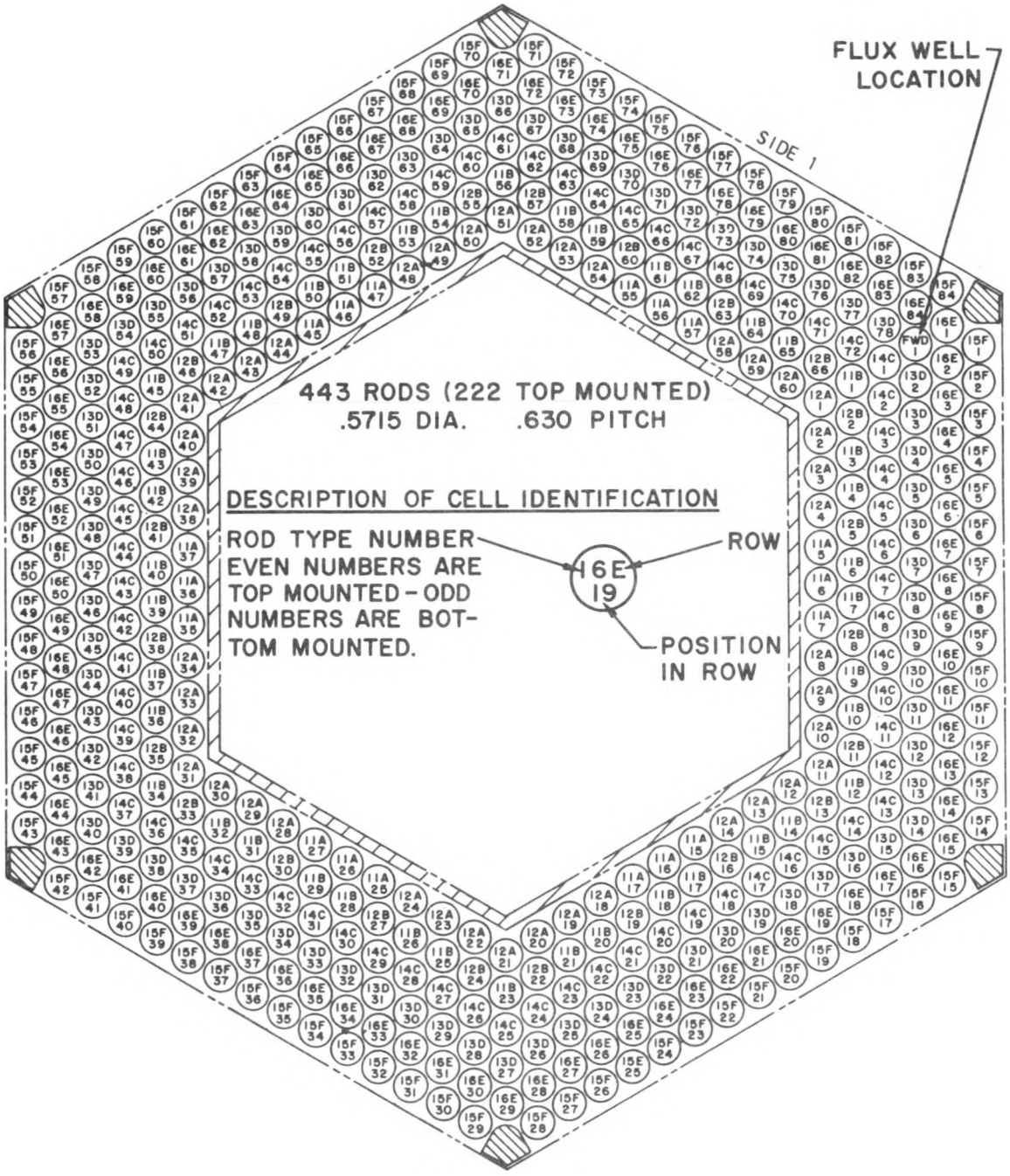

Figure A1-2 - LWBR Type I Blanket Module
Rod and Cell Identification

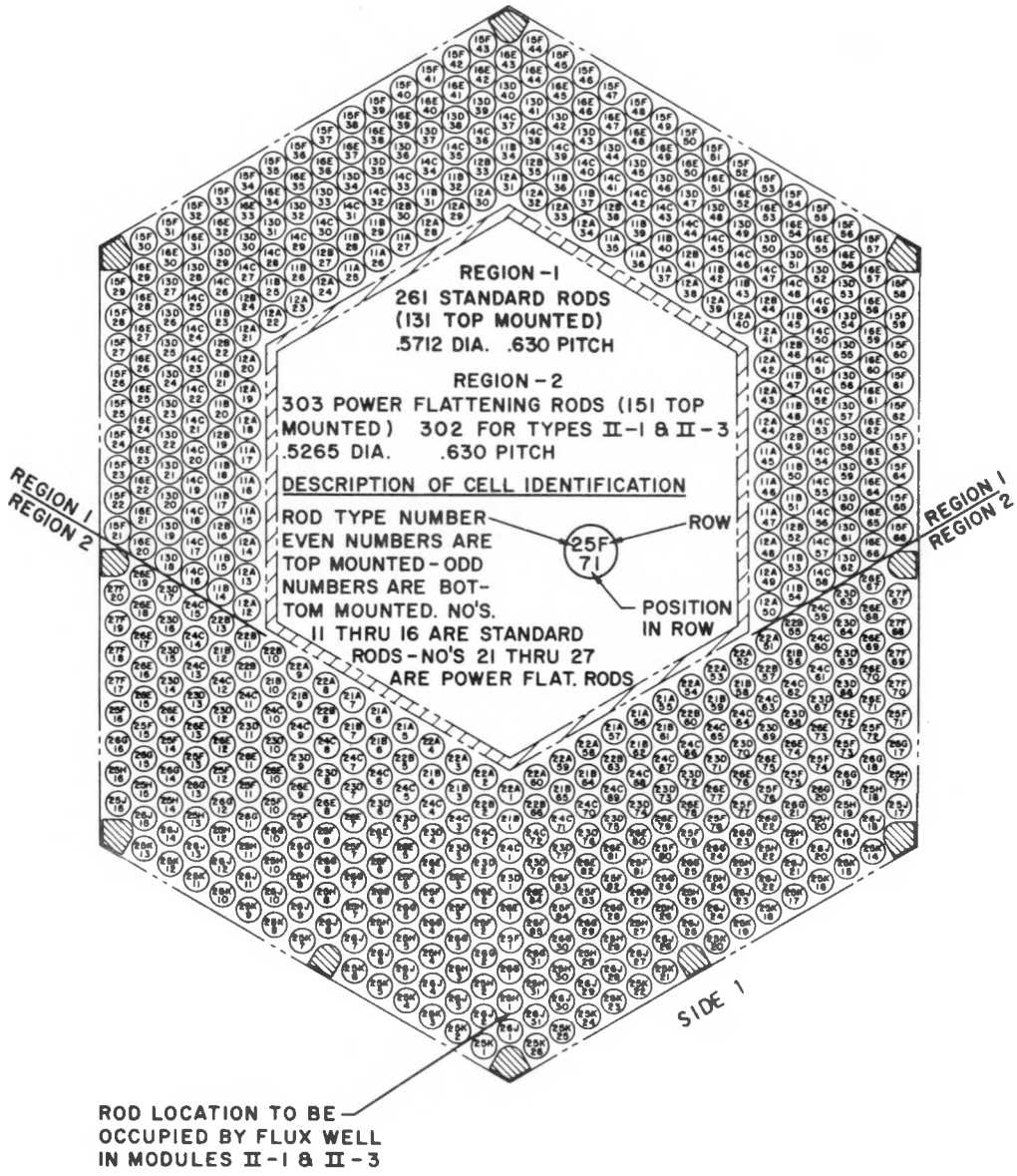

Figure A1-3 - LWBR Type II Blanket Module
Rod and Cell Identification

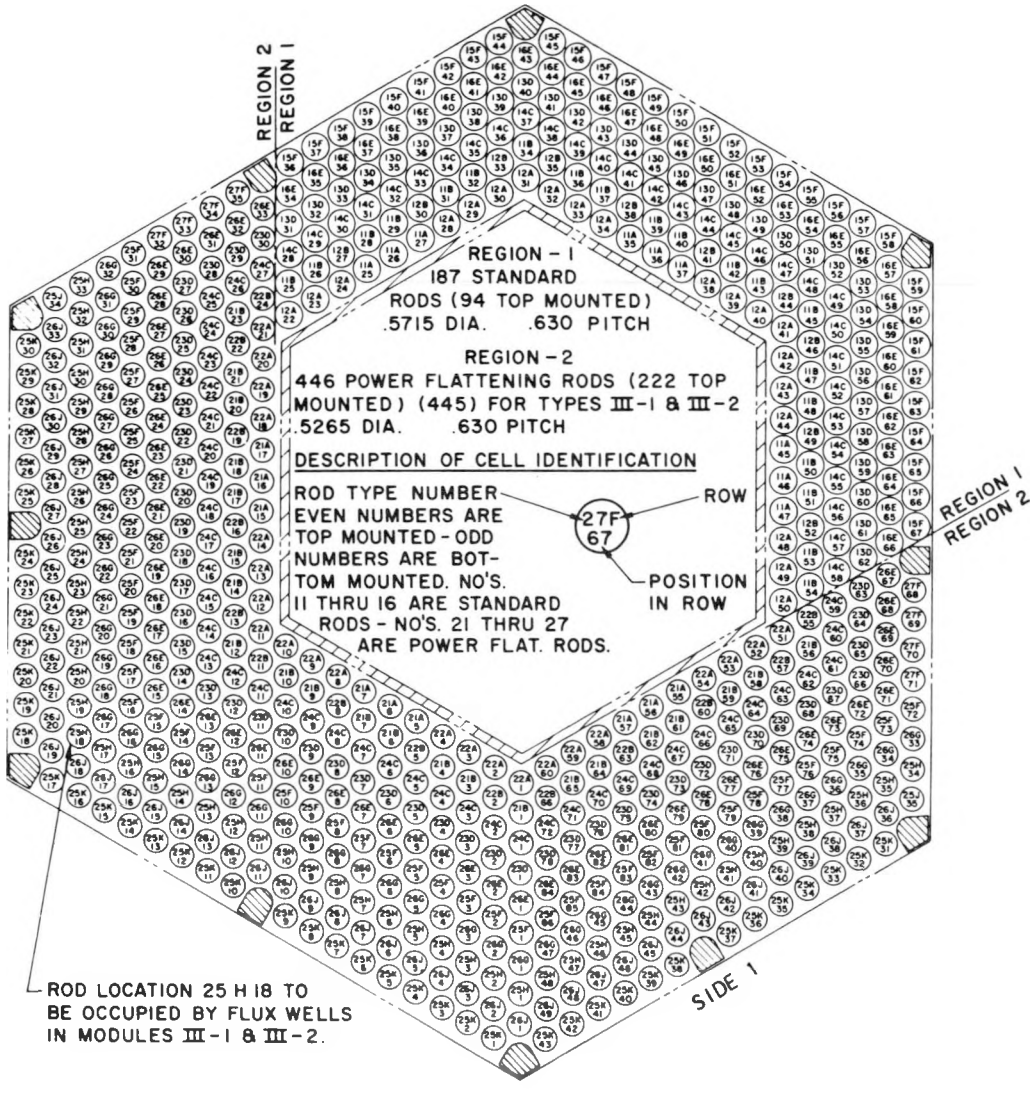

Figure A1-4 - LWBR Type III Blanket Module
Rod and Cell Identification

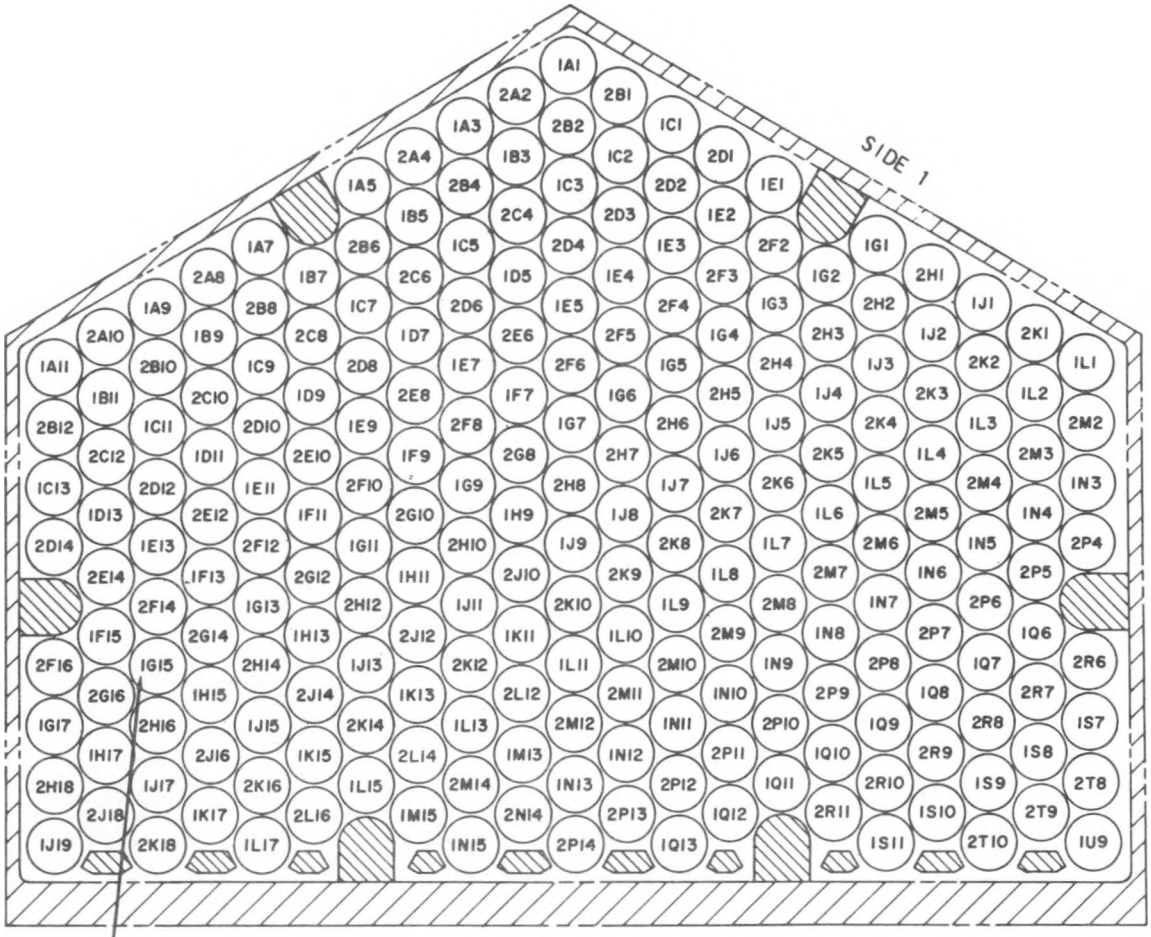

IDENTIFICATION LEGEND
EXAMPLE:

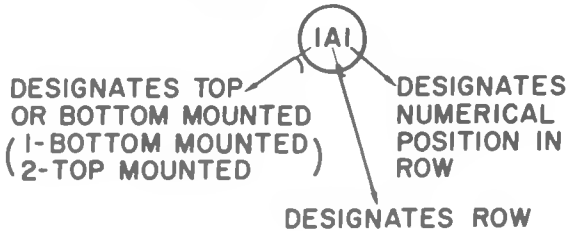

228 RODS (113 TOP MOUNTED)
.832 DIA.
.900 PITCH

Figure A1-5 - LWBR Type IV Reflector Module
Rod and Cell Identification

APPENDIX A2 - AS-BUILT DATA FOR REX NONDESTRUCTIVE EXAMINATION RODS

Table A2-1 - As-Built Data for REX Nondestructive Examination Rods

Rod Serial Number	Module	Cell	Fuel Blend Data: Fuel Binary Blend	% TD	Grain Size (ASTM-No.)	Granular Segregation	Fuel OD (in.)	Cladding Data: Rod Avg. OD (in.)	Avg. Wall (in.)	Calculated: Cladding ID (in.)	Fuel/Clad Diam. Gap (in.)
0606773	SI-1	6B4	103-2-87	97.30	7.0-8.0	67-1,33-2	0.2520	0.3068	0.0228	0.0261	0.0092
0507672	SI-1	5L31	105-2-07	97.58	6.0-8.0	97-1,3-2	0.2518	0.3056	0.0219	0.2618	0.0100
0504502	SI-1	5L32	128-2-85	97.66	5.5-9	100-1	0.2519	0.3053	0.0217	0.2619	0.0100
0201746	SI-1	2Q41	141-1-85	97.73	7.5-12	93-1,7-2	0.2519	0.3063	0.0222	0.2619	0.0100
0400736	SI-1	4M33	135-85 RS	98.00	9-10,8.5-10,9.5-10.5	100-1	0.2520	0.3064	0.0224	0.2616	0.0096
0604555	SI-1	6B3	101-2-09	97.45	7.5-10.5	70-1,30-2	0.2516	0.3053	0.0221	0.2611	0.0095
1606710	BI-3	16E57	540-5-07(85) 540-5-01RS(22)	98.06 98.13	4.5-6,5-6.5,6-9.5 5-5.5,5-5.5,5.5-6.5	84-1,16-2 67-1,30-2,3-3	0.5105 0.5104	0.5712	0.0282	0.5148	0.0043
1605629	BI-3	16E58	540-5-08(36) 540-5-17RS(71)	98.03 98.13	4.5-5.5,6.5-7.5,8.5-9.5 5-6,5-7,5.5-9	50-1,39-2,11-3 97-1,302	0.5105 0.5105	0.5716	0.0284	0.5148	0.0043 0.0043
1504272	BI-3	15F11	509-4-13CR(81) 509-4-02(16)	98.38 98.07	5.5-6.5,5-8.5,5-8.5 6-7,6.5-8.6,6.5-8.5	99-1,1-3 100-1	0.5105 0.5105	0.5712	0.0277	0.5758	0.0053 0.0053
1105717	BI-3	11A46	533-3-01	98.66	5-7.5,5-7.5,8-9	100-1	0.5105	0.5720	0.0281	0.5158	0.0054
1601036	BI-3	16E71	539-5-06(85) 539-5-03(22)	98.12 98.08	4-5,6.5-9.5,9-10 4-5.5,6-8,8.5-10	94-2,6-2 4-1,44-2,52-3	0.5105 0.5104	0.5708	0.0277	0.5154	0.0049 0.0050
1612146	BII-2	16E20	540-5-13(85) 540-5-11(22)	98.28 97.72	5.5-6.5,7-9,10.4-10.8 5-6.5,5.5-7,8.5-10	100-1 70-1,24-2,6-3	0.5103 0.5106	0.5724	0.0287	0.5150	0.0047 0.0046
1208823	BII-2	12A12	533-3-10XRS(67) 551-3-85(12)	98.53 98.34	4.5-5.5,4.5-6,5.5-7.5 5-6.5,5.5-9.5,8.5-9.5	100-1 77-1,23-2	0.5104 0.5105	0.5721	0.0284	0.5153	0.0049 0.0048
2610746	BII-2	26E68	545-8-16	97.76	5.5-7,5.5-9.5,6-11	97-1,3-2	0.4696	0.5278	0.0266	0.4746	0.005
2607600	BII-2	26E19	545-8-16	97.76	5.5-7,5.5-9.5,6-11	97-1,3-2	0.4696	0.5278	0.0265	0.4748	0.0052
2514164	BII-2	25K13	545-8-20	97.75	4.5-6.5,6-9,9.5-10.5	84-1,16-2	0.4696	0.5276	0.0267	0.4742	0.0046
3102657	RIV-3	1A1	048-3-14	97.59	8.5-9.5,11-12,11-11.5	82-1,18-2	0.7418	0.8320	0.0415	0.7490	0.0072
3107082	RIV-4	1A1	047-3-07	97.39	7.5-10,9.5-11,10.5-11	70-1,30-2	0.7421	0.8314	0.0414	0.7486	0.0065
3206304	RIV-4	2D10	037-3-13	97.86	9.5-11,10-11,10.5-11	62-1,38-2	0.7422	0.8318	0.0419	0.7480	0.0058

APPENDIX A3 - REX EXAMINATION ROD PULL FORCES AND AVERAGE PULL FORCE HISTOGRAMS

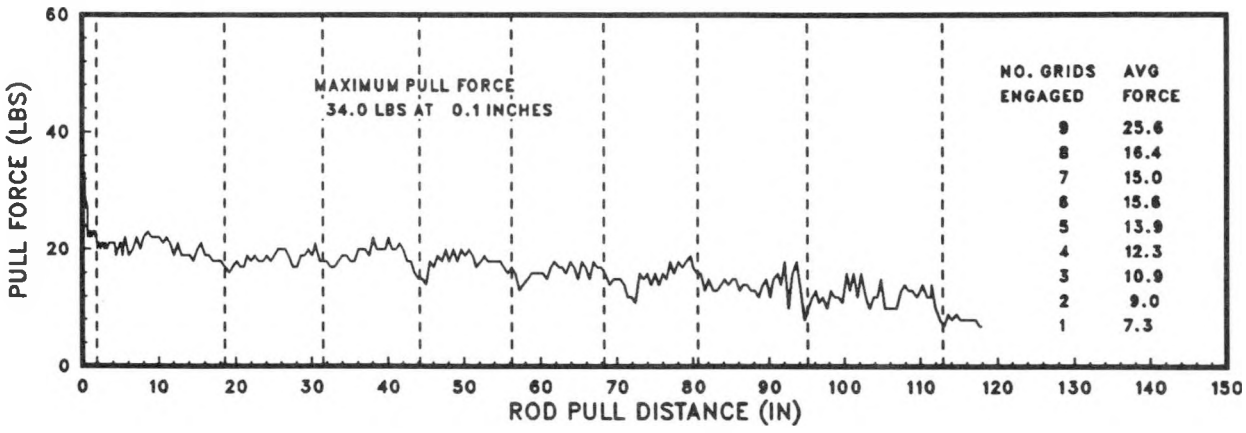

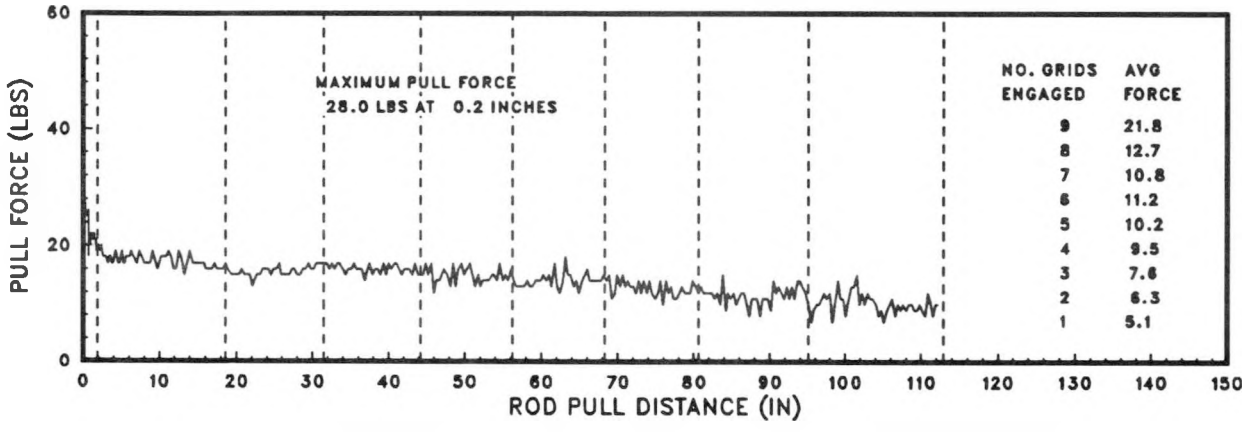

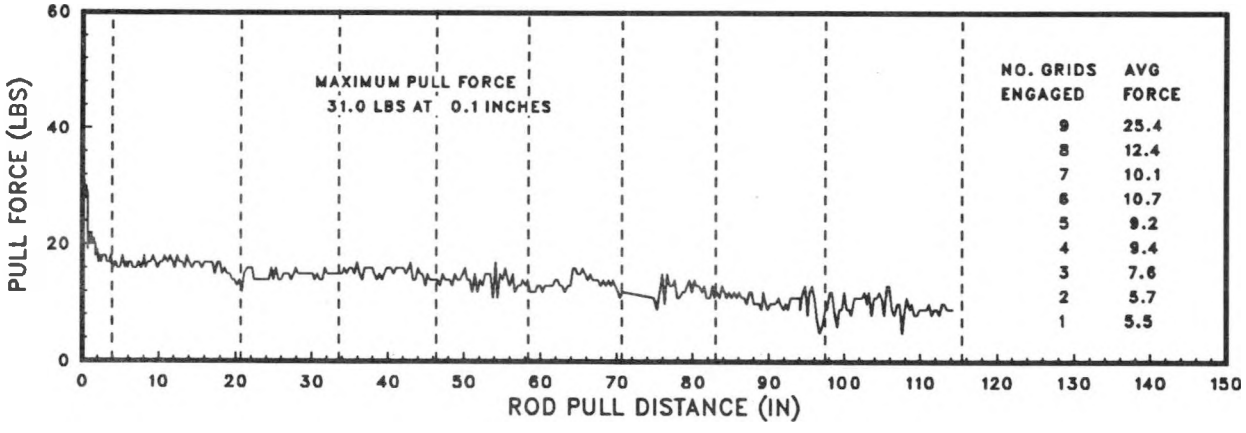

Figure A3-1 - REX Examination Rod Pull Forces

PULL FORCE ROD 0507672 CELL L31 MODULE SI-1

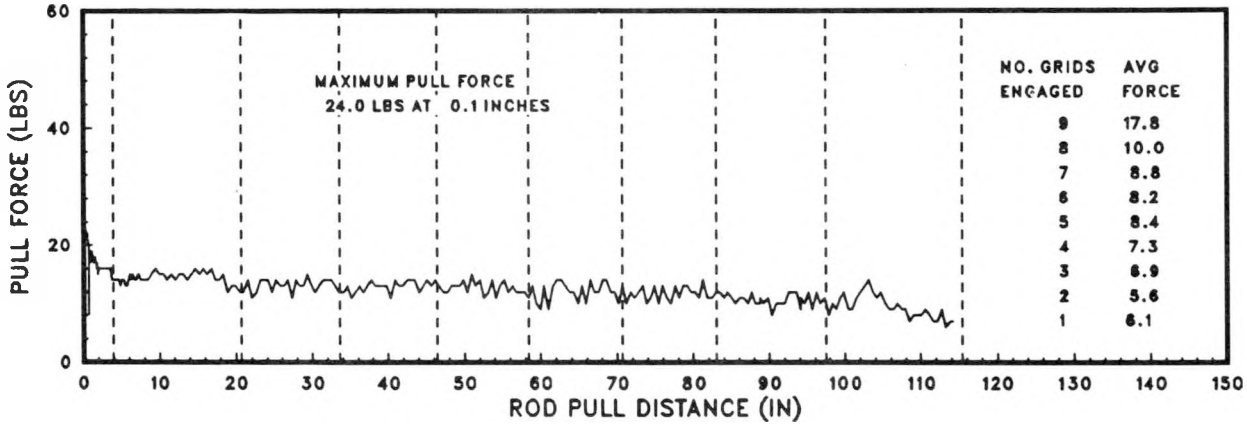

PULL FORCE ROD 0606773 CELL B4 MODULE SI-1

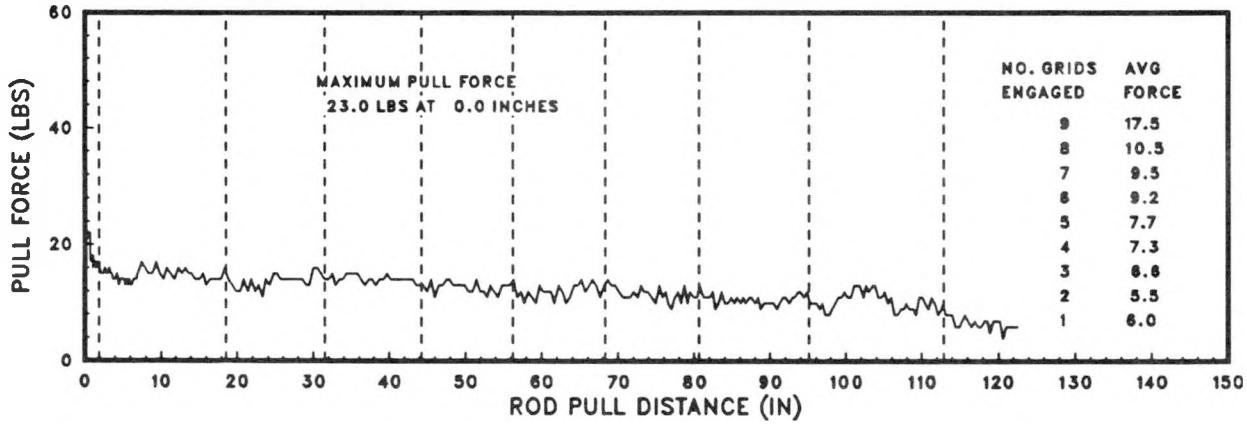

PULL FORCE ROD 1105717 CELL A46 MODULE BI-3

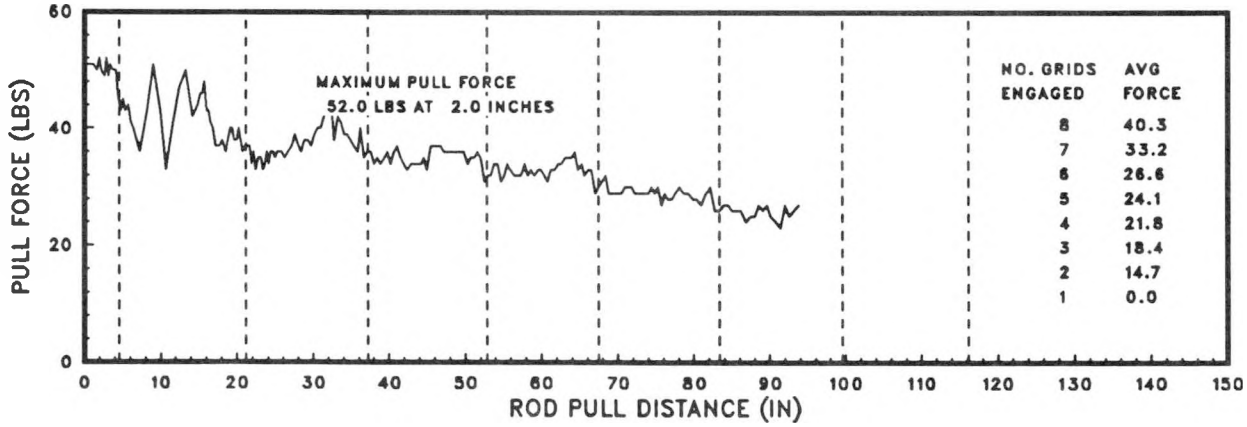

Figure A3-1 - REX Examination Rod Pull Forces (Cont)

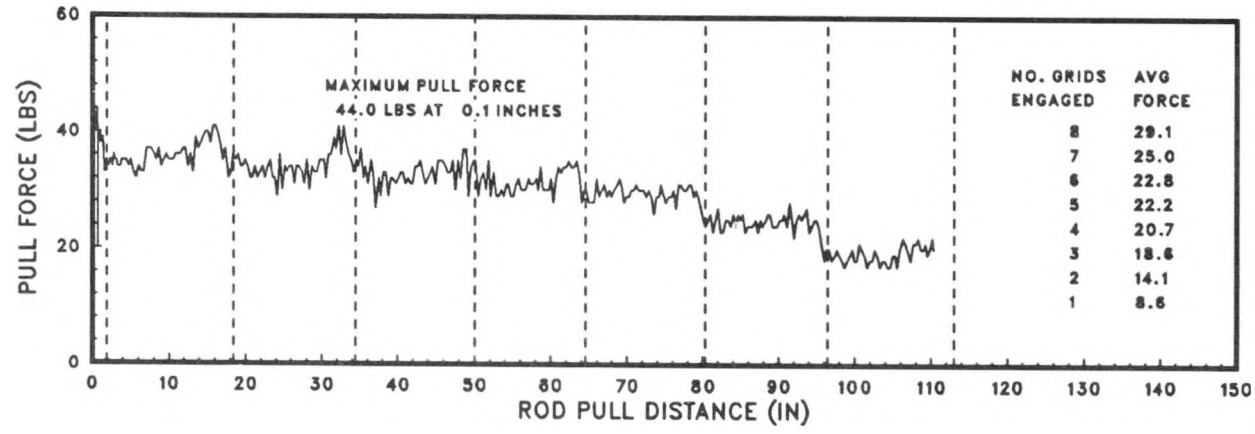

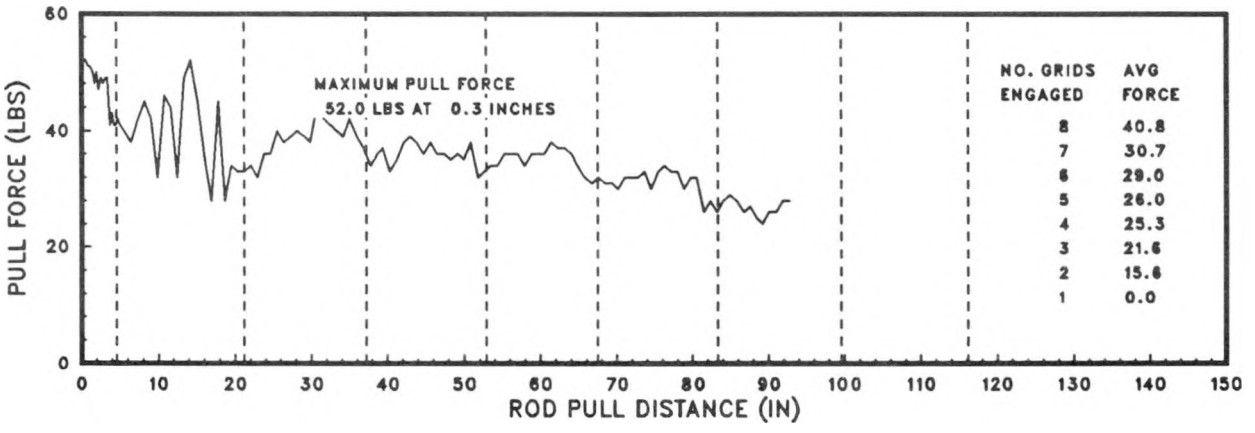

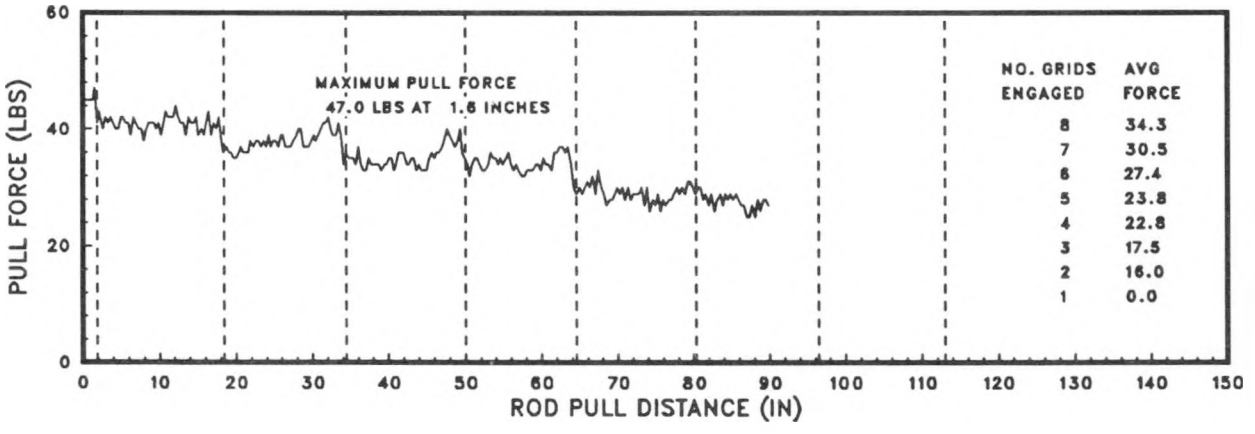

Figure A3-1 - REX Examination Rod Pull Forces (Cont)

PULL FORCE ROD 1605629 CELL E58 MODULE BI-3

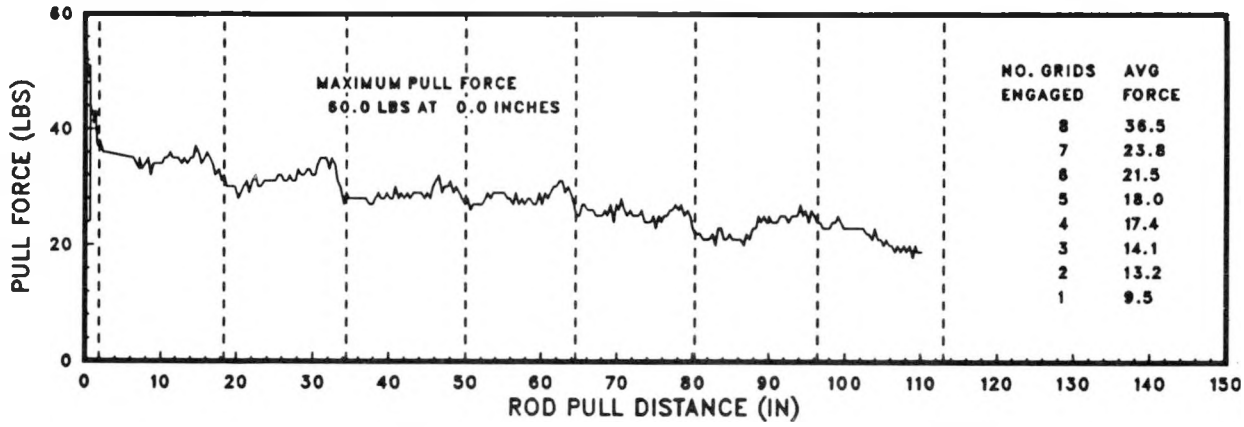

PULL FORCE ROD 1606710 CELL E57 MODULE BI-3

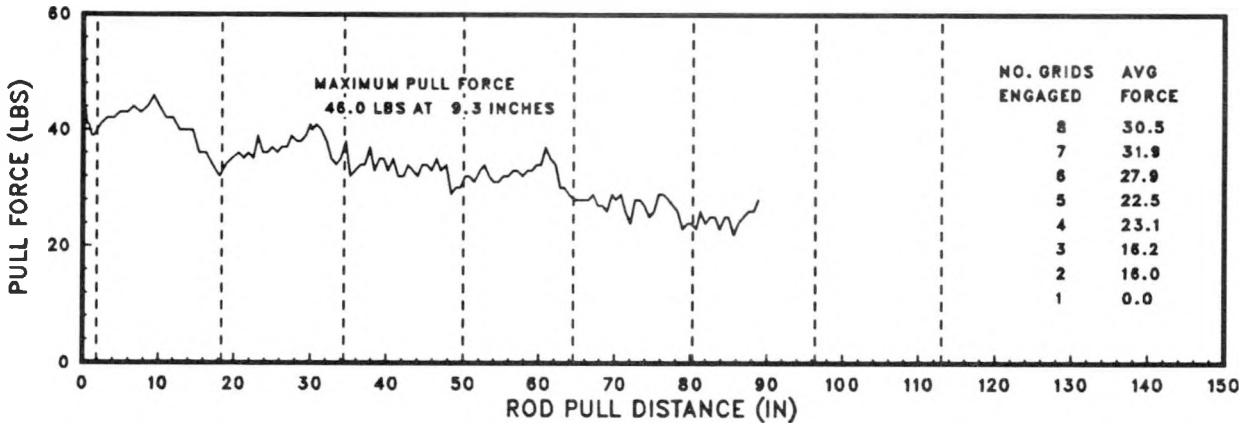

PULL FORCE ROD 1612146 CELL E20 MODULE BII-2

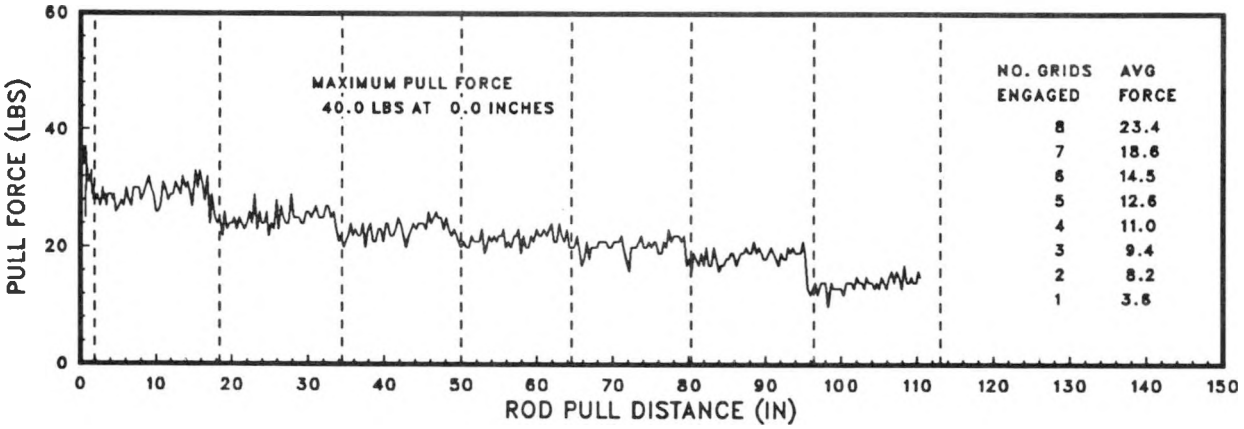

Figure A3-1 - REX Examination Rod Pull Forces (Cont)

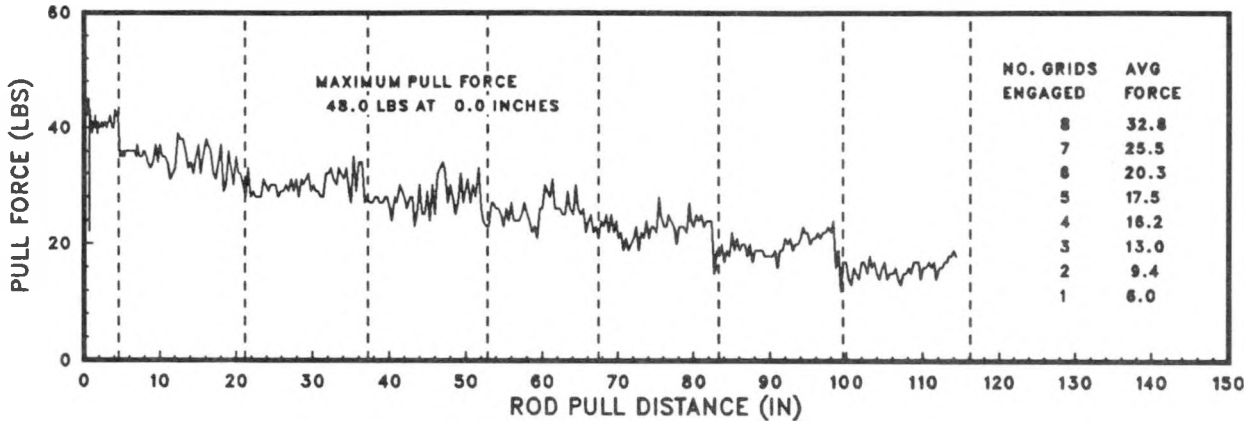

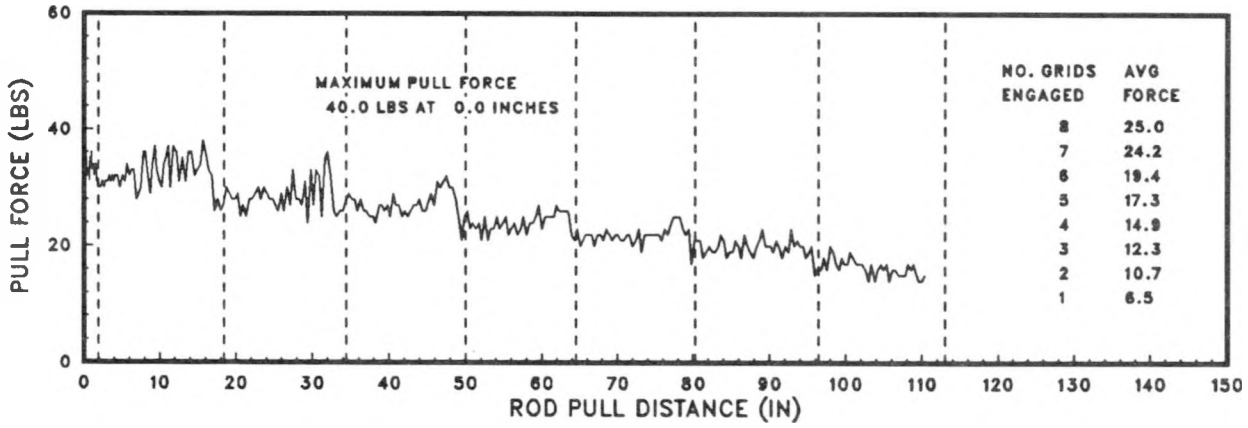

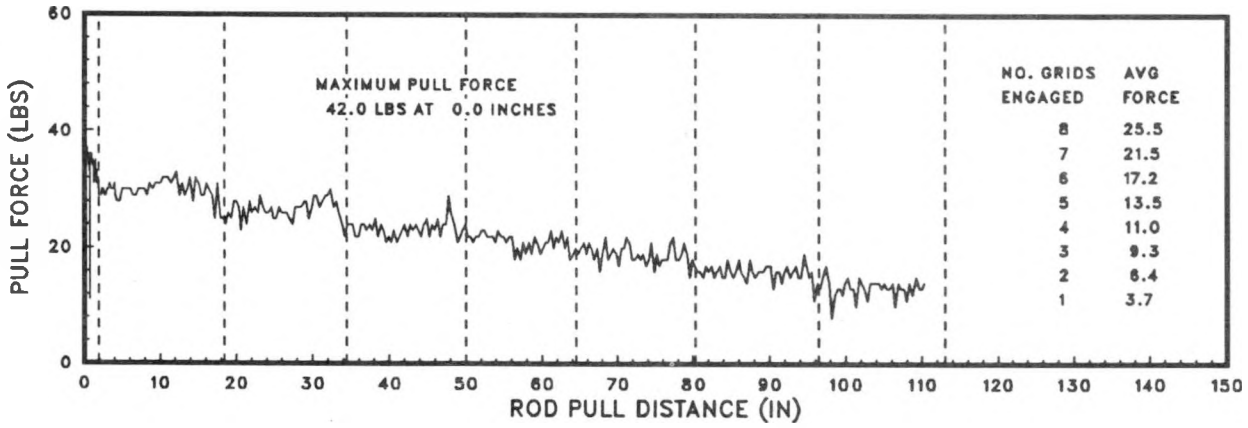

Figure A3-1 - REX Examination Rod Pull Forces (Cont)

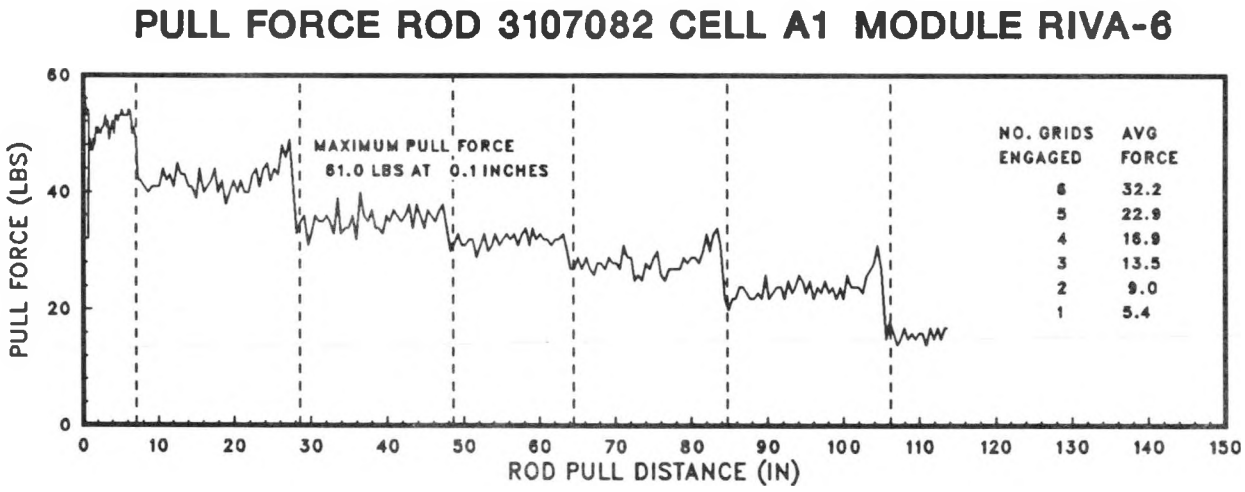

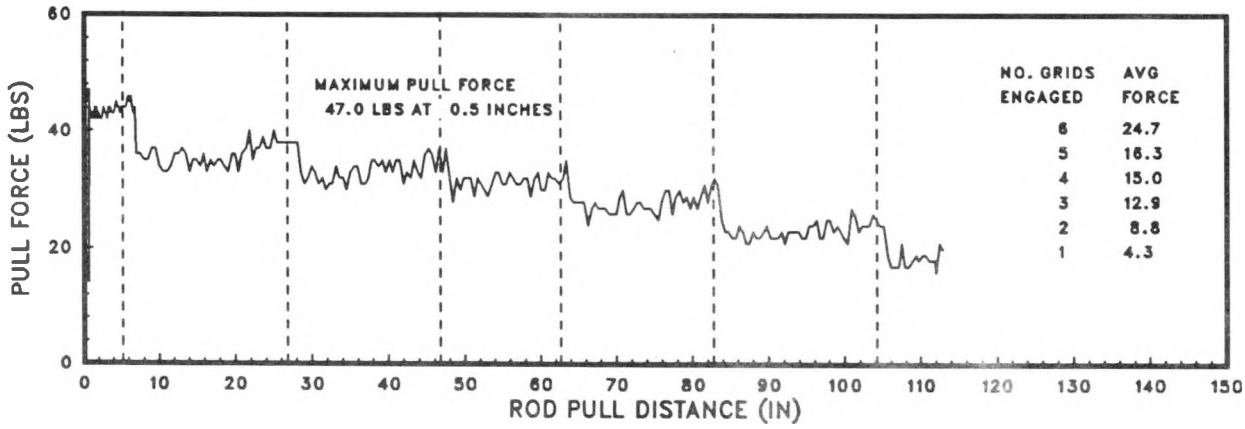

Figure A3-1 - REX Examination Rod Pull Forces (Cont)

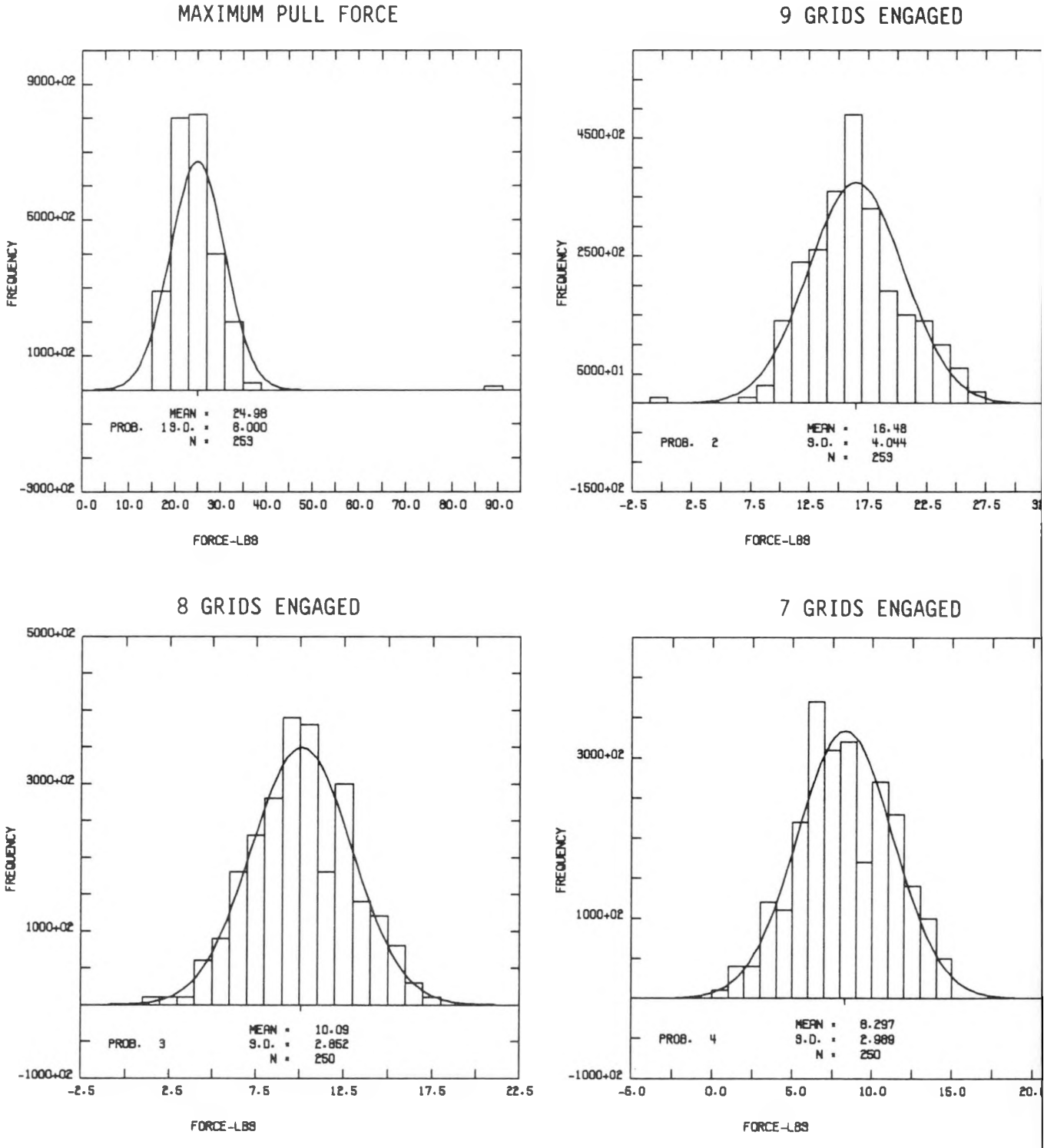

Figure A3-2 - Seed Pull Force Histograms

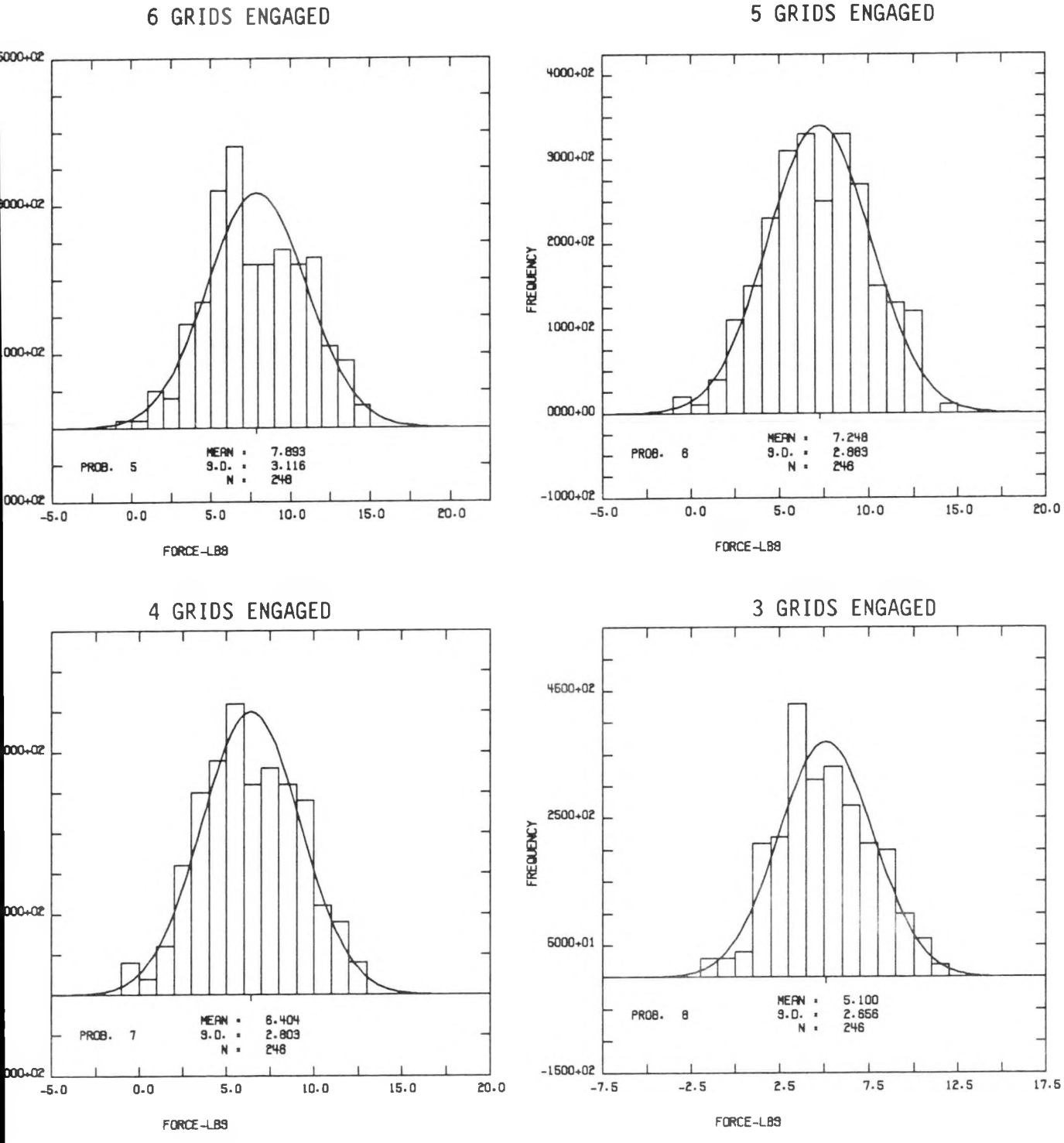

Figure A3-2 - Seed Pull Force Histograms (Cont)

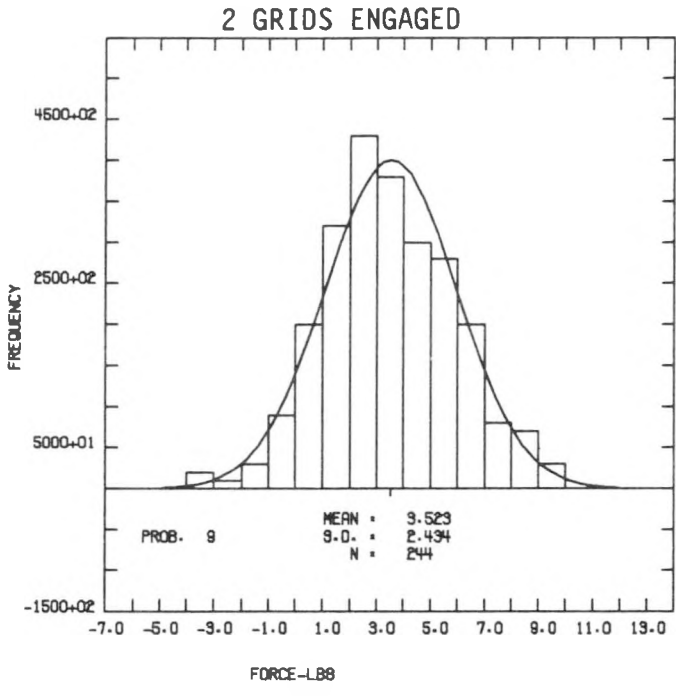

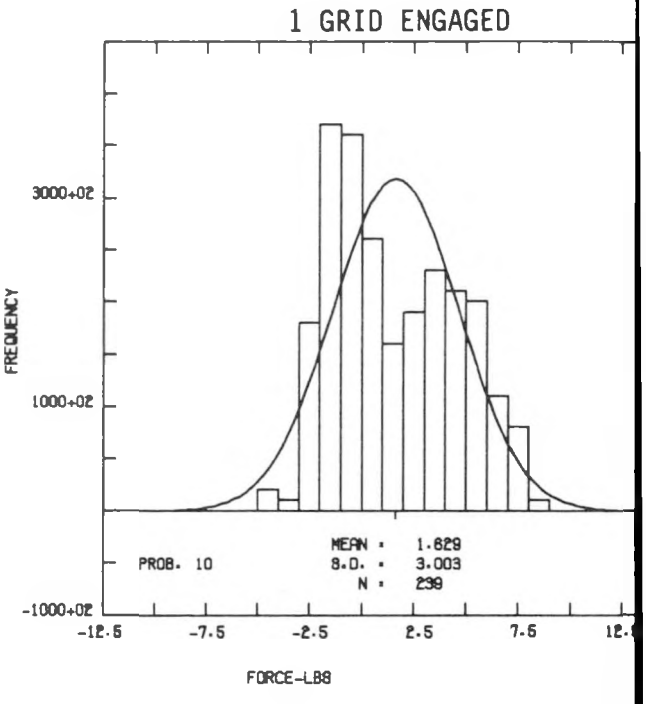

Figure A3-2 - Seed Pull Force Histograms (Cont)

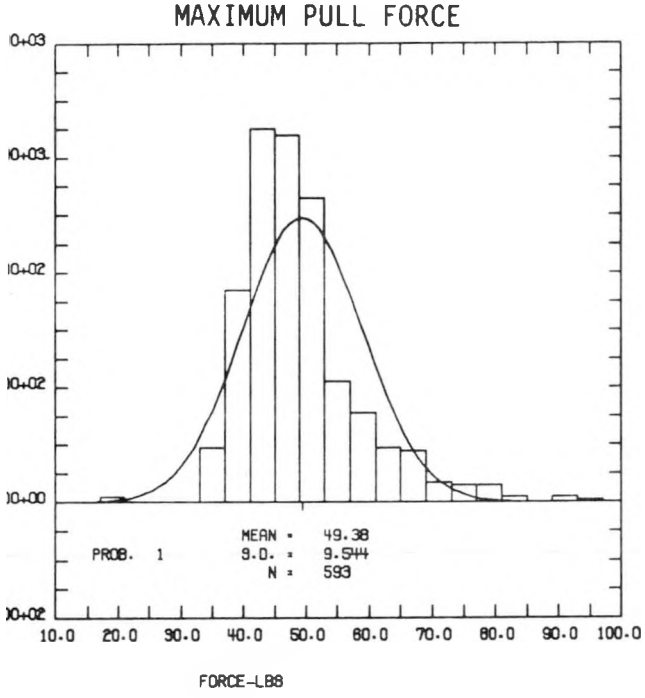

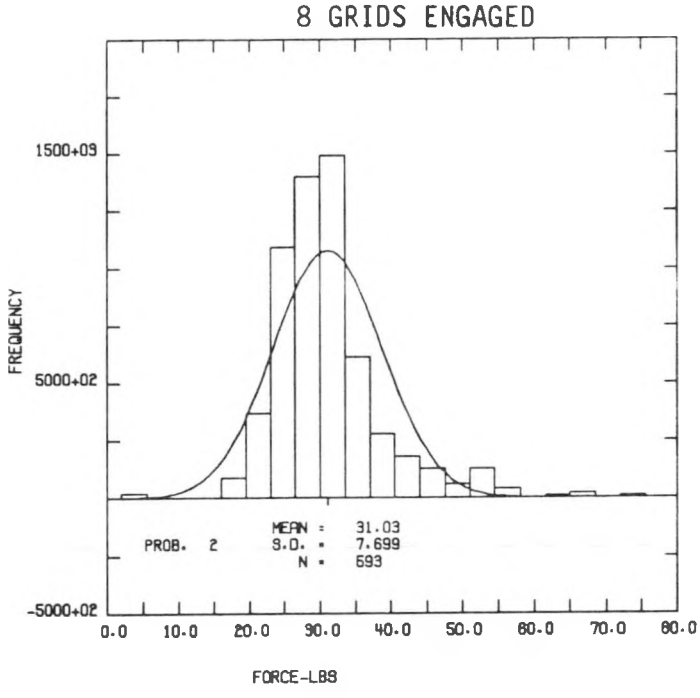

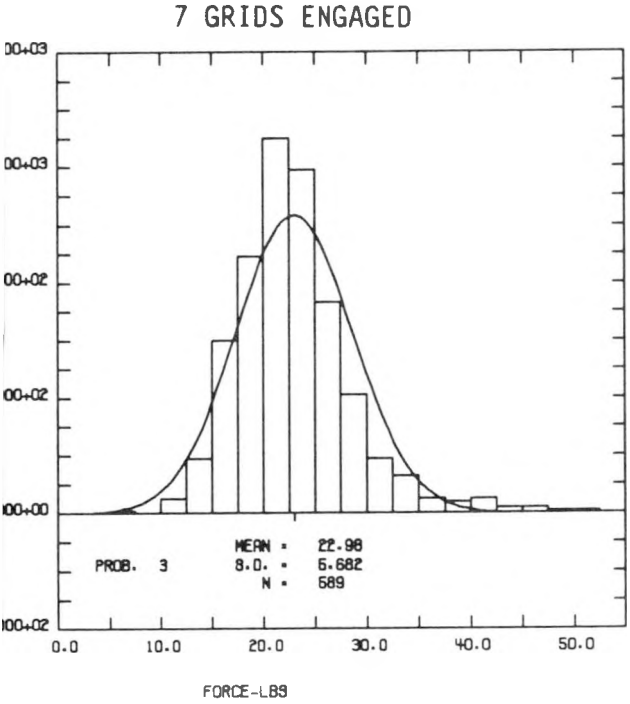

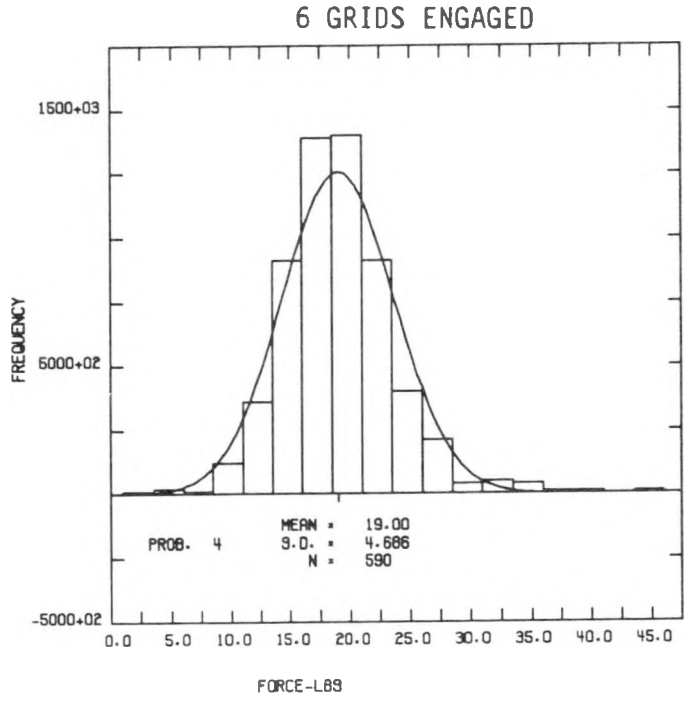

Figure A3-3 - Blanket Pull Force Histograms

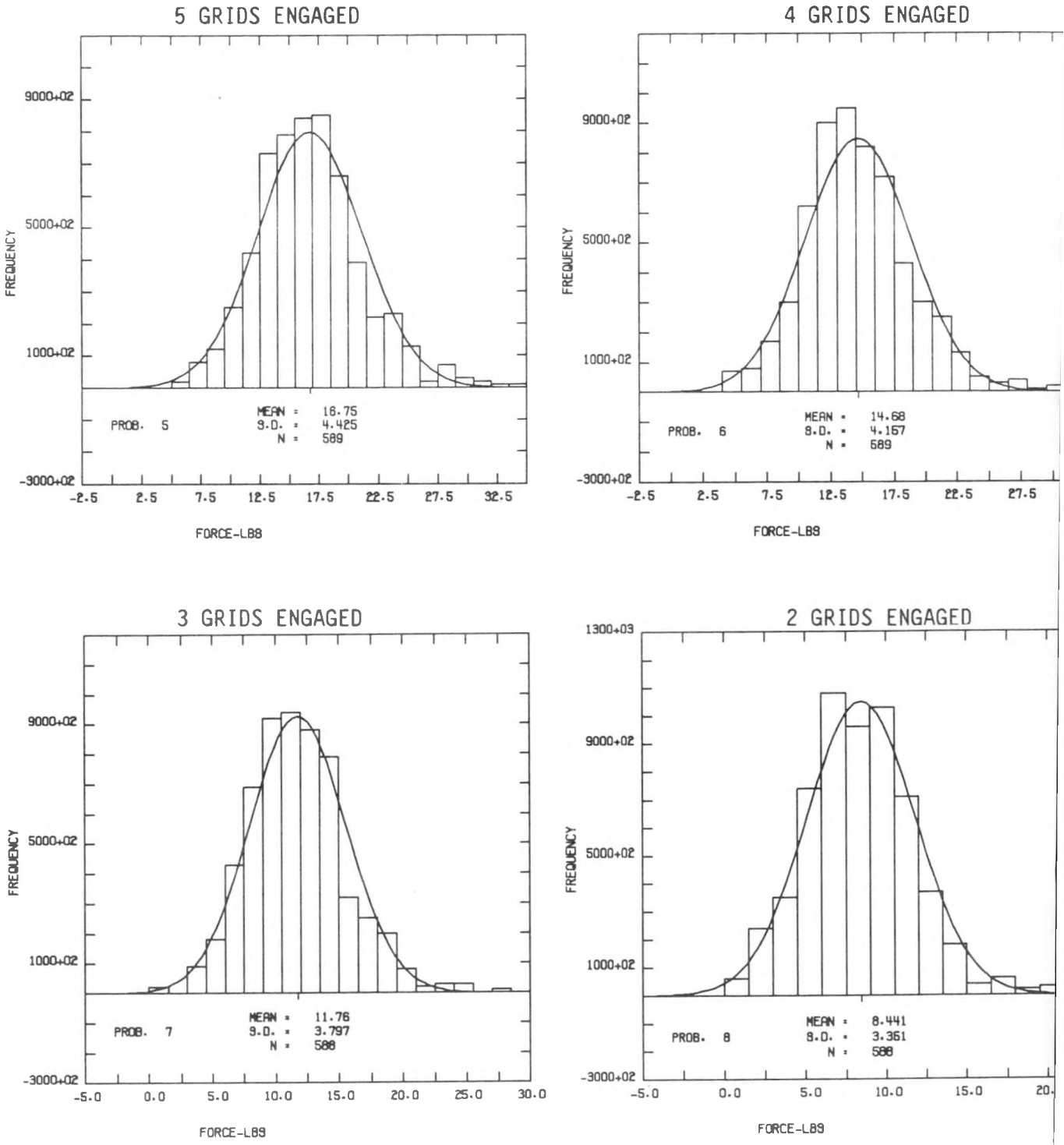

Figure A3-3 - Blanket Pull Force Histograms (Cont)

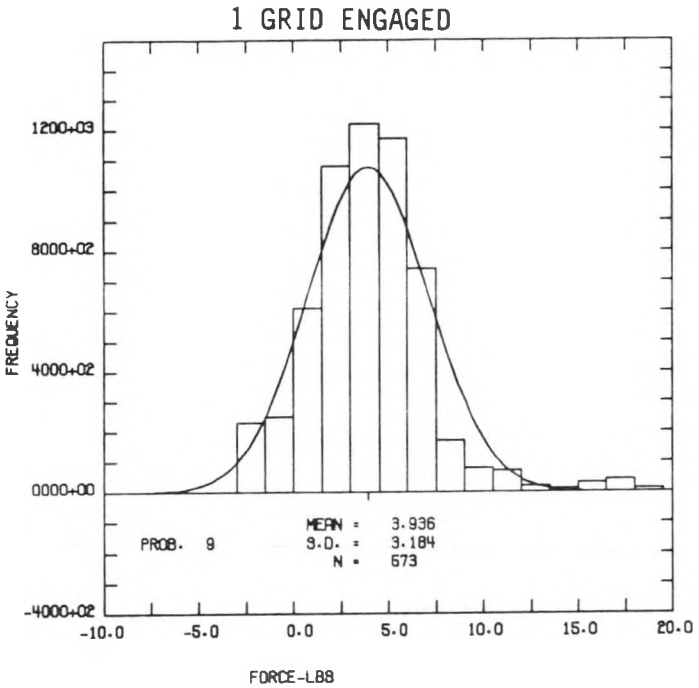

Figure A3-3 - Blanket Pull Force Histograms (Cont)

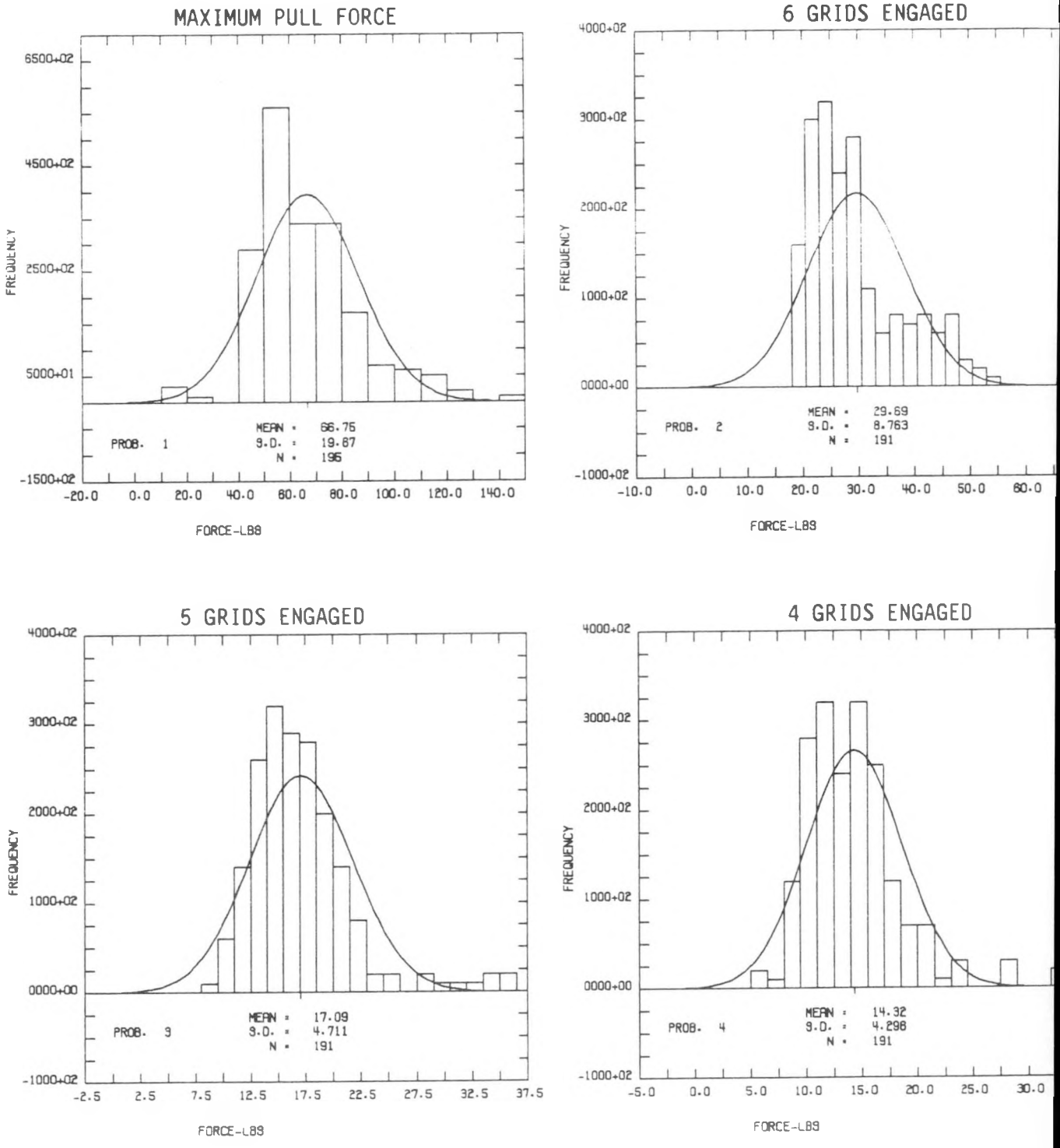

Figure A3-4 - Reflector Pull Force Histograms

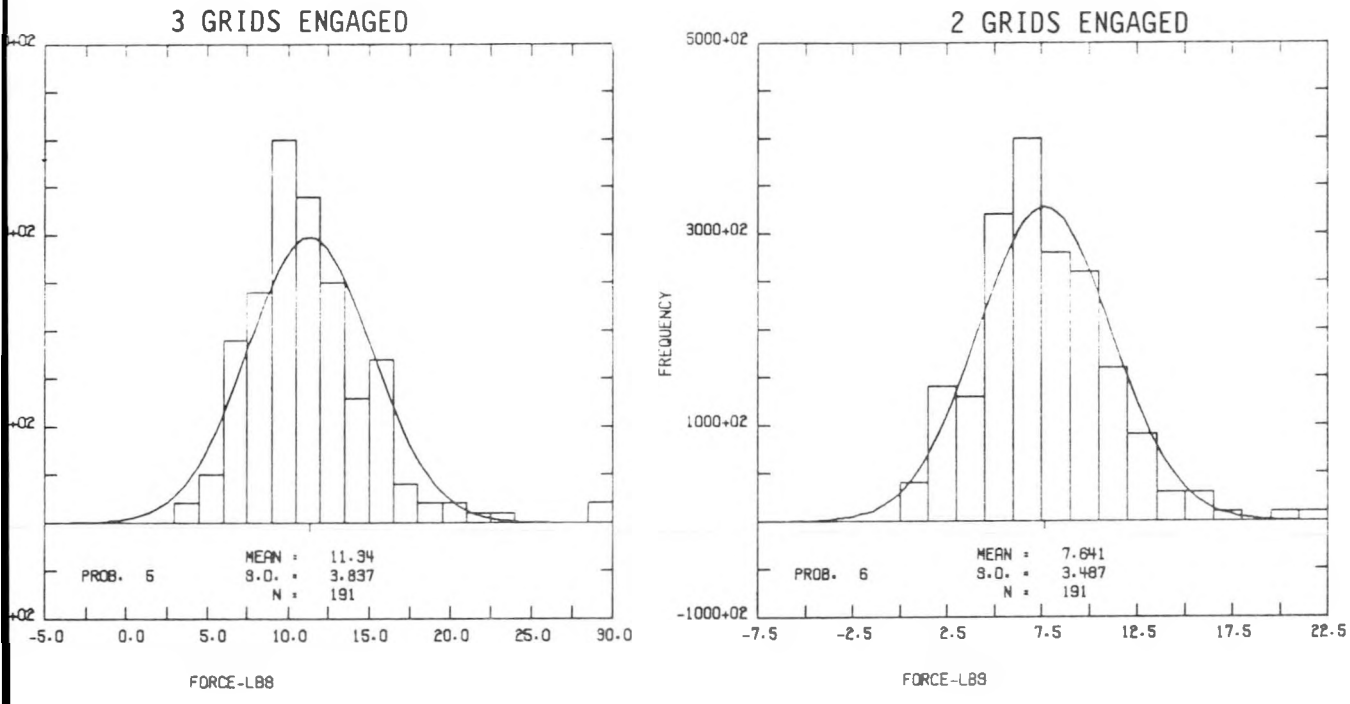

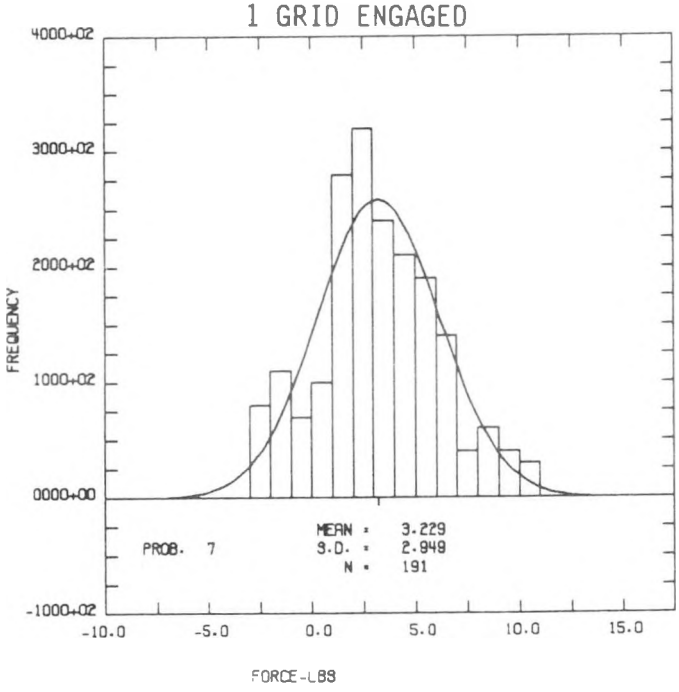

Figure A3-4 - Reflector Pull Force Histograms (Cont)

(Intentionally Blank)

APPENDIX A4 - FUEL ROD IN-BUNDLE BOW PLOTS FOR SELECTED MODULES

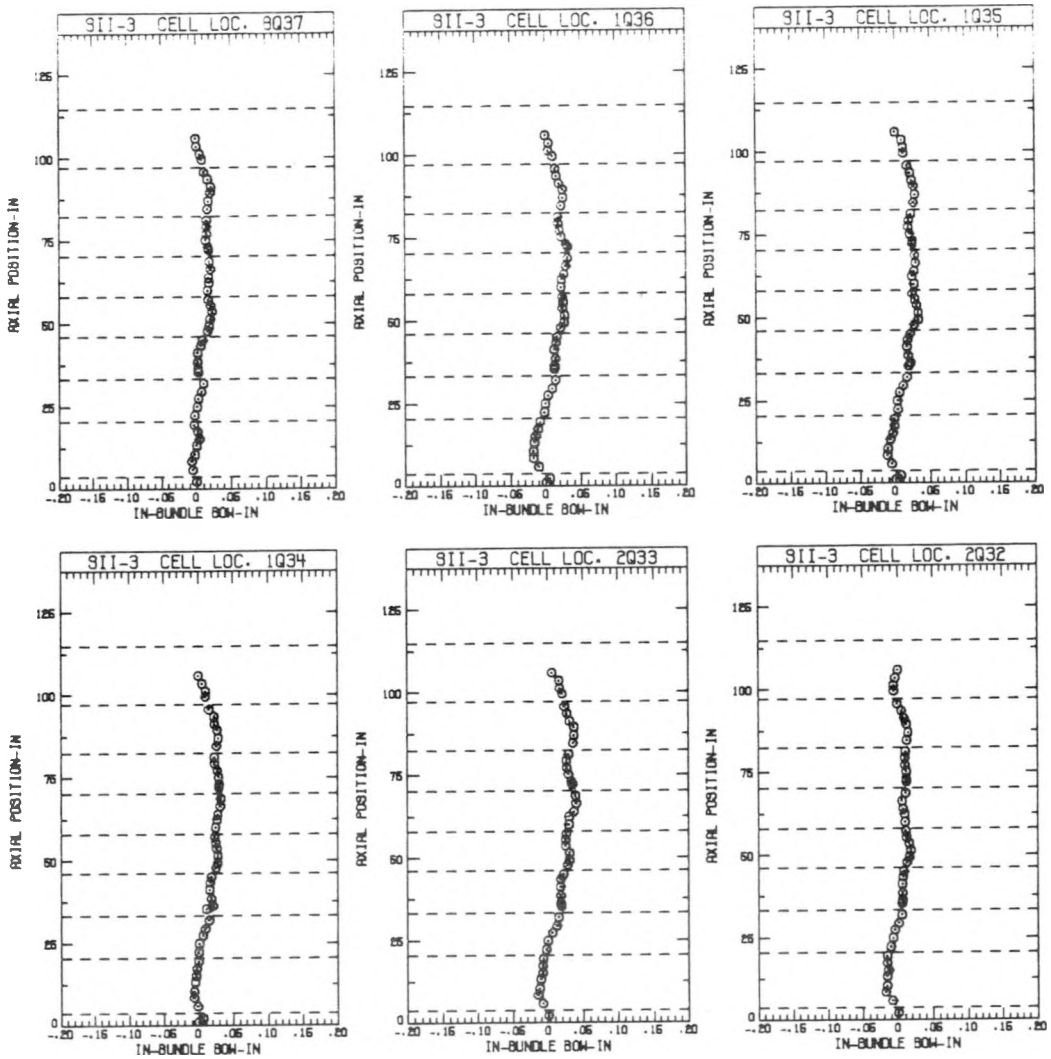

Figure A4-1 - SII-3 Rod Bow Side 4

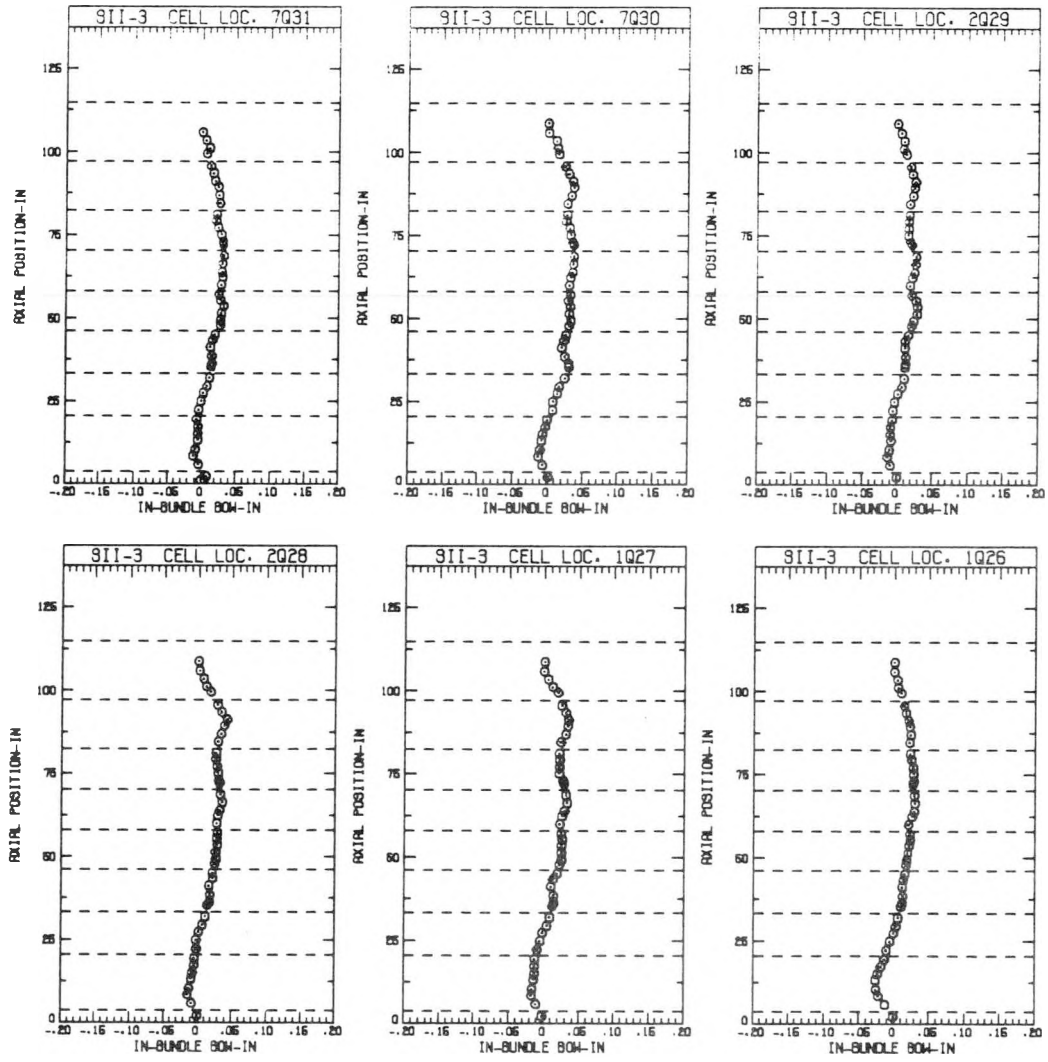

Figure A4-1 - SII-3 Rod Bow Side 4 (Cont)

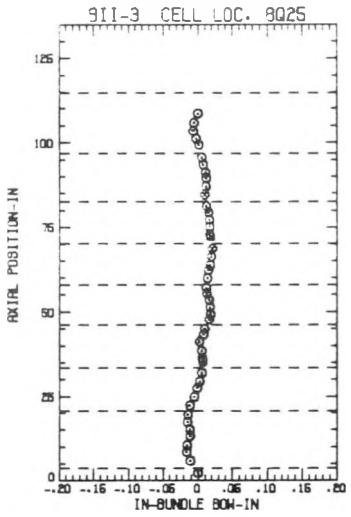

Figure A4-1 - SII-3 Rod Bow Side 4 (Cont)

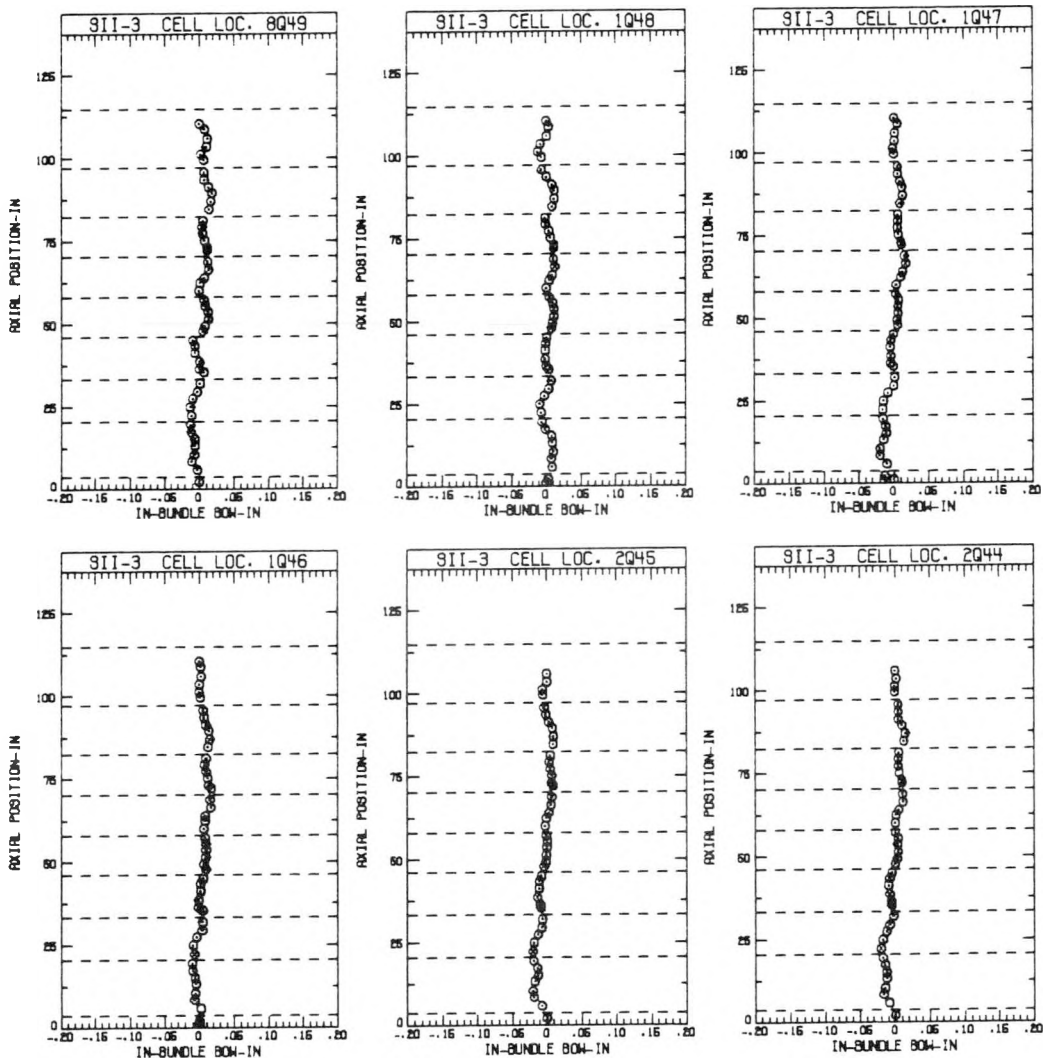

Figure A4-2 - SII-3 Rod Bow Side 5

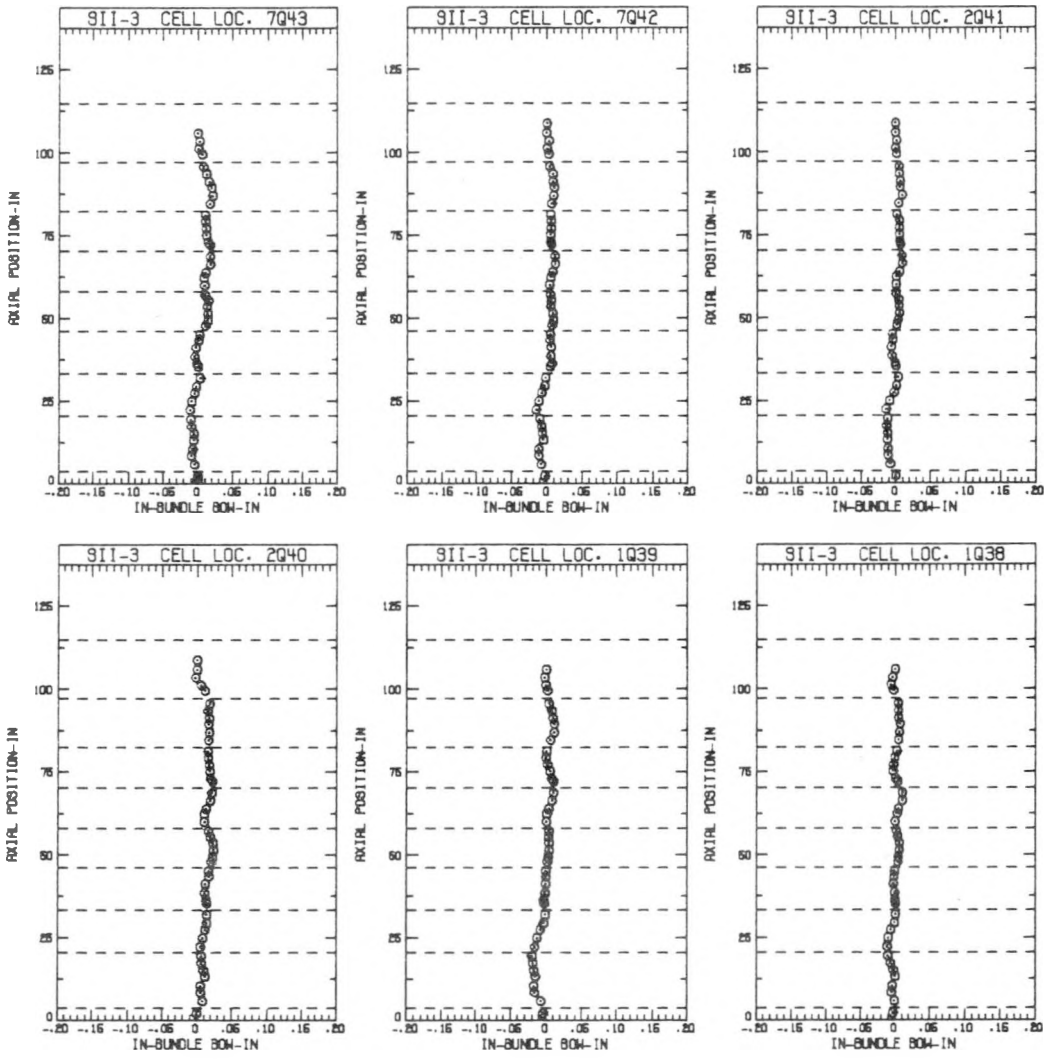

Figure A4-2 - SII-3 Rod Bow Side 5 (Cont)

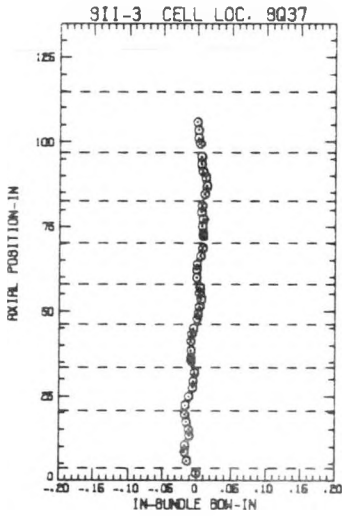

Figure A4-2 - SII-3 Rod Bow Side 5 (Cont)

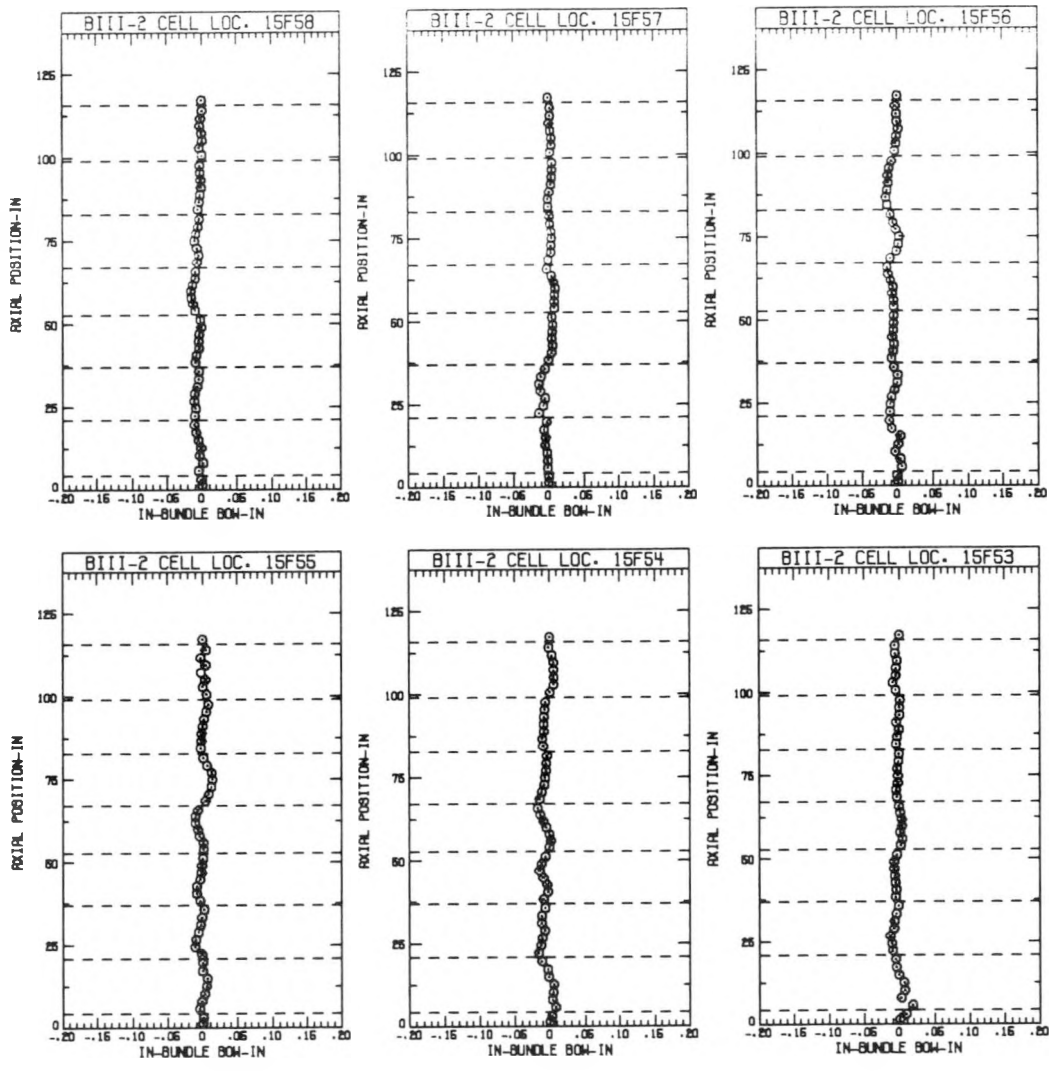

Figure A4-3 - BIII-2 Rod Bow Side 5

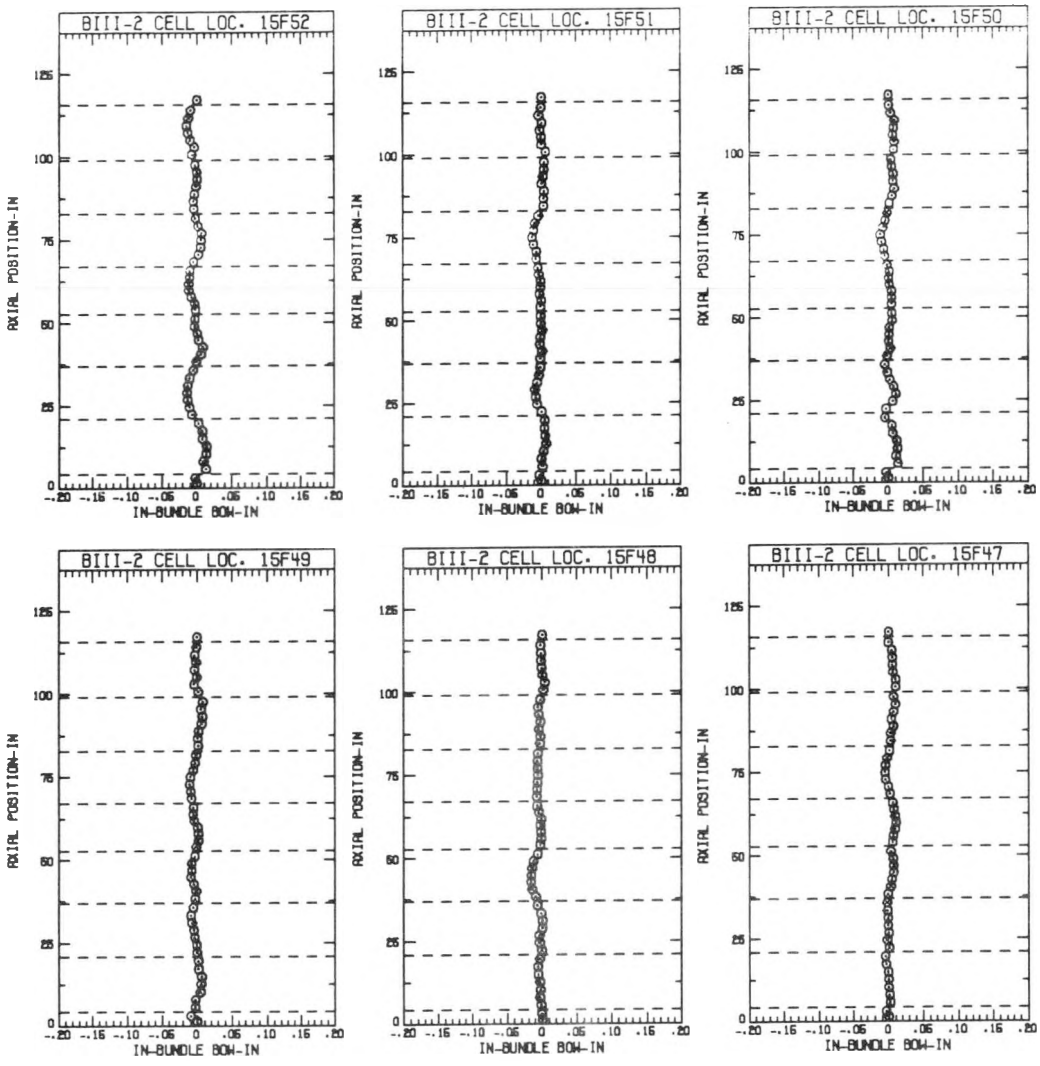

Figure A4-3 - BIII-2 Rod Bow Side 5 (Cont)

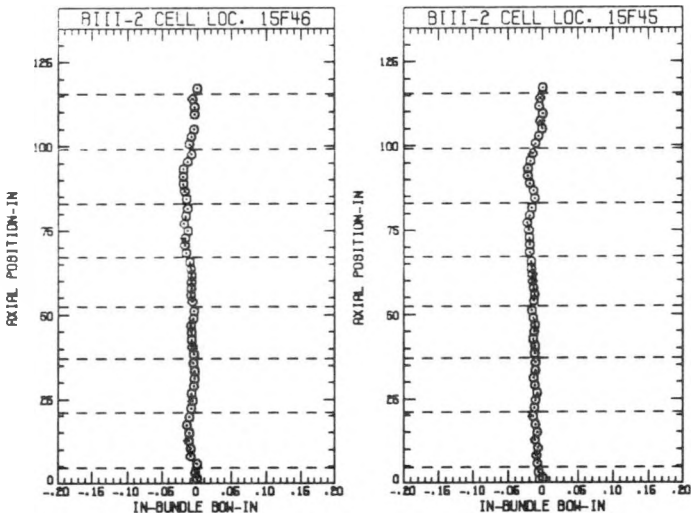

Figure A4-3 - BIII-2 Rod Bow Side 5 (Cont)

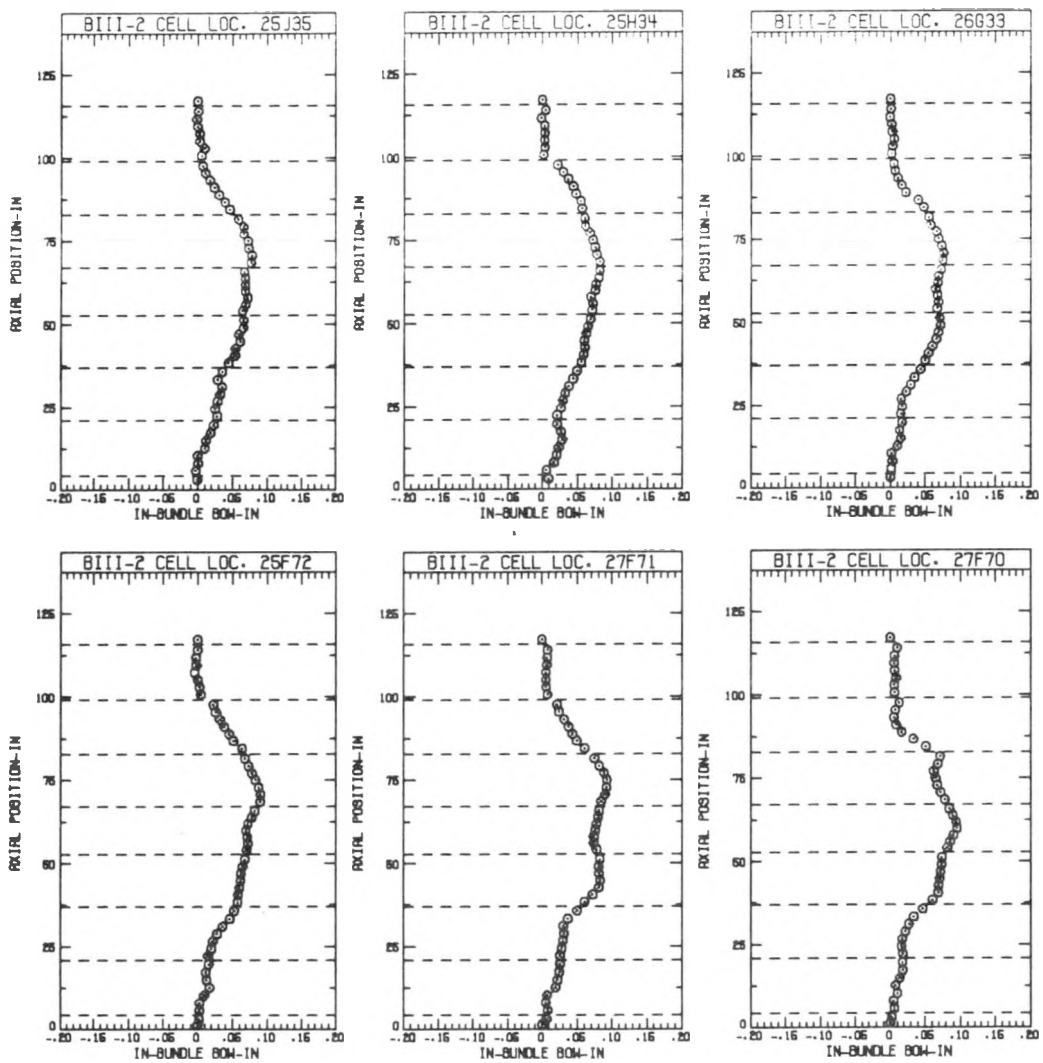

Figure A4-4 - BIII-2 Rod Bow Side 6

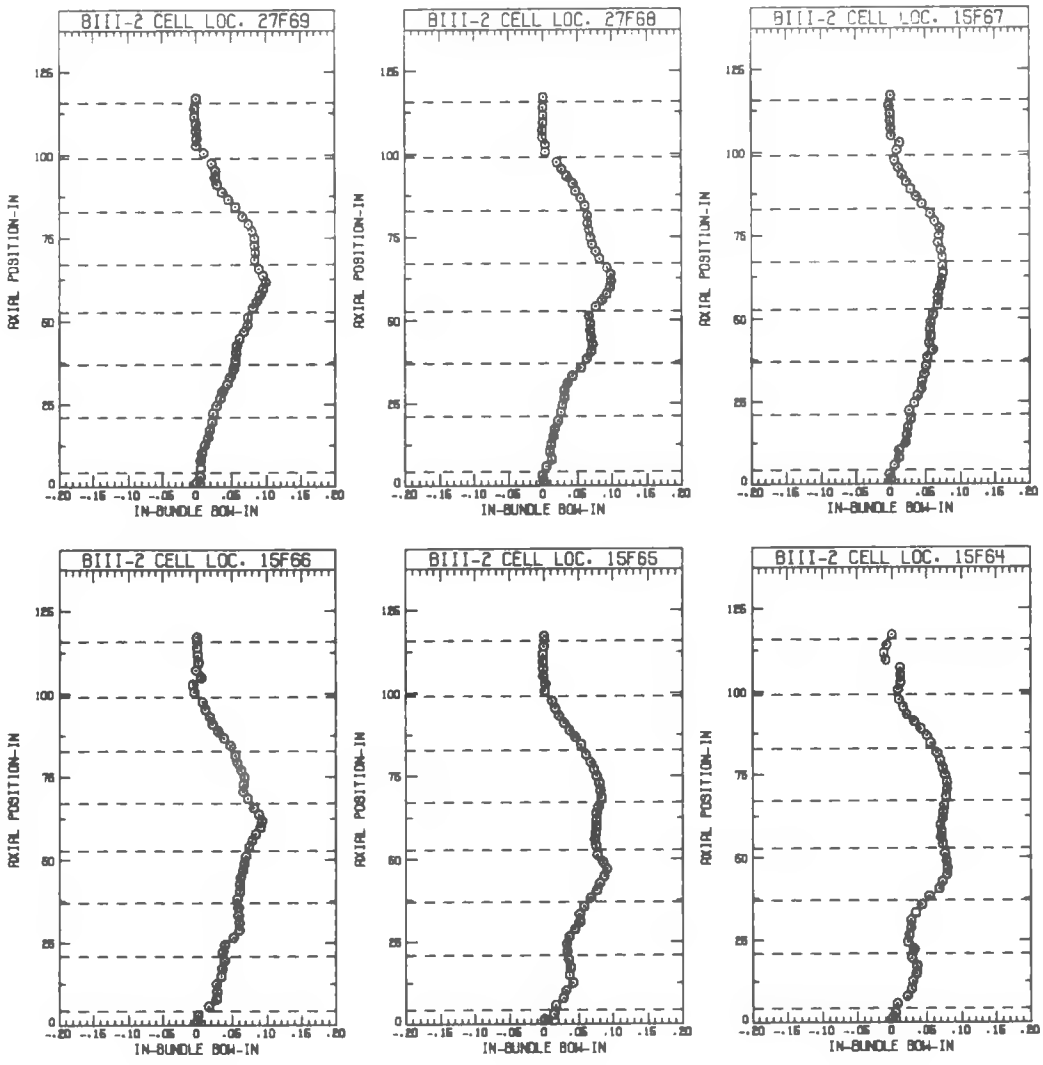

Figure A4-4 - BIII-2 Rod Bow Side 6 (Cont)

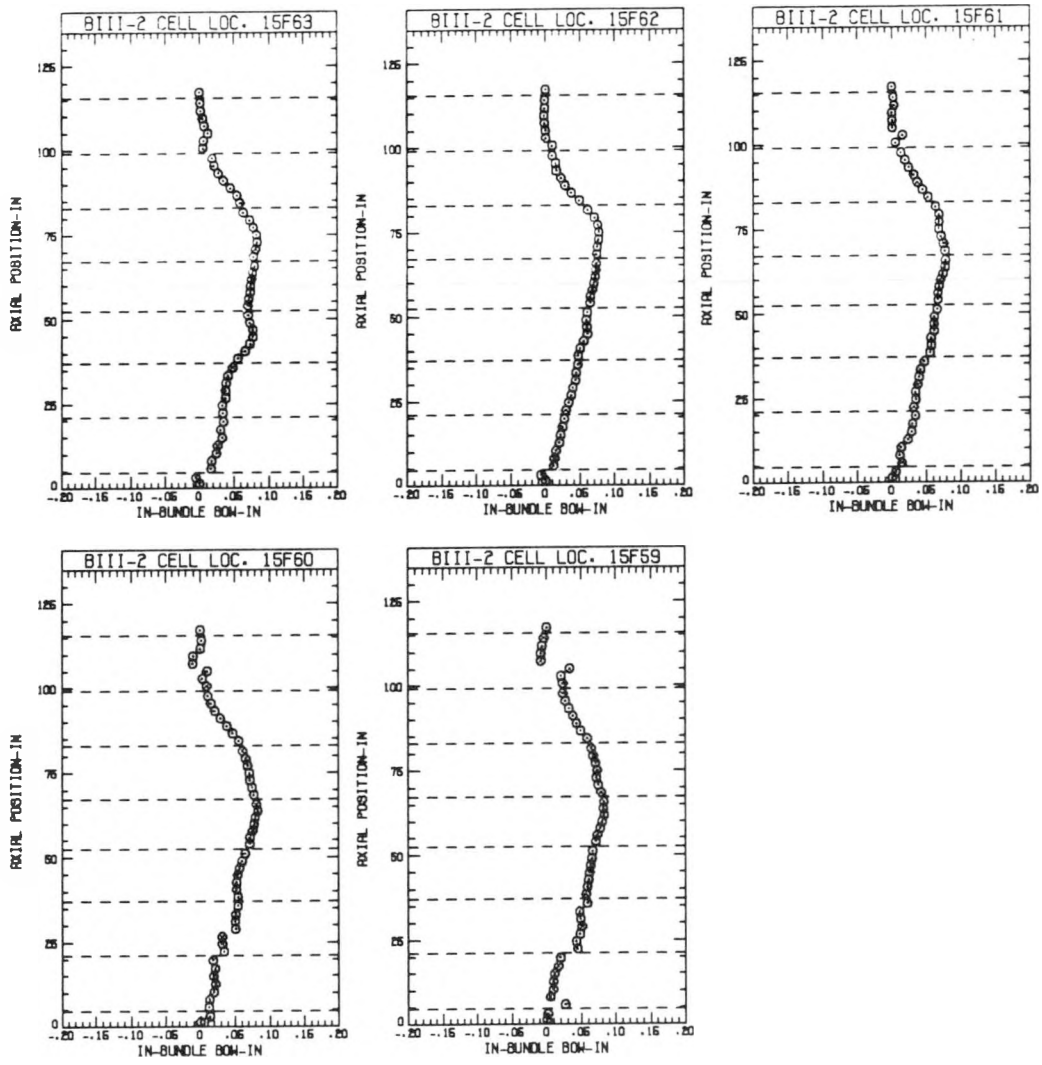

Figure A4-4 - BIII-2 Rod Bow Side 6 (Cont)

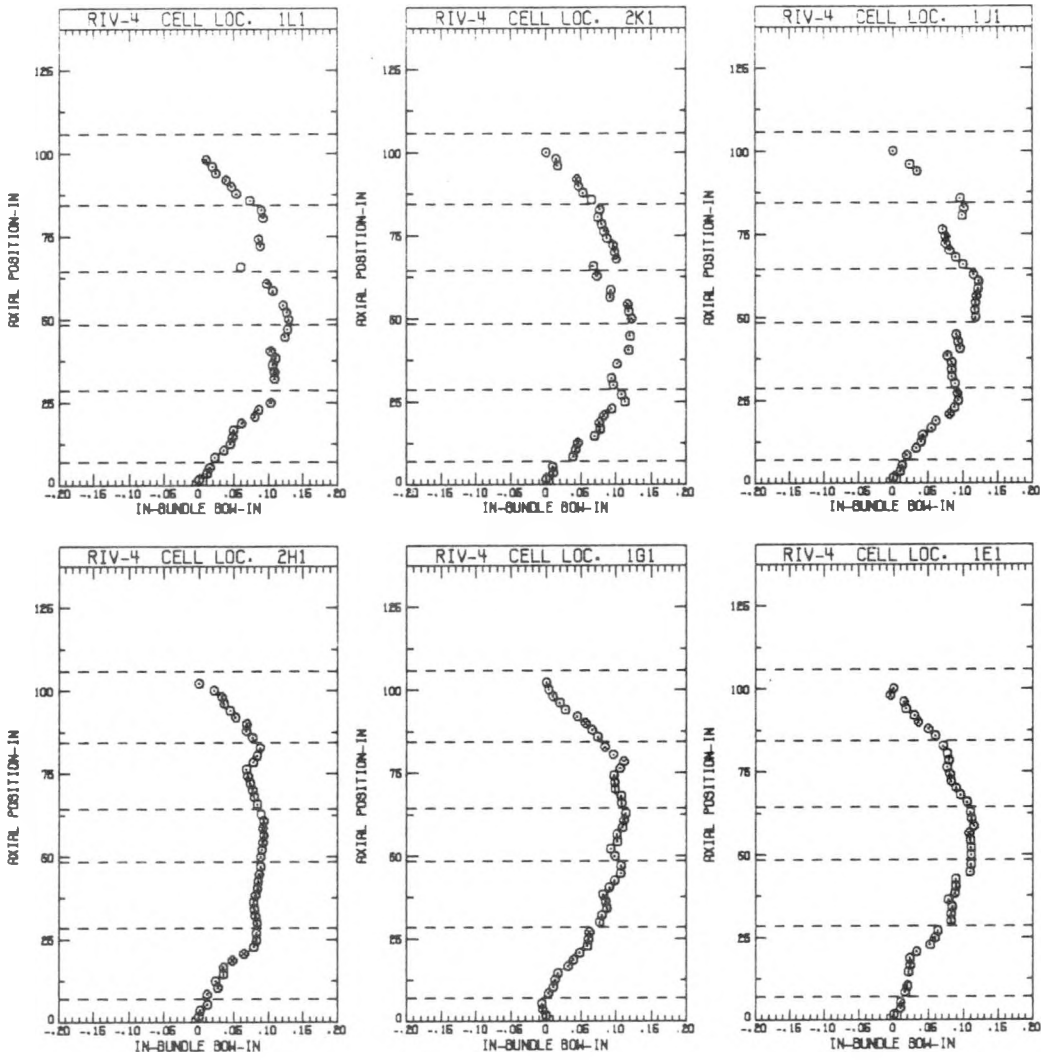

Figure A4-5 - RIV-4 Rod Bow Side 1

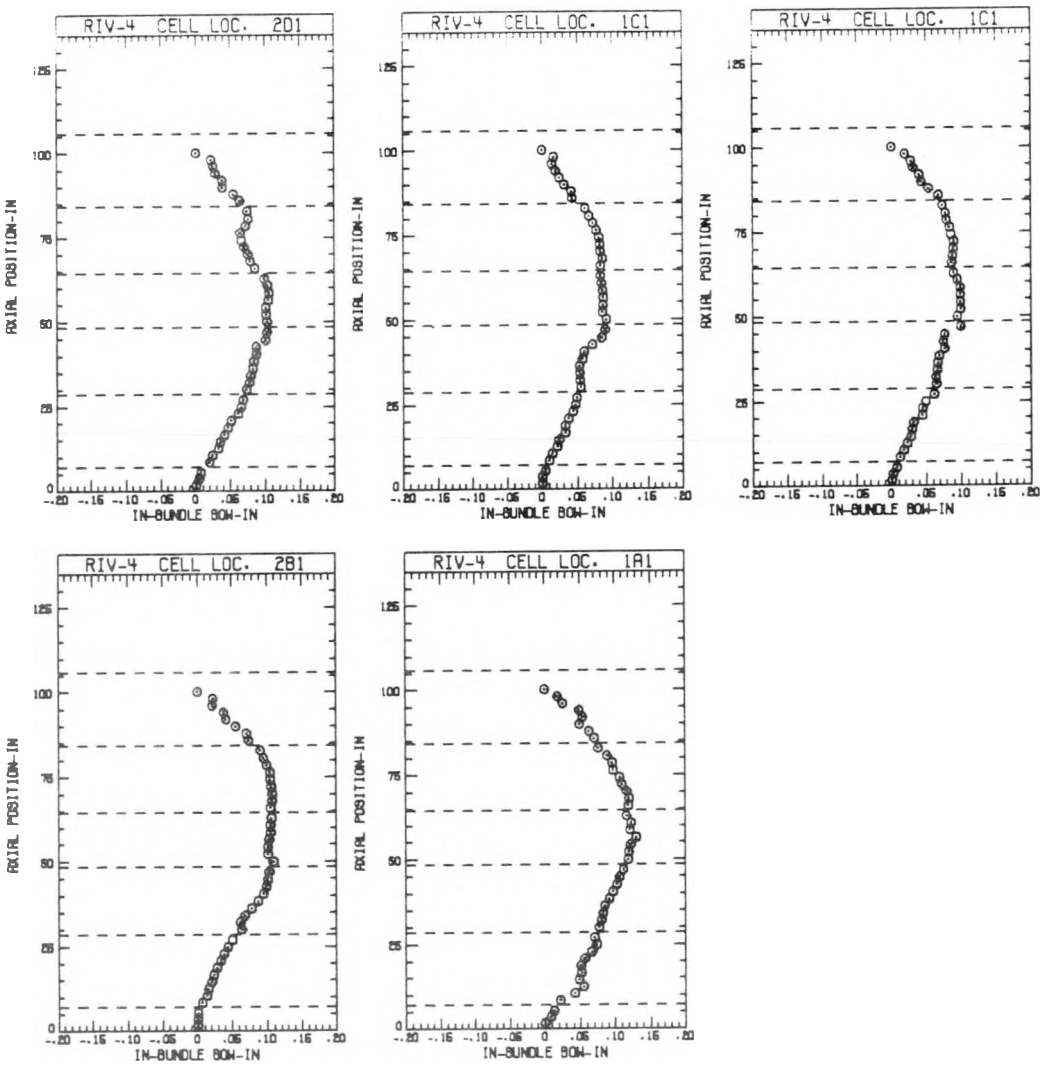

Figure A4-5 - RIV-4 Rod Bow Side 1 (Cont)

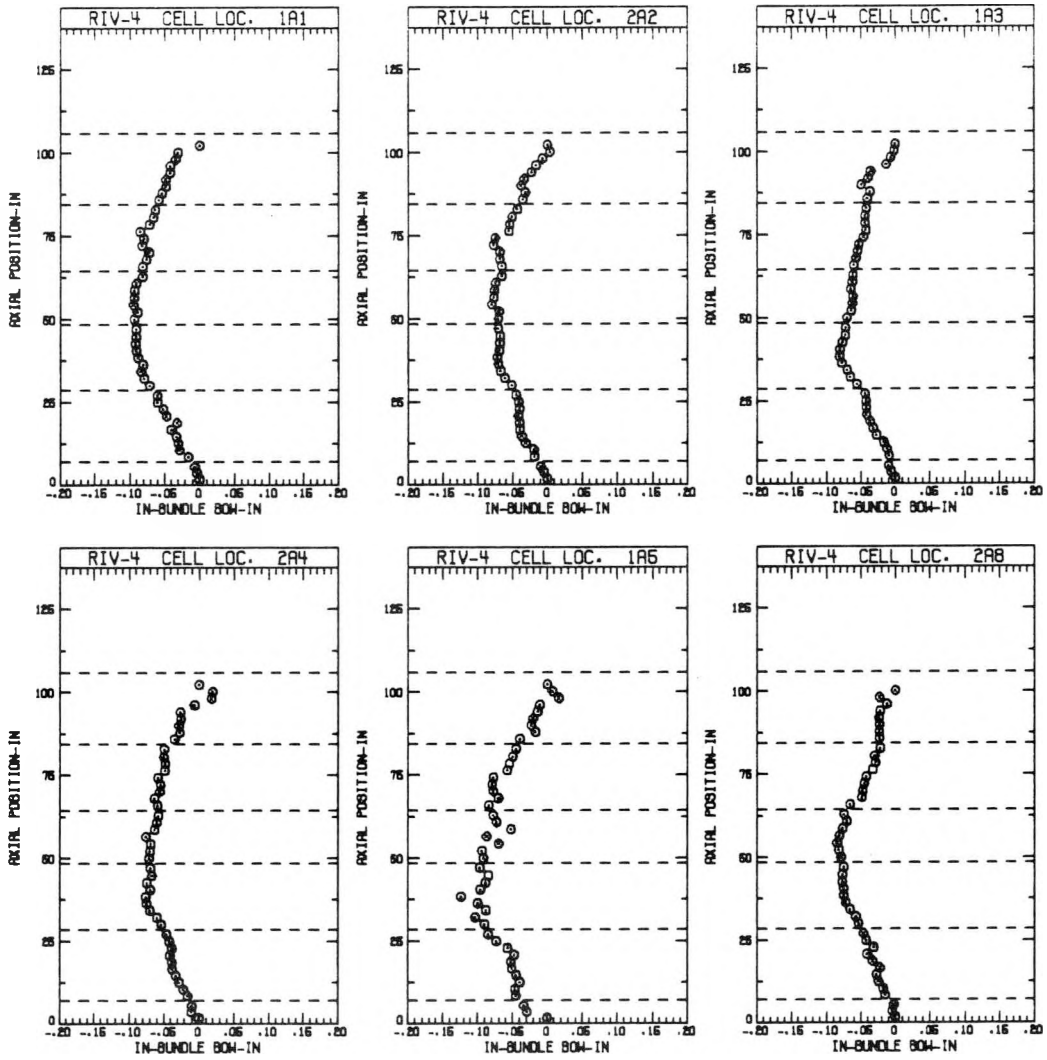

Figure A4-6 - RIV-4 Rod Bow Side 5

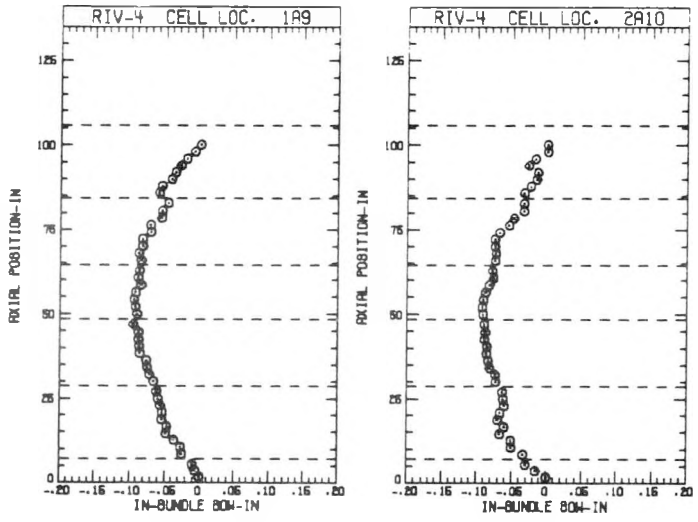

Figure A4-6 - RIV-4 Rod Bow Side 5 (Cont)

(Intentionally Blank)

APPENDIX A5 - FUEL ROD IN-BUNDLE GAP PLOTS FOR SELECTED MODULES

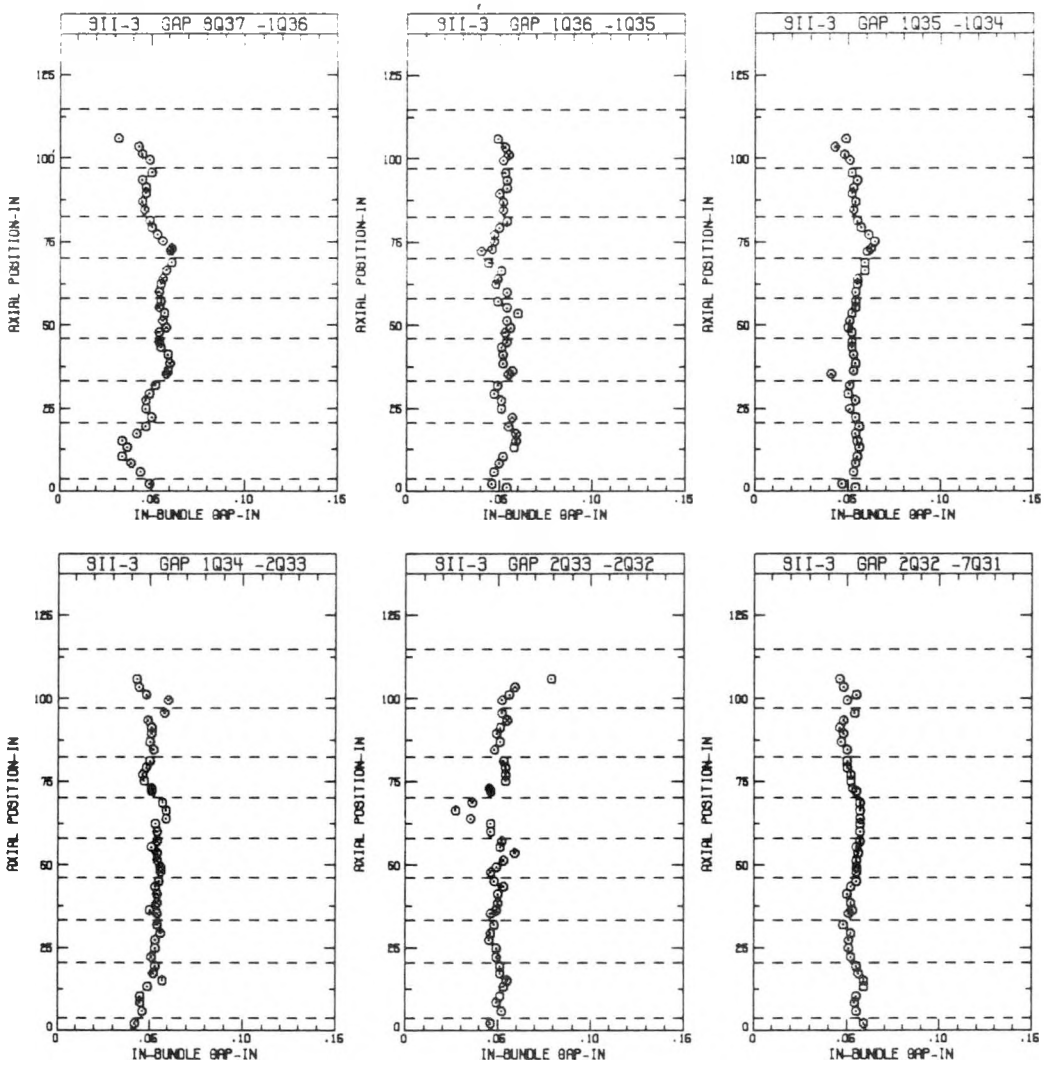

Figure A5-1 - SII-3 Rod Gaps Side 4

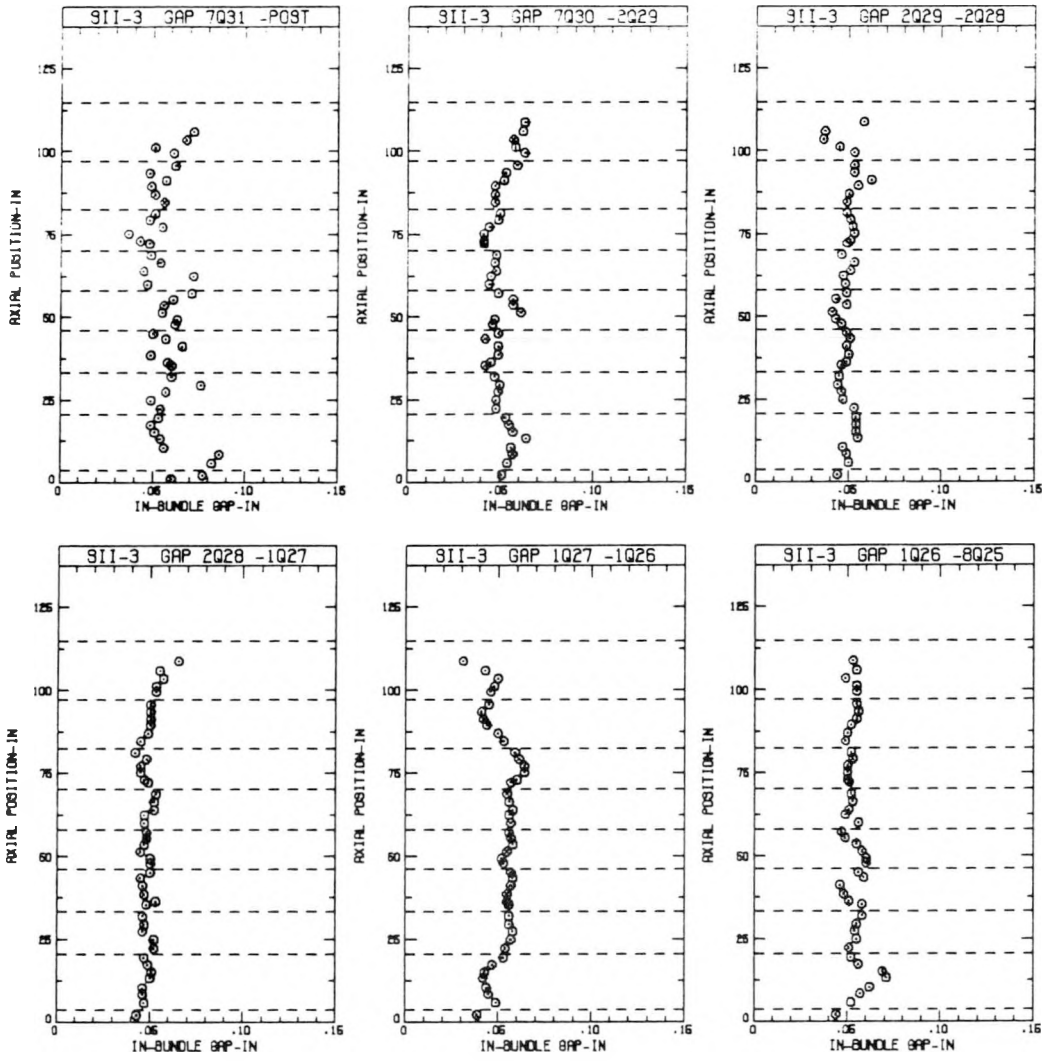

Figure A5-1 - SII-3 Rod Gaps Side 4 (Cont)

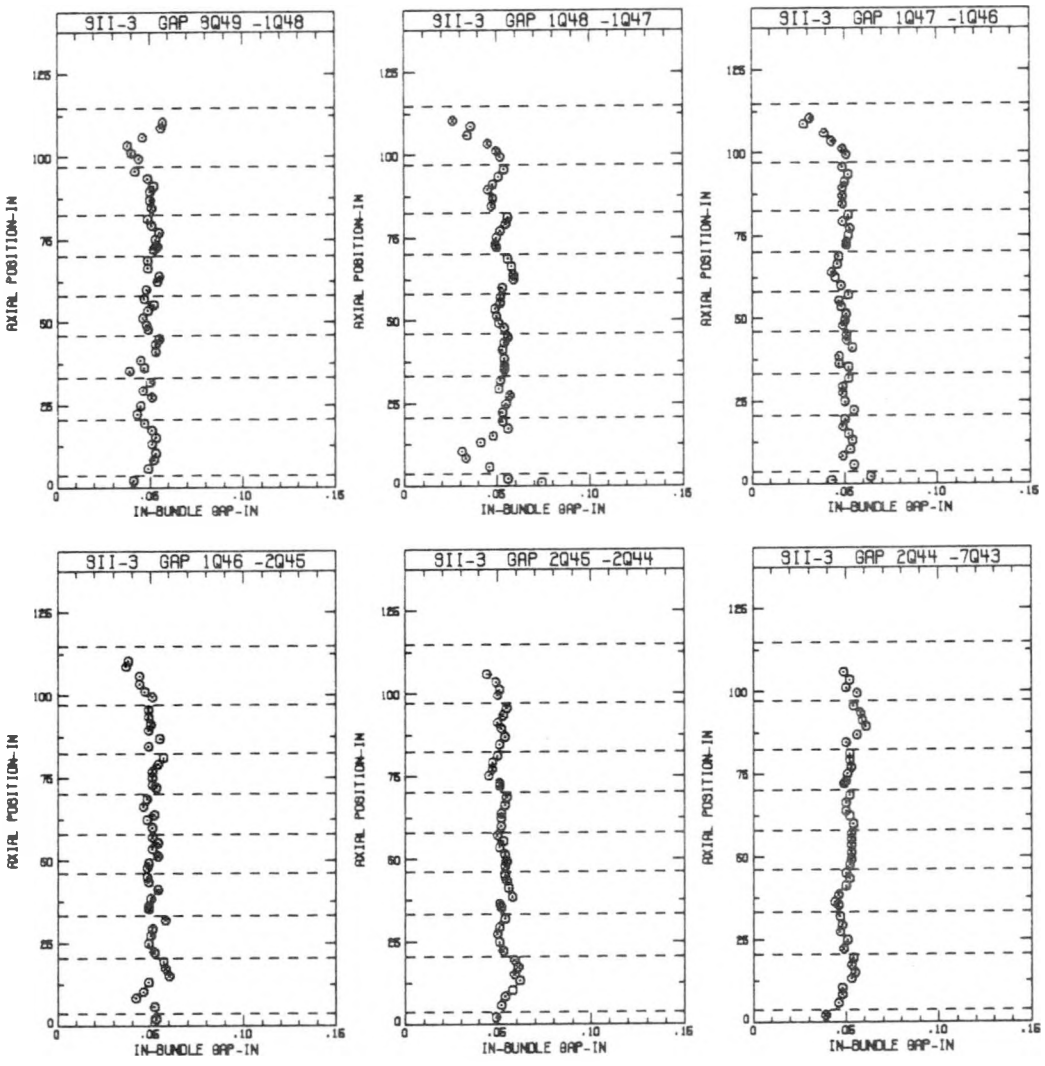

Figure A5-2 - SII-3 Rod Gaps Side 5

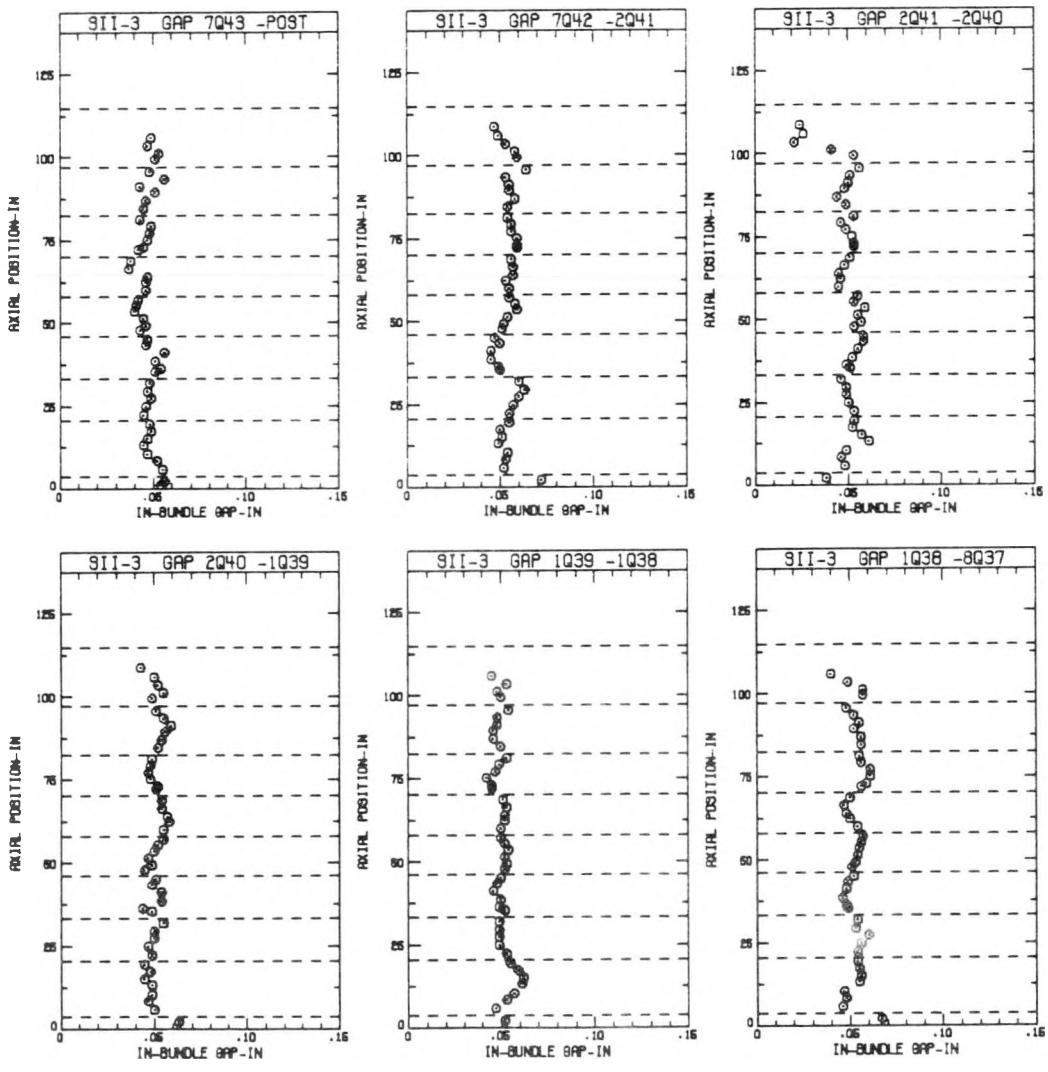

Figure A5-2 - SII-3 Rod Gaps Side 5 (Cont)

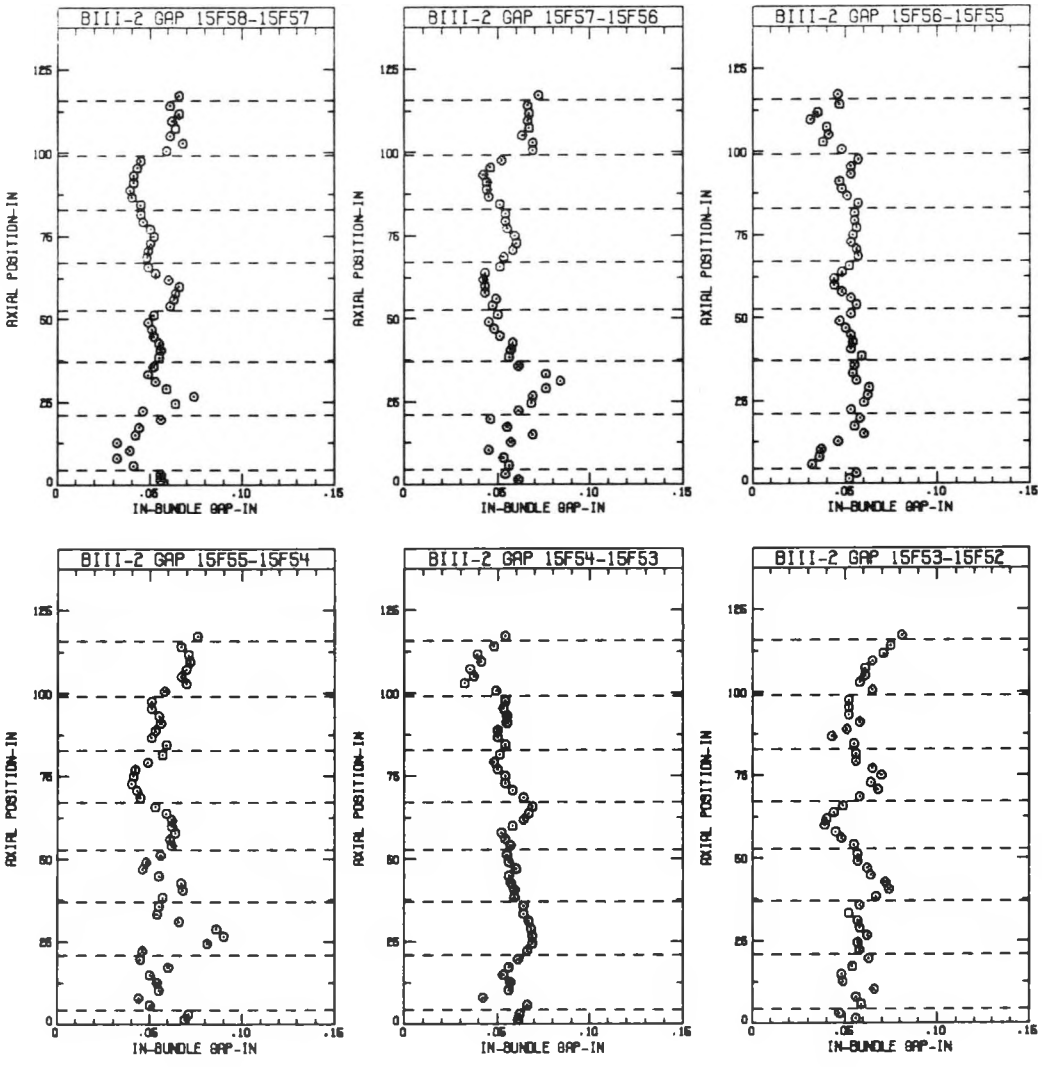

Figure A5-3 - BIII-2 Rod Gaps Side 5

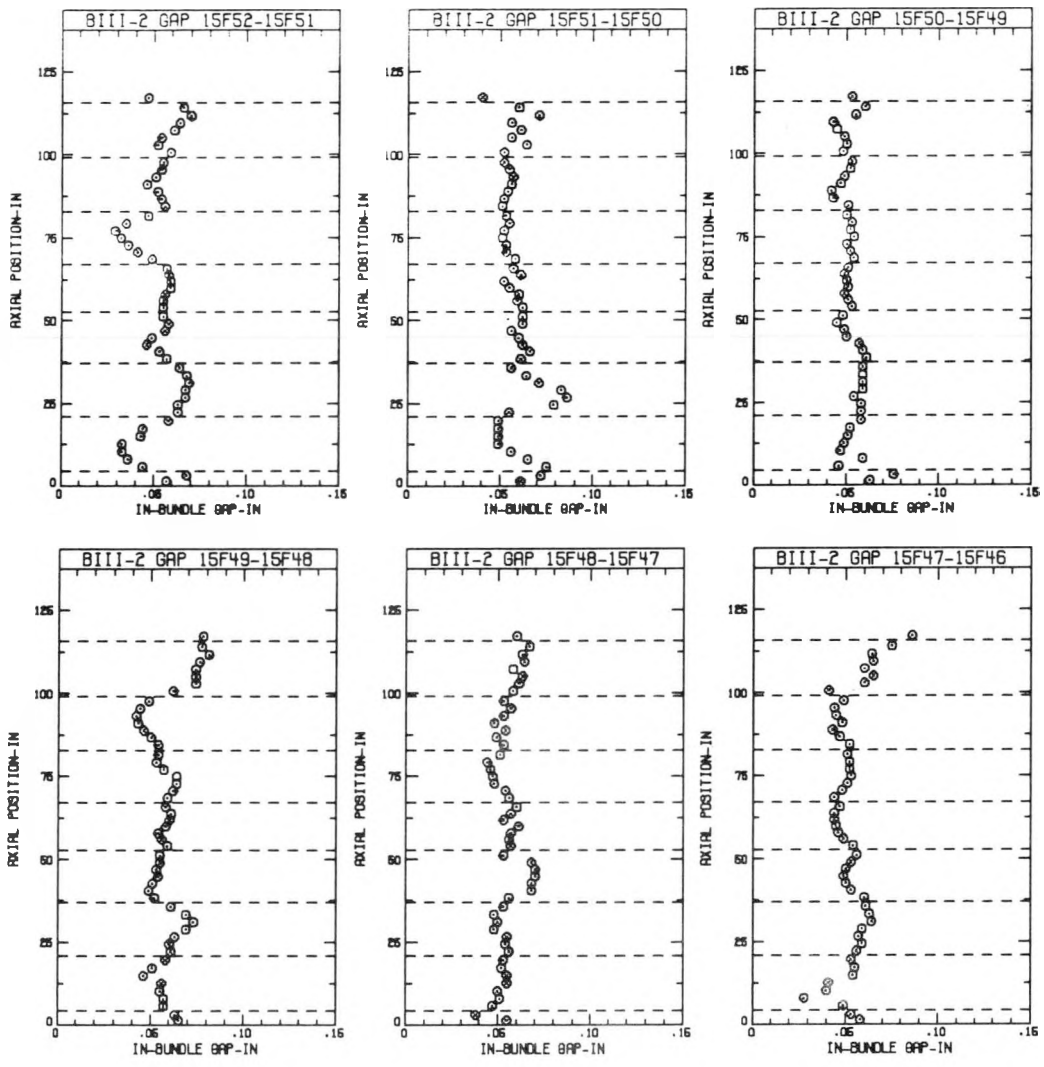

Figure A5-3 - BIII-2 Rod Gaps Side 5 (Cont)

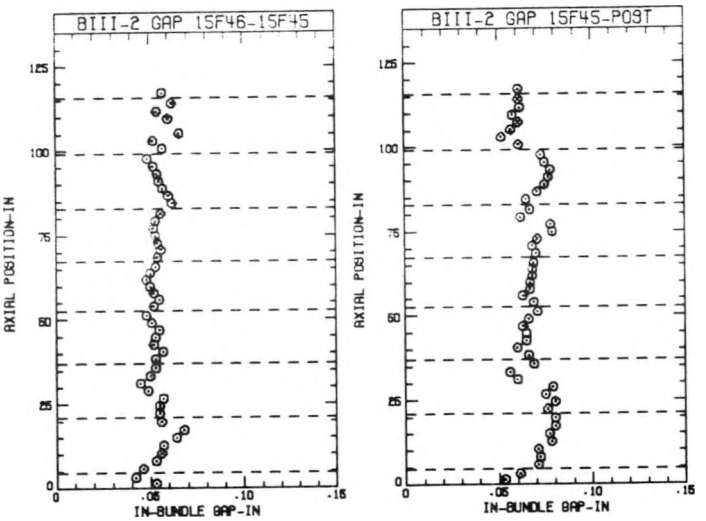

Figure A5-3 - BIII-2 Rod Gaps Side 5 (Cont)

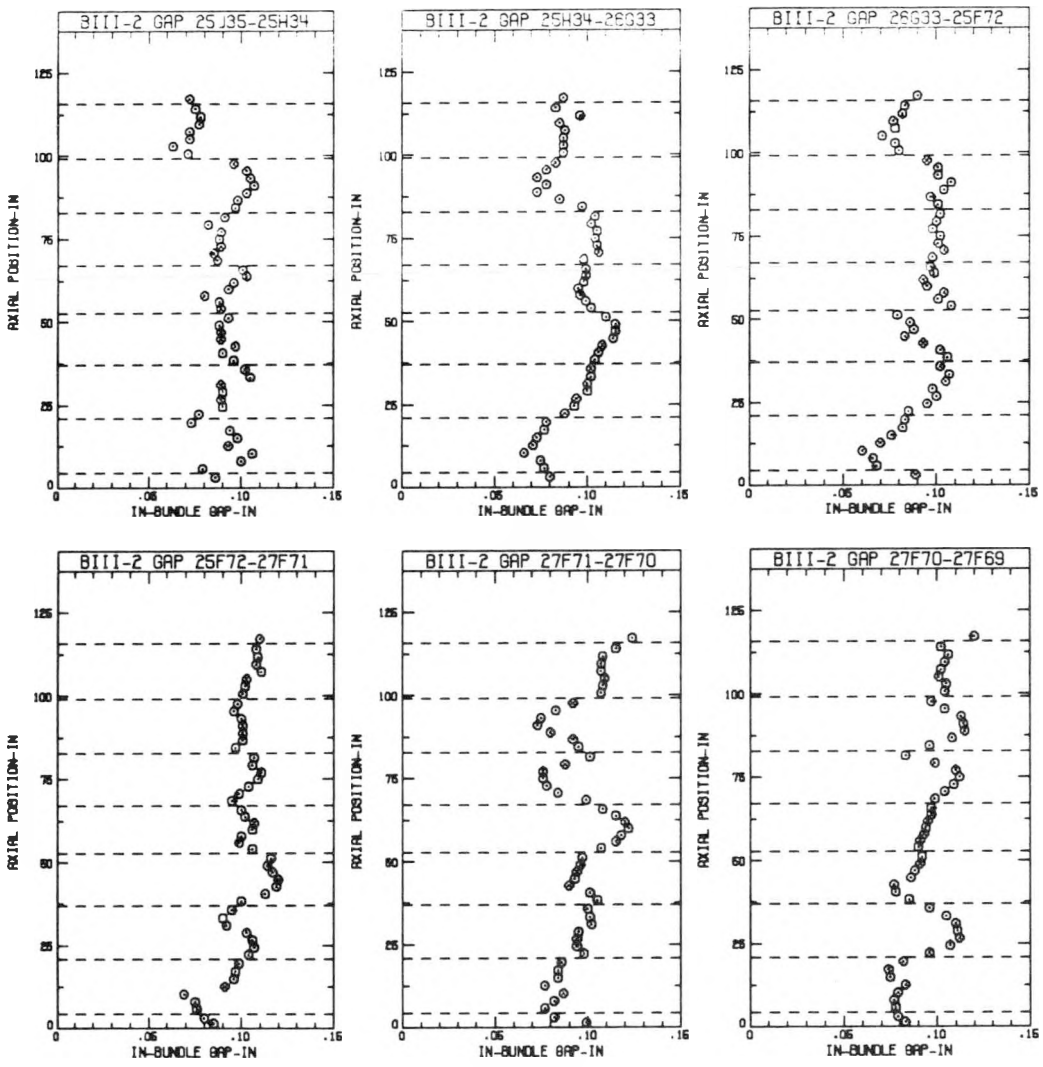

Figure A5-4 - BIII-2 Rod Gaps Side 6

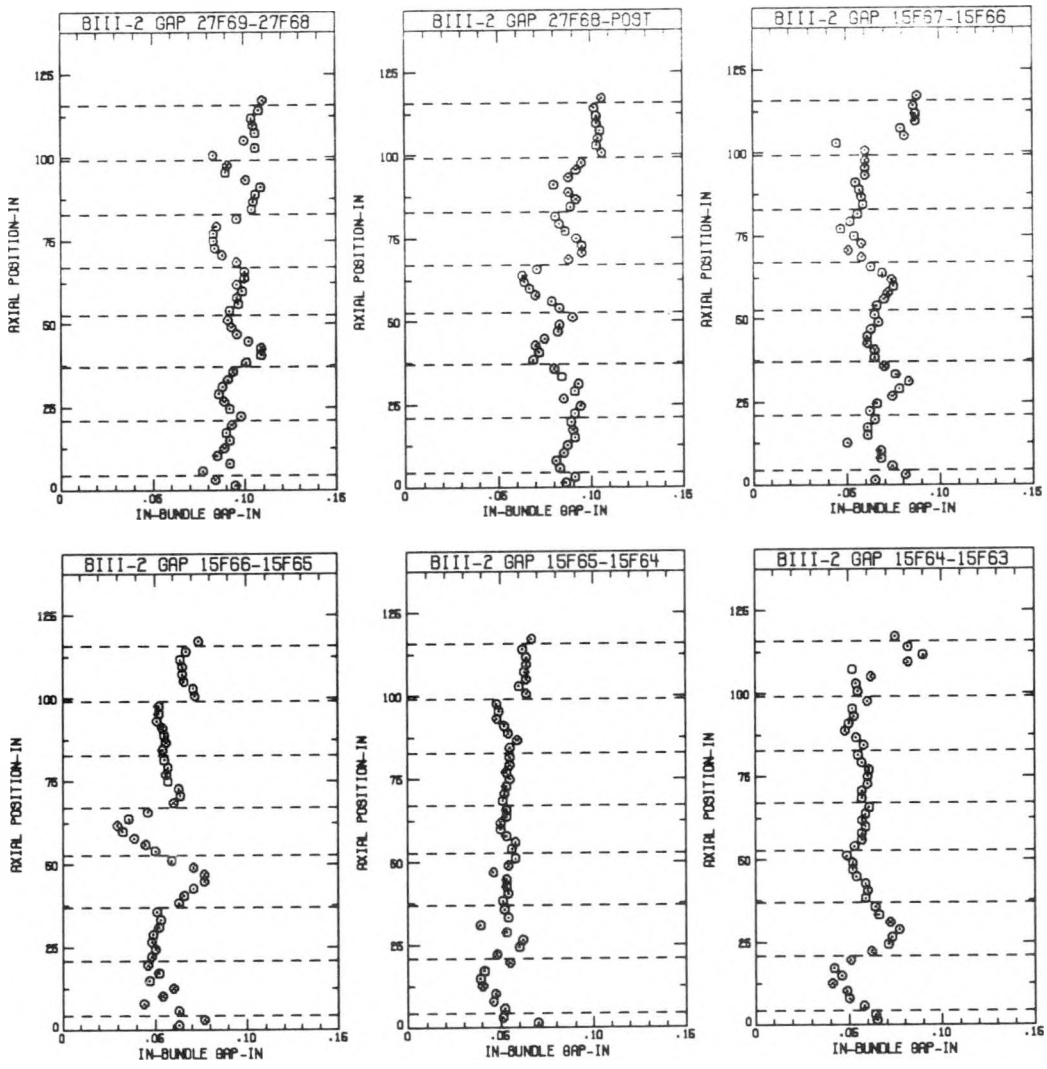

Figure A5-4 - BIII-2 Rod Gaps Side 6 (Cont)

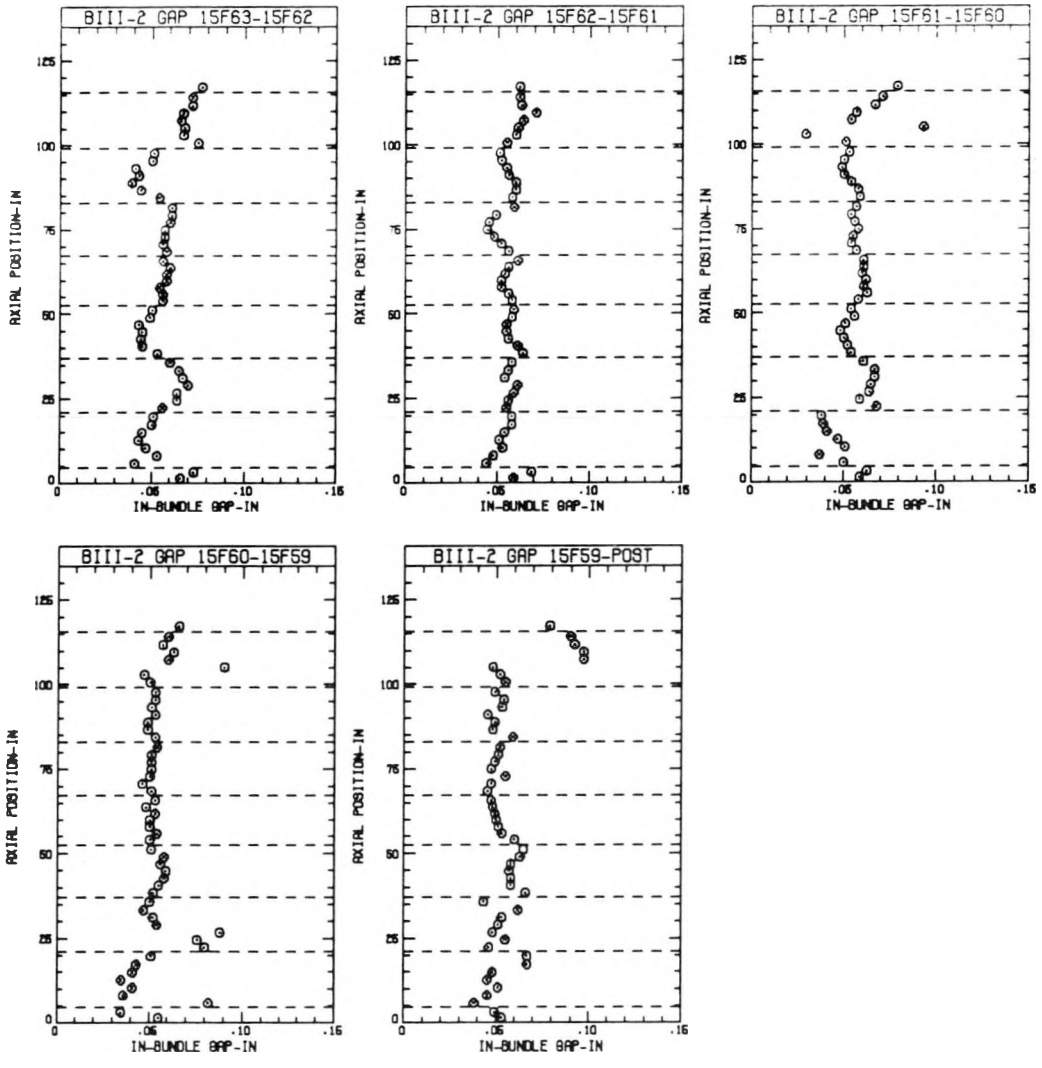

Figure A5-4 - BIII-2 Rod Gaps Side 6 (Cont)

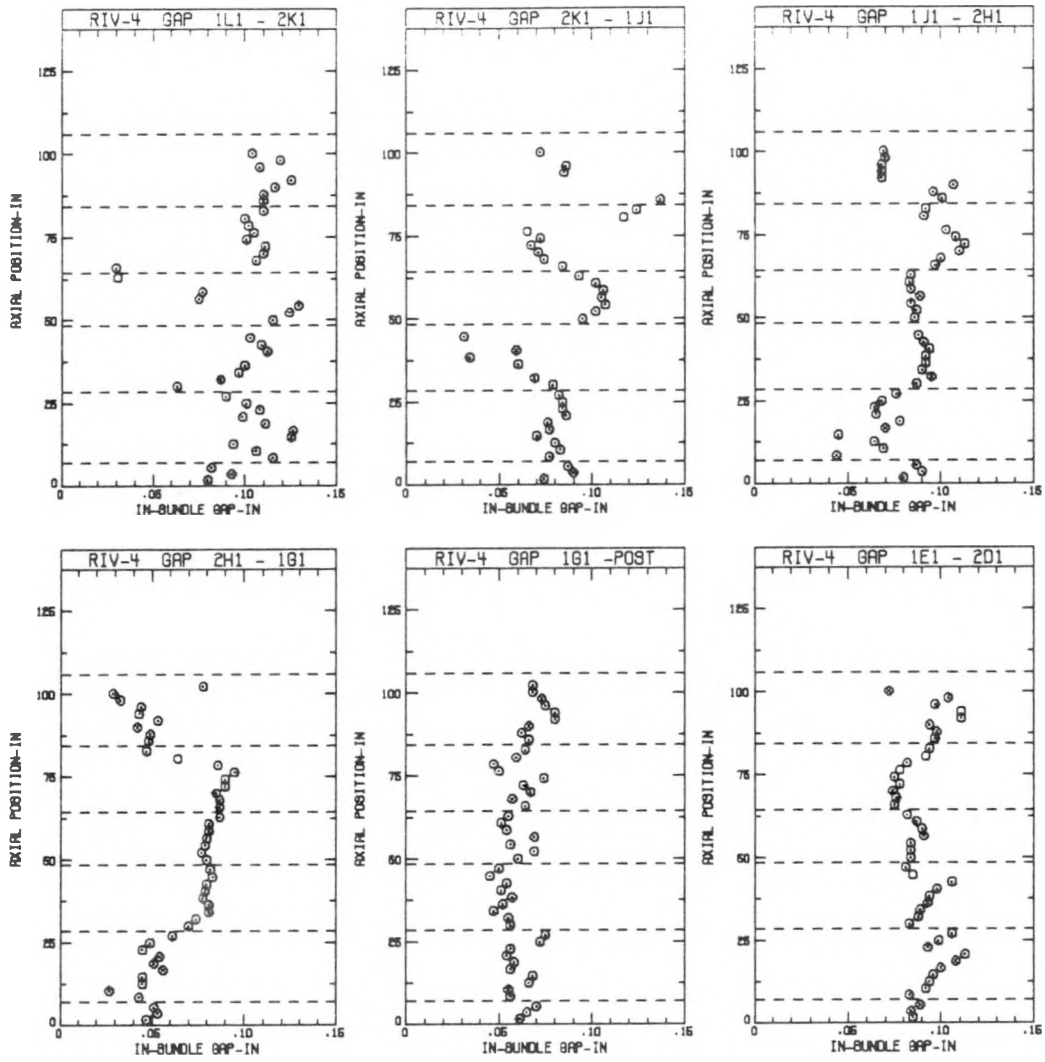

Figure A5-5 - RIV-4 Rod Gaps Side 1

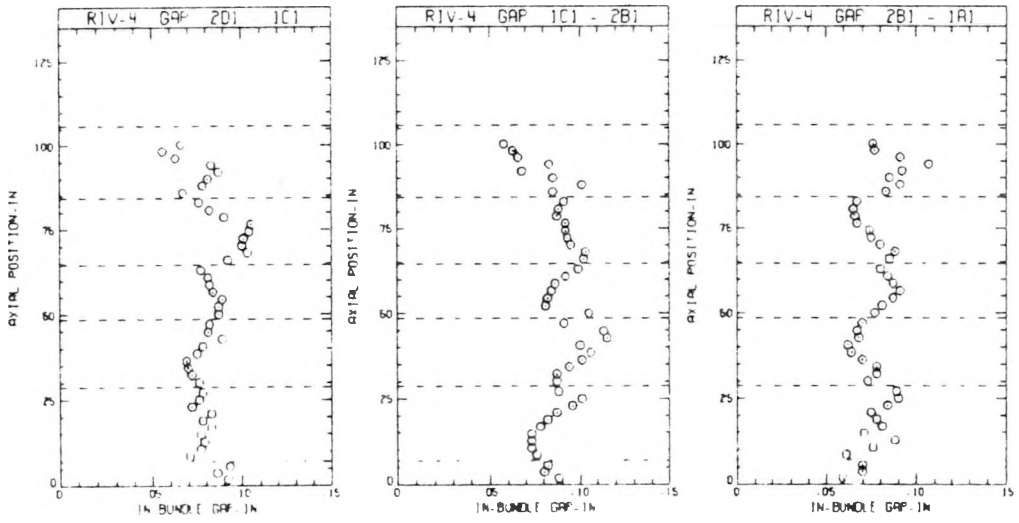

Figure A5-5 - RIV-4 Rod Gaps Side 1 (Cont)

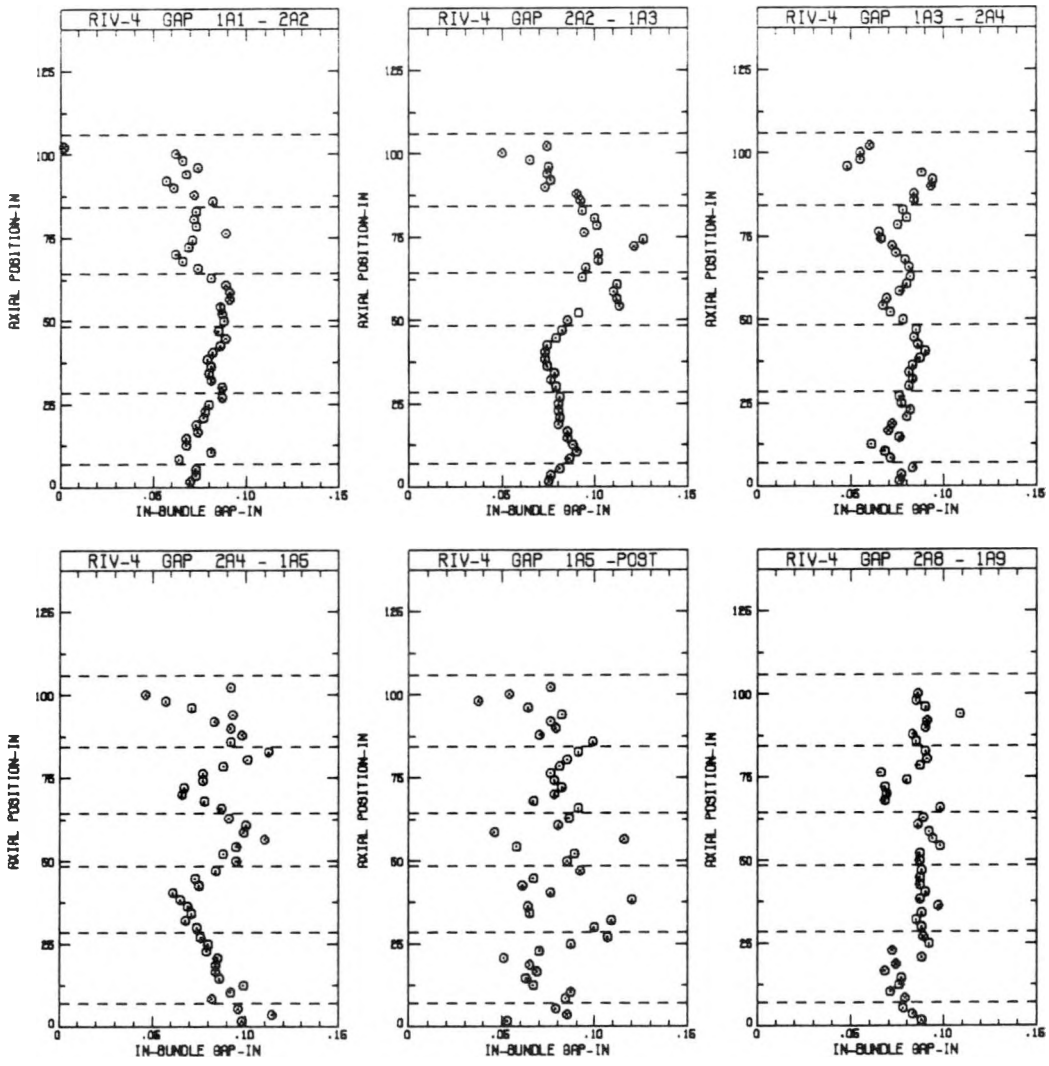

Figure A5-6 - RIV-4 Rod Gaps Side 5

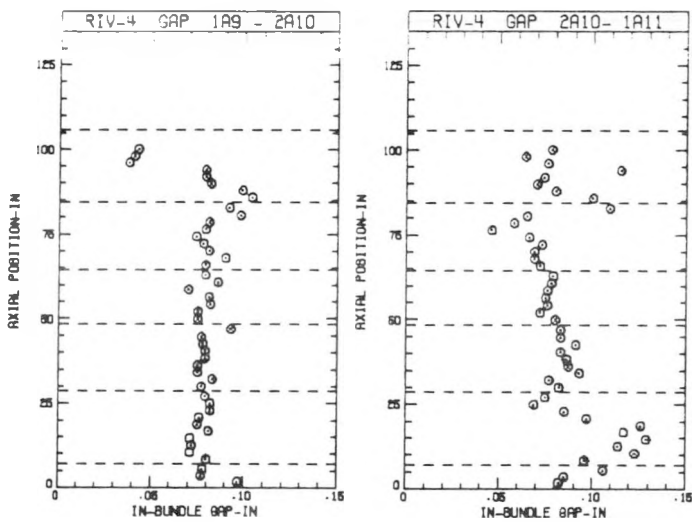

Figure A5-6 - RIV-4 Rod Gaps Side 5 (Cont)

(Intentionally Blank)

APPENDIX A6 - AVERAGE DIAMETER AND OVALITY PROFILES FOR TWELVE DESTRUCTIVE EXAMINATION RODS

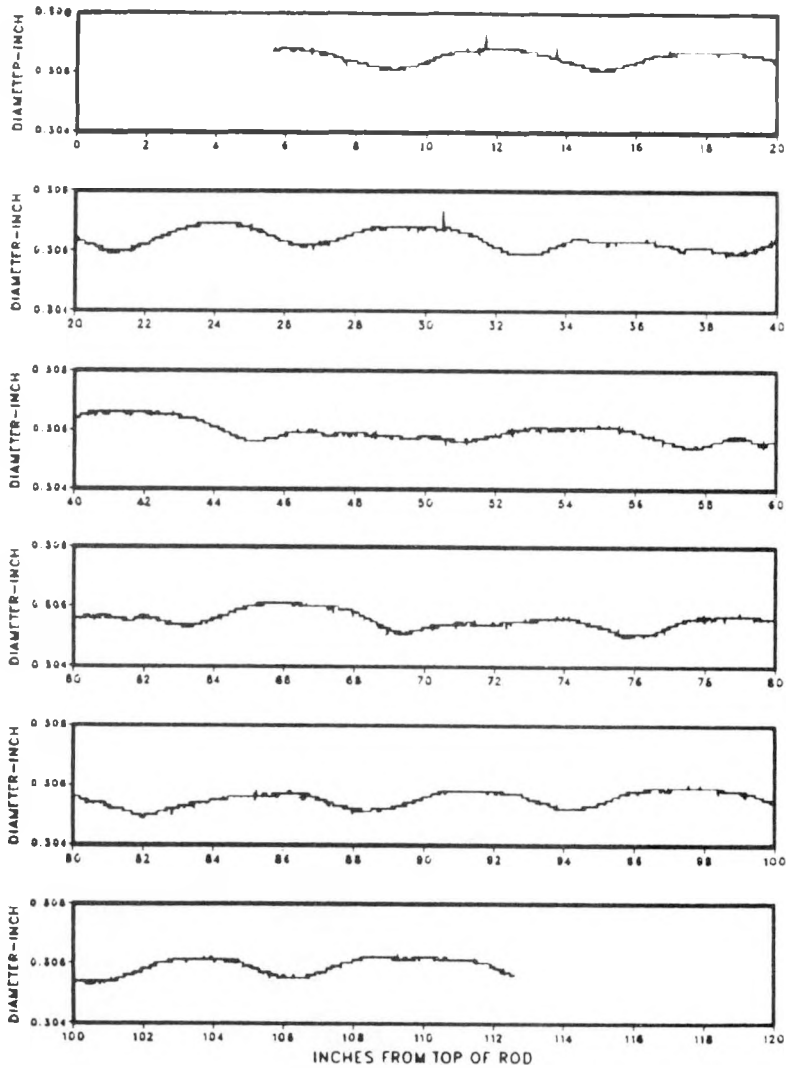

Average Diameter

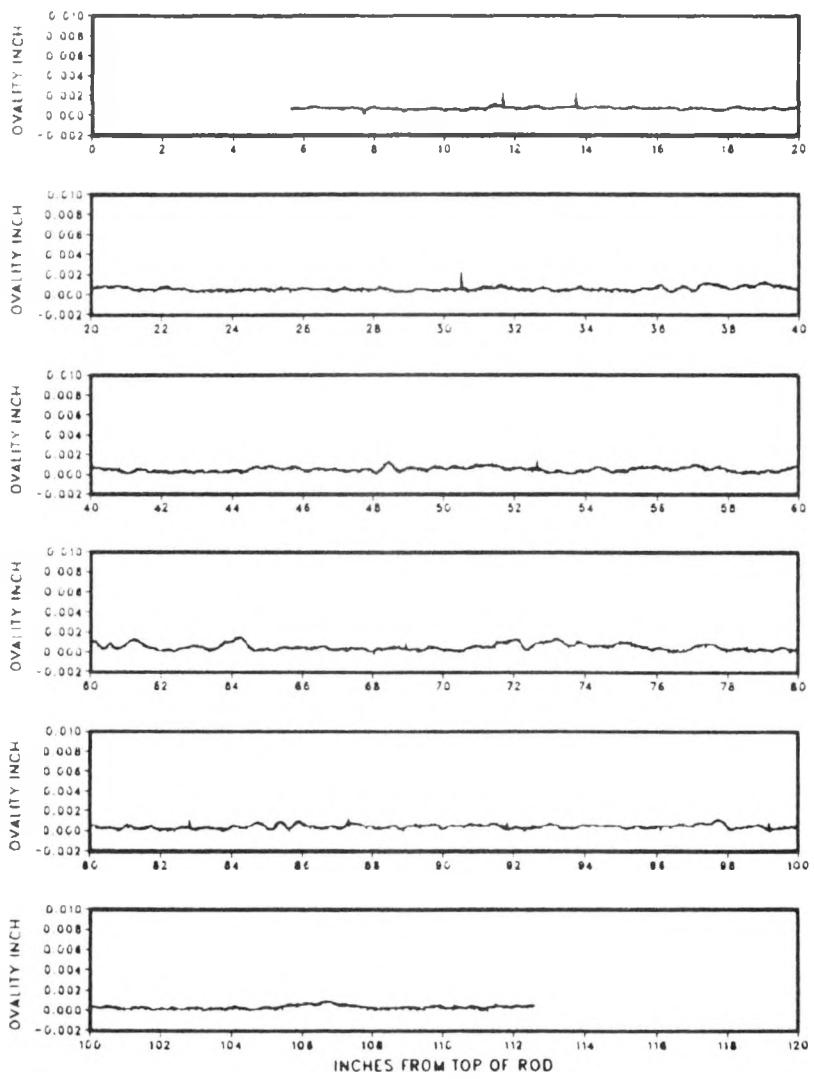

Ovality

Figure A6-1 - Rod 4M33

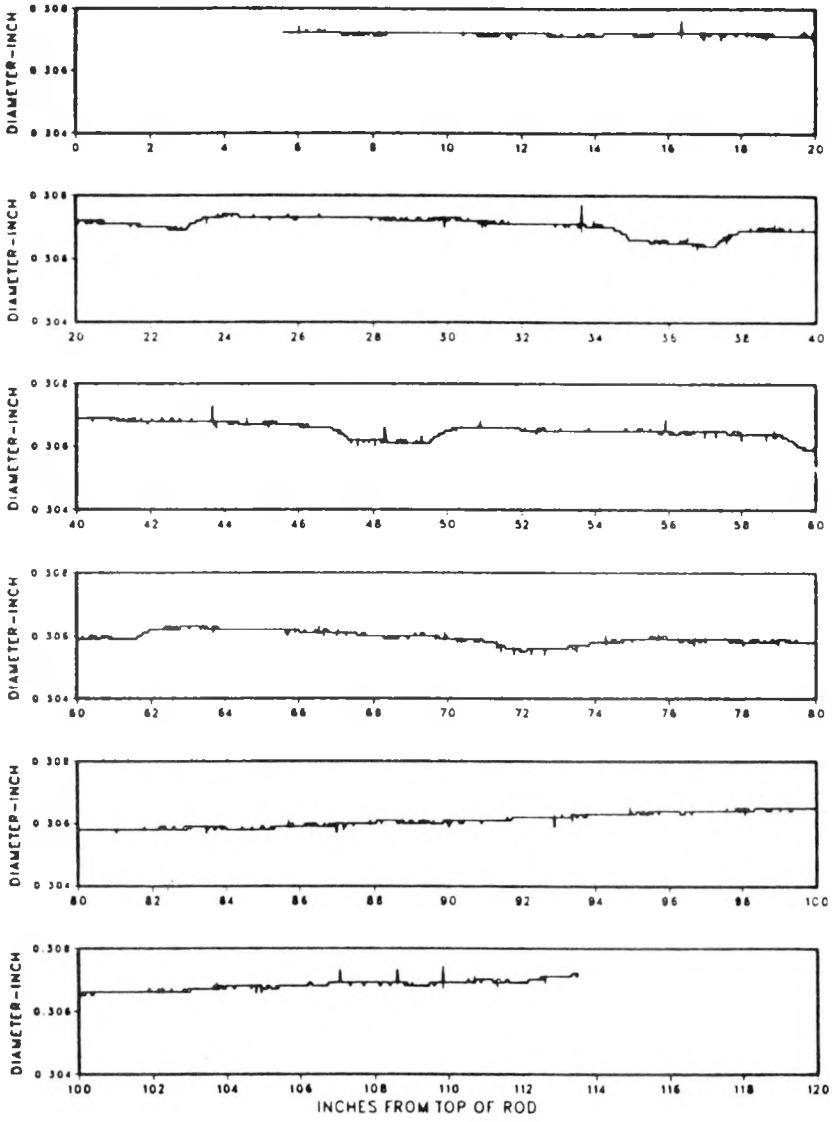

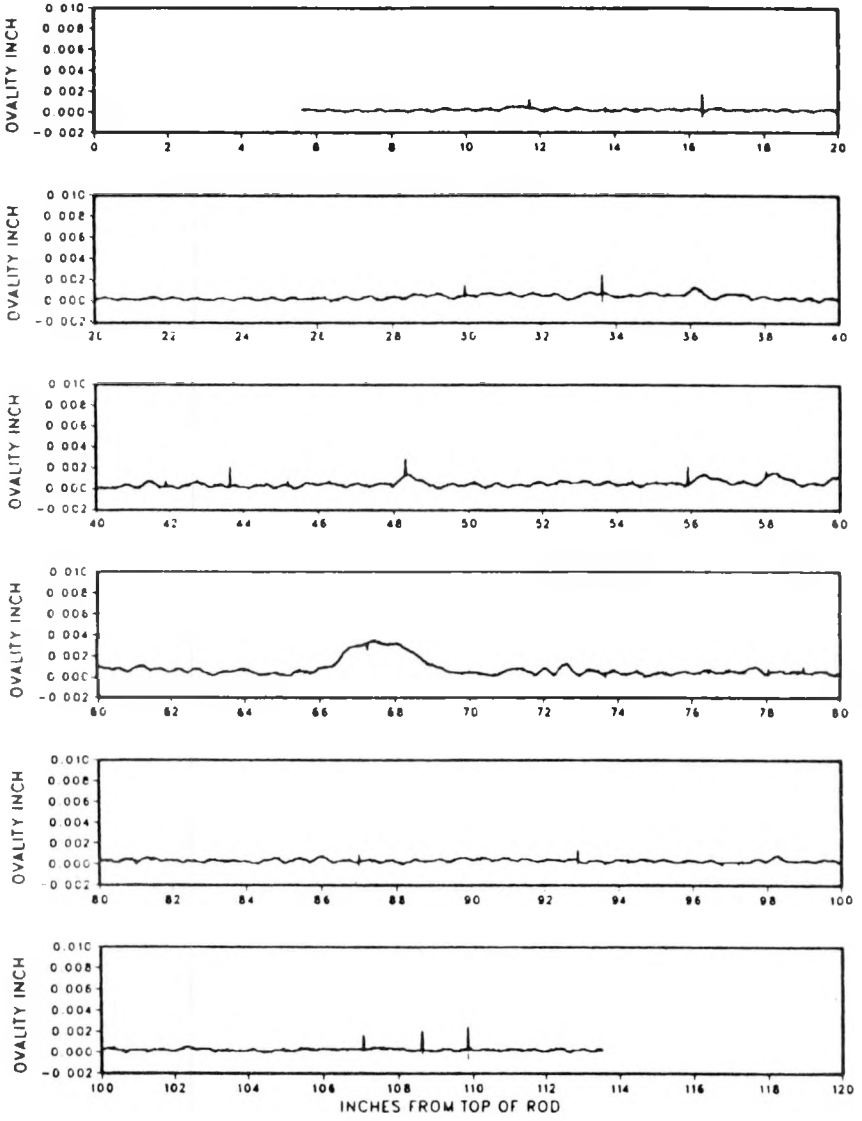

Average Diameter

Ovality

Figure A6-2 - Rod 684

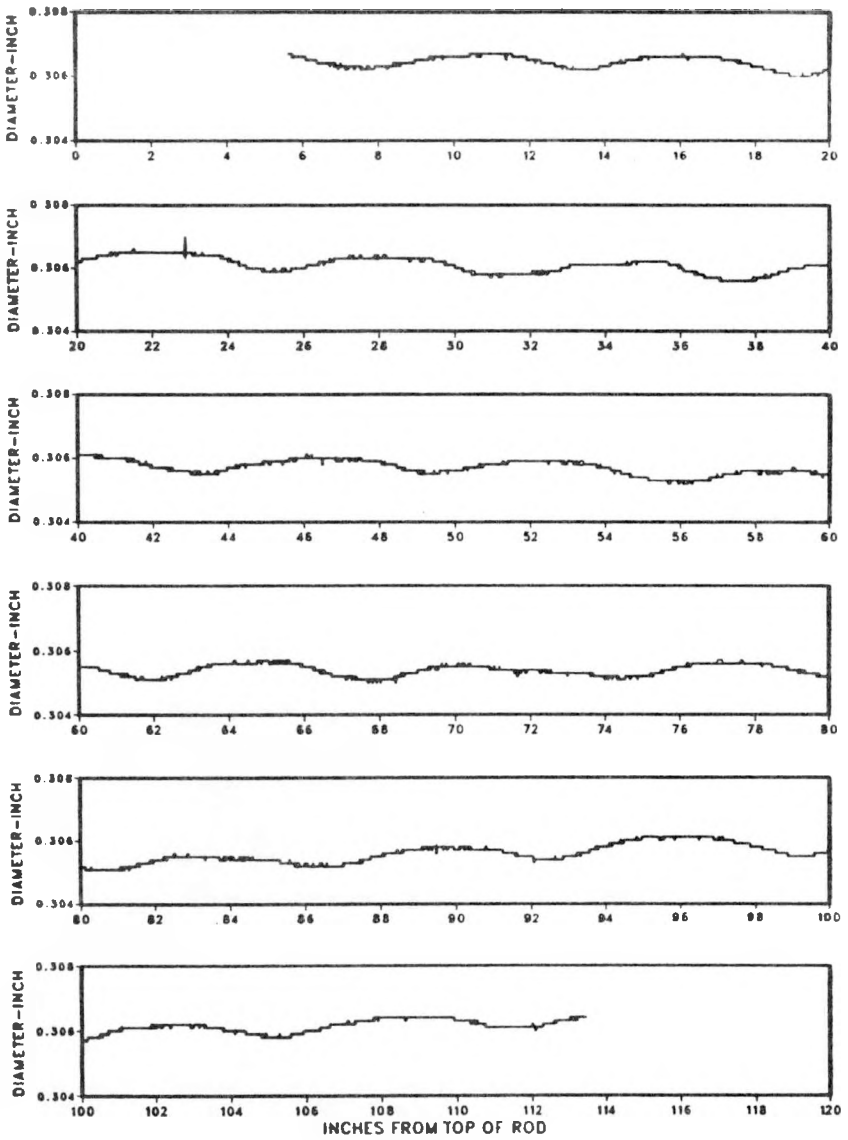

Average Diameter

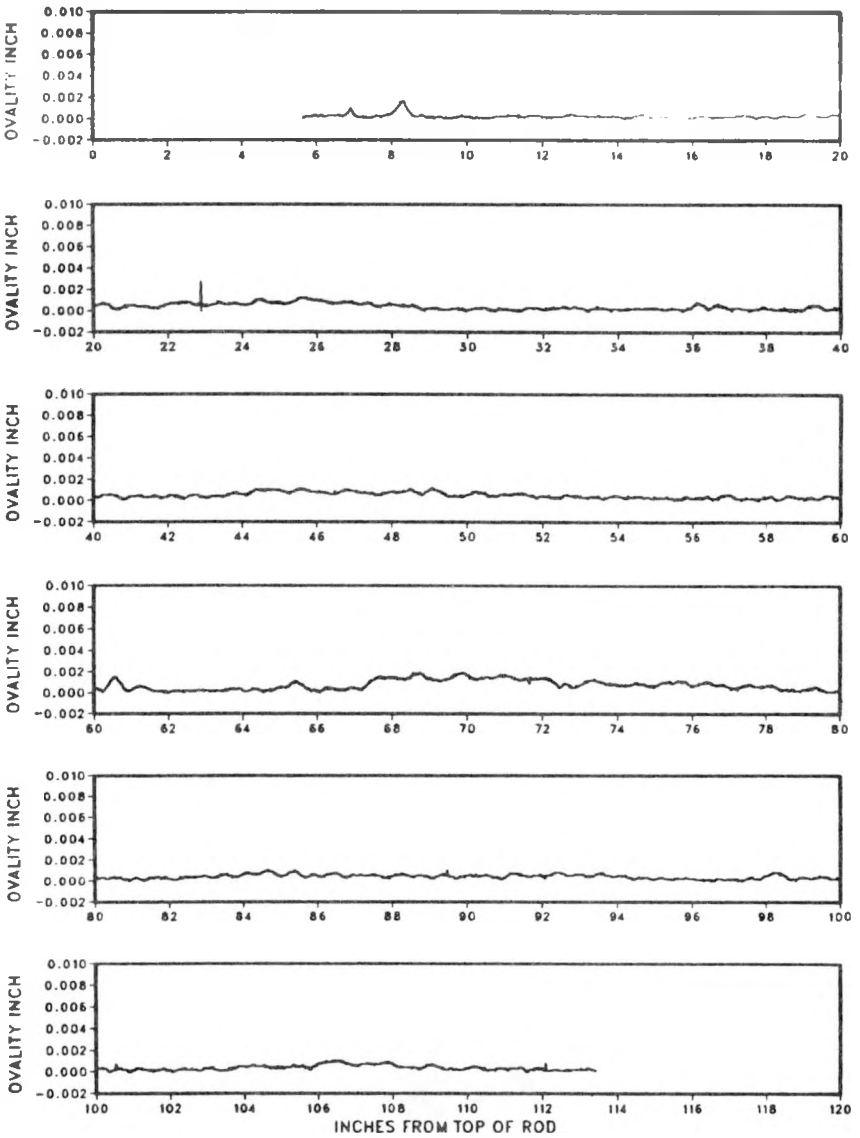

Ovality

Figure A6-3 - Rod 0205071

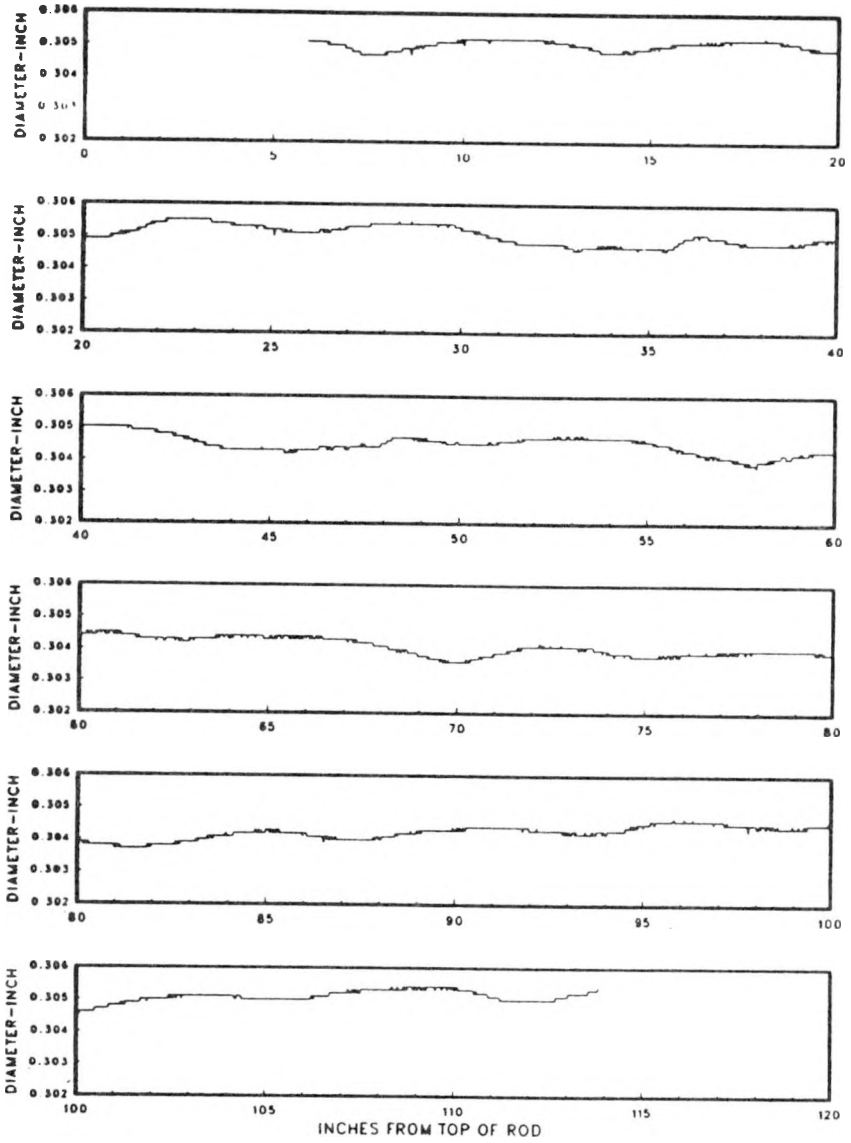

Average Diameter

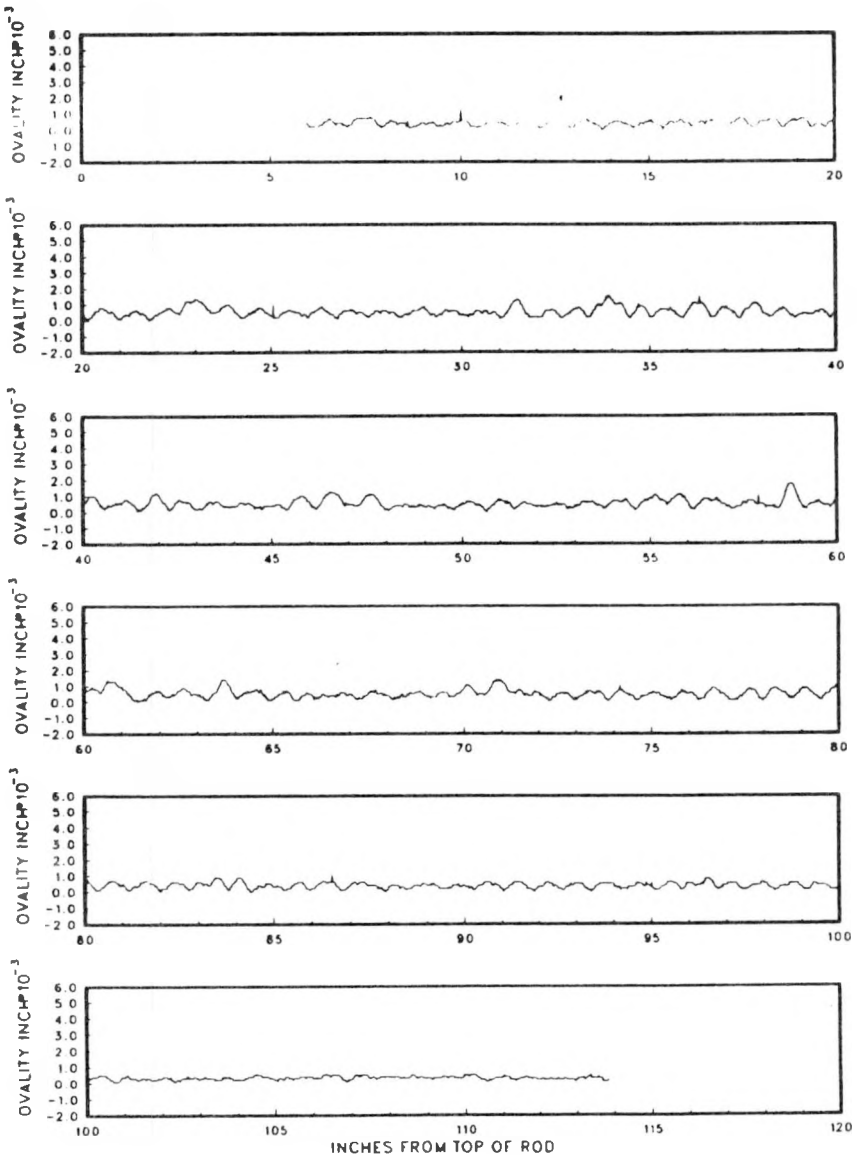

Ovality

Figure A6-4 - Rod 0507672

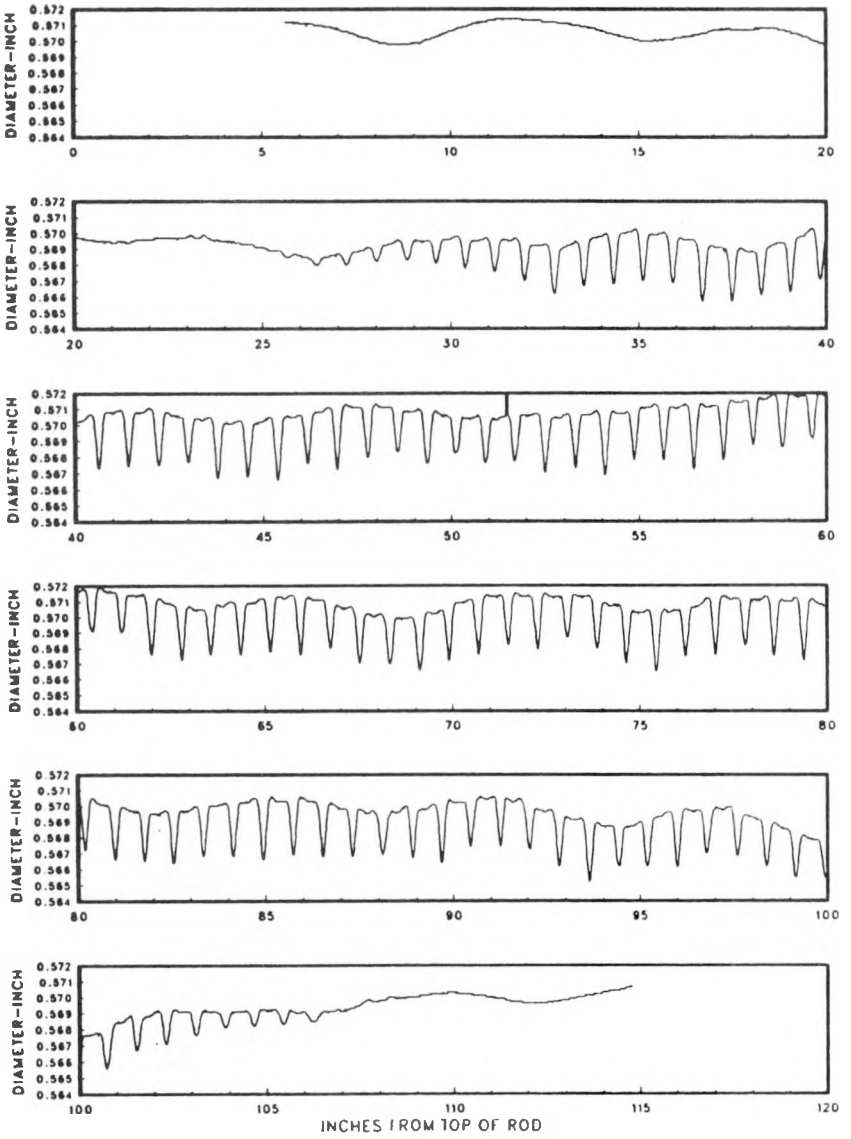

Average Diameter

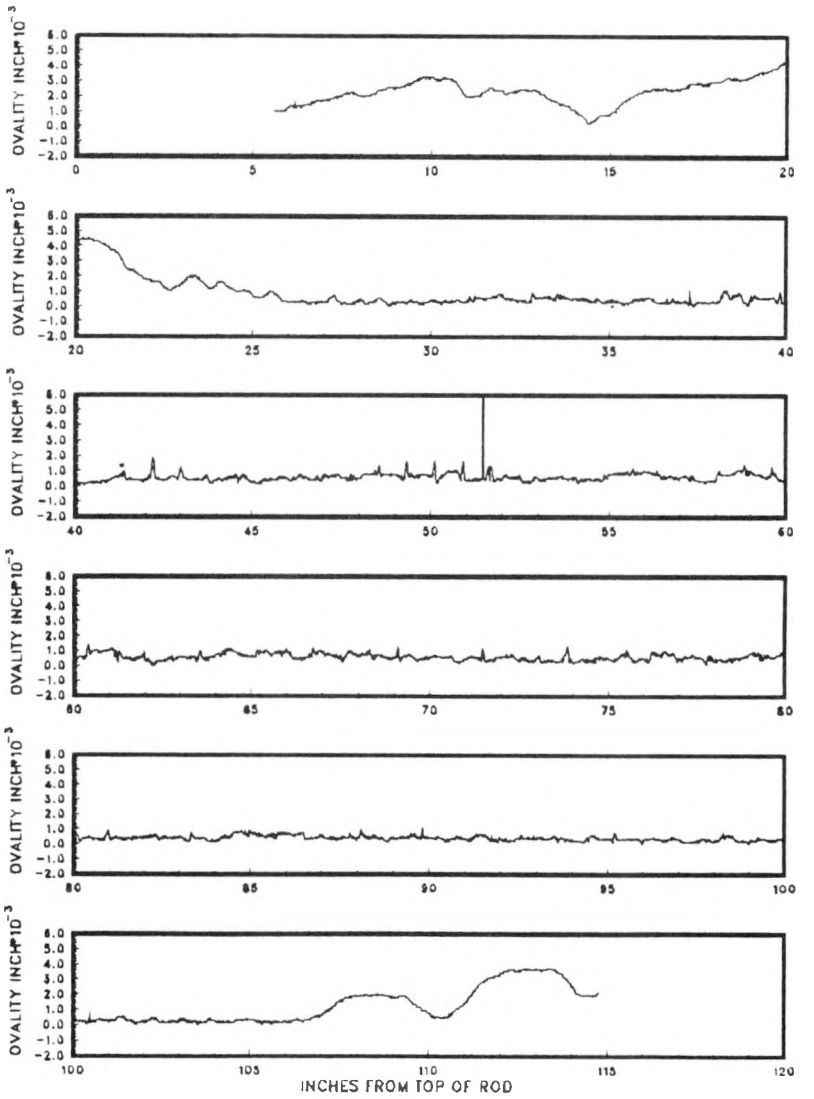

Ovality

Figure A6-5 - Rod 1606710

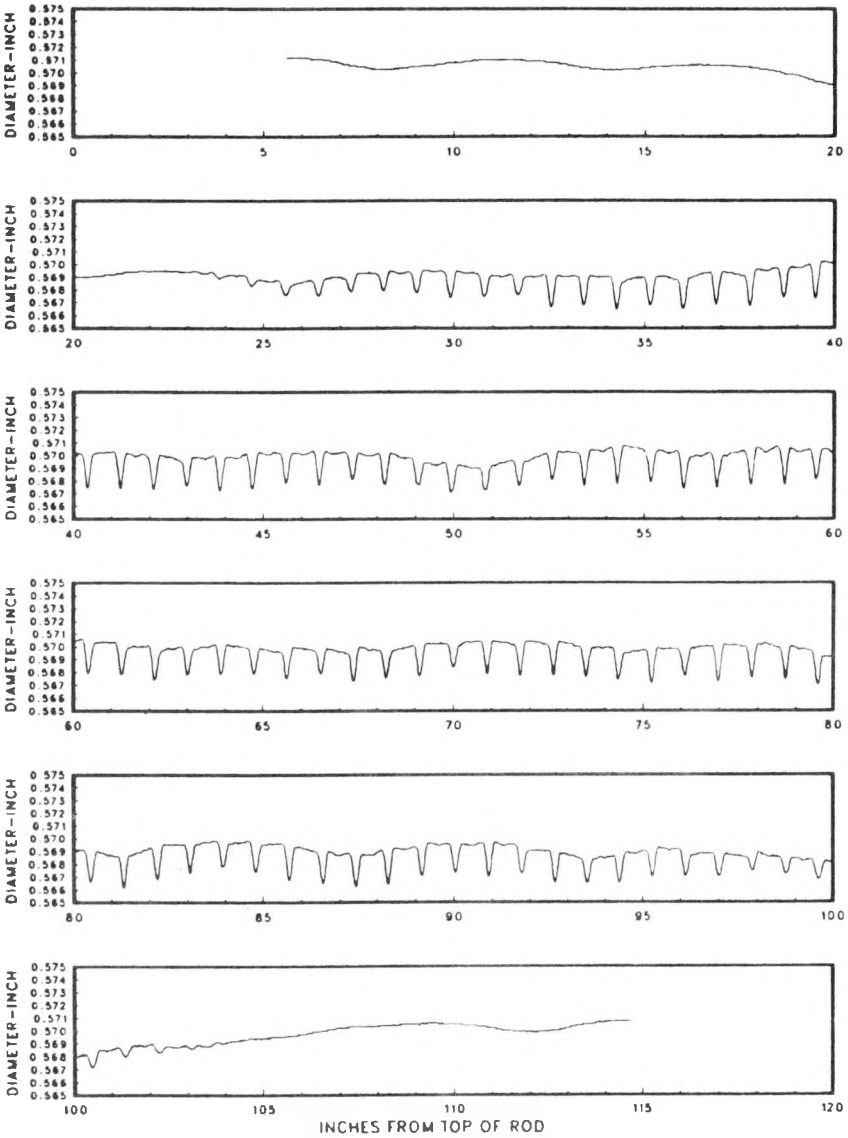

Average Diameter

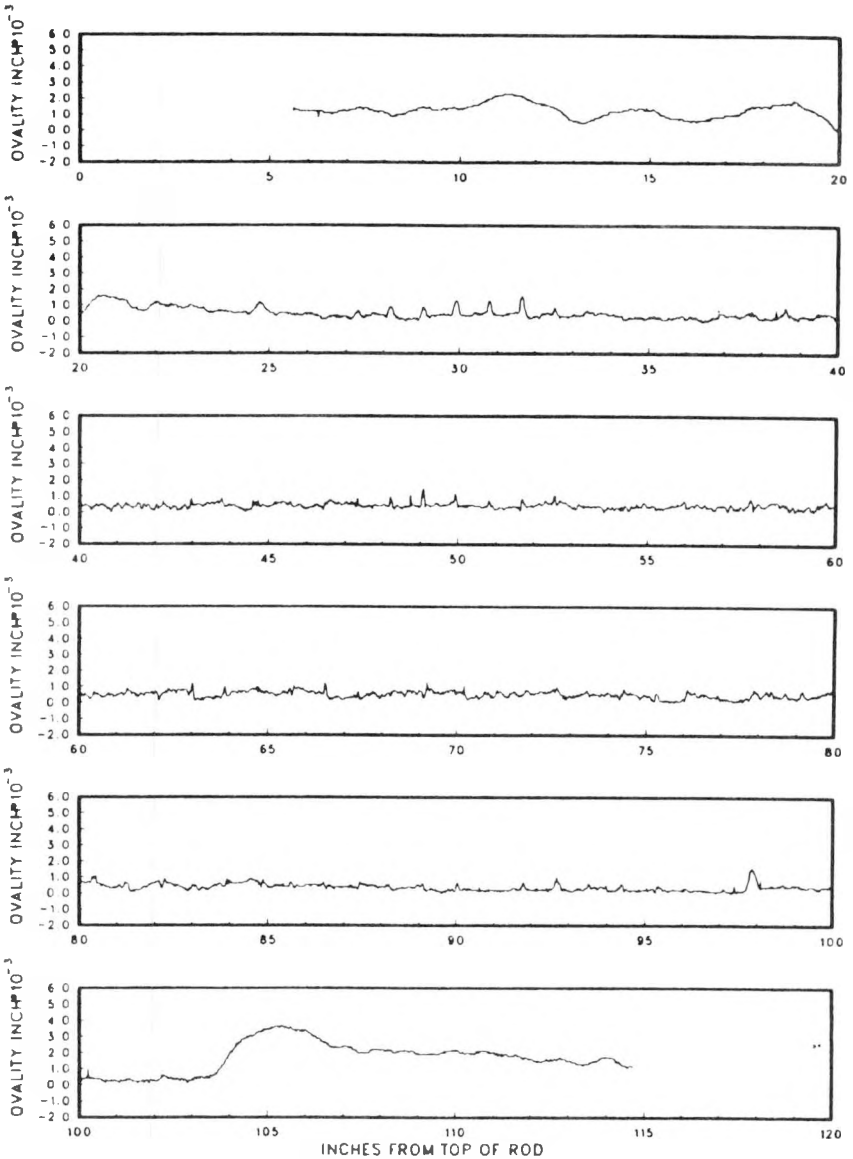

Ovality

Figure A6-6 - Rod 1504272

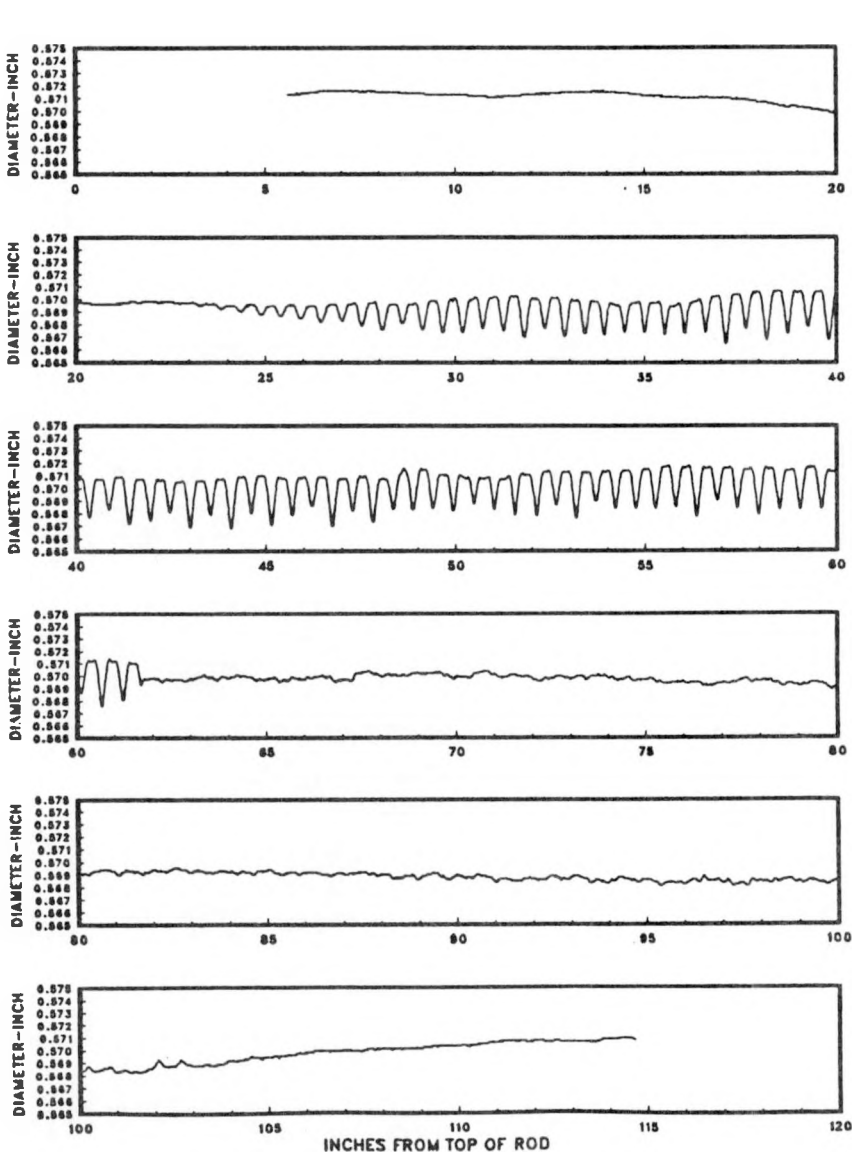

Average Diameter

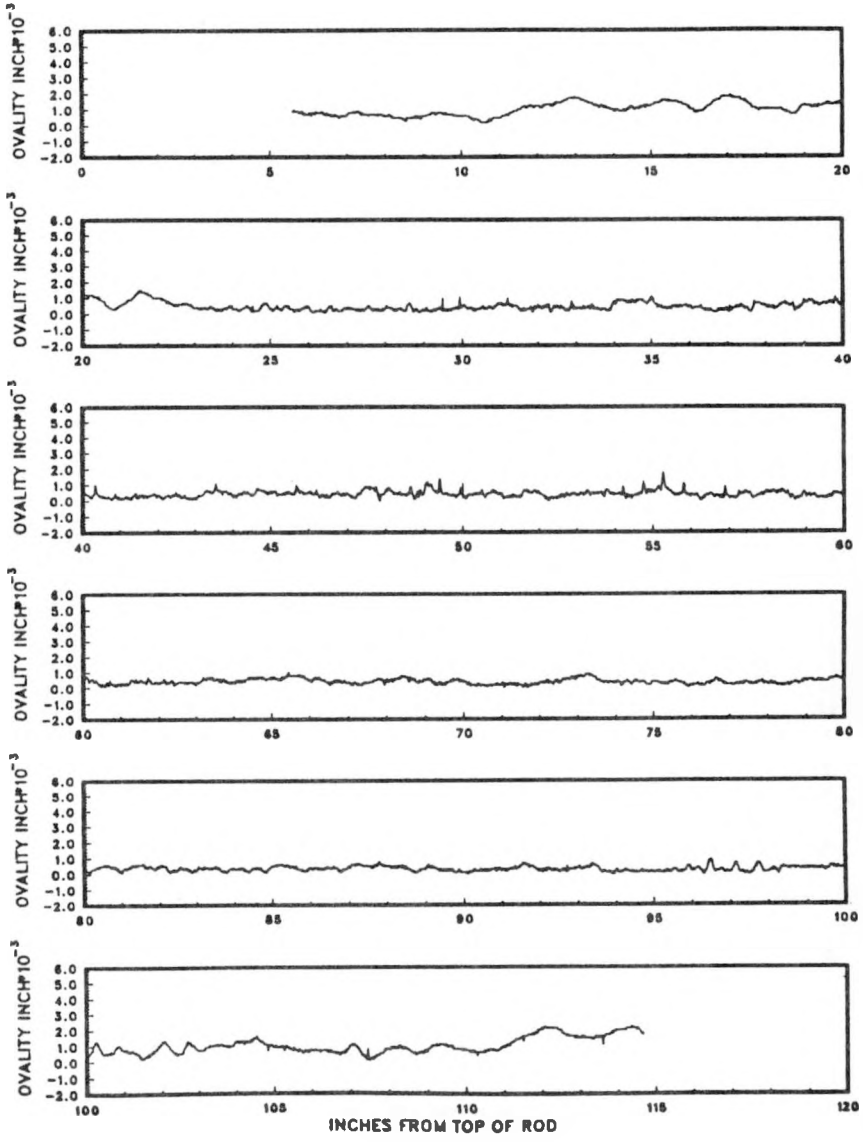

Ovality

Figure A6-7 - Rod 1105717

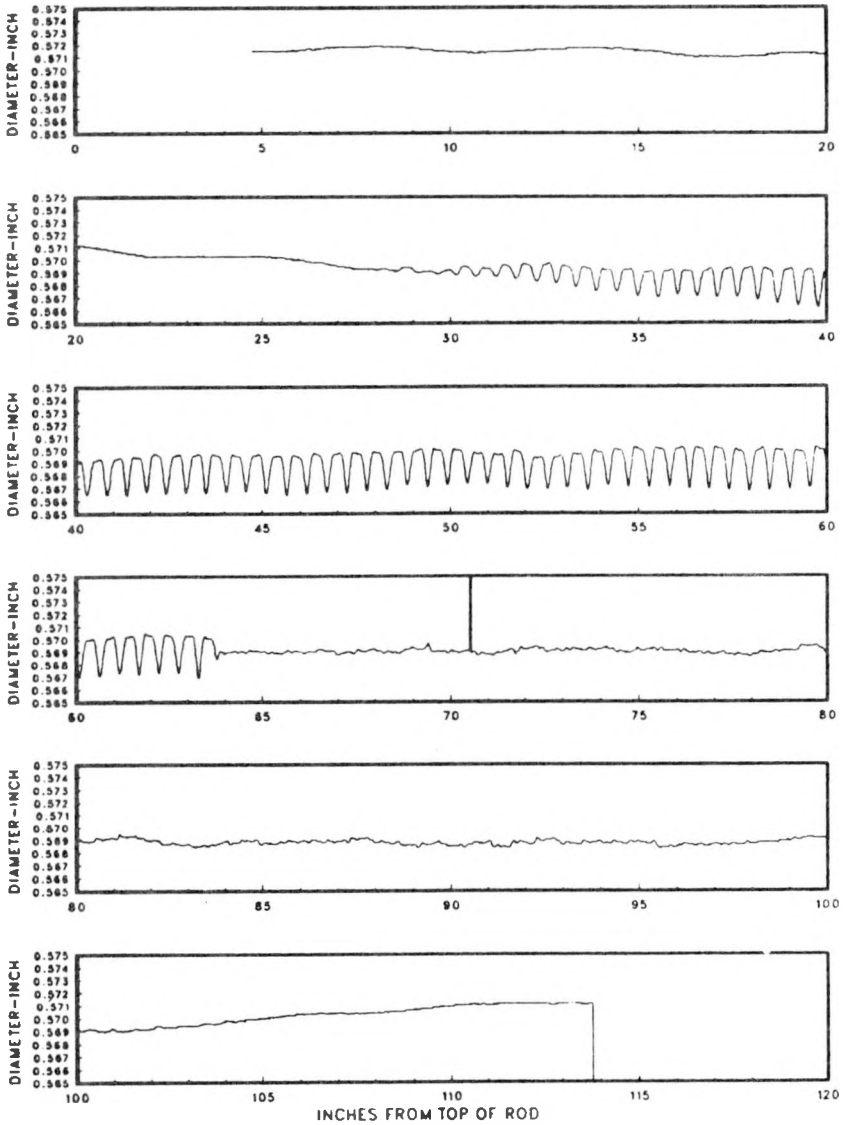

Average Diameter

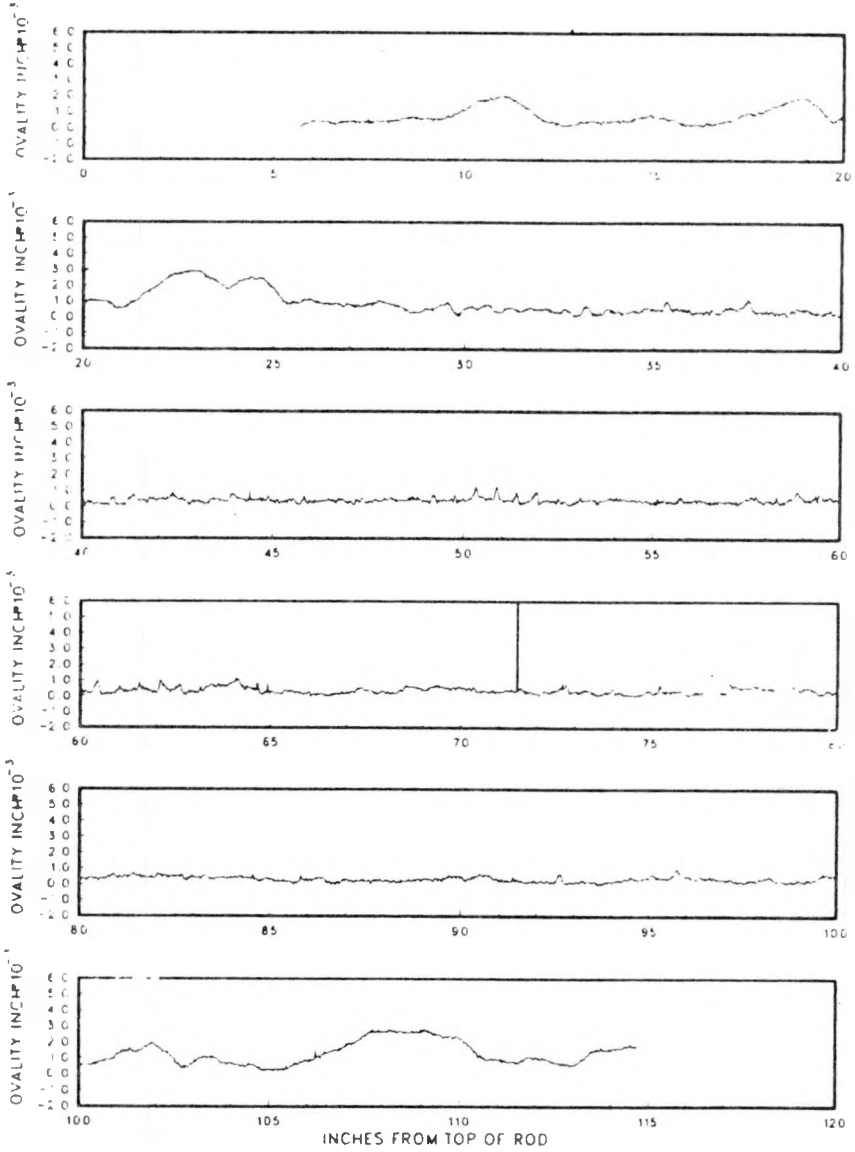

Ovality

Figure A6-8 - Rod 1208823

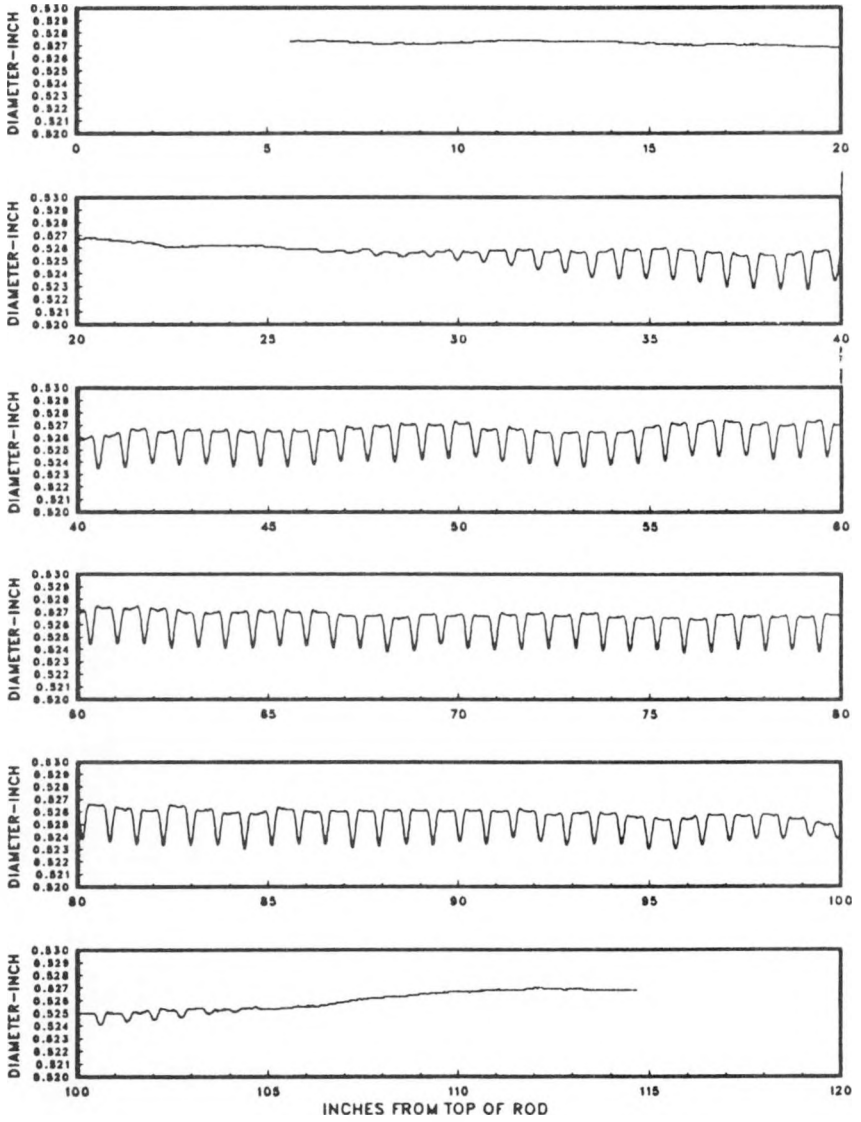

Average Diameter

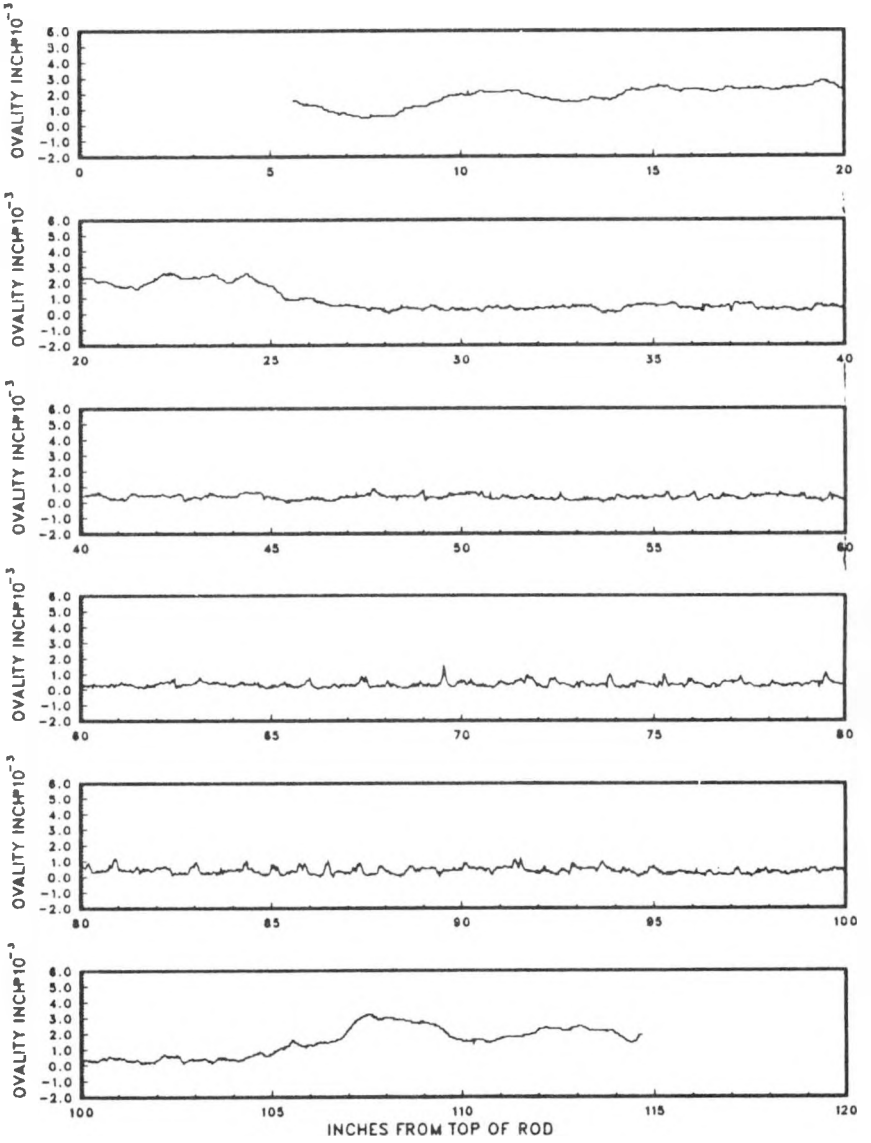

Ovality

Figure A6-9 - Rod 2610746

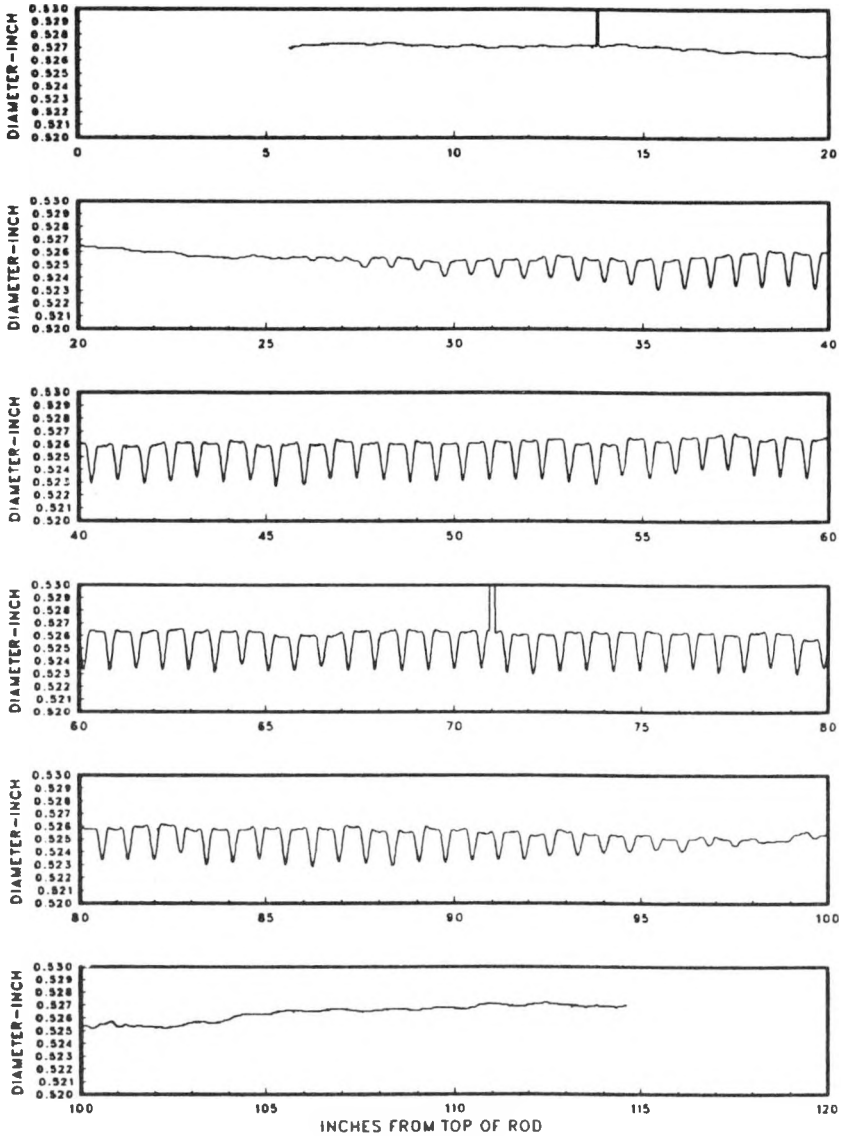

Average Diameter

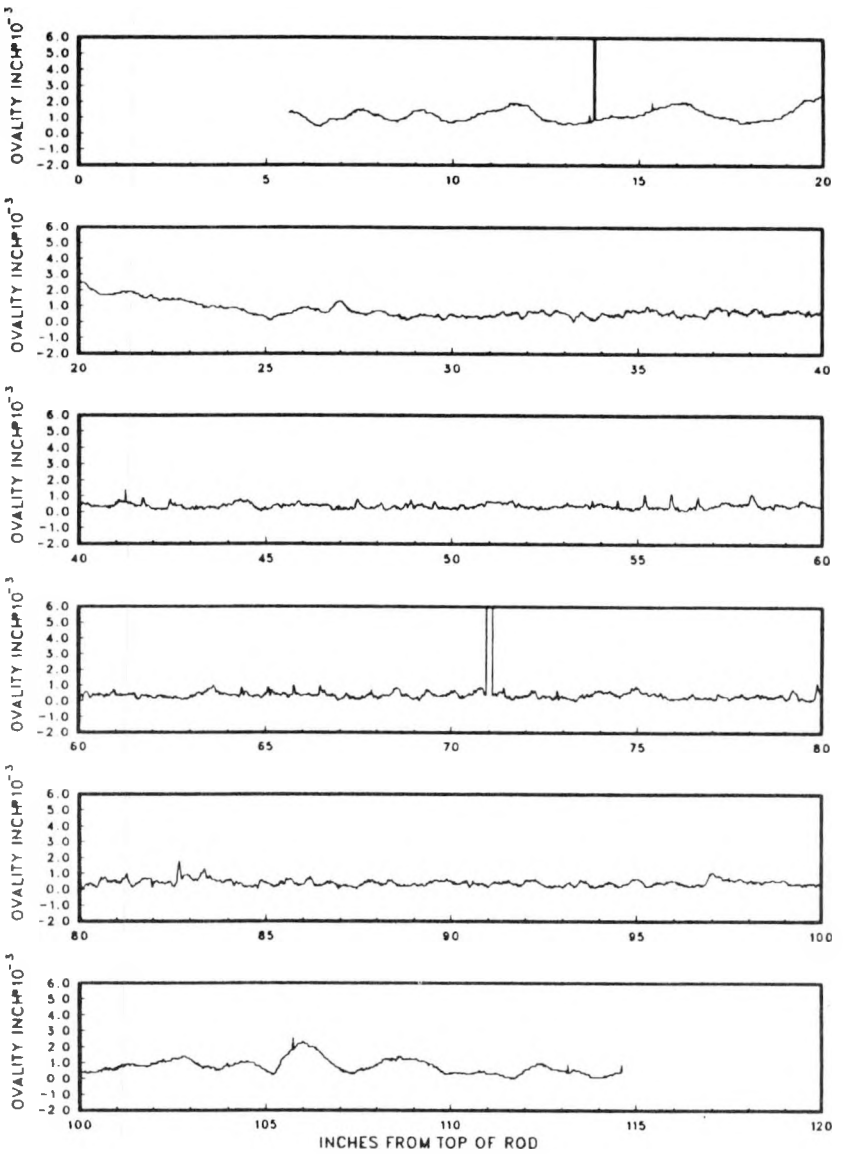

Ovality

Figure A6-10 - Rod 2514164

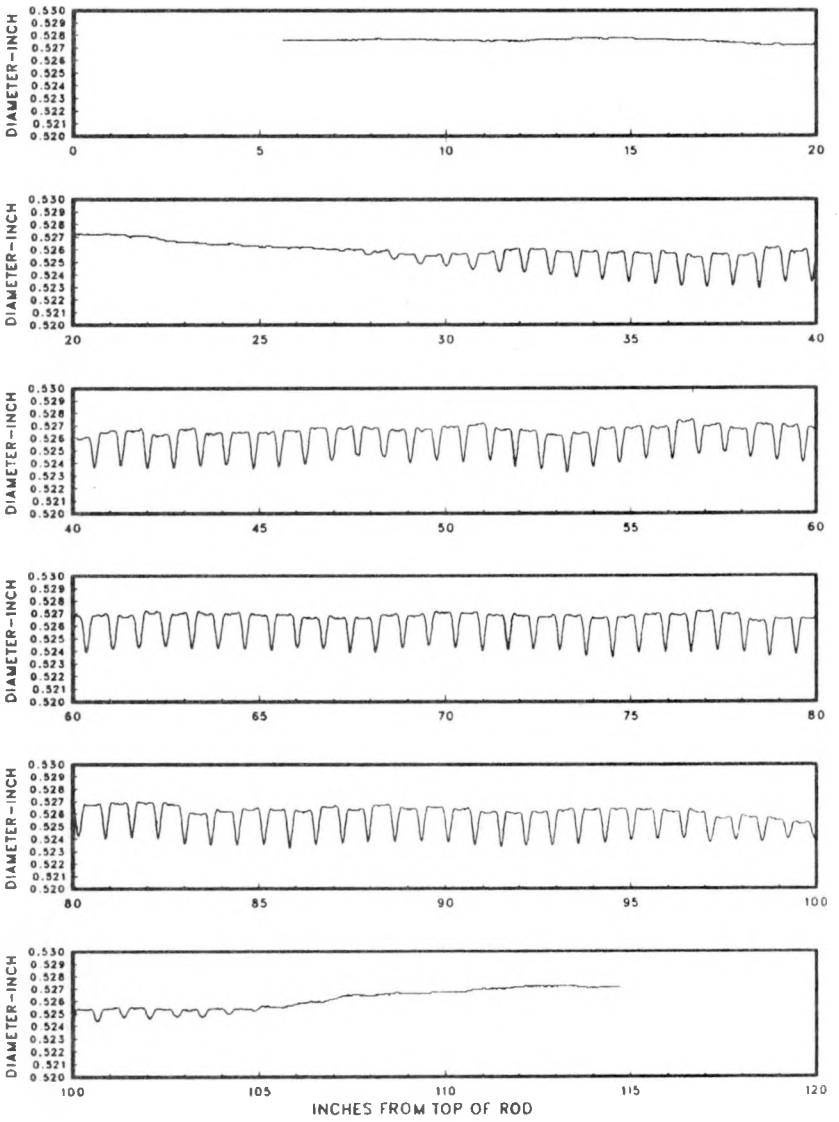

Average Diameter

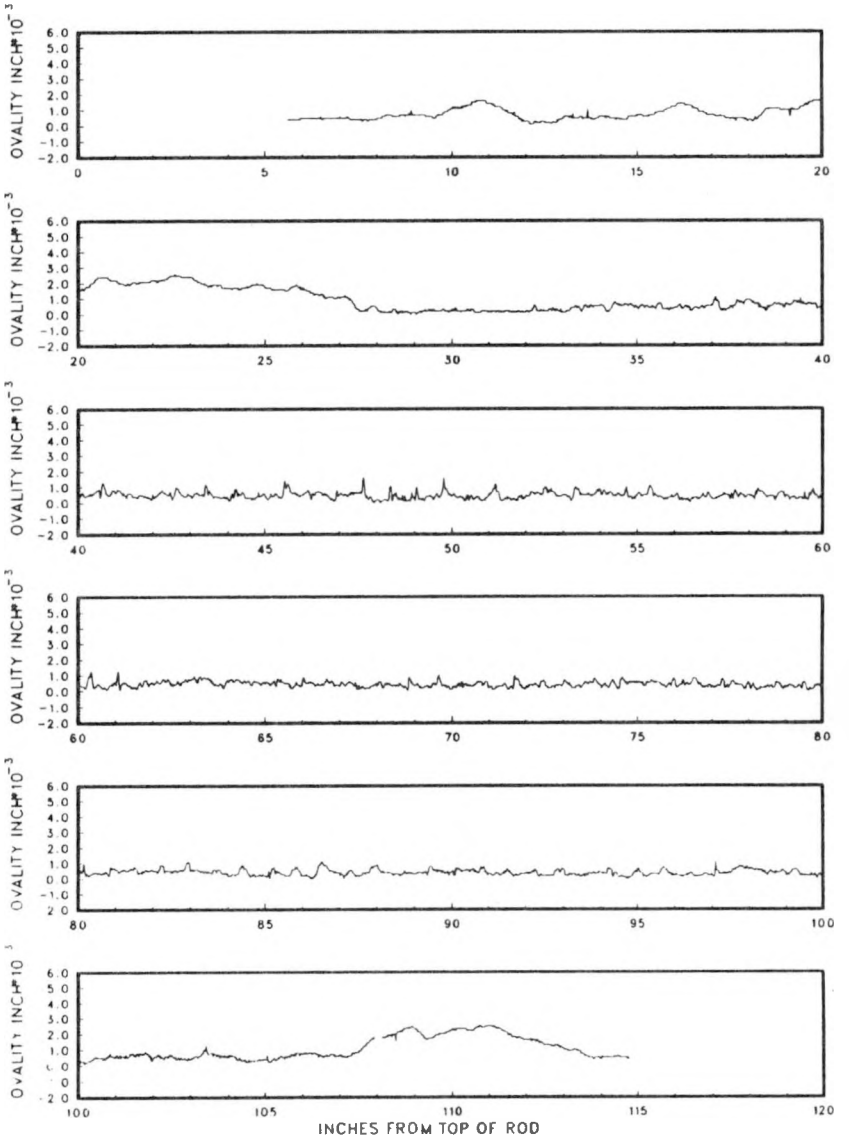

Ovality

Figure A6-11 - Rod 2607600

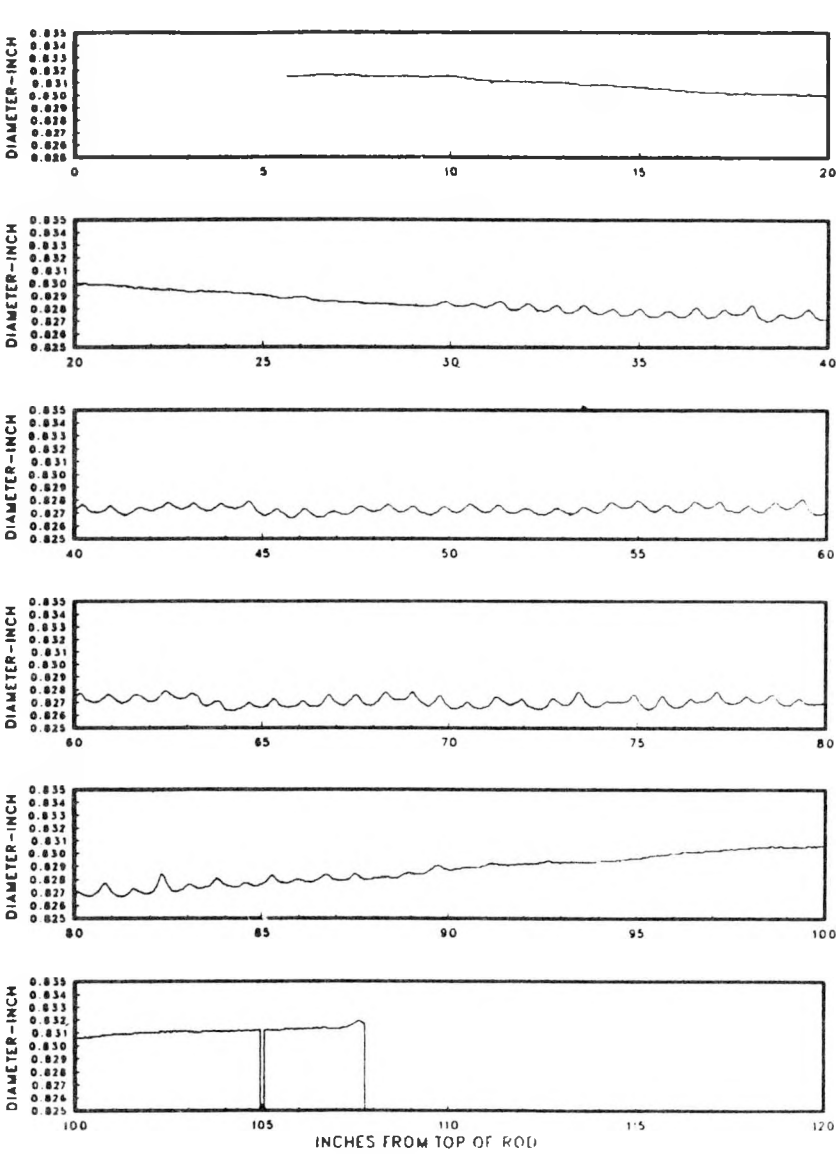

Average Diameter

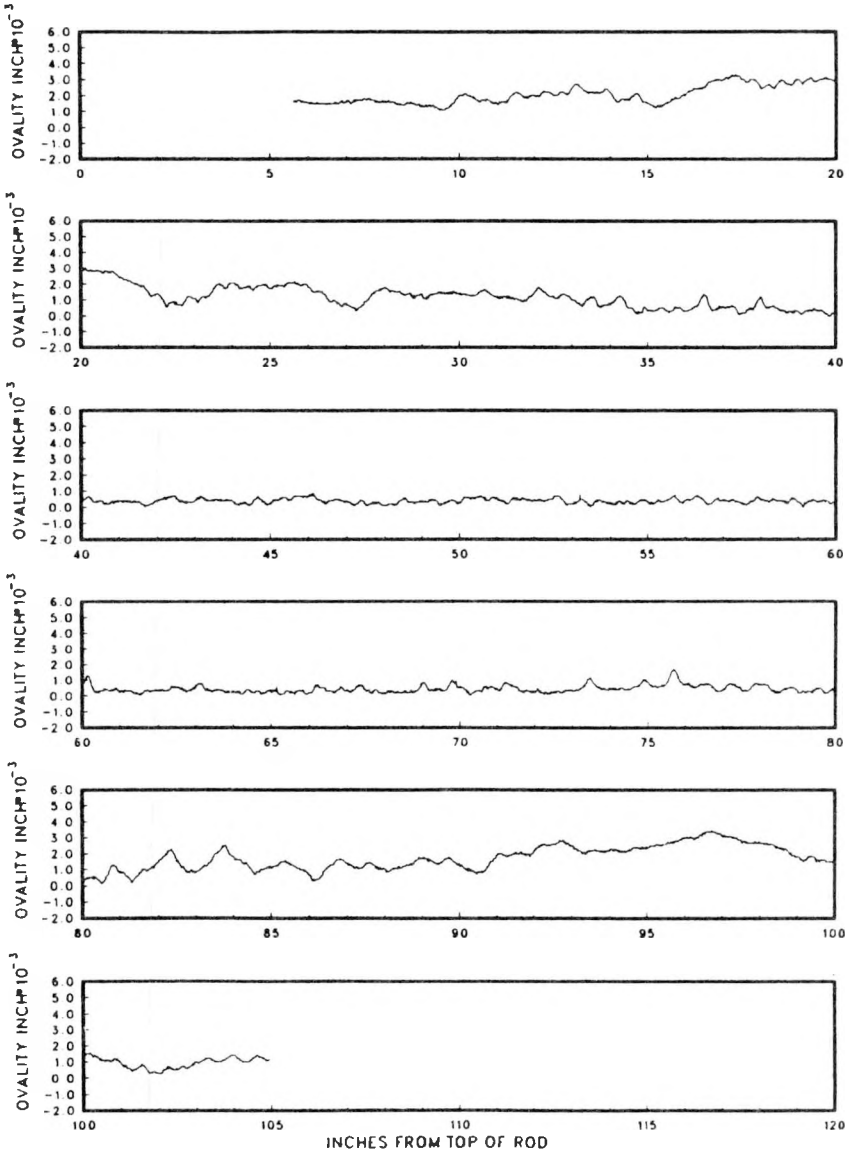

Ovality

Figure A6-12 - Rod 3102657

(Intentionally Blank)

APPENDIX A7 - OXIDE THICKNESS PROFILES

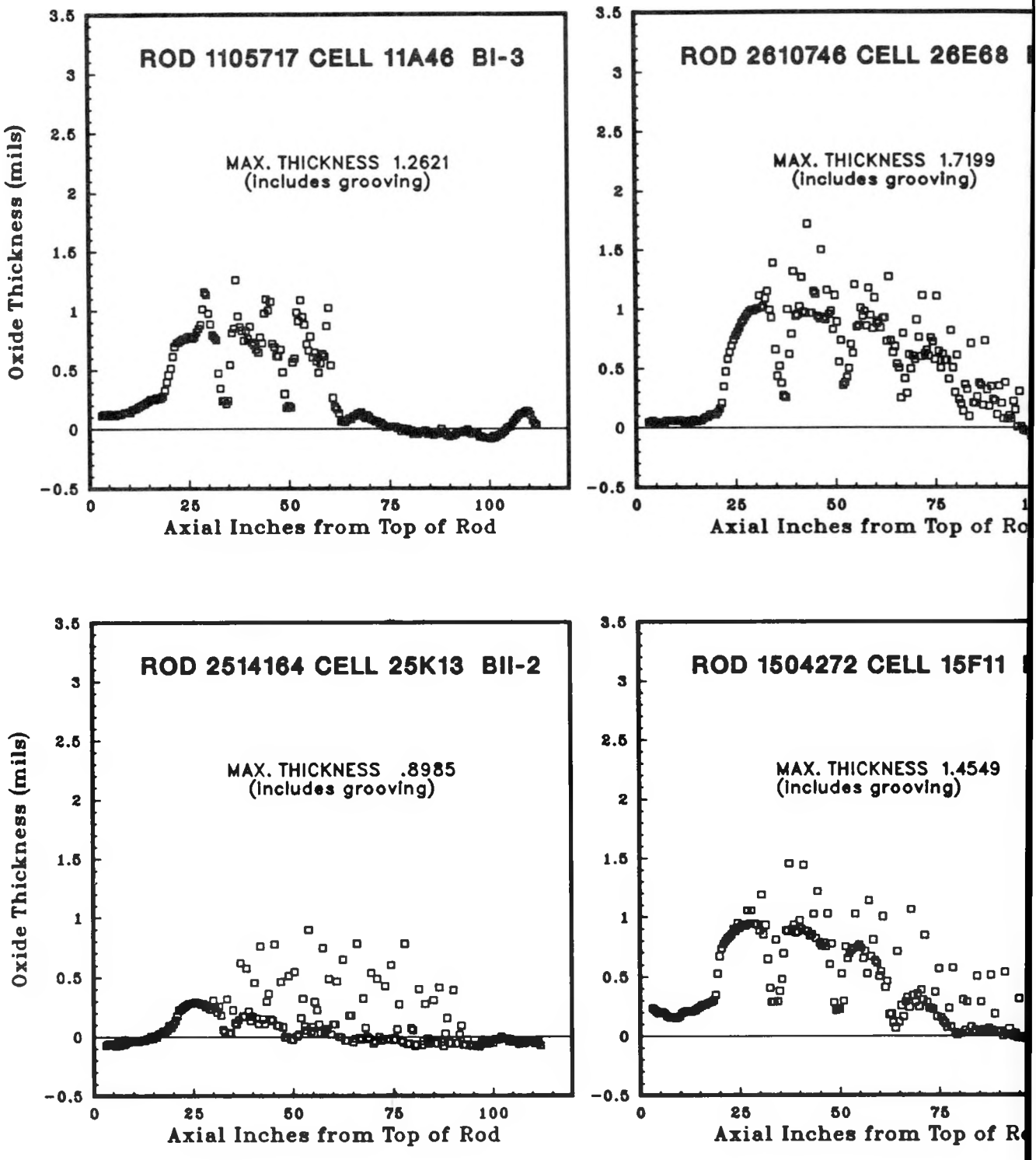

Figure A7-1 - Axial Profile of Measured Oxide Thickness
Average of Four Tracks

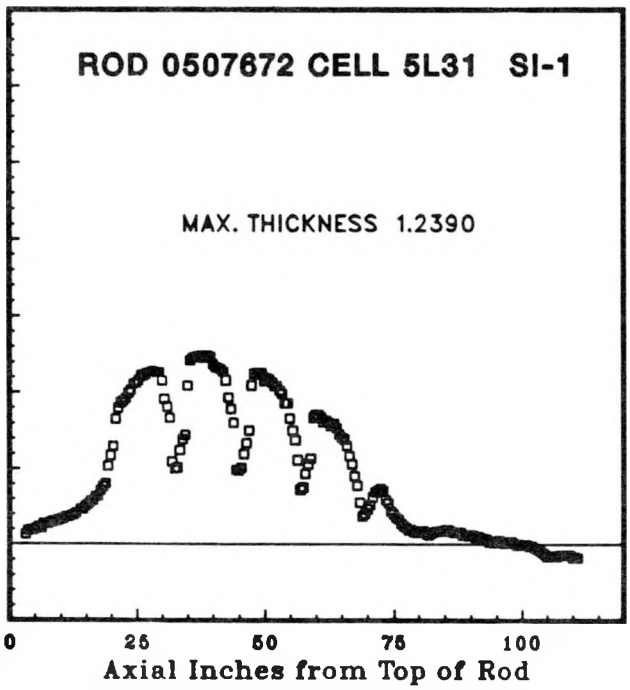

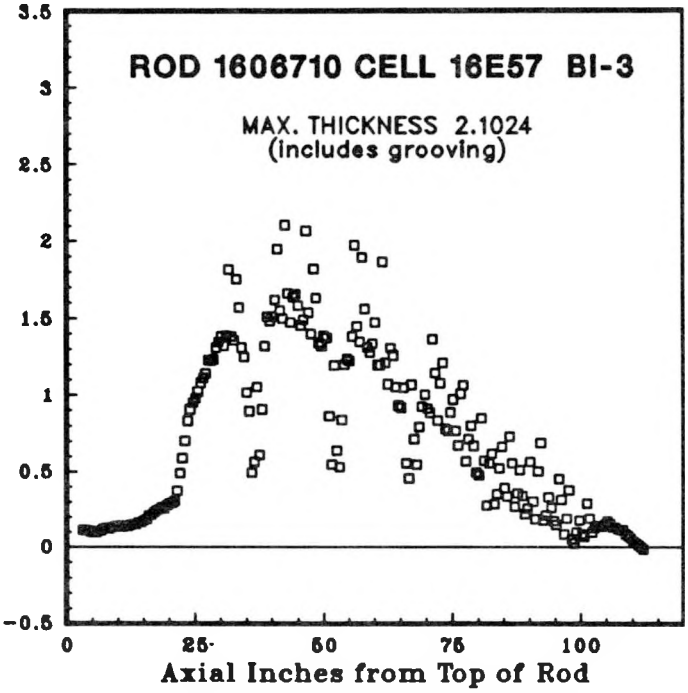

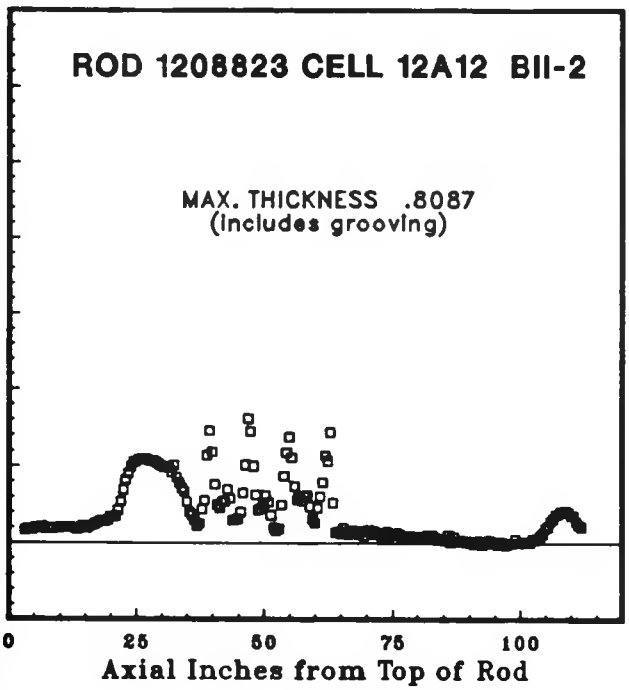

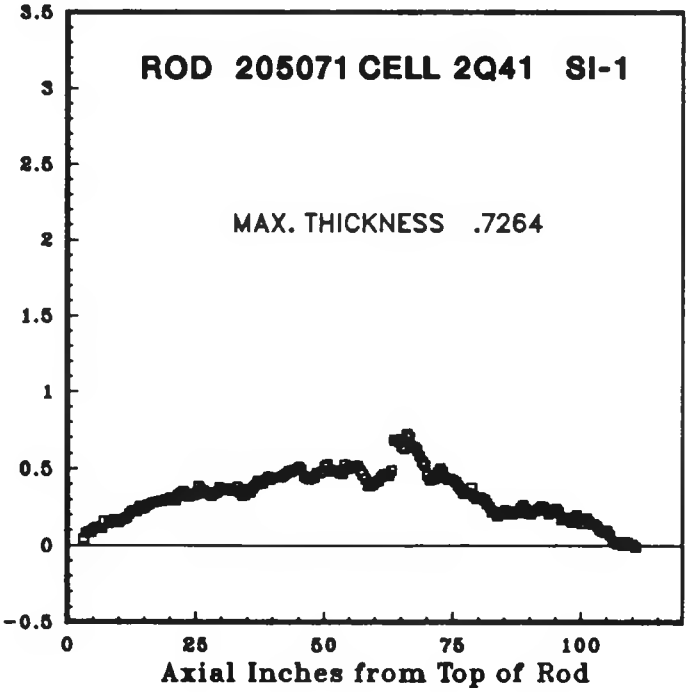

Figure A7-1 - Axial Profile of Measured Oxide Thickness
Average of Four Tracks (Cont)

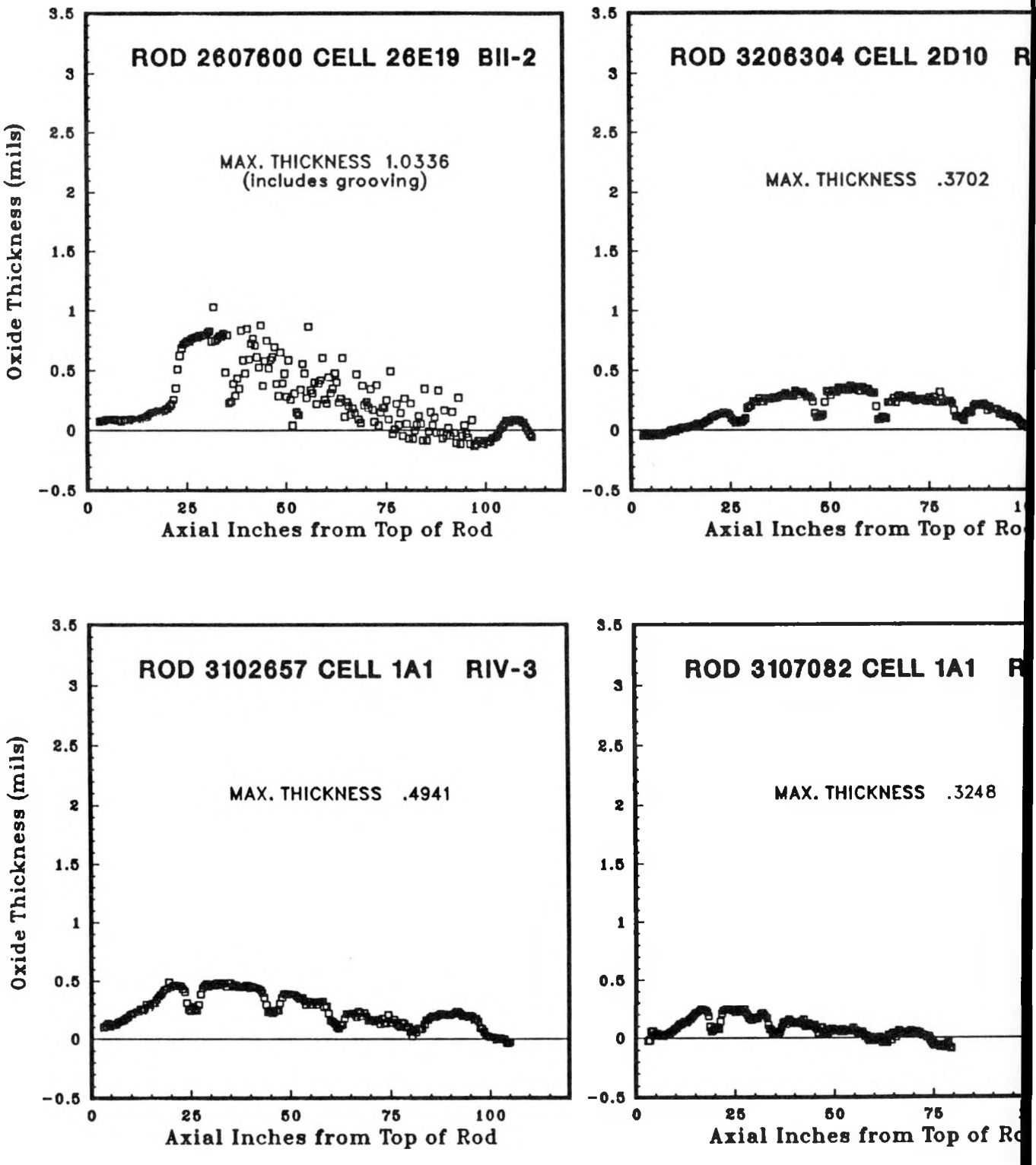

Figure A7-1 - Axial Profile of Measured Oxide Thickness
Average of Four Tracks (Cont)

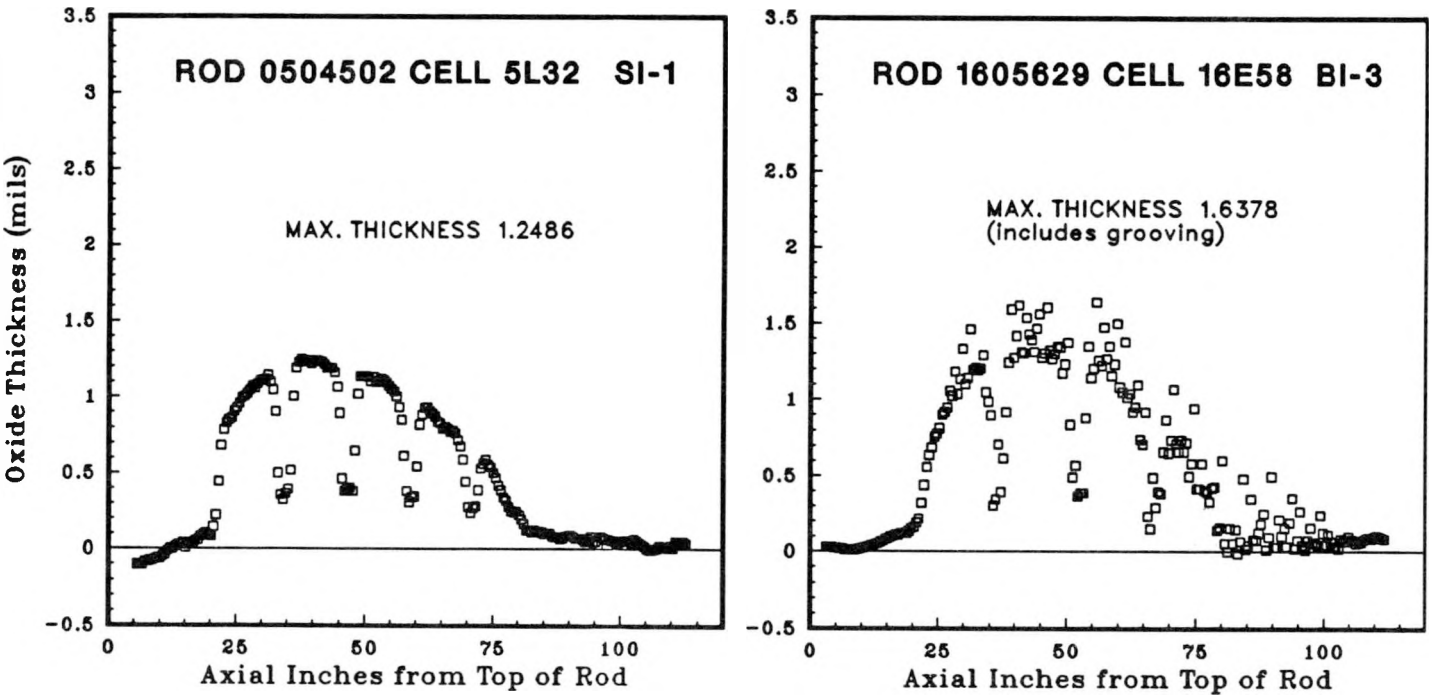

Figure A7-1 - Axial Profile of Measured Oxide Thickness
Average of Four Tracks (Cont)
(Chemically Decrudded)

(Intentionally Blank)

APPENDIX A8 - CRUD THICKNESS PROFILES

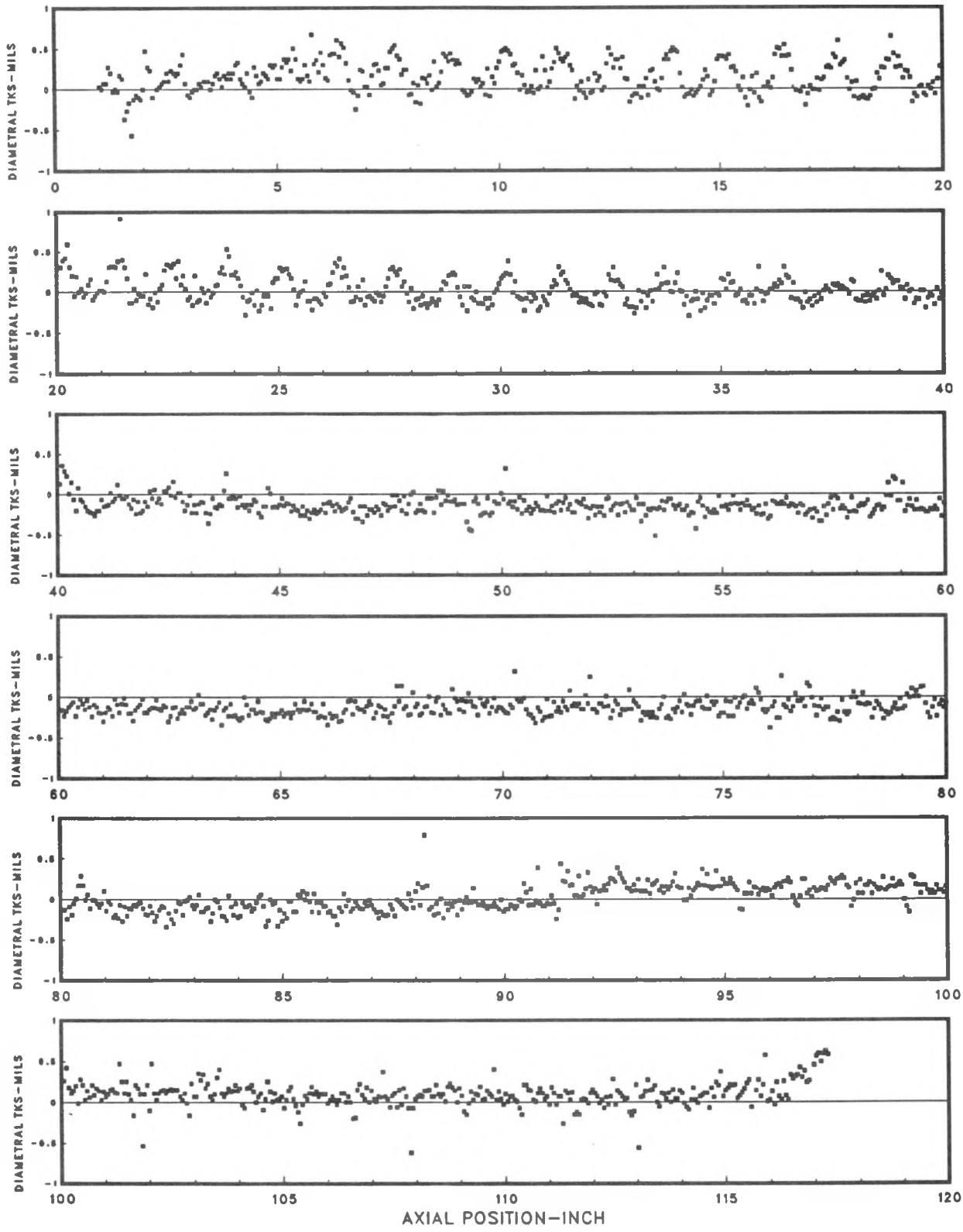

Figure A8-1 - Rod 0504502 Crud Thickness

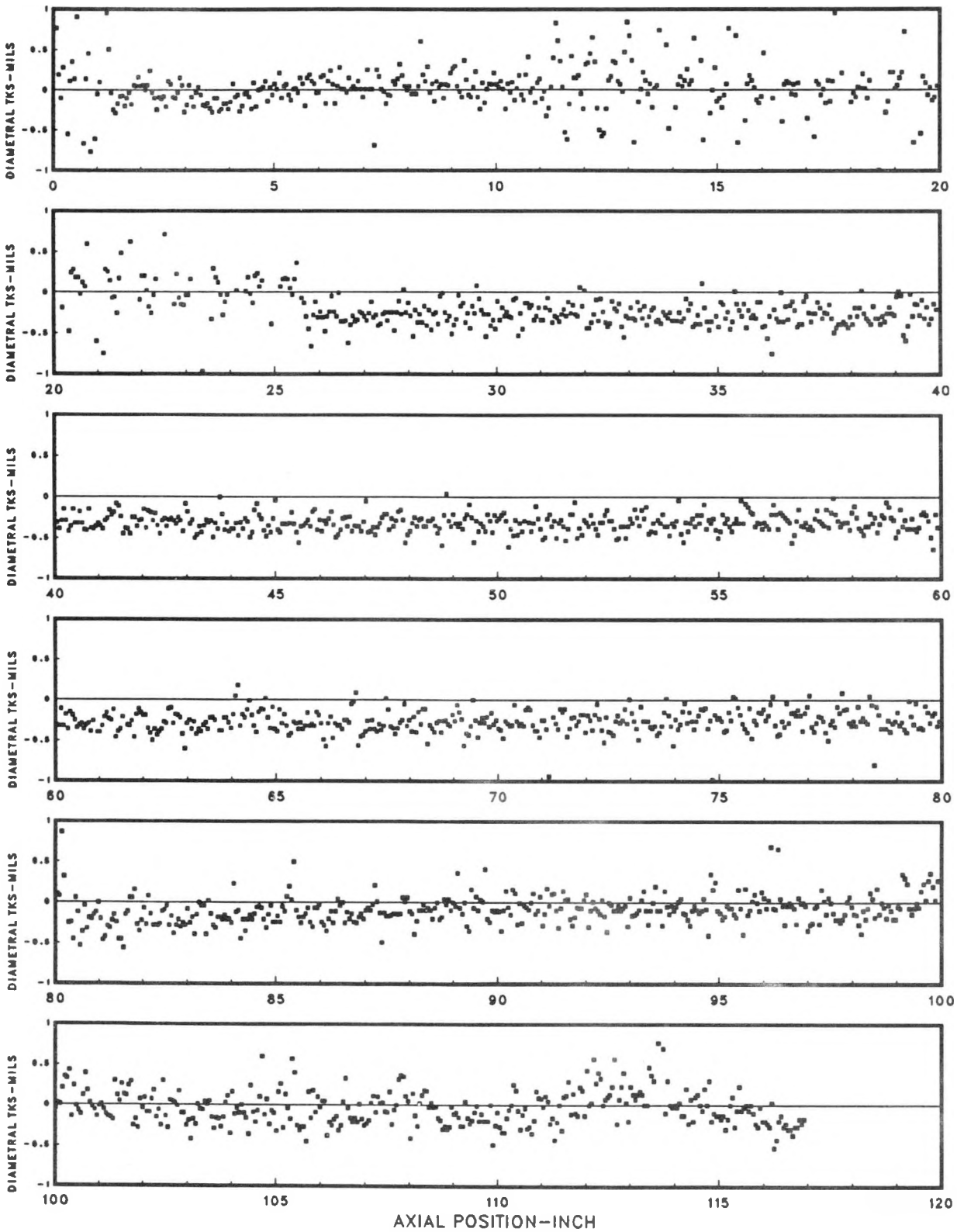

Figure A8-2 - Rod 1605629 Crud Thickness

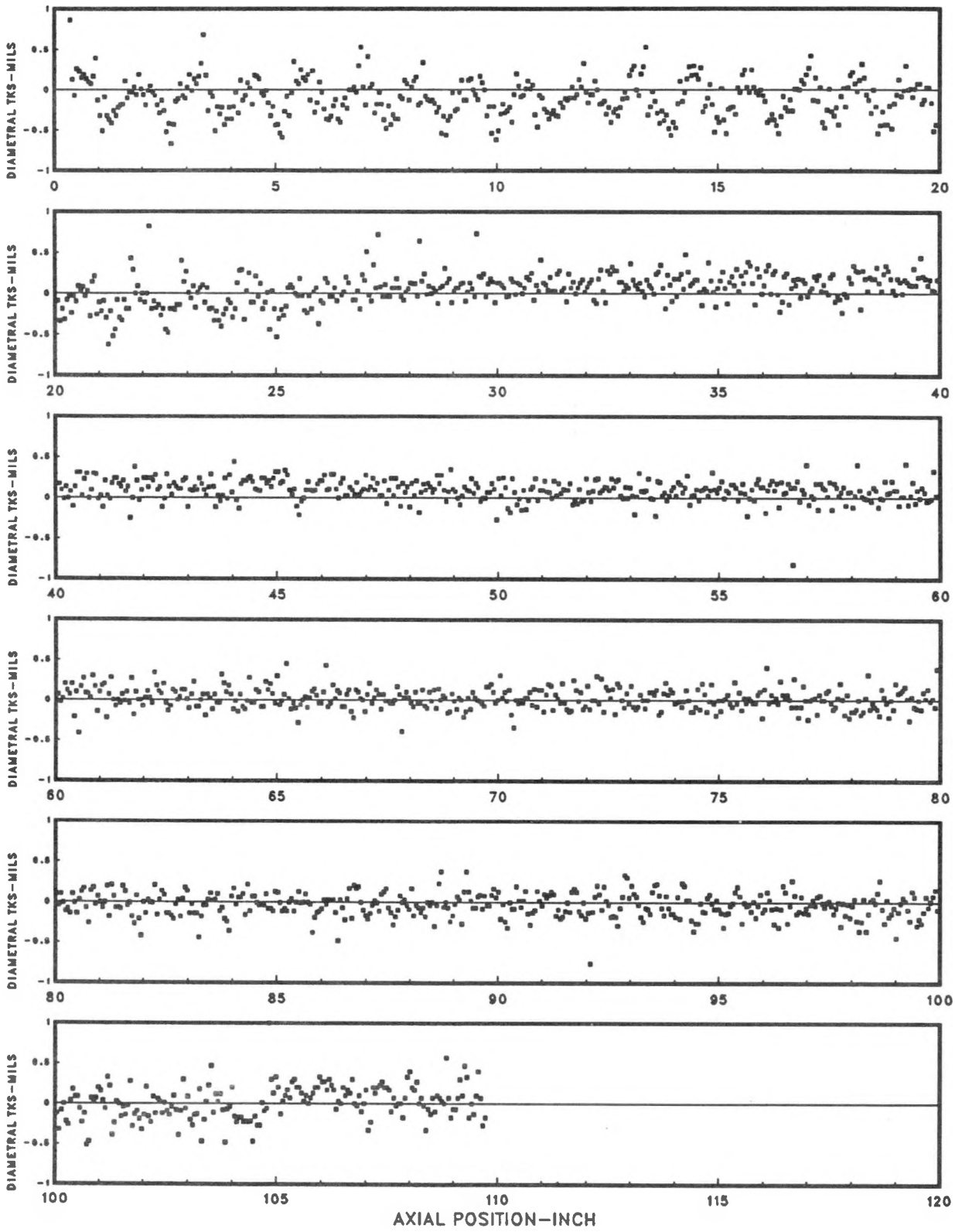

Figure A8-3 - Rod 3220018 Crud Thickness

*U.S. GOVERNMENT PRINTING OFFICE: 1988-505-001/80131